Faculty of Pharmaceutical, Biomedical and Veterinary Sciences
Department of Pharmaceutical Sciences
Medicinal Chemistry

Design, synthesis, and evaluation of trans-cyclooctene (TCO) and cis-dioxolane fused TCO (d-TCO) probes for bioorthogonal pretargeted PET imaging

Ontwerp, synthese en evaluatie van trans-cyclooctene (TCO) en cis-dioxolane gefuseerd TCO (d-TCO) probes voor bioorthogonale pretargeted PET beeldvorming

PhD thesis submitted for the degree of doctor in pharmaceutical sciences at the University of Antwerp to be defended by

Karuna Adhikari

Promotors (s):
Prof. Koen Augustyns
Prof. Filipe Elvas
Prof. Sigrid Stroobants
Antwerp, 2024

Members of the jury

- Prof. dr. Koen Augustyns (promotor)
- Prof. dr. Filipe Elvas (promotor)
- Prof. dr. Sigrid Stroobants (promotor)
- Prof. dr. Alexander van Nuijs (chair of the IDC and chair of the jury)
- Prof. dr. Nina Hermans (internal member of the jury)
- Prof. dr. Frederik Cleeren (external member of the jury)
- Prof. dr. François Guérard (external member of the jury)

Financial support:

This project has received funding from the Research Foundation Flanders (FWO) grant agreement No 1156820N, 1156822N, and V433320N and from the University of Antwerp BOF-umbrella grant agreement number 541200003.

Cover image: Ricardo Lopes

Cover design: Niki Nagels

Table of contents

List of Abbreviations

Ab: Antibody

ADC: Antibody-drug conjugate

Am: Molar activity

AML: Acute myeloid leukemia

AUC: Area under curve

BSA: Bovine serum albumin

CAR: Chimeric antigen receptor

CuAAC: Cu(I)-catalyzed [3+2] azide-alkyne cycloaddition

CT: Computed Tomography

DBCO: Dibenzocyclooctyne

DCM: Dichloromethane

DMF: Dimethylformamide

d-TCO: cis dioxolane fused TCO

EDG: Electron-donating group

EGFR: Epidermal growth factor receptor

ELISA: Enzyme-linked immunosorbent assay

EOB: end of bombardment

EPR: Enhanced permeability and retention

ESI: Electron-spray ionization

EWG: Electron-withdrawing group

Fab: Fragment antigen-binding region

FcRn: Neonatal Fc receptor

FDA: Food and drug administration

FDG: 2-fluoro-2-deoxy-D-glucose

FMO: Frontier molecular orbital theory

GFP: Green Fluorescent protein

HER2: Human epidermal growth factor receptor 2

HOMO: highest occupied molecular orbital

HPLC: High-performance liquid chromatography

HRMS: high-resolution mass spectrometry

i.v.: intravenous

ID/g: Injected dose per gram

ID/mL: injected dose per mL

IEDDA: inverse electron-demand Diels-Alder

Ig: immunoglobulin

Immuno-PET: Immuno-positron emission tomography

J: coupling constant

K_{obs}*:* observed rate constant

K2: second order rate constant

K222: Kryptofix 2.2.2

LUMO: Lowest unoccupied molecular orbital

mAbs: monoclonal antibodies

MeBA: 6-Methyl benzyl amine tetrazine

MIP: Maximum intensity projections

MMAE: Monomethyl auristatin E

MRI: Magnetic resonance imaging

MS: Mass spectrometry

m/z: mass-to-charge ratio

NMR: nuclear magnetic resonance

NHS: N-hydroxysuccinimide

NOTA: 1,4,7-triazacyclononane-1,4,7-triacetic acid

ns: not significant

oxTCO: oxazolone-fused *trans*-cyclooctene

OxoTCO: *trans*-5-oxocene

p.i.: post injection

PBS: Phosphate buffered saline.

PBSF: Perfluoro-1-butanesulfonyl fluoride

PEG: Polyethylene glycol

PET: Positron emission tomography

PSMA: Prostate-specific membrane antigen

Q-TOF: quadrupole-time-of-flight

SPECT: Single-photon emission computed tomography

RCP: radiochemical purity

RCY: radiochemical yield

RGD: Arginine-glycine-aspartic acid peptide

RT: room temperature

SD: standard deviation

SDS-PAGE: Sodium dodecyl sulfate polyacrylamide gel electrophoresis

SEC-HPLC: Size Exclusion-High performance liquid chromatography

SPAAC: Strain-promoted azide-alkyne cycloaddition

sTCO: strained cyclopropane fused TCO

SUV: Standardized uptake values

$t_{1/2}$: half-life

TAC: Time-activity curves

TCO: *trans*-cyclooctene

TFA: Trifluoroacetic acid

THF: tetrahydrofuran

Trx: Thioredoxin

Tz: Tetrazine

UPLC: ultra high performance liquid chromatography

UV: ultraviolet

VOI: Volume of interest

$2Pyr_2$: 3,6-di-2-pyridyl-1,2,4,5-tetrazine

CHAPTER 1

General Introduction

Chapter 1 Introduction

1.1 PET Imaging

Molecular imaging is defined as a technique that allows the visualization, characterization, and quantification of biological processes at the molecular and cellular levels *in vivo.*[1] Molecular imaging techniques include a range of anatomical and functional imaging modalities such as magnetic resonance imaging (MRI), X-ray computed tomography (CT), positron emission tomography (PET), and single-photon emission computed tomography (SPECT). Over the past century, these imaging modalities have found important clinical applications in the diagnosis and management of patients. Other *in vivo* molecular imaging techniques often used in preclinical settings include magnetic resonance spectroscopy, optical imaging, ultrasound, and photoacoustic imaging.[2]

Among different molecular imaging techniques, PET provides the highest sensitivity. The radioisotopes used in PET are positron emitters and mainly exhibit β^+ decay. As the radioisotope decays, the emitted positron travels a certain path length (e.g. 1-2 mm for ^{18}F, 3.5 mm for ^{68}Ga) in tissue and annihilates with an electron, resulting in the emission of two gamma photons with 511 keV energy at 180-degree angle from each other. These high energy γ-photons are detected by a ring of scintillation detectors placed around a volume of interest. The detectors register all the events but only the coincident events measured within a time frame of approximately 5 ns are used for the reconstruction of a three-dimensional image (Figure 1.1). This allows for a dynamic imaging of biological processes with high temporal and spatial resolution based on the radionuclide distribution within the volume of interest.[3, 4]

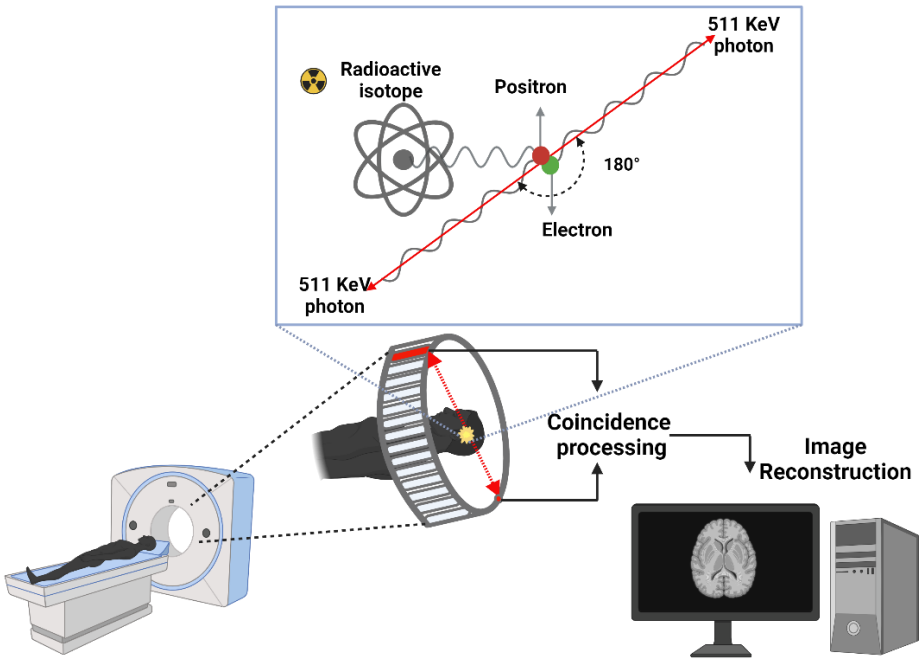

Figure 1.1 *Schematics of a PET scanner and the detection of gamma photons following β^+ decay and subsequent annihilation of a positron and an electron. Figure adapted from Wikimedia commons.*[5]

PET is an important tool for disease diagnosis and patient management in oncology as it provides crucial information on the tumor's position, size, presence of metastases, or therapy response. In contrast to standard tumor biopsies or volumetric tumor analysis, PET imaging allows for accurate differentiation between benign and malignant tissues, while providing information on tumor heterogeneity. This allows for early assessment of therapy response since metabolic changes precede the volumetric reduction of tumors. The most frequently used PET radiotracer is 2-[^{18}F]fluoro-2-deoxy-D-glucose ([^{18}F]FDG), an analog of glucose. It is selectively taken up by cells with a high rate of glucose metabolism, a hallmark feature of most malignant tumors. [^{18}F]FDG is the current reference standard in clinical practice for evaluating, staging, and monitoring therapy response in many different cancers, such as non-small cell lung cancer, lymphomas, colorectal carcinoma, malignant melanoma, esophageal carcinoma, head and neck cancer, thyroid carcinoma, and breast cancer.[6, 7] However, [^{18}F]FDG is not a tumor-target-specific tracer and also accumulates in other tissues with high glucose metabolism, such as the brain and areas of inflammation or infection. In addition, not all cancer types exhibit high metabolic rates. Moreover, with the expansion in targeted therapeutic approaches, characterization and understanding of tumor heterogeneity are important factors for effective patient selection to increase the therapeutic benefits of anticancer treatments. Consequently, target-specific radiotracers are required for precision oncology.

1.2 Immuno-PET

With progress in the discovery of the molecular mechanisms of cancer pathogenesis and novel biomarkers, specific tumor targeting for imaging and therapy has become possible with tracers that target specific biological processes or tumor-specific antigens. Different targeting agents such as small molecules, peptides, peptidomimetics, antibodies and their fragments, and nanoparticles in combination with a PET-radiolabel have been applied for imaging of tumor-specific biomarkers. The targets of these tracers include cell surface receptors, kinases, epigenetic regulatory proteins, DNA damage repair enzymes, and proteases allowing for a deeper understanding of underlying pathophysiological processes.[8] Among these vectors, antibodies have emerged as an important tool as many therapeutic antibodies are used for targeted cancer therapies.[9] These antibodies are considered magic bullets as they selectively bind to tumor-specific antigens with high affinity and accumulate at the target site. Given their high specificity and binding affinity, antibodies are attractive targeting vectors for imaging and can be used as a companion diagnostic tool.

Immuno-positron emission tomography (immuno-PET) is a molecular imaging technique that combines the targeting specificity of monoclonal antibodies (mAbs) with the superior sensitivity of PET. Immuno-PET relies on radiolabeled antibodies (Abs) or smaller fragments of antibodies such as antigen-binding fragments (fab), nanobodies, or affibodies. These vectors can be radiolabeled with positron-emitting radionuclides for PET, or gamma-emitting radionuclides for SPECT. Imaging radiolabeled antibodies can provide valuable information on the expression of tumor-specific biomarkers and tumor heterogeneity within or between patients, thereby facilitating diagnosis, prognosis, and therapy selection.[10, 11] Additionally, radiolabeled antibodies can also be used as a tool in drug discovery to evaluate the targeting, biodistribution, and pharmacokinetics of therapeutic antibodies or antibody-drug-conjugates (ADC) to maximize their therapeutic effects and safety.[12] One of the important features of molecular imaging techniques including immuno-PET imaging is its non-invasive character. This enables longitudinal and quantitative assessment of tumor target expression and distribution throughout the different stages of diagnosis and treatment. This allows for patient stratification, effectively differentiating responsive and non-responsive individuals in the context of targeted therapeutic interventions.

Initially, Ab radiolabeling involved the use of SPECT radioisotopes, such as ^{131}I,^{123}I, ^{111}In, and ^{99m}Tc. However, with the advancements in radionuclide synthesis and purification procedures, PET radioisotopes such as ^{89}Zr, ^{64}Cu, or ^{124}I have found a broader interest. In general, PET scanners have greater sensitivity and higher spatial and temporal resolutions than SPECT cameras. This results in better images at lower injected radioactivity doses and more accurate image quantification, thereby making it a preferred imaging method in clinical settings. Nonetheless, the choice of a suitable radioisotope is predominantly influenced by the long physiological half-life of mAbs. Specifically, the physical half-life of the radioisotope should match the biological half-life of mAb, to ensure the visualization of the target site following the mAb binding with good target-to-non-target ratios. As a result, full mAbs are often labeled with long-lived radioisotopes such as ^{89}Zr ($t_{1/2}$ 78.4 hrs; β^+ 23%; E_{Mean} = 396 KeV) or $_{124}I$ ($t_{1/2}$ 100.3 hrs; β^+ 12 % E_{Mean} = 687 KeV).

1.2.1 Clinical applications of Immuno-PET

The clinical application of immuno-PET imaging has deepened our understanding of tumor heterogeneity and improved disease management strategies. Immuno-PET as a companion diagnostic tool aids in identification and precise quantification of the biomarker enabling the prediction and monitoring the therapeutic response of a targeted treatment. For instance, a clinical trial (ZEPHIR trial) of HER2-positive breast cancer demonstrated that combining baseline target-specific immuno-PET/CT imaging of HER2 using [^{89}Zr]Zr-trastuzumab PET with early assessment of tumor metabolism using [^{18}F]FDG-PET/CT identified a subset of patients benefitting from the treatment with an ADC trastuzumab emtansine (T-DM1).[13] Moreover, immuno-PET/CT with [^{89}Zr]Zr-trastuzumab guided the treatment approach in patients with clinical dilemmas when HER2 status could not be determined by standard methods. Following the scan, the choice of treatment was altered in 40% of the patients, whereas the physician's confidence in the unaltered treatment choice was improved in 50% of patients.[14] Similarly, the evaluation of programmed death ligand-1 (PD-L1), with ^{89}Zr-atezolizumab immuno-PET, effectively predicted the therapeutic response of atezolizumab in patients with three different tumor types, which was not possible through immunohistochemistry or RNA-sequencing-based biomarker analysis.[15] In a recent study, the use of ^{89}Zr-pertuzumab allowed for the identification of HER2-positive metastases in patients with HER2-negative primary breast cancer, enabling the identification of patients for treatment with HER2-targeted therapy which otherwise might not have been considered.[16]

Besides imaging, a mAb can also be radiolabeled with therapeutic radioisotopes. Ibritumomab tiuxetan labeled with ^{90}Yttrium, a β-emitting radioisotope (Zevalin) was the first FDA approved radioimmunotherapy for the treatment of non-hodgkin's lymphoma.[17] It is a powerful tool in drug development and many clinical trials are being conducted using radiolabeled mAbs for either diagnosis or for targeted radioimmunotherapy (Table 1.1).[18, 19]

Table 1.1: Examples of clinical trials evaluating radiolabeled mAbs for diagnostics and therapy

Antigen	Radiolabeled antibody	Application	Tumor	Phase
PD-L1 and PD1	^{89}Zr-Atezolizumab	Diagnostic	RCC	I
	^{18}F-PDL1	Diagnostic	Lung cancer	Pilot
	^{89}Zr-Crefmirlimab	Diagnostic	Melanoma, MCC, RCC, NSCLC	II
CAIX/MN	^{89}Zr-Girentuximab	Diagnostic	Triple-negative breast cancer	II
EGFR	^{89}Zr-Nimotuzumab	Diagnostic	Lung and colorectal cancers	I/II
	^{89}Zr-Panitumumab	Diagnostic	Colorectal cancer	
HER2	^{89}Zr-Pertuzumab	Diagnostic	HER2-Positive Solid Tumors	I
	^{64}Cu-Trastuzumab	Diagnostic	Stage III Breast cancer	II
CD25	^{90}Y-Basiliximab	Therapeutic	Hodgkin Lymphoma	II
CD66	^{90}Y-Anti-CD66	Therapeutic	Leukemia	II
B7H3	^{131}I-Omburtamab	Therapeutic	Medulloblastoma and Ependymoma	II
CD33	^{225}Ac-Lintuzumab	Therapeutic	AML (older patients ≥ 60 years)	I/II (completed)
IGF-1R	^{225}Ac-FPI-1434	Therapeutic	IGF-1R expressing solid tumors	I/II

Abbreviations: MCC, Merkel cell carcinoma; RCC, renal cell carcinoma; NSCLC, non-small-cell lung cancer; PD-L1, programmed death ligand-1; AML, Acute myeloid leukemia

1.2.2 Limitations of Immuno-PET

Despite the promising clinical outcomes, immuno-PET suffers from some disadvantages. Notably, mAbs have high molecular weights (~150 kDa), which far exceeds the clearance cut-off value of glomerular filtration (60 kDa). Furthermore, the interaction between the Fc domain of an immunoglobulin (IgG) and the neonatal Fc receptor (FcRn) in endothelial cells protects the mAb against degradation, resulting in prolonged physiological half-life.[20] The FcRn-mediated mAb slavage pathway is similar across different species however, the affinity of a mAb for FcRn varies among them. For instance, the average half-life of IgG in mice is 6-8 days whereas in humans, it is about 21 days.[21] Similarly, the half-life of different marketed mAbs vary between 11-30 days. Consequently, long-lived radionuclides matching the biological half-life of mAbs should be employed for imaging.

Moreover, an interval of several days post-mAb radiotracer injection is required for an optimal accumulation of the radiotracer in the tumor and clearance from circulation and non-target organs to obtain the best tumor-to-background (T/B) ratios. This leads to a higher radiation burden for patients associated with higher photon energies of the long-living radioisotopes combined with the slow pharmacokinetics of the mAb.[22] The effective dose values of such radionuclides can result in 40-50 mSv per scan in patients, which is twice the annual dose constraint recommended by the International Commission on Radiological Protection (20 mSv) for patients under diagnosis or treatments with radiopharmaceuticals.[23] Therefore, the use of radiolabeled mAbs with long-living radioisotopes restricts repeated applications within a shorter time frame, hampering the study of disease progression. Additionally, most long-lived positron emitters currently in use have low β^+-branching fractions which leads to lower-quality images and a decrease in the accuracy of quantification. Moreover, some long-lived PET radionuclides emit long-range positrons resulting in decreased spatial resolution.[22] In comparison, short-lived radioisotopes such as Fluorine-18 or Carbon-11 show almost exclusively positron emission and also translate into lower effective dose values in patients. For instance, the effective dose value resulting from the injection of [^{18}F]FDG in patients is 9 mSv per scan, which is substantially lower in comparison to long-lived radioisotopes.[24] However, the short half-life of Fluorine-18 is not compatible with directly radiolabeled antibodies.

1.3 Pretargeted Immuno-PET Imaging

Pretargeted Immuno-PET imaging is an *in vivo* labeling strategy developed to circumvent the shortcomings associated with the prolonged residence time and high radiation burden of the radiolabeled mAbs. In this approach, the mAb and the radionuclide are injected as two separate components which will subsequently react *in vivo*. In the first step, a mAb is initially modified with a tag, and upon administration, it binds to its target while simultaneously clearing from non-target sites. In the second step, after sufficient clearance of the mAb, a small, fast-clearing radiolabeled probe is administered. This radiolabeled probe binds or interacts specifically with the tag present on the target-bound antibody, while the unbound fraction is excreted rapidly from the circulation (Figure 1.2).[25, 26]The physical separation of mAb and radioisotope allows the use of short-lived radioisotopes which would normally be incompatible with mAb-based imaging agents. Moreover, pretargeting with short-lived radionuclides allows the *in vivo* imaging of the target at earlier time points following the administration of the radiotracer leading to reduced radiation doses and superior image contrast compared to directly labeled antibodies.[27] In certain cases, an additional clearing agent or a masking agent may be administrated before the radiotracer injection to eliminate or mask the unbound antibodies from circulation to enhance the T/B ratios.

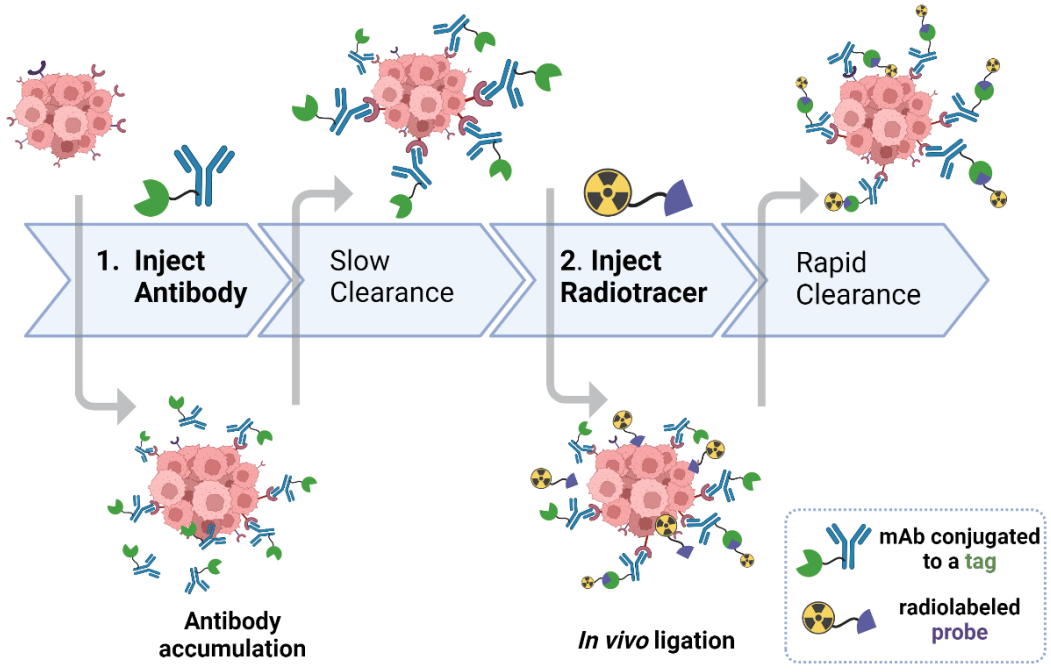

Figure 1.2 *Schematics of in vivo pretargeting approach for immuno-PET imaging. An immunoconjugate is administered and allowed to slowly accumulate at the tumor and clear from the circulation. Subsequently, a radioligand is injected which selectively reacts or binds to the tag on the tumor-bound immunoconjugate while the unbound fraction is cleared rapidly.*

Numerous strategies with different recognition pairs of secondary target/tag on mAb with radiolabeled probes for *in vivo* pretargeting have been explored. Four different strategies have been reported: 1) the non-covalent interaction between (strept)avidin and biotin; 2) a bispecific antibody that binds to both antigen and a radiolabeled chelates or haptens; 3) hybridization of complementary oligonucleotides; and finally, 4) bioorthogonal ligation via inverse electron-demand Diels-Alder (IEDDA) reaction (Figure 1.3). Although each of the approaches has demonstrated success in pre-clinical models, they are also accompanied by their limitations.

The first strategy relies on the high affinity between (strept)avidin-conjugated mAbs and biotin-modified radiolabels.[28] Streptavidin and biotin-based pretargeting demonstrated clinical feasibility in both imaging and radiotherapy.[29-32] However, the immunogenicity associated with the streptavidin-modified mAbs poses a substantial concern.[30]

The pretargeting system based on bispecific antibody (BsAb) uses mAbs capable of binding a tumor antigen as well a radiolabeled chelates or haptens (a non-immunogenic small molecule, that binds specifically to an Ab with high affinity). The BsAb/hapten when initially developed showed low tumor retention due to a lower binding affinity of the hapten which was later improved through the use of bivalent haptens.[33, 34] Although extensively studied in both preclinical and clinical studies, its broad applicability is limited by the complexity, expense, and lack of modularity of the system for generating BsAbs.[35]

An optimized strategy for pretargeting based on bispecific antibodies is the Self-Assembling and DisAssembling domains fused BsAbs which results in formation of a stable tetrameric complexes. These tetrameric complexes bind to tumor antigen with high avidity but are able to dissassemble into small dimers or monomers after some time in circulation. This facilitates a rapid renal clearance of the unbound tetramers, resulting in higher tumor-to-background ratios of the radiolabeled probe. This improved strategy has shown promising results in a pretargeted radioimmunotherapy setting.[36]

The binding of DNA and RNA oligonucleotides sequences with their complementary strands are highly specific and demonstrate high affinity. The hybridization of complementary oligonucleotides using nuclease-resistant DNA analogs such as morpholino nucleic acids (cMORF) and peptide

nucleic acids (PNAs) sequence have shown successful results in pretargeting as natural DNA degrades *in vivo.*[37-39] However, no clinical studies have been reported so far.

Finally, the *in vivo* covalent bond formation *via* a bioorthogonal reaction between a mAb conjugated to *trans*-cyclooctene (TCO) and a radiolabeled tetrazine (Tz) is the most recent mechanism which is currently under active investigation.[40-43] Bioorthogonal reactions have attractive properties for *in vivo* pretargeting. Their fast reaction kinetics and selectivity in biological environments without interfering with endogenous functional groups make them a perfect candidate. In the following sections, a brief overview of bioorthogonal chemistry and the pretargeting studies based on bioorthogonal click chemistry are described.

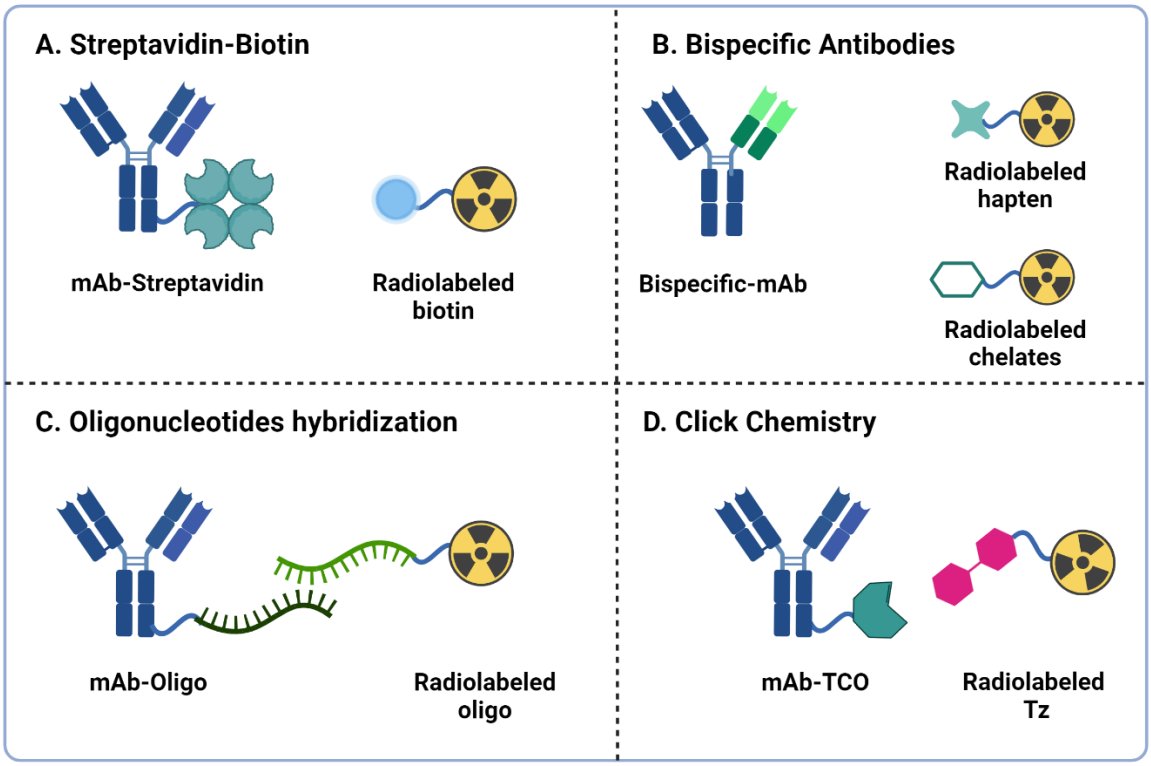

Figure 1.3 *Different recognition pairs used for in vivo pretargeting studies. (A) Noncovalent interaction between streptavidin and biotin (B) Bispecific antibodies and hapten interaction (C) Hybridization of complementary oligonucleotides (D) Covalent binding through click reaction between a trans-cyclooctene and tetrazine.*

1.3.1 Bioorthogonal chemistry

Bioorthogonal chemistry refers to a group of chemical reactions that proceed in living organisms under physiological conditions without interfering or interacting with the biological system.[44-47] The term likely originates from the mathematical concept of "orthogonality" which describes independent events that do not affect each other's outcome. These reactions allow the modification of biomolecules with non-native functional groups through a covalent bond formation, which can be employed to study biological processes. Bertozzi (Nobel prize laureate) and co-workers defined the ideal bioorthogonal reaction as one (i) proceeds in physiological conditions, (ii) is selective and inert towards the biological system, (iii) has fast kinetics at low concentrations, and (iv) should not contain functional groups naturally found in biological systems.[44] However, not all the bioorthogonal reactions satisfy all of these criteria simultaneously.

The **Copper-Catalyzed Azide-Alkyne Cycloaddition (CuAAC)** reaction, discovered independently by Sharpless and Meldal (Nobel prize laureates), is the most widely used click reaction for bioorthogonal labeling of proteins, glycans, lipids, nucleic acids, and for activity-based protein profiling.[48-50] It is an improvement over the **1,3-dipolar cycloaddition** reaction between an alkyne and an azide which requires elevated temperatures or pressure and often results in regioisomers. With the presence of copper(I) catalyst, the reaction proceeds at room temperature at much higher rates (10 - 100 $M^{-1}s^{-1}$) yielding only the 1,4-substituted regioisomer (Scheme 1.1). CuAAC has found applications in bioconjugation, and selective modification of proteins, nucleic acids, and virus particles.[51-54] However, its application in *in vivo* systems has posed challenges due to the cytotoxicity of copper Cu(I), which induces oxidative damage to cells. Efforts have been made to minimize the toxicity of Cu(I) by employing ligands such as tris(triazolymethyl)amines which stabilize the Cu(I) catalyst and reduce copper redox reactions. The development of various biocompatible ligands has facilitated the use of CuAAC in living systems. Additionally, efforts to enhance the reaction rate through chelation-assisted CuAAC have also been pursued.[55]

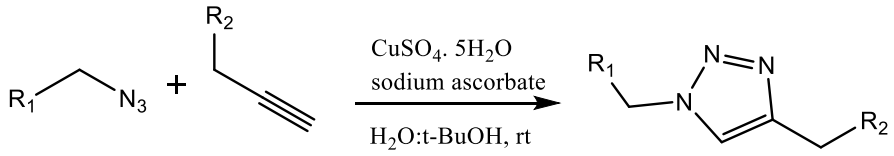

Scheme 1.1 *Copper-catalyzed Azide Alkyne Cycloaddition (CuAAC) of azide with terminal alkyne in the presence of a copper Cu(II) salt and sodium ascorbate for Cu(I) generation. The reaction yields a 1,4-disubstituted 1,2,3-triazole.*

Moreover, ruthenium (II)-catalyzed azide alkyne cycloaadition (RuAAC) reaction to selectively form the 1,5-disubsituted triazoles has also been described. While CuAAC can only be perfomed with terminal alkynes, RuAAC also allows the reaction with internal alkynes. Although the reaction broadens the scope to 1,5 disubstituted triazoles, the reaction requires higher temperature than CuAAC and can be problematic in reactions containing acidic functional groups.[56] Nevertheless, there has been a growing interest in the development of alternative click chemistry reactions that proceed without catalysts. Notably, bioorthogonal reactions such as the Staudinger ligation, Strain-promoted alkyne-azide cycloaddition (SPAAC), and the Inverse electron-demand Diels-Alder reaction (IEDDA) have attracted a significant amount of interest in the field of nuclear imaging.[40, 57] Other bioorthogonal ligation reactions described include oxime ligations, photoclick 1,3-dipolar cycloadditions between tetrazoles and substituted alkenes, and strain-promoted cycloadditions of nitrones and alkynes. Similarly, transition metal-catalyzed reactions that form carbon-carbon bonds such as Suzuki and Sonagashira couplings or olefin metathesis have also been described. These reactions are often explored for labeling proteins *in vitro* and on the cell surface.[42] The following section describes the bioorthogonal click reactions used for *in vivo* pretargeting.

1.3.1.1 *Staudinger Ligation*

One of the first bioorthogonal reactions developed was Staudinger Ligation, which involves the reaction of azides and functionalized phosphines. The reaction forms an iminophosphorane intermediate which hydrolyses into an amine and a phosphine oxide in the presence of water. The potential of this reaction for biological applications was described by Bertozzi and co-workers.[44] The Staudinger ligation is selective and occurs rapidly at room temperature. However, the aqueous instability of the iminophosphorane adduct limits its use *in vivo*. By introducing an ester group as an electrophilic trap within the phosphine, the nitrogen of iminophosphorane reacts with the ester to form a stable amide bond (Scheme 1.2).[46] The Staudinger ligation is a robust method for *in vitro* and *in vivo* labeling and its variations have been applied in the labeling of glycans in zebrafish, proteins, lipids, and DNA.[58, 59] The Staudinger ligation was also successfully used to label glycoproteins in living mice.[54] Despite its biocompatibility, the reaction suffers from oxidation of phosphine and suboptimal kinetics with a second-order rate constant in the low 10^{-3} $M^{-1}s^{-1}$ range, which limits its *in vivo* applicability for pretargeted imaging.[60] The pretargeting strategy using an antibody-azide conjugate as a targeting vector and a radiolabeled phosphine probe administered sequentially showed no evidence of ligation products *in vivo*.[60]

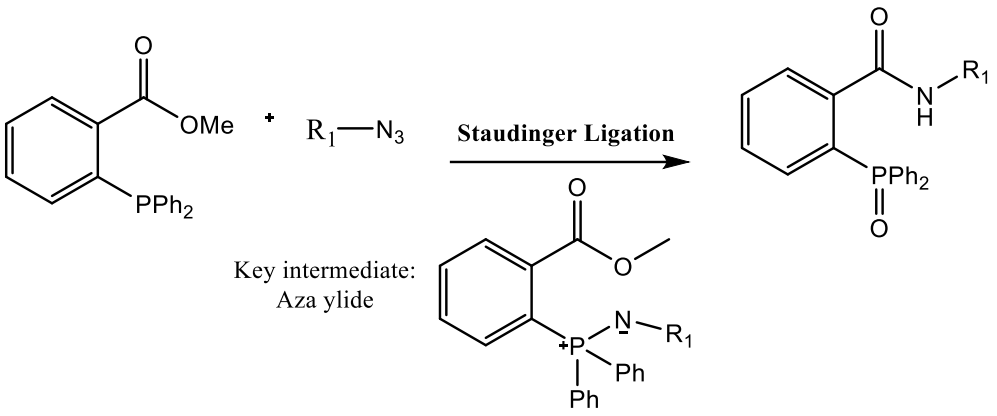

Scheme 1.2 *The Staudinger ligation reaction between an azide and a triarylphosphine consisting of an ester group as an electrophilic trap. The iminophosphorane intermediate is trapped intramolecularly forming a stable covalent adduct.*

1.3.1.2 *Strain-promoted [3+2] azide-alkyne cycloaddition (SPAAC)*

Strain-promoted [3+2] azide-alkyne cycloaddition (SPAAC) is a strategy re-discovered by Bertozzi *et al.* to optimize the biocompatibility of azide-alkyne cycloaddition.[45] It is a copper-free azide-alkyne reaction, where the terminal alkyne is replaced by cyclooctyne (Scheme 1.3). The introduced ring strain into the alkyne reagent serves as the driving force of SPAAC. Although biocompatible, the first generation of SPAAC was considerably slower than CuAAC (1.2 - 2.4 x 10^{-4} $M^{-1}s^{-1}$).[61] Rate enhancements were achieved through the introduction of electron-withdrawing groups to the cyclooctyne, nitrogen-containing cyclooctynes, or fused rings (DIFO, DIBO, BCN, DIBAC, DBCO).[62, 63] Several studies utilizing the cyclooctyne derivatives have shown their ability to react with azides *in vitro*, in zebrafish as well as in live mice.[64-67] However, the synthesis of these compounds remains a challenging aspect and cyclooctyne rings can potentially react with nucleophiles present in living systems.

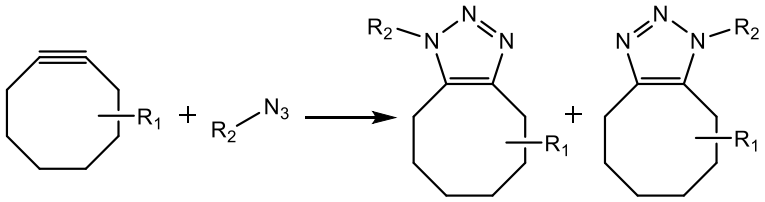

Scheme 1.3 *Strain-promoted azide-alkyne cycloaddition (SPAAC) between an azide and a highly strained cyclooctyne forming the triazole. The reaction proceeds in physiological conditions without catalysts.*

Robillard and co-workers evaluated the use of ^{177}Lu-cyclooctyne derivatives and an azido-conjugated anti-CD20 mAb (Rituximab) for pretargeted radiotherapy. The study showed covalent and non-covalent interactions of cyclooctynes with serum proteins. This led to decreased reactivity

of cyclooctynes towards azides *in vivo*, precluding their use for *in vivo* pretargeting.[68] However, a study reported by Kim and coworkers demonstrated a successful pretargeted imaging using a dibenzocyclooctyne (DBCO)-functionalized pegylated mesoporous silica nanoparticles (MSNs) administered 24 h before ^{18}F-labeled azides. PET-CT imaging showed a significant accumulation of radioactivity in tumors in mice treated with MSNs in comparison to the untreated group.[69] The difference in the pretargeting efficiency between these two studies is possibly related to the 4-fold higher reactivity of the cyclooctyne used and the high loading capacity of nanoparticles used in the latter study. Nevertheless, SPAAC ligation shows promise in an *in vivo* pretargeting approach given favorable kinetics, and a suitable protocol is applied.[39, 70]

1.3.1.3 *Inverse electron-demand Diels-Alder (IEDDA)*

Significant progress toward achieving a universal approach for *in vivo* pretargeted imaging was offered by the bioorthogonal inverse electron-demand Diels-Alder (IEDDA) reaction between strained *trans*-cyclooctene (TCO) and electron-deficient tetrazine (Tz).[71, 72] The reaction between a TCO and a tetrazine proceeds through a [4+2] cycloaddition forming a highly strained bicyclic intermediate. Subsequently, a retro-Diels-alder reaction occurs with N_2 evolution, resulting in the formation of a stable six-membered 4,5-dihydropyridazine ring which further oxidizes to a pyridazine (Scheme 1.4). The TCO-Tz cycloaddition is extremely fast, with measured rate constants up to 10^7 $M^{-1}s^{-1}$. No catalyst is required, and the reaction proceeds in high yields in organic solvents, water, buffer, cell media, or lysate.[71, 73] The reaction is extremely selective and can thus tolerate a broad range of functional groups commonly present in peptides and proteins.[74, 75] Since its rediscovery as a bioorthogonal reaction, the number of research published featuring tetrazine-TCO ligation has increased consistently.[76] The interest is continued as the reaction satisfies the conditions needed for biological applications, including pre-targeted imaging. The detailed mechanism of IEDDA and its reaction partners are described in detail in Chapter 2. This chapter entails a comprehensive review of TCOs and provides an overview of TCO derivatives and their biomedical applications.

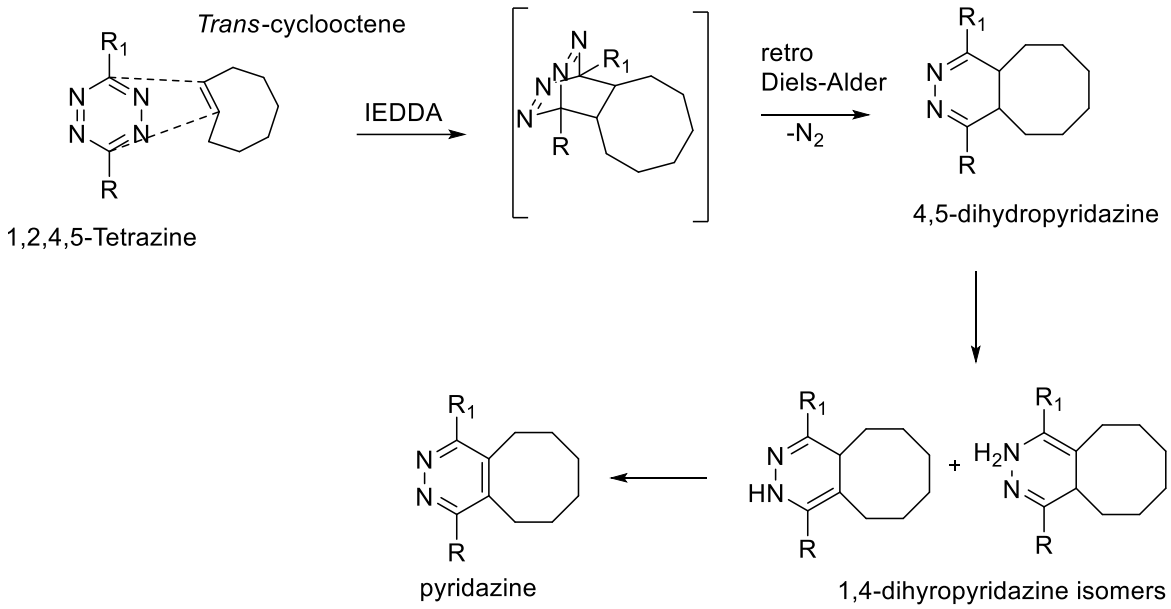

Scheme 1.4 *IEDDA reaction scheme between trans-cyclooctene and a 1,2,4,5-tetrazine.The cycloaddition results in the formation of a 4,5-dihydropyridazine which is oxidized to a pyridazine.*

1.4 Pretargeting using IEDDA

In a pretargeting approach based on the IEDDA reaction between a TCO and tetrazine, the mAb can be modified with either Tz or TCO and injected into a living subject. Then, a radiolabeled reaction partner (either TCO or Tz), is administered which will selectively and covalently bind to the pretargeted mAb conjugate, while the unbound radiolabeled TCO or Tz is rapidly cleared from the body. The ultrafast reaction kinetics between TCO and tetrazine plays a pivotal role in the feasibility of *in vivo* pretargeting, as this allows the reaction to take place *in vivo* conditions at low micromolar to nanomolar concentrations. Another advantage of this approach is the versatility of the system. It can be adapted to different tumor targets as many clinically approved anti-tumor antibodies are already available. Apart from imaging, the application of pretargeting approach for radioimmunotherapy holds promise in enhancing the therapeutic efficacy by increasing tumor uptake while reducing the dose limiting hematotoxicity which is often associated with directly radiolabeled mabs.[77] Furthermore, by separating the tumor-targeting from the radioisotope, pretargeting also enables the use of different radioisotopes for diagnositic and therapeutic purposes, thereby leaning towards a theranostic approach.

In an *in vivo* pretargeting approach based on IEDDA, different factors play a role in determining the efficacy of *in vivo* chemical reaction. Besides the fast reaction kinetics of the reactants, *in vivo*

stability and the serum half-life of the reactants are important factors. In general, a trade-off between reactivity and stability is observed. Faster-reacting tetrazines are prone to hydrolysis in aqueous media. Consequently, the vast majority of IEDDA-based pretargeting is performed employing a TCO-labeled antibody and a tetrazine-based radioligand. For TCO, the *in vivo* isomerization of the trans double bond to its *cis* isomer is the main concern. However, shortening the linker length between mAb and the TCO-tag increased the serum half-life of TCO up to 5 days.[78] Numerous studies have applied the strategy with the first clinical trial in humans using [^{64}Cu]Cu-Tz-SarAr and hu5B1-TCO in patients with pancreatic cancer recently being approved.[78-88]

One of the earliest works on pretargeting based on IEDDA was reported by Rossin *et al.* In their pioneering work, an mAb conjugated to TCO (CC49-TCO) and a ^{111}In-labeled DOTA-tetrazine radioligand were used for the imaging of TAG-72 expressing colorectal cancer xenografts.[89] TAG - 72 antigen is an ideal target for pretargeting given its limited internalization, shedding, and overexpression in a wide range of solid tumors. The study demonstrated a pronounced accumulation of radioactivity at the tumor with excellent image contrast. The same group has since then investigated alternative TCO moieties with improved properties for pretargeting, tetrazine functionalized clearing agents, and pretargeting with diabodies and affibodies.[79, 81, 90, 91] Zeglis *et al.* also described a ^{64}Cu-labeled tetrazine-based pretargeted PET imaging of SW1222 colorectal carcinoma xenografts, showing comparable images and tumor-to-muscle ratios when compared to directly labeled mAb. The study also demonstrated that the pretargeted imaging approach led to a 3-fold reduction in the effective dose to the whole body when compared to directly labeled mAb.[85] Additionally, pretargeting studies of TCO-5B1-Ab targeting carbohydrate antigen 19.9 on pancreatic cancer xenografts with ^{64}Cu-labeled tetrazine showed the viability of the approach even in the difficult circumstances presented by a circulating antigen and internalization of antibody.[82]

Initially, pretargeted imaging studies were carried out with longer living isotopes (^{111}In ($t_{1/2}$ = 67 h), ^{64}Cu ($t_{1/2}$ = 12.7 h), and ^{177}Lu ($t_{1/2}$ = 162 h) as efforts to directly radiolabel tetrazines with nucleophilic fluorine-18 were not successful due to the instability of tetrazines under basic conditions. But with the recent advances in tetrazine labeling strategies, several pretargeted imaging studies employing Fluorine-18 have been reported (Figure 1.4). Early efforts to radiolabel tetrazine included indirect methods such as labeling with prosthetic groups or through the Aluminum fluoride strategy. In 2016, Lewis *et al.* reported the imaging of a TCO- 5B1 mAb conjugate with an Al^{18}F-NOTA-labeled

tetrazine radiotracer (**[^{18}F]1**), in BxPC3 pancreatic cancer xenografts expressing A19.9. PET imaging data demonstrated tumor uptake values up to 6.4% ID/g at 4 h postinjection.[92]

In 2017, Keinänen *et al.* investigated the efficacy of the pretargeting strategy in A431 epidermoid carcinoma and a BT-474 ductal carcinoma as *in vivo* tumor models. ^{18}F-radiolabeled glycosylated tetrazine tracer **[^{18}F]2** was used in combination with two internalizing antibodies, cetuximab, and trastuzumab conjugated with TCO. For both antibodies, the tumor could be visualized through PET imaging with the highest tumor uptake of 3.7 ± 0.1 %ID/g for [^{18}F]2-TCO-cetuximab and 1.5 ± 0.1 %ID/g for [^{18}F]2-TCO-trastuzumab, 4 h after **[^{18}F]2** injection. However, relatively low tumor-to-background (T/B) ratios were observed with high amounts of radioactivity observed in blood for both mAbs, but to a much lesser degree with trastuzumab.[84]

In 2021, Steen *et al.* used copper-mediated click chemistry for ^{18}F labeling of six different tetrazine alkene derivatives with ^{18}F-labeled azides. Pretargeted PET imaging in LS174T-xenografted tumor-bearing mice pretreated 72 h earlier with CC49-TCO followed by **[^{18}F]3** showed a mean tumor uptake of 1.7 ± 0.6% ID/g 1 h after the injection and moderate target-to-background ratios.[80] Although a good tumor-to-muscle ratio of 4.8 was observed, the tumor-to-blood ratio remained rather low (0.78) which contributed to a high background signal.

In 2021, direct aromatic radiolabeling of highly reactive Tzs was successful *via* Cu-mediated fluorination using stannane precursors.[93] Pretargeted PET imaging in mice bearing LS174T xenograft with CC49-TCO 72 h prior to **[^{18}F]4** injection resulted in a mean tumor uptake of 1 ± 0.1% ID/g. The tracer displayed rapid clearance and showed a good tumor-to-muscle ratio of 10, an improvement compared to Tzs labeled with ^{64}Cu and ^{111}In.[93] The same group further extended their approach to directly label base-sensitive tetrazines through aliphatic nucleophilic substitution. Using this approach, H-Tz and bis-pyridyl-Tzs were radiolabeled and both tracers showed a significantly higher tumor uptake (1.87 ± 0.31 for **[^{18}F]5** and 1.81 ± 0.3% ID/g for **[^{18}F]6**) than controls. A high tumor-to-muscle (T/M) ratio was determined for both tracers (20 for **[^{18}F]5** and 8 for **[^{18}F]6**). A tumor-to-muscle ratio of 20, 1 h post tracer injection is thus far the highest ratio observed for pretargeting with ^{18}F-labeled radiotracers.[94, 95] Similarly, pretargeting studies using ^{18}F-labelled TCO and d-TCO probes have been reported. These TCO probes will be discussed in Chapter 2.

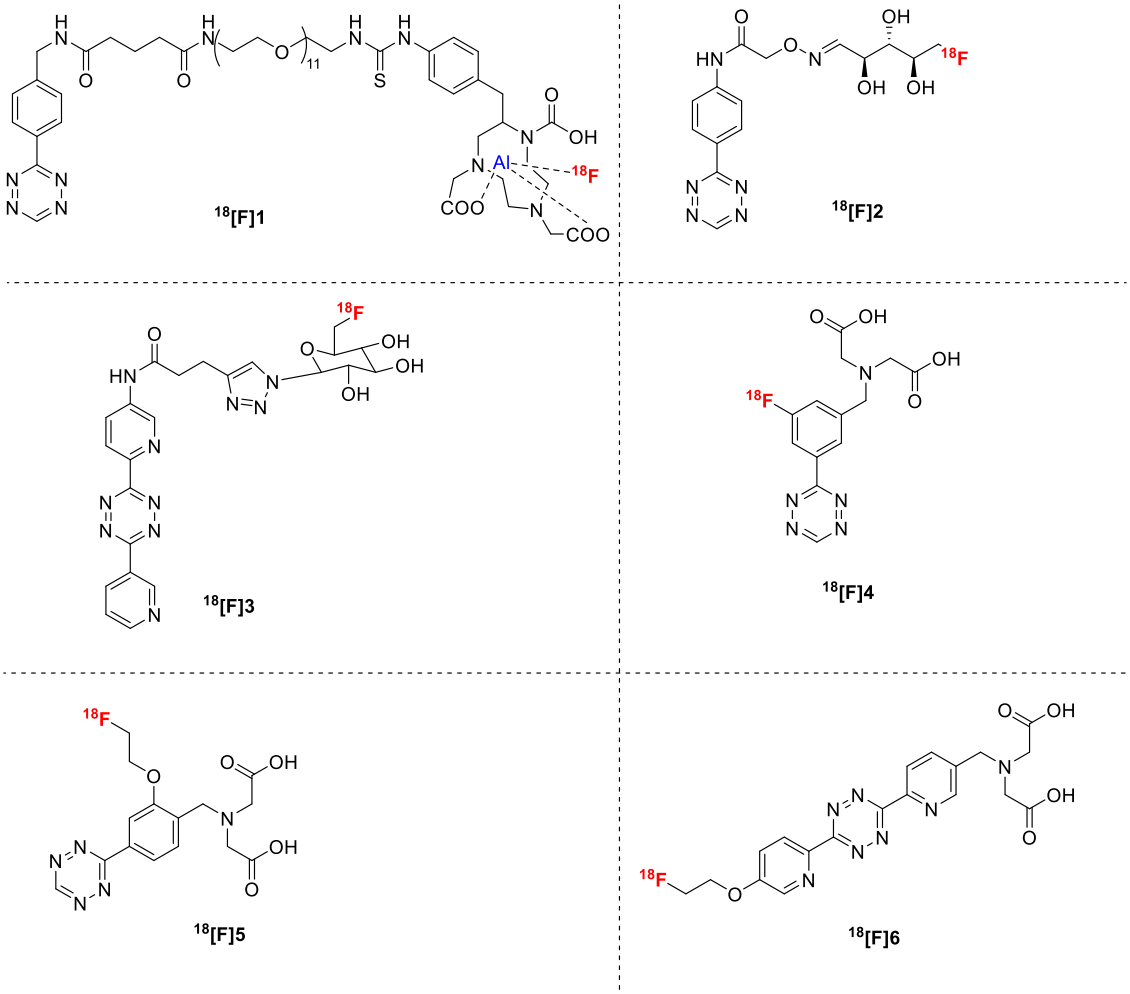

Figure 1.4 *Structures of ^{18}F-labeled tetrazines used in pretargeting studies through IEDDA reaction with TCO-modified mAb conjugates.*[80, 84, 92-95]

1.5 Radiolabeling strategies for Fluorine-18

Fluorine-18 is a short-lived ($t_{1/2}$ = 109.8 min) positron-emitting radioisotope with favorable chemical and nuclear properties for PET imaging. Fluorine is a small but highly electronegative element, and a C-F bond has greater stability when compared to a C-H bond. In medicinal chemistry, fluorine often serves as a bioisostere for hydrogen. Fluorine atoms can be used as a replacement for hydrogen atoms or hydroxyl groups to influence the physiochemical and or pharmacokinetic properties of pharmaceutically active compounds.[96] Moreover, many medicinally active compounds often contain fluorine in their structure, and labeling such compounds with ^{18}F allows the visualization of targets without altering their binding affinity. Additionally, ^{18}F has attractive nuclear properties when compared to other positron-emitting radioisotopes. Fluorine-18 has a

favorable decay profile with 97% positron emission and 3% electron capture. Additionally, it displays a low positron energy (E_{Mean} = 250 KeV) with a short positron range (max. 2.4 mm in water) resulting in high spatial resolution for imaging with lower radiation burden to patients. Moreover, fluorine-18 has a half-life of 109.8 minutes allowing for multi-step radiosynthesis and transport to satellite nuclear medicine facilities.[97] Additionally, different fluorination methods are available allowing the labeling of a broad range of molecules or peptides. Thus, fluorine-18 is a perfect candidate for use in pretargeted PET imaging approaches.

1.5.1 Fluorine-18 production

Fluorine-18 is often produced from a cyclotron by proton irradiation of ^{18}O-enriched water through the nuclear reaction $^{18}O(p, n)^{18}F$. The aqueous fluoride anions ($[^{18}F]F^-$) are transferred from the target and used for nucleophilic substitution reactions. Gaseous $[^{18}F]F_2$ can be produced through the reaction $^{20}Ne(d, \alpha)^{18}F$, where deuterons are accelerated onto a neon-20 target. The electrophilic ^{18}F is isolated with a small amount of nonradioactive F_2 gas added to the ^{20}Ne gas. Carrier addition is needed to quench the highly activated electrophilic ^{18}F species, which otherwise adsorbs to the target wall. The addition of nonradioactive F_2 gas allows for the exchange of the ^{19}F atom with the ^{18}F atom and traps the activity as ^{18}F-^{19}F fluorine ($[^{18}F]F_2$).

The advantage of non-carrier added $[^{18}F]F^-$ is the high specific activity of the produced ^{18}F isotope. Specific activity is the ratio of the amount of $[^{18}F]$fluoride ion to its mass of carrier ^{19}F or total fluoride ion and is expressed in becquerel per gram (Bq/g).[98] High specific radioactivity is required when targeting saturable binding sites. Low specific radioactivity causes the target protein to be saturated with non-radioactive ligands and leads to lower signals from radiotracer binding. High specific activity also enables radiotracers to be administered to human subjects in low mass doses (typically less than 1–10 nmol), without toxic or pharmacological effects.[97, 99]

Fluorine-18 can be introduced through electrophilic substitution, nucleophilic substitution, or through chelation of the metal-Fluoride complex. In the light of the work presented in the thesis, only nucleophilic substitution and $Al^{18}F$ labeling are described.

1.5.1.1 *Nucleophilic substitution*

Nucleophilic substitution with non-carrier added $[^{18}F]F^-$ is the most commonly applied method for radiofluorination. Aqueous fluoride ion $[^{18}F]F^-$ is obtained following irradiation of ^{18}O enriched water. However, the fluoride ion forms hydrogen bonds with water molecules inactivating $[^{18}F]F^-$ ion for further nucleophilic reaction. To increase nucleophilicity, $[^{18}F]F^-$ is first trapped on an anion exchange resin, which is then eluted with a solution of a weak base such as potassium carbonate and a phase transfer catalyst, in water/acetonitrile. The water is subsequently removed by azeotropic distillation with acetonitrile. The use of a phase transfer catalyst enhances the solubility of $[^{18}F]KF$ in polar aprotic solvents such as DMF, DMSO, or ACN, conditions necessary for nucleophilic substitution reactions (S_N2 or S_NAr). Additionally, the phase transfer catalyst increases the nucleophilic character of the $[^{18}F]F^-$ by separating the charges between K^+ and $[^{18}F]F^-$ as it forms a strong complex with the potassium cation. The most used phase-transfer catalyst is $Kryptofix_{2.2.2}$. For base-sensitive reactions, organic salts such as tetra butyl ammonium bicarbonate can be used. Tetraalkylammonium carbonates and $[^{18}F]$tetraalkylammonium fluoride are soluble in polar aprotic solvents and facilitate nucleophilic substitution similar to a phase-transfer catalyst.[97, 99-101]

Aliphatic nucleophilic substitution proceeds via an S_N2 mechanism and thus requires a good leaving group. Different leaving groups can be used based on their leaving ability: Cl < Br < I < 4-methyl benzenesulfonate (tosylate) ~ methanesulfonate (mesylate) < 4-nitrobenzenesulfonate (nosylate) < trifluoromethanesulfonate (triflate). However, the tendency for E2 elimination is also higher with a better leaving group in basic conditions.

Nucleophilic aromatic fluorination can be achieved with I < Br < Cl < F < NO_2 < NMe^{3+} as leaving groups. However, an activated aromatic ring toward nucleophiles is required. The installation of electron-withdrawing groups at the ortho or para position to the leaving group stabilizes the negative charge of the Meisenheimer complex intermediate, facilitating the S_NAr. The following groups can be used to activate the aromatic ring in the following order: 2-NO_2 < 4-Ac < 4-CHO < 4-CN ≈ 4-CF_3 < 4-NO_2. Moreover, the reaction conditions required are often harsh with high temperatures. Similarly, ^{18}F-labeling of heteroaromatic compounds which favor nucleophilic substitution has also been studied. Heteroarene such as pyridine allows for radiofluorination in the activated 2- or 4-position.[100, 101]

1.5.1.2 *Prosthetic groups*

Direct radiofluorination requires harsh conditions that are often not compatible with biologically active molecules. Additionally, late-stage fluorination of temperature and base sensitive peptides is not a viable strategy. A more indirect method to label such biomolecules is using ^{18}F-labeled prosthetic groups which contain reactive groups and can be reacted with an appropriate functional group of the biomolecule under mild conditions. The biomolecules can be attached to the prosthetic groups on amine or thiol functional groups via acylation, alkylation, amidation, imidation, oxime formation, or through click chemistry (Figure 1.5). A broad spectrum of both aliphatic and aromatic radiofluorinated precursors have been reported and many are widely used for the synthesis of PET tracers.[102] Although this approach allows for the labeling of broad ranges of compounds and biomolecules, it also requires longer synthesis times and additional purification times.[97, 99, 100, 102]

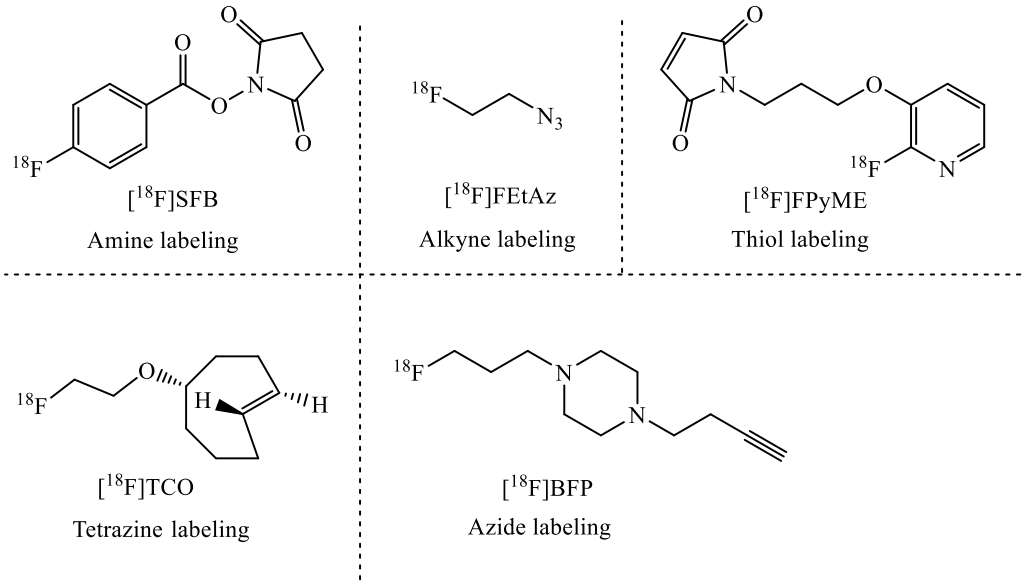

Figure 1.5 *Examples of prosthetic groups applied for ^{18}F labeling.*

1.5.1.3 *Al^{18}F labeling*

The aluminum-[^{18}F]fluoride ([^{18}F](AlF)$^{2+}$) complex is a "pseudo-radiometal" which is used in the metal-based radiochemistry for labeling with Fluorine-18 through the chelation of Al^{18}F complex. Aluminum-fluoride forms a stable and inert chelate with an aluminum-fluoride bond strength of 670 kJ/mol.[103, 104] The complex is formed by the reaction of $AlCl_3$ with nucleophilic [^{18}F]F^- in an aqueous milieu at pH~4 which is subsequently chelated using a suitable chelator. Among the different chelators, azamacrocyclic chelator 2,2′,2″-(1,4,7-triazacyclononane-1,4,7-triyl)triacetic

acid (NOTA) is often preferred for Al^{18}F chelation due to the superior stability of the chelation complex in serum.[105, 106] NOTA and other cyclic bifunctional chelators binding with N_3O_2 donor set form stable Al^{18}F complexes at elevated temperatures (100-120 °C). Based on this method, a range of Al^{18}F-based radiolabeled peptides have already been developed.[106, 107] Wan *et al.* reported the first use of a lyophilized kit for the synthesis of [^{18}F]AlF-NOTA-RGD dimer peptide for the imaging of αvβ3 expressing tumors.[108] Recently, [^{18}F]AlF-NOTA-octreotide was used successfully in clinical trial and outperformed the ^{68}Ga-DOTATATE/NOC, the current gold standard for imaging in patients with neuroendocrine tumors.[109, 110] Although promising, the labeling method requires high temperatures and could not be applied for the labeling of temperature-sensitive peptides/proteins. To circumvent the issue, Cleeren *et al.* reported the development of a new complexing agent, ((±)-H_3RESCA) which allows the chelation of [^{18}F](AlF)$^{2+}$ at room temperature expanding the possibilities to label heat-sensitive biomolecules.[111]

One of the advantage of chelation chemistry is that it offers the possibility of labeling the same precursor with either diagnostic or therapeutic radio-metals. Apart from diagnostic radionuclides Al^{18}F or ^{68}Ga, NOTA is also compatible for labeling with therapeutic radionuclide ^{67}Cu leaning towards a theranostic approach. Study using NOTA for ^{67}Cu chelation for radioimmunotherapy has been reported.[112] However, NOTA is not suitable for chelation of other therapeutic radiometals such as ^{177}Lu or ^{213}Bi. Recently, 3p-C-NETA has been introduced as a potential theranostic Al^{18}F chelator which allows the chelation of a wider range of therapeutic radionuclides (^{77}Lu, ^{161}Tb, ^{213}Bi, ^{225}Ac and ^{67}Cu).[113]

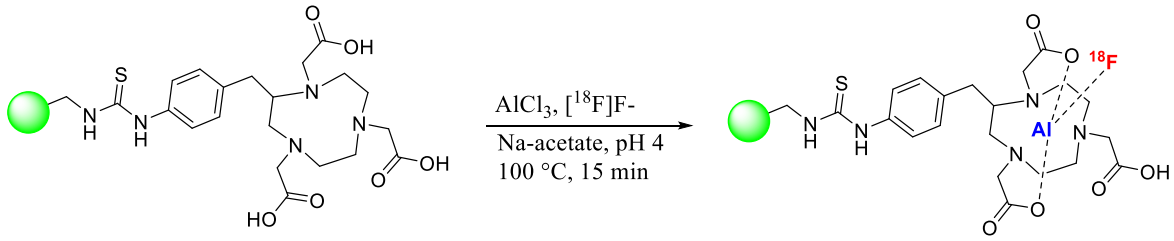

Scheme 1.5 *[^{18}F]AlF labeling with NOTA chelator.*

CHAPTER 2

Trans-cyclooctene- A Swiss army knife for bioorthogonal chemistry: Exploring the synthesis, reactivity, and applications in biomedical breakthroughs

Review article: Manuscript in preparation

Karuna Adhikari, Maarten Vanermen, Gustavo Da Silva, Tim Van den Wyngaert, Koen Augustyns and Filipe Elvas

Contribution: Literature search and writing manuscript

Chapter 2 *Trans*-cyclooctene- A Swiss army knife for bioorthogonal chemistry: Exploring the synthesis, reactivity, and applications in biomedical breakthroughs

2.1 Abstract

Trans-cyclooctenes (TCOs) are highly strained alkenes with remarkable reactivity towards tetrazines (Tzs) in inverse electron-demand Diels-Alder (IEDDA) reactions. Since their discovery as a bioorthogonal reaction partner, novel TCO derivatives have been developed to improve their reactivity, stability, and hydrophilicity, and thus expanding their utility in diverse applications. Here, we discuss the IEDDA reaction mechanism to unravel the key factors that determine TCO's high reactivity and provide a comprehensive list of TCOs, and derivatives used in both IEDDA-based ligation reactions as well as in click-to-release settings. In chemical biology, TCOs serve as tools for bioconjugation, enabling precise labeling and manipulation of biomolecules. Moreover, their role in nuclear medicine is substantial, with TCOs being employed in the radiolabeling of peptides and other biomolecules. This led to their utilization in pretargeted nuclear imaging and therapy, where they function as both bioorthogonal tags or as radiotracers, facilitating targeted disease diagnosis and treatment. Beyond these applications, TCOs have also found utility in targeted cancer therapy through a "click-to-release" approach, where they act as key components in the selective delivery of therapeutic agents to cancer cells, thereby enhancing treatment efficacy while minimizing off-target effects. This review provides a comprehensive overview of the current state of knowledge regarding TCOs, the synthetic challenges, and their development throughout the years. We describe their wide range of applications in bioconjugation, radiolabeling, and targeted therapy and aim to showcase the versatility and potential of TCOs as valuable tools in advancing biomedical research and application.

2.2 Introduction

Trans-cyclooctenes (TCOs) are a class of planar chiral alkenes that exhibit unusual reactivity and have often been the subject of physical organic studies.[114-116] Their structural features have been extensively studied. TCO is conformationally stable and displays a high barrier to racemization (35.6 kcal/mol).[117] TCO's most stable crown conformer consists of an alternating arrangement of equatorial and axial hydrogens similar to a chair conformer of cyclohexane.[118, 119] The double bond in TCO is severely twisted in crown conformation.[117, 120, 121] Consequently, the highest occupied molecular orbital (HOMO) of TCO is in a relatively high energy state. This distinctive electronic structure imparts unusual reactivity to TCOs, particularly in HOMO-alkene-controlled cycloaddition reactions with dienes, dipoles, and ketenes.[122-125] Due to their particular reactivity profile, TCOs have become the subject of study for numerous applications in synthesis and biology. In the field of organic synthesis, TCOs serve as ligands for transition metals, catalysts for halolactonization, and monomers for polymerization reactions catalyzed by radical initiators or metathesis catalysts.[126-132] TCOs are widely employed as bioorthogonal labeling reagents in the domain of bioorthogonal chemistry through reactions with tetrazines (Tzs).[42, 133-135]

The term "bioorthogonal chemistry" is used to describe a group of chemical reactions that can take place within living organisms under physiological conditions without interfering or interacting with the biological system of the host.[44-47] These reactions allow the modification of biomolecules with non-native functional groups through covalent bond formation and can be employed to study biological processes. According to the work done by the Bertozzi Group, a perfect bioorthogonal reaction should fulfill the following four requirements: (i) the reaction should take place under physiological conditions, (ii) the reaction should be selective and inert towards the biological system, (iii) the reaction should have fast kinetics at low concentrations, and (iv) the reaction should not contain any functional groups that are naturally found in biological systems.[44] Although several bioorthogonal reactions have been described, such as the Staudinger Ligation, the Copper-Catalyzed Azide-Alkyne Cycloaddition (CuAAC), or the Strain-promoted [3+2] azide-alkyne cycloaddition (SPAAC), not every bioorthogonal reaction concurrently satisfies all of these conditions.

The inverse electron-demand Diels-Alder (IEDDA) cycloaddition, involving a strained dienophile, such as TCO, and a diene, such as a tetrazine (Tz), is widely regarded as the most favorable bioorthogonal reaction for *in vivo* applications. This preference stems from its remarkably fast reaction kinetics, with rate constants reaching up to 10^7 $M^{-1}s^{-1}$.[136] The IEDDA reaction between tetrazines (Tzs) and strained alkenes has been the subject of substantial research in the fields of physical and organic chemistry. However, its application as a bioorthogonal ligation reaction was only reported in 2008 by three independent research groups.[71, 72, 137] Subsequently, the use of TCO-Tz ligation has become prevalent in several fields such as chemical biology, biomedical imaging, radiochemistry, and material sciences.[27, 42, 133-135]

This review aims to present a comprehensive overview of the recent progress made in the field of TCO development, specifically focusing on its role as a crucial reactant in the IEDDA reaction. We will present the synthesis of TCOs and their derivatives and provide a comprehensive understanding of the mechanisms that govern their reactivity. Furthermore, we will emphasize the wide range of applications that TCOs have in the fields of chemical biology, biomedical imaging/therapy, and drug delivery. By exploring these aspects, this review aims to provide valuable insights into the current state-of-the-art in TCO research and its implications in various scientific disciplines.

2.3 Inverse Electron-Demand Diels-Alder (IEDDA) reaction and mechanism

The reactivity of Tzs with unsaturated compounds has been previously elucidated by Lindsey and Carboni in 1959.[138] The initial discovery of IEDDA as a bioorthogonal ligation was reported by Fox and Hilderbrand in 2008.[71, 72] In contrast to the normal electron-demand Diels-Alder reaction, the IEDDA proceeds through a [4+2] cycloaddition between electron-poor diene (1,2,4,5-Tz) and electron-rich dienophile (alkene or alkyne) forming a highly strained bicyclic intermediate. Subsequently, a retro-Diels-Alder reaction occurs with N_2 evolution, resulting in the formation of a stable six-membered 4,5-dihydropyridazine ring. Upon reaction with alkenes, the 4,5-dihydropyridazine undergoes isomerization to yield the corresponding 1,4-dihydro-isomers, or it can be oxidized to form a pyridazine. In contrast, alkyne dienophiles undergo a direct transformation, leading to the formation of pyridazine (Figure 2.1).

The kinetics of the IEDDA reaction are determined by the energy gap between the HOMO of the dienophile and the lowest unoccupied molecular orbital (LUMO) of the diene, as postulated by the

frontier molecular orbital theory (FMO).[42] Consequently, a smaller energy difference between the HOMO and LUMO results in a faster reaction rate. Hence, fine-tuning the tetrazine and the dienophile pairs can significantly enhance the rate of the reaction. The subsequent section examines various parameters that can influence the kinetics of IEDDA.

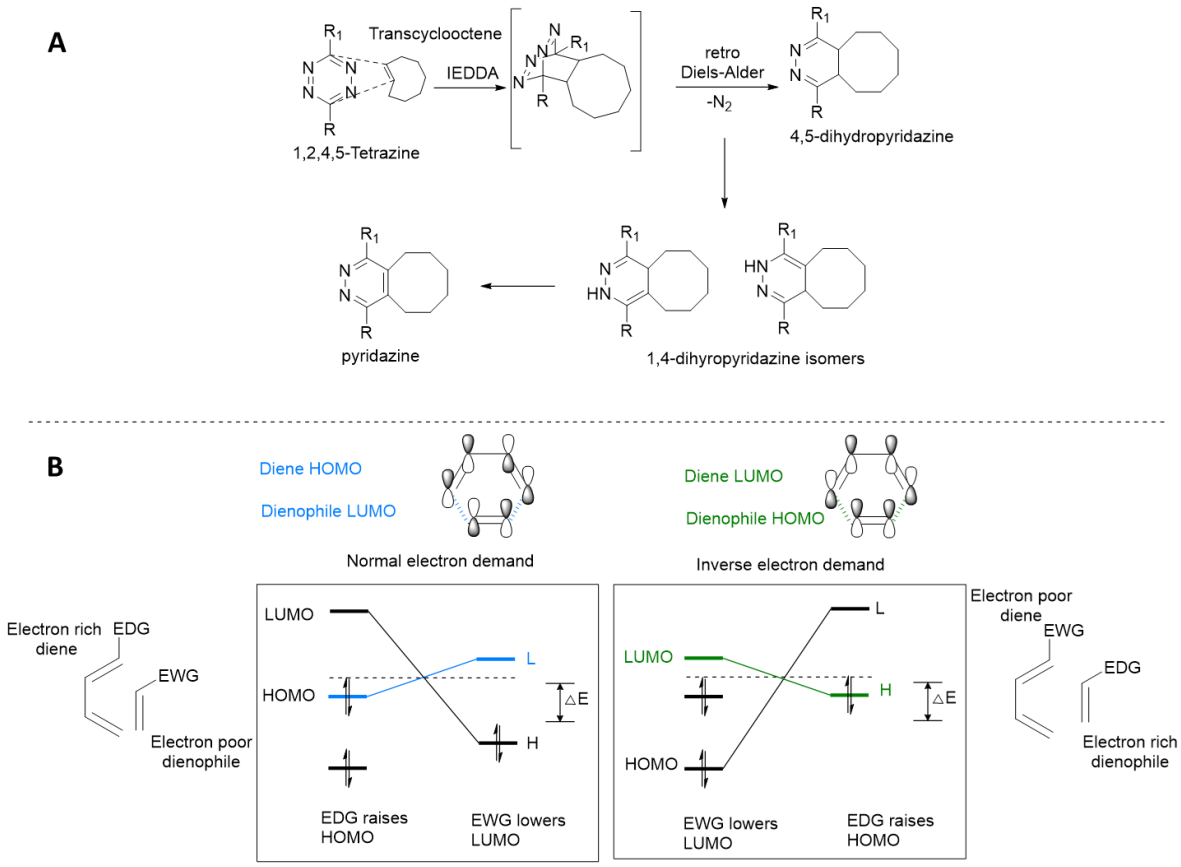

Figure 2.1 *(A) Mechanism of an inverse electron-demand Diels-Alder [4+2] (IEDDA) cycloaddition between a tetrazine and trans-cyclooctene. (B) Frontier molecular orbital (FMO) model of Diels-Alder reaction and the IEDDA reaction. EDG: electron donating group, EWG: electron withdrawing group, HOMO: highest occupied molecular orbital, LUMO: lowest unoccupied molecular orbital. ΔE: energy gap $LUMO_{Diene}$-$HOMO_{Dienophile}$. Adapted from Oliveira et al. with permission from Royal Society of Chemistry.*[42]

2.3.1 Reactivity of tetrazines

Tzs are the most common dienes used in IEDDA. The substitutions performed on the tetrazine backbone can influence its reactivity. Electron-withdrawing groups (EWG) lower the energy level of LUMO of the diene, decreasing the $HOMO_{dienophile}$-$LUMO_{diene}$ energy gap. Thus, the reactivity of the tetrazines can be increased through the installation of EWG on the tetrazine scaffold. Experimental and computational studies of 3,6-disubstituted-1,2,4,5 Tzs revealed that the most reactive tetrazines always have a lower LUMO energy.[139] Tzs containing EWGs such as carboxylates,

pyridines, and pyrimidines have faster kinetics than tetrazines bearing methoxy or methyl groups.[140, 141] However, Tz-bearing strong EWGs are also unstable in aqueous conditions, which can be a limiting factor for biorthogonal reactions. From a structural point of view, diaryl Tzs are known to have a good balance between moderate stability and reactivity. Steric effects also play an important role as hydrogen-substituted Tz show faster kinetics (70-fold increased reactivity) than di-substituted Tzs.[140, 141] Furthermore, unfavorable steric repulsions were reported when Tzs were substituted with bulky *tert*-butyl groups.[142] A study by Svatunek *et al.* showed that reduced Tz distortion energy caused by repulsive intramolecular interactions also increases the reactivity of Tz toward dienophiles.[143] The reactivity is not only determined by the type of substituents but also by their position on the aromatic ring attached to Tzs (Figure 2.2).[144] Although the pH of the solvent has a minor effect on the reaction rate, the interaction with solvents should be taken into account. Protic solvents stabilize the interaction with the activated complex while enhancing the hydrophobic interaction between the cycloaddends, which accelerates the reaction rate. Also, the hydrogen bonding of water with Tzs accelerates the reaction rate.[144-146]

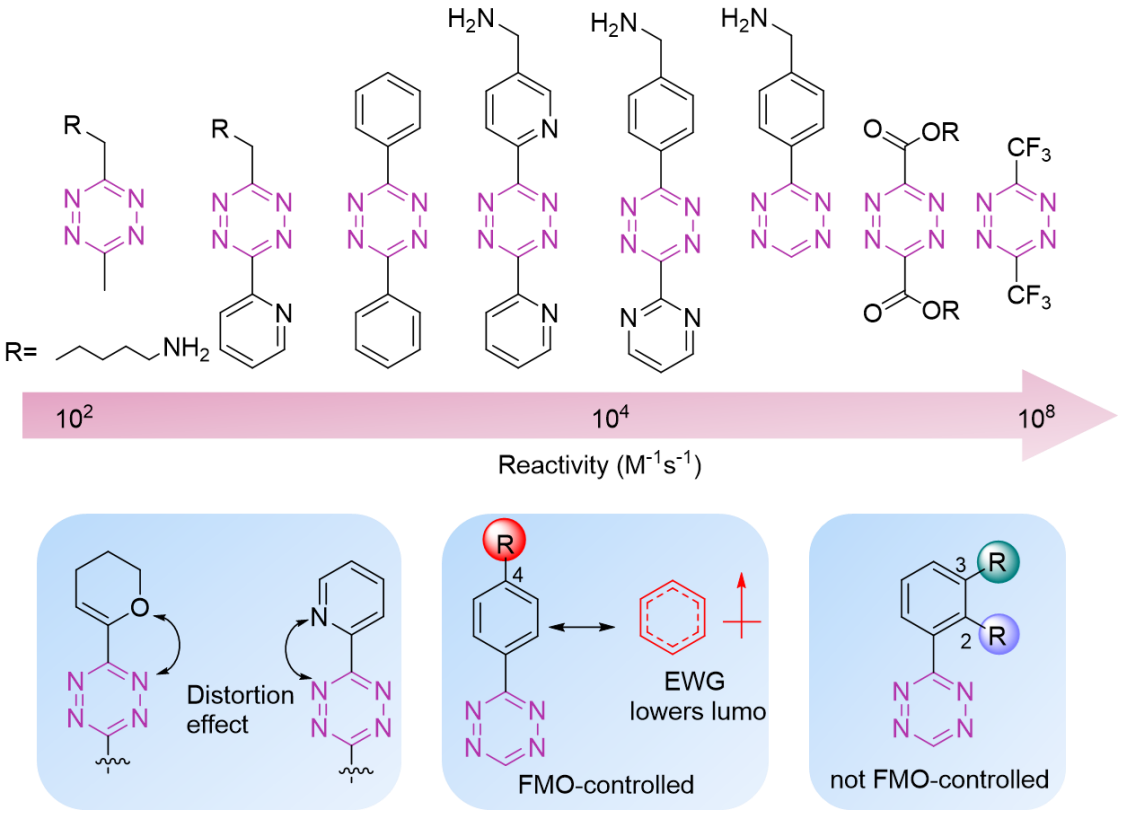

Figure 2.2 *Structure and reactivity of tetrazine influenced by the electronic, steric, and distortion effects. EWG groups increase the reactivity of tetrazines. Repulsive intramolecular interactions reduce Tz distortion energy and increase the reactivity. The reactivity of 4-substituted tetrazines is FMO-controlled whereas 2-substituted or 3-substituted tetrazines are not FMO-controlled.*

2.3.2 Reactivity of dienophiles

In contrast to dienes, dienophiles exhibit greater reactivity in the presence of electron-donating groups (EDG). EDGs raise the energy of both the HOMO and LUMO orbitals of the dienophile and consequently decrease the $HOMO_{dienophile}$-$LUMO_{diene}$ energy gap.[42] The effect of electronic substituents on unstrained dienophiles has been extensively studied, where electron-rich groups are favored for faster kinetics. Sauer and coworkers investigated the reaction kinetics of various Tzs and dienophiles and established that the rate constant increases with increasing ring strain of the dienophiles (cyclopropene > cyclobutene > cyclopentene > cyclohexene > cyclooctene).[147] However, the strain effect is the most crucial factor affecting dienophile reactivity. Houk *et al*. demonstrated through computational analyses that greater reactivity of the strained dienophiles is attributed to their pre-distorted conformation towards the transition state structures. Therefore, less distortion energies are needed for the dienophile to react.[148] The most reactive dienophile known is TCO, which is 7 orders of magnitude more reactive than the *cis*-cyclooctene (CCO).[147] TCO shows a remarkable increase in reactivity when compared to other cyclic alkenes with higher ring strain (e.g., cyclopropene).[149] Computational studies have shown that this higher reactivity is linked to the 'crown' conformation adopted by the TCO, which is energetically more favorable than the 'half-chair' conformation of *cis*-cyclooctene.[120, 149-151]

In recent years, computational studies have obtained additional insights into the design of reactive dienophiles. Fox *et al*. demonstrated the increased reactivity of dienophiles through the introduction of conformational strain. Based on *ab initio* calculations, a TCO with cis-fused cyclopropane ring (s-TCO) was designed to enforce a highly strained half-chair conformation for the eight-membered ring. Transition state calculations predicted that the s-TCO would react much faster than the crown conformation of TCO ($\Delta\Delta G^{\ddagger}$ = 3.34 kcal/mol). When experimentally determined the s-TCO showed $\Delta\Delta G^{\ddagger}$ = 3.0 kcal/mol and reacted 160 times faster with 3,6-diphenyl-s-tetrazine than the original TCO.[152] Similarly, *cis*-dioxolane fused *trans*-cyclooctene (d-TCO) was designed to increase the stability and hydrophilicity while retaining the highly strained 'half-chair' conformation, which showed 27-fold rate enhancement in comparison to the original TCO (Figure 2.3).[73]

The stereochemistry of the strained dienophiles also plays a crucial role in determining the reactivity.[153] Density functional theory (DFT) calculations showed that the axial isomer of functionalized TCO is higher in energy by 1.1 kcal/mol than the corresponding equatorial isomer.[153] Experimentally, the axial isomer showed 4-fold higher reactivity than the equatorial isomer.[73, 78, 154] Similarly, the syn-diastereomer of d-TCO showed a higher rate constant compared to the anti-diastereomer (~1.2 x).[73] Similar trends were also observed with other dienophiles such as norbornene and bicyclononyne (BCN) which has been discussed in detail elsewhere.[42]

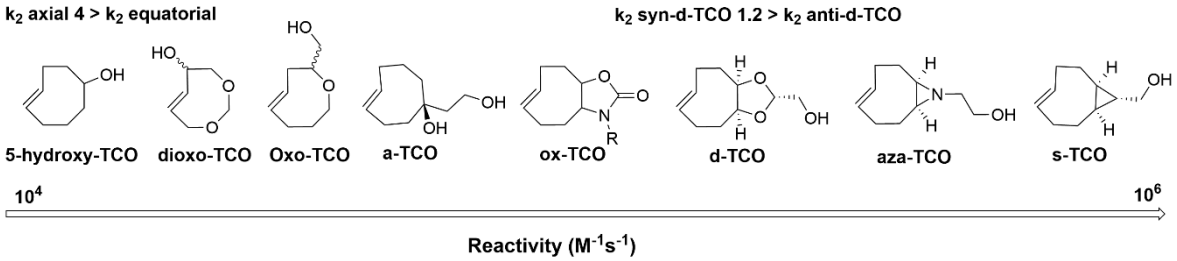

Figure 2.3 *Reactivity of different TCO derivatives. The reactivity of TCO is enhanced by increasing the ring strain via cis-ring fusion to the cyclooctene core. Stereochemistry and inclusion of endocyclic or exocyclic heteroatoms also influence the reactivity.*

2.4 Synthesis of *trans*-cyclooctenes

TCO was originally prepared in 1950 via the Hoffman elimination of trimethylcyclooctyl ammonium iodide as a mixture with cis-cyclooctene.[114] In 1953, TCO was separated from CCO through the formation of the water-soluble TCO•$AgNO_3$ complex, which was subsequently decomplexed by aqueous NH_4OH to provide the pure trans-alkene.[115] While there are established routes for the synthesis of parent TCO, the number of strategies for the preparation of functionalized derivatives was limited.[155-158] Several stereospecific methods for preparing TCO from CCO have also been described.[159-162] An illustrative example involves a synthetic procedure that entails a sequence of epoxidation steps of the double bond, subsequent addition of $LiPPh_2$, and ultimately elimination, resulting in the pure inverted TCO as a product (Figure 2.4).[163] However, one limitation of this protocol is the complex multistep synthesis procedure required to invert the alkene stereochemistry. Additionally, the use of harsh reaction conditions restricts the scope of TCO derivatives that can be prepared using this protocol.

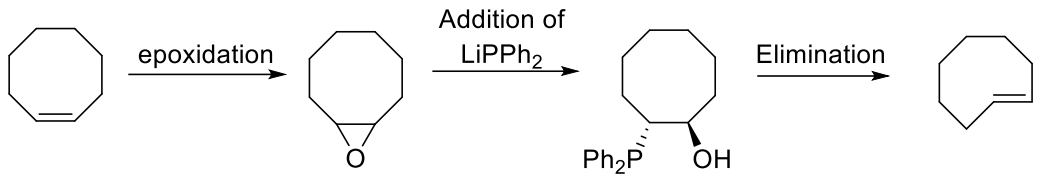

Figure 2.4 *Example of multistep synthesis of trans-cyclooctene from cis-cyclooctene via inversion of alkene stereochemistry.*

In 2008, Fox *et al.* described a one-step closed-loop flow photoisomerization of CCO to TCO.[74] Currently, this procedure stands as the most commonly used approach for obtaining TCO derivatives. In a recent study conducted by Hsung *et al.*, significant progress was made in the preparation of TCOs by 4-π electrocyclic ring opening.[164-166] Novel synthetic routes have been established for the synthesis of heteroatom-containing trans-cycloalkenes.[167] Woerpel *et al.* described the synthesis of trans-dioxasilacyclooctenes, whereas Tomooka *et al.* introduced the dialkoxysilane cyclooctene.[168-170] Recently, Fox *et al.* also reported a diastereoselective method for synthesizing TCOs in high yield through stereo-controlled additions of nucleophiles to *trans*-cyclooct-4-enone.[171] Similarly, more accessible synthetic pathways toward click-cleavable TCO-linker were also reported.[172-175]

2.4.1 Photochemical isomerization of *cis*-cyclooctene to *trans*-cyclooctene

The photoisomerization of *cis*-cyclooctene in the presence of a singlet sensitizer represents a direct method for the synthesis of TCO.[176] The concept was first introduced by Inoue *et al*. in a series of papers on the enantioselective photoisomerization of cyclooctene, cycloheptene, and 1,3-cyclooctadiene to their *trans*-isomers, where chiral ester function was found to be the most optimal sensitizers.[176-184] When irradiated at 254 nm, the chiral aromatic ester forms a singlet excited state, which combines with CCO to form diastereomeric exciplexes (pS-1b and pR-1b; Figure 2.5). These "twisted singlet" exciplexes subsequently disassociate into the corresponding TCO and CCO (Figure 2.5). The photoisomerization process is enantioselective as the relative rates for the formation of the twisted singlet exciplexes for chiral sensitizers are not equal.

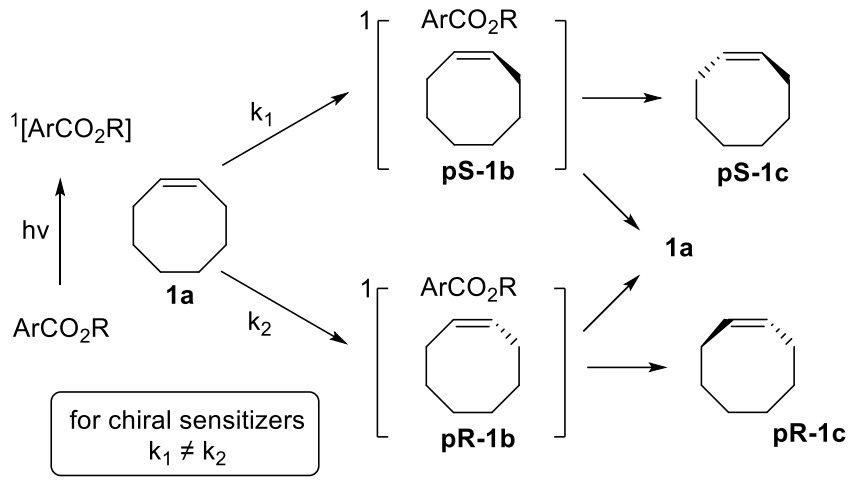

Figure 2.5 *Enantioselective photoisomerization based on chiral exciplex formation. Reproduced with permission from Pigga et al. Copyright 2019 Wiley-VCH Verlag GmbH & Co. KGaA, Weinheim.*[185]

The photochemical synthesis of functionalized *trans*-cyclooctenes showed, unfortunately, limitations in terms of low yields, with a maximum of 23% conversion. When using a functionalized TCO, the formation of diastereomers was observed, which further decreased the yield of the desired product.[186] Additionally, photodegradation of functionalized TCO was also observed as the yield dropped to <5% when irradiated up to 18h.[74]

The flow-photoisomerization strategy introduced by Fox *et al.* is based on the selective metal complexation of the *trans*-isomer.[74] TCO interacts strongly with metals which is facilitated by the strain relief in the hydrocarbon framework with the relatively minimal energetic cost associated with the reorganization.[187, 188] As originally reported, the setup consists of a closed-loop photoreactor where a quartz reaction flask containing methyl benzoate and a solution of a *cis*-cyclooctene derivative is irradiated at 254 nm. During irradiation, the reaction mixture continuously flows through a column filled with $AgNO_3$-impregnated silica gel. The TCO derivative selectively binds to the $AgNO_3$-impregnated silica, while the *cis*-isomer elutes back to the reaction flask, where it is photoisomerized and recirculated through the column (Figure 2.6).[74] After complete consumption of the CCO, the silica is removed and stirred with NH_4OH, liberating the TCO from the $AgNO_3$. For base-sensitive molecules, NaCl can be used instead of NH_4OH for $AgNO_3$ decomplexation. The TCO derivative is subsequently recovered by extraction. This innovative strategy provides a selective and efficient means for obtaining TCO derivatives, opening new possibilities for their application in various chemical processes.

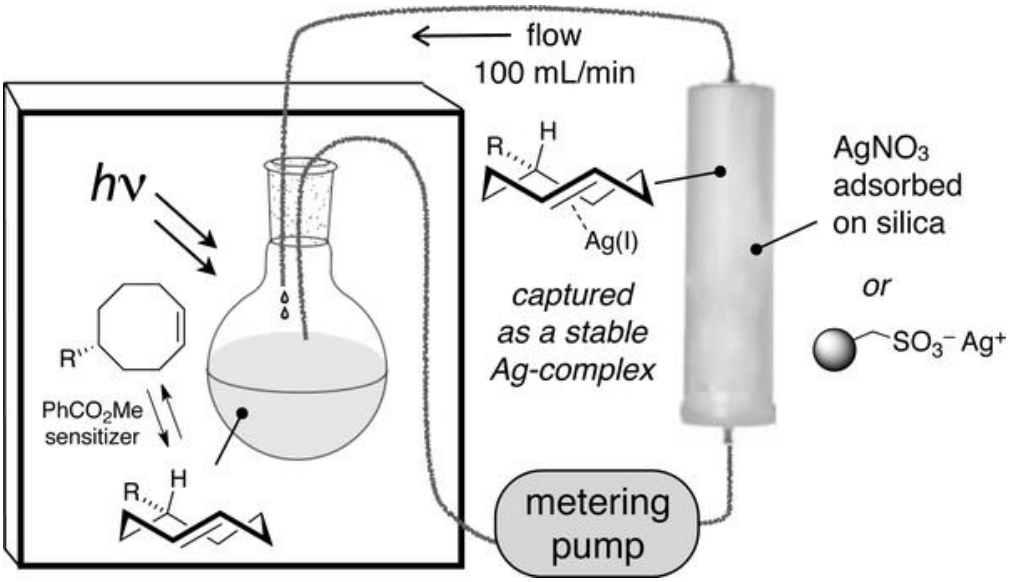

Figure 2.6 *Schematic of Flow-Photoisomerization apparatus for the synthesis of trans-cyclooctene. Adapted from Fox. et al. with permission from Copyright 2018 Georg Thieme Verlag KG.*[74]

Since its original description, flow-photoisomerization has been used by several research groups for the synthesis of TCO for different applications.[154, 189-209] While the flow procedure has proven effective, some modifications and alternative setups have been explored. One approach involved mimicking flow photoisomerization by periodically stopping irradiation, filtering the reaction mixture through $AgNO_3$-impregnated silica to capture the TCO, and resubjecting the filtrate to photoisomerization.[210, 211] Although it avoids the cost of the flow equipment, it is more labor-intensive and the yields are lower. Another variation to the setup utilized a quartz tube along with a UV light where the bulk of the reaction solution residing in a reservoir flask was continuously pumped through the irradiated quartz tube. The use of the reservoir flask enabled upscaling of the reaction without the use of expensive quartz flasks in different dimensions since containers of any size and shape could be used.[212] A microflow flow system reported utilized two microreactors coiled around a UV lamp and several beds of $AgNO_3$-impregnated silica, exchangeable during irradiation.[213] Fox *et. al* also further modified their setup by using Ag(I) immobilized on Tosic acid-functionalized silica gel (TAg silica) to capture TCO at higher silver loadings without leaching, as the metal is covalently bound to the solid support. This facilitated the upscaling of photoisomerization of TCOs with a variety of substitutions such as hydroxyl, carboxylic acid, hydroxyethylether, diol, and protected amines.[214]

A low-cost and readily accessible apparatus was recently described. This setup incorporates the use of fluorinated ethylene propylene (FEP) tubing coiled placed within an aluminum vent pipe in combination with a household germicidal lamp and flash chromatography system for photoisomerization.[215] This make-shift apparatus yielded 48-76% of different TCOs and avoided the high cost of photoreactors.

A recent technique developed by Rutjes *et al.* applies a liquid-liquid extraction method.[186] The setup consists of a UV lamp and a continuous flow of heptane solution containing CCO over an aqueous $AgNO_3$ solution. The organic phase flows through UV-permeable FEP tubing wrapped around a UV lamp (254 nm) and into an $AgNO_3$ aqueous solution, where TCO is trapped while CCO returns to the organic phase. This system is scalable as it allows for a consistent concentration of CCO in heptane via the external addition of substrate. With this method up to 2.2 g/h of TCO could be produced and was applied to synthesize several of the commonly utilized TCOs.[186] This efficient and scalable technique represents a valuable advancement in the field of TCO synthesis, facilitating large-scale production of TCO derivatives.

2.5 *Trans*-cyclooctenes in ligation reactions

The following section summarizes the different TCO derivatives that have been used for IEDDA ligation reactions over the years.

2.5.1 *Trans*-cyclooct-4-enol and its derivatives

Blackman *et al.* reported the very fast kinetics of parent TCO with electron-deficient Tzs (k_2 = 2.0 x 10^3 $M^{-1}s^{-1}$). The study demonstrated the bioorthogonality of the reaction as the reaction proceeded successfully in organic solvents, water, cell media, or cell lysates with a quantitative yield.[71] The group synthesized an alcohol-functionalized derivative *trans*-cyclooct-4-enol (2.1) (TCO-OH) through photoisomerization of cis-cyclooct-4-enol. *Trans*-cyclooct-4-enol is by far the most used TCO derivative for different biological applications. In the initial investigation by Fox *et al.*, *trans*-cyclooct-4-enol was further derivatized with thioredoxin (Trx) and reacted with 2x excess Tz, and complete consumption of the reagents was observed within 5 minutes, illustrating the biocompatibility of TCO-Tz ligation for the conjugation of proteins (Figure 2.7).[71]

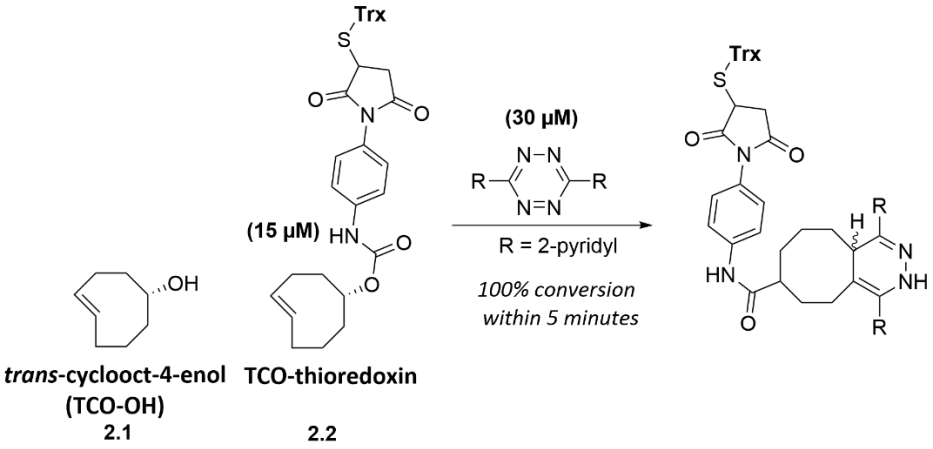

Figure 2.7 *Structure of trans-cyclooct-4-enol and reaction between a thioredoxin-derivatized trans-cyclooct-4-enol and 3,6-dipyridyl-s tetrazine. Adapted with permission from Fox et al. Copyright 2008, American Chemical Society.*[71]

Encouraged by these results, Rossin *et al*. studied the potential use of TCO-Tz ligation in more demanding *in vivo* conditions, where metabolism, side reactions, and prolonged residence times play an important role. TCO conjugated to CC49 antibody (mAb) showed a second order rate constant of 13,090 ± 80 $M^{-1}s^{-1}$ with ^{111}In-labelled-Tz in PBS at 37°C. Importantly, 75% of the CC49-bound TCO was still reactive after 24 hours in circulation. However, a slow deactivation (25% in 24 h) of TCO in serum was observed. This in turn limited the interval between the mAb conjugate and the Tz probe administration for the *in vivo* pretargeted imaging study.[89] In a follow-up study, the sole mechanism of deactivation of mAb-bound TCO in serum was found to be the *trans-to-cis* isomerization mediated by copper-containing serum proteins.[78] This was circumvented by omission of the PEG-linker between the TCO and the lysine residue on mAb consequently increasing the steric hindrance on the TCO for interaction with serum proteins. Additionally, they also demonstrated that the axial substituent is up to 4-fold more reactive due to the increased strain in axially substituted isomers.[78] When reacted with 3,6-dipyridyl-s-tetrazine in aqueous media, the measured k_2 values for the equatorial and the axial diastereomer were 22,600 ± 40 $M^{-1}s^{-1}$ and 80,200 ± 200 $M^{-1}s^{-1}$, respectively.[73]

Other ring-substituted isomers are also reported. The genetic encoding of TCO-based noncanonical amino acid (ncAA) using a double-mutant synthetase MmPylRS (Y306A, Y384F) was reported to enable site-specific labeling of proteins in a short time for super-resolution microscopy.[216] However, the genetic encoding of lysine-modified *trans*-cyclooct-4-enol was unsatisfactory. Lemke and coworkers explored the ***trans*-cyclooct-2-enol** and ***trans*-cycloocte-3-enol** ring isomers as an

alternative.[217] The lysine-modified 3-ene and the 2-ene amino acid isomers showed significantly higher genetic incorporation into green fluorescent protein (GFP) in E. *coli* expression cultures by the mutant tRNA synthetase than the 4-ene isoform. Their studies revealed that the diastereomeric mixture of 3-enol isomer displayed similar reaction kinetics to the 4-enol isomer. However, the 2-enol isomer showed slower kinetics but a 10-fold increase in stability showing a lower level of *trans to cis* isomerization.[217] In a follow-up study, the axial isomer of *trans*-cyclooct-2-enol showed higher reactivity when compared with the equatorial isomer, just as *trans*-cyclooct-4-enol.[154] Notably, the bicyclic product of the [4+2] cycloaddition reaction of *trans*-cyclooct-2-enol with Tz undergoes β-elimination releasing the conjugated lysine bond under certain conditions. This property was further exploited as a click-to-release strategy for targeted drug release which will be referred to later in this review.[218]

2.5.2 Axial-5-hydroxy-*trans*-cyclooctene (a-TCO)

The widely used photoisomerization process produces the equatorial and axial diastereomers in a 2.2:1 ratio, yielding the axial isomer in a low isolated yield of ≤ 24% and necessitating a tedious separation process. For some TCO derivatives, separation of both diastereomers through flash chromatography can be challenging or not feasible at all. Pigga *et al.* devised a diastereoselective method for synthesizing TCOs through the additions of nucleophiles to *trans*-cyclooct-4-enone in a stereocontrolled manner. This approach addresses the problem of low stereoselectivity during TCO production. The preparation of *trans*-cyclooct-4-enone (2.4) proceeded in two steps by the Wacker oxidation of 1,5-cyclooctadiene followed by photoisomerization (Scheme 2.1). As the ketone lacks a stereocenter, it can be isomerized without the complication related to diastereoselectivity during isomerization. Computational studies predicted that nucleophilic additions to ketone take place exclusively from the equatorial face to produce only axial substituted diastereomers. In agreement with the computational data, nucleophilic substitutions with hydride afforded exclusively the axial diastereomer (Scheme 2.1).[171] The described route shows significant advantages for the synthesis of TCOs as it is short, selective, and scalable. Several a-TCO conjugates were prepared from the central ketone intermediate. A diol-derivatized a-TCO (2.6) showed rapid kinetics with a 3,6-dipyridyl-s-tz derivative with a rate constant (k_2) of 150,000 ± 8,000 $M^{-1}s^{-1}$, which is two times faster than the axial diastereomer of ***trans*-cyclooct-4-enol** (k_2 = 70,000 ± 1,800 $M^{-1}s^{-1}$). The faster kinetics was attributed to an increase in olefinic strain for a-TCO due to the steric effect of geminal substitution in the eight-membered ring backbone. The a-TCO (2.6) was also predicted to show

improved hydrophilicity when compared to other TCO derivatives with a lower calculated logP (cLogP) value of 1.11 when compared to TCO (cLogP 1.95), oxo-TCO (cLogP 1.33) and d-TCO (cLogP 1.76). When applied in a cell-imaging assay, the increased hydrophilicity of a-TCO allowed for a rapid washout of the fluorophore-conjugated a-TCO leading to lower background fluorescence when compared to the less hydrophilic oxo-TCO.[171]

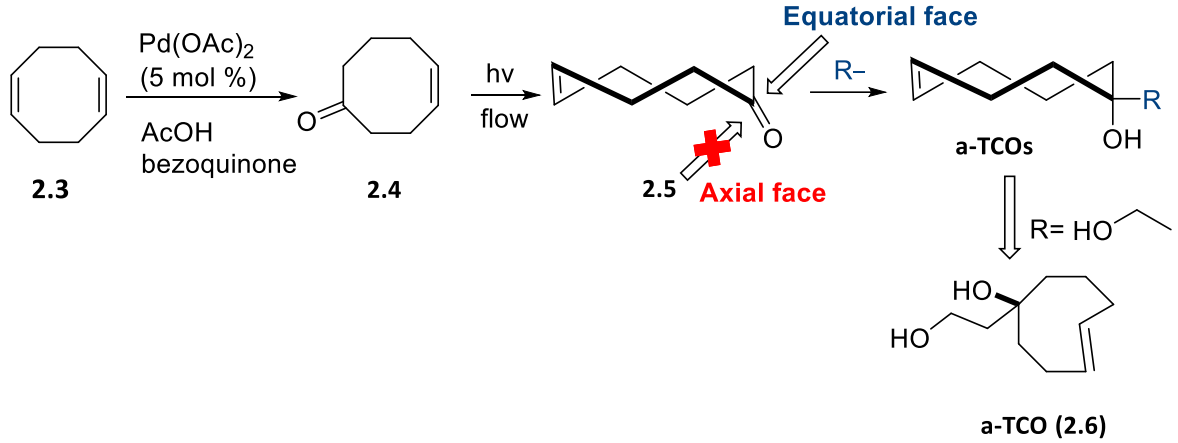

Scheme 2.1 *Diastereoselective synthesis of a-TCO with nucleophilic addition preferred at the equatorial face. Adapted with permission from Pigga et al. Copyright 2021 Wiley-VCH GmbH.*[171]

2.5.3 Conformationally strained *trans*-cyclooctene (s-TCO) and derivatives

Computational studies have provided important insights into the development of TCOs with faster reaction kinetics. Calculations by Bach *et al.* found the strain energy of half chair conformation of a TCO to be 5.9 kcal/mol higher than the crown conformation (0 kcal/mol).[149] Based on their increased strain energy, non-crown conformers were speculated to accelerate the reactivity towards Tzs. Studies by Dommerholt *et al*. using the ring fused strained cycloalkyne, BCN showed that the reactivity towards azide in SPAAC reaction could be accelerated through the fusion of a cyclopropane ring.[219] In parallel, Fox and coworkers recognized that the introduction of conformational strain on TCO with a fused cyclopropane ring forces the bicyclic system to adopt a highly strained half-chair conformation, increasing the TCO's reactivity. The strained TCO annealed to a cyclopropane with a *cis* ring fusion was termed s-TCO.[152] The group synthesized an alcohol-functionalized analog of s-TCO (2.7) through cyclopropanation of 1,5-cyclooctadiene with ethyl diazoacetate, followed by ester reduction and a photochemical *cis-trans* isomerization (Figure 2.8 Scheme B). To prove the hypothesis that the increased reactivity of s-TCO is caused by additional ring strain resulting in a half-chair conformation, the barrier for the reaction between s-tetrazine and *trans*-fused s-TCO was investigated. The calculated reaction barrier was $\Delta G^{\ddagger}$ = 8.24 kcal/mol,

which is significantly higher in comparison to *cis*-ring fused s-TCO ($\Delta G^{‡}$ = 6.95 kcal/mol). A *trans*-ring fusion allows the eight-membered ring to adopt a crown conformation, similar to parent TCO and thus explains the difference in reactivity between the two diastereomers (Figure 2.8 A). Specifically, when compared with TCO, the augmented ring strain in s-TCO led to a 160-fold increase in reactivity with 3,6-diphenyl-s-tetrazine.[152] A water-soluble derivative of s-TCO showed a remarkable rate constant (k_2) of 3,300,000 $M^{-1}s^{-1}$ ± 40,000 $M^{-1}s^{-1}$ with 3,6-dipyridyl-s tetrazine derivative, making it the fastest TCO to date.[73] With its ultra-fast kinetics, s-TCO allowed rapid fluorogenic labeling inside living bacteria in combination with a tetrazine-modified GFP.[220] However, the inherent reactivity of s-TCO is accompanied by a trade-off in terms of stability. In the presence of high thiol concentrations (30 mM), the s-TCO isomerizes rapidly.[152, 221] *In vivo*, s-TCO conjugated to a mAb showed rapid deactivation to the cis-isomer with a half-life of 0.67 days.[78] Moreover, these derivatives exhibit limited stability to prolonged storage and must be stored as cold solutions to avoid polymerization and isomerization. The shelf-life of these derivatives can be extended by storing them as stable silver(I) (Ag(I)) metal complexes.[222] Additionally, the synthesis lacks stereoselectivity, necessitating chromatographic separation of syn- and anti-product diastereomers, limiting its widespread use.[73]

To incorporate an additional vector for functionalization, Ravasco *et al*. modified the s-TCO at the cyclopropane moiety (2.8) (Figure 2.8, Scheme C).[223] The cyclopropane ring was double-functionalized with an aromatic substituent and alcohol on a quaternary carbon. DFT calculation for the cycloaddition between s-tz and the double-functionalized s-TCO (2.8) demonstrated that the introduction of an aromatic ring had no significant impact on the energy barrier for the reaction. A ΔG‡ value of 7.0 kcal/mol was observed for the double-functionalized s-TCO (2.8), which was comparable with that of parent s-TCO (ΔG‡ = 7.1 kcal/mol). Similarly, the distortion energy in the transition state of double-functionalized s-TCO (ΔE_{dist} = 1.6 kcal/mol) remained comparable to parent s-TCO (ΔEdist = 1.7 kcal/mol). In ^{1}HNMR competition experiments, double functionalized sTCO (krel = 1.54 ± 0.1) was estimated to react 1.5 times faster than sTCO (krel = 1) with 3,6-dipyridyl-s tetrazine confirming the results from the DFT calculations and indicating that the additional linker on the scaffold did not affect the reactivity.

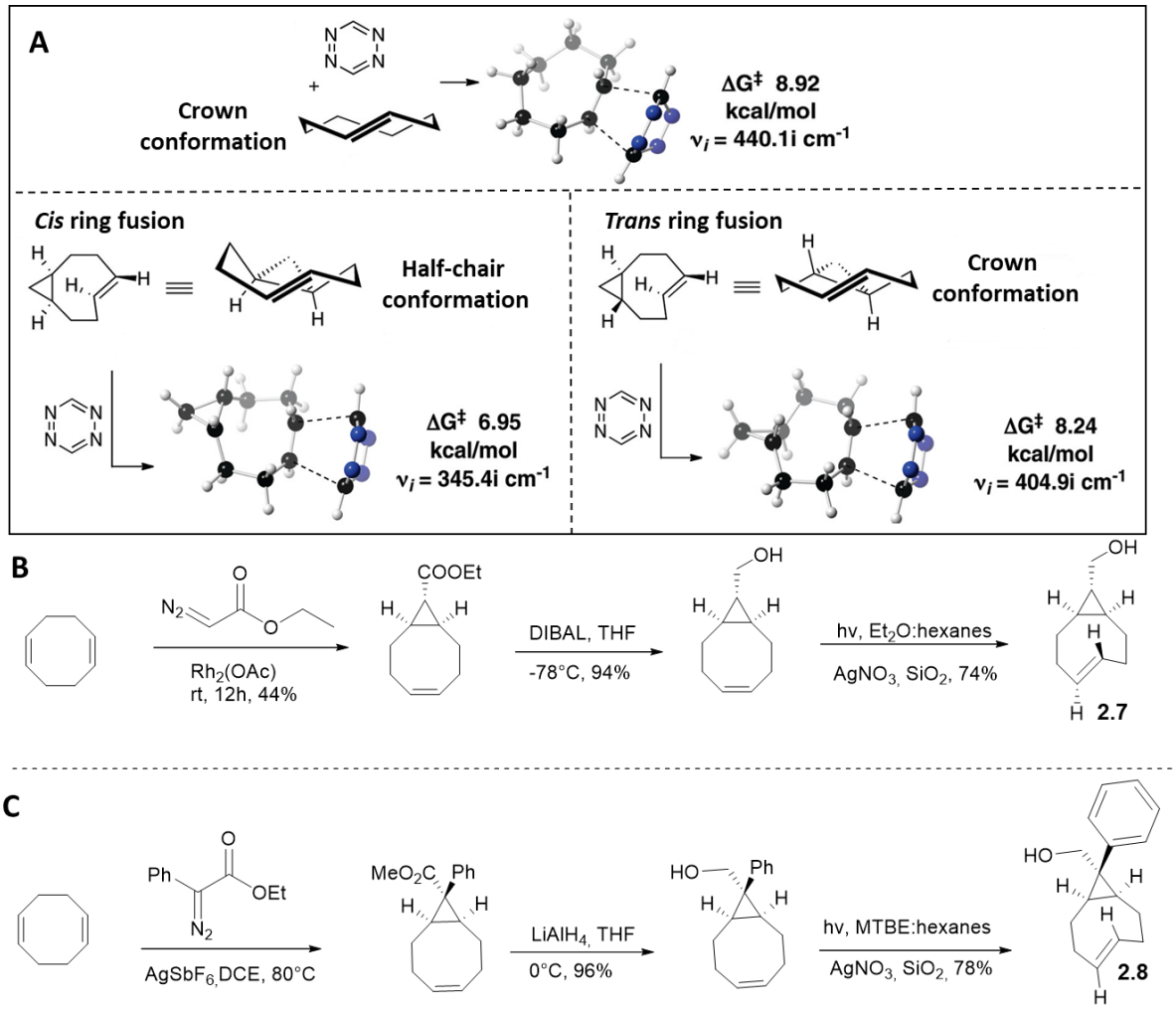

Figure 2.8 (**A)** *Transition structures and respective energy barriers for the Diels-Alder reaction of s-tetrazine with the crown conformer of trans-cyclooctene, cis-ring fused s-TCO, and trans-ring fused s-TCO. Adapted with permission from Fox et al. Copyright 2011, American Chemical Society.*[152] **Scheme (B)** *Synthetic scheme of s-TCO.* **Scheme (C)** *Synthetic scheme of double-functionalize s-TCO.*[223]

When assessed for stability, double functionalized s-TCO remained stable for over 70 h in deuterated phosphate buffer (pH 7.4 and 6, 1:1 DMSO/PBS) and up to 24 h when exposed to amine nucleophiles (30 mM n-pentylamine in CD_3OD-d_4). Similar to other TCO derivatives, isomerization of the compound was observed (12 % after 12 h) in the presence of concentrated ethanethiol (30 mM in CD_3OD-d_4) or when exposed to the high concentration of reduced glutathione (GSH) (60 % in 12 h in DMSO/PBS 1:1, pH 7.4). Overall, the compound showed slightly increased stability compared to s-TCO.[223] In general, the established synthetic pathway presents an opportunity for the incorporation of additional functional groups. However, to enhance the compound's suitability for biological assays, it may be required to incorporate additional polar groups. The reason for this

is that the s-TCO core comprises a hydrophobic core, which has the potential to result in increased nonspecific uptake in biological environments.

2.5.4 *cis*-Dioxolane-fused *trans*-cyclooctenes (d-TCO)

In 2014, Fox and coworkers developed another conformationally strained TCO variant based on computational studies, termed *cis*-dioxolane-fused *trans*-cyclooctene (d-TCO).[73] The incorporation of a *cis*-fused dioxolane ring imposed a strained half-chair conformation of the cyclooctene ring, resulting in enhanced reactivity. The introduction of inductive electron-withdrawing oxygen also increased the hydrophilicity and stability of the compound due to the reduction of electron density from the alkene.[73] However, this reduction in electron density also lowers the $HOMO_{dienophile}$ resulting in decreased reactivity, creating a compromise between reactivity and stability.

Derivatives of d-TCO were prepared on a multigram scale through a diastereoselective synthesis. Upjohn dihydroxylation of 1,5-cyclooctadiene, followed by dioxolane formation in the presence of an aldehyde afforded the syn diastereomer (2.9) in greater yield, which was subsequently photoisomerized to d-TCO (2.10, Scheme 2.2). Although slower than s-TCO, d-TCO showed excellent reactivity towards tetrazines. Additionally, the dioxolane functionality increased the overall hydrophilicity of the molecule (logP 0.94), allowing the kinetics measurements in an aqueous solution. At 25 °C in water, the syn-diastereomer of d-TCO reacts with the water-soluble derivative of 3,6-dipyridyl-s-tetrazine with a rate constant k_2 of 366,000 ± 15,000$M^{-1}s^{-1}$ whereas the anti-diastereomer showed k_2 value of 318,000 ± 2,900 $M^{-1}s^{-1}$. Moreover, d-TCO derivatives demonstrated improved stability compared to the more reactive s-TCO, showing no decomposition when stored in aqueous solutions at room temperature. No degradation or isomerization of d-TCO was in observed phosphate-buffered D_2O for up to 14 days. The compound remained as a *trans*-isomer (> 97%) after incubation in human serum at room temperature for 4 days. Similar to other TCOs, d-TCO is also susceptible to thiol-promoted isomerization (43% after 5h at pH 7.4).[73] Due to its improved hydrophilicity, stability, and remarkable kinetics d-TCOs have been a compound of interest in several biological applications.

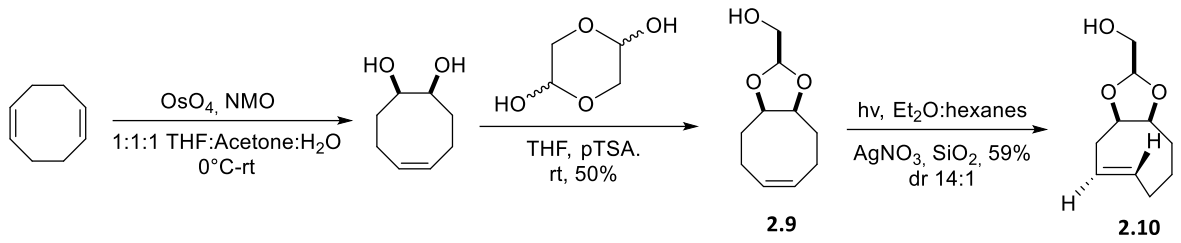

Scheme 2.2 *Diastereoselective synthesis of d-TCO.*

2.5.5 Strained aziridine-fused *trans*-cyclooctene (aza-TCO)

In 2016, Vázquez *et al.* reported on the formation of fluorescent 1,4-dihydropyridazines product following an IEDDA reaction between an s-tetrazine and axial *trans*-cyclooct-4-enol.[199] The authors hypothesized the involvement of the axially substituted hydroxy group in the tautomerization of the dihydropyridazine product. Through conformational analysis and DFT modeling, the key step for the formation of the 1,4-dihydropyridazine fluorophore was identified as the hydrogen atom transfer from one of the bridgehead carbon atoms to a heteroatom on the 4,5-dihydropyridazine intermediate. Importantly, this hydrogen transfer was only feasible when the heteroatom and the hydrogen atom were in close proximity. Notably, this phenomenon was observed for the dihydropyridazine intermediate formed with the axial substituted TCO but not for the equatorial isomer. Additionally, modifications of the alcohol group either altered the fluorogenic properties of the reaction or completely disappeared.[199]

To maintain the fluorogenic nature of the reaction while allowing the attachment of useful functional groups, Siegl *et al*. designed a *cis*-fused aziridine ring to the *trans*-cyclooctene (aza-TCO, 2.15).[195] Computational studies confirmed that this fusion resulted in the desired "half-chair" conformation, enhancing the reaction rate. Further conformational analysis of 4,5-dihydropyridazine intermediate revealed that a low energy conformer of 4,5-dihydropyridazine contains a bridgehead hydrogen-aziridine nitrogen distance of 2.29 Å, facilitating the hydrogen migration to yield a fluorescent product. Encouraged by the computational results aza-TCO was synthesized (Scheme 2.3).[195] The synthesis involved the ring opening of the epoxide, yielding azido alcohol which was subsequently converted into the aziridine (2.11) through Staudinger reduction-cyclization, resulting in a *cis*-ring fusion. Protection of the aziridine nitrogen with trimethylsilylethoxycarbonyl was found to be crucial for photoisomerization. After further

deprotection and alkylation of the aziridine nitrogen, an ethyl ester (2.14) was obtained which was reduced to aza-TCO-alcohol (2.15).

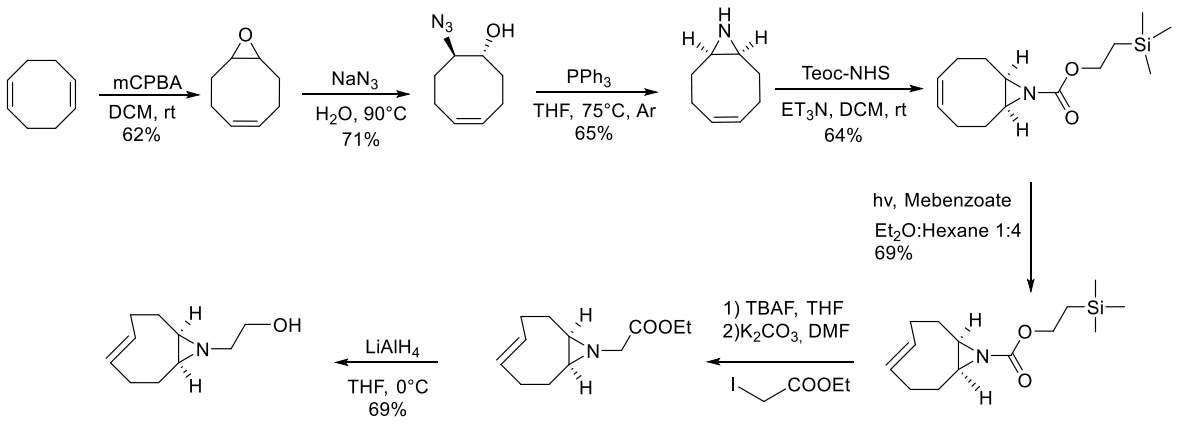

Scheme 2.3 *Synthetic scheme of aza-TCO.*

As anticipated, the click products of aza-TCO with tetrazines yielded fluorescent 1,4-dihydropyridazine products. The click products exhibited large Stokes shift and tunable emission maxima, depending on the substitution of tetrazine. Furthermore, a 20-70-fold fluorescence enhancement was observed upon reaction. While the reported fluorescence quantum yield was relatively low, the authors claimed that it was sufficient for bioimaging applications. When reacted with diphenyl-s-tetrazine, aza-TCO exhibited a reaction rate that was 20 times faster (k_2= 690 ± 20 $M^{-1}s^{-1}$) compared to axial diastereomer of TCO-OH (k_2 = 38 ± 3 $M^{-1}s^{-1}$) and 1.5 times faster than the d-TCO (470 ± 8 $M^{-1}s^{-1}$), while it was slower than the s-TCO (2,000 ± 18 $M^{-1}s^{-1}$). Additionally, aza-TCO showed good stability in the CD_3OD-d_4 solution at room temperature. Similar to other TCOs, exposure to thiol-containing groups led to a 1:1 mixture of *cis* and *trans* isomers within seven days in deuterated PBS.[195]

In the same study, an activated ester derivative of aza-TCO was successfully used for the fluorescent labeling of proteins. Moreover, when applied for fluorogenic imaging of peptidoglycans in live bacteria, aza-TCO-modified D-amino acid was effectively incorporated in the peptidoglycan after a 2-hour incubation. A weak fluorescence signal persisted on the surface of bacteria after a 12 h incubation period with aza-TCO, indicating that a fraction of the aza-TCO remained in its reactive *trans*-conformation.

2.5.6 **Oxazolone fused-TCO (Ox-TCO)**

Oxazolone fused TCO was first reported to be used in a biological assay by Kozma *et al.* as a hydrophilic ncAA.[203] Dienophile-modified ncAAs are often hydrophobic leading to a non-specific uptake [217, 221, 224] To achieve easy and faster washout of reactive ncAAs from cells, a TCO with exocyclic heteroatoms was developed. The incorporation of a heteroatom increases the hydrophilicity while preserving the reactivity of TCOs.[62, 225] The synthesis described started by microwaving (Z)-9-oxabicyclo[6.1.0]non-4-ene with 2-(2-aminoethoxy)ethanol at 130°C. The intermediate was subsequently reacted with *N, N*-disuccinimidyl carbonate yielding the fused oxazolidine ring (2.16). The photoisomerization of the fused oxazolidine ring leads to the formation of a mixture of two *trans* isomers in a 4:1 ratio (Scheme 2.4). Attempts to isolate the isomers (2.17 and 2.18) remained unsuccessful. Additionally, a long isomerization time (80 h) was required to obtain the desired product, which complicates the synthesis as silver leeching is observed over time.[226] Although, the synthesis of oxazolone fused TCOs and its ring isomers have been attempted by a few groups, often low yields and fast compound degradation were reported.[74, 214]

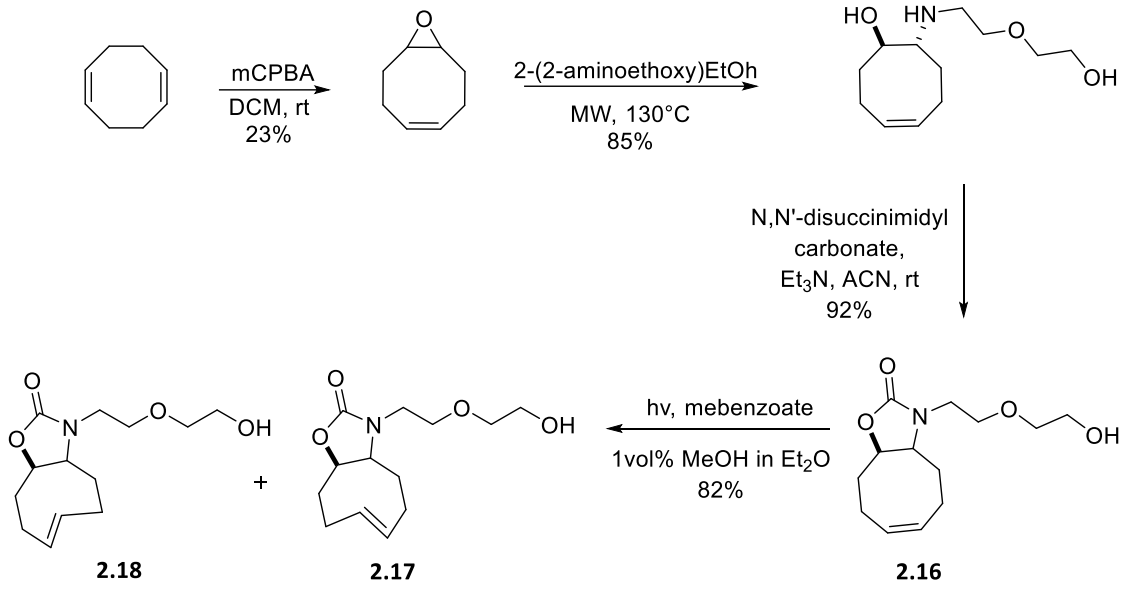

Scheme 2.4 *Synthetic scheme of Ox-TCO.*

When reacted with benzylamino tetrazine, the 4:1 mixture of Ox-TCO isomers showed a k_2 of 29,242 ± 636 $M^{-1}s^{-1}$ which is in the same range of *trans*-cyclooct-4-enol reactivity (26,000 $M^{-1}s^{-1}$). Ox-TCO was stable when stored in D_2O at room temperature. In the presence of cysteine, Ox-TCO showed no degradation for up to 16 hours, showing similar stability to that of TCO-OH.[226] Unfortunately, no

genetic incorporation of lysine-conjugated ox-TCO was observed when incubated in bacterial cell culture media. It was speculated that linker attachment at the five-membered oxazolidine ring might account for inefficient recognition by the bacterial synthetase.[203] In another study, hydrophilic Ox-TCO was used to study the turn-on fluorescence of Tz-quenched phenoxazine fluorogenic labels.[227]

2.5.7 4,6-dioxo-TCO (DO-TCO)

Effects of endocyclic oxygen on the reactivity of TCO was first studied by Jendrella in 1983, where 4,6-dioxo-TCO showed a 20-1000-fold faster reaction rate than *trans*-cyclooctene in cycloadditions with cyclopentadiene, 2,3-dimethyl butadiene, and diphenylketene.[225] Studies by Sletten *et al.* also showed that the introduction of heteroatoms on cyclooctynes led to improved kinetics as well as increased hydrophilicity.[62] Later on, *in silico* investigations by Gold *et al*. showed that the fast reactivity displayed by 3-oxocyclooctynes was partially attributed to the hyperconjugation effect of allylic oxygens.[228] Heterocyclic 4,6-dioxo-TCO was initially synthesized by Jendrella.[225, 229] To enhance the washout times in fluorescence imaging, Kozma *et al.* introduced a modified version of DO-TCO for imaging of cell surface or cytosolic proteins via genetic incorporation. Notably, DO-TCO-Lys showed a remarkably fast washout from cytoplasm within 5 min, allowing labeling with fluorophore-conjugated tetrazine without any additional washing procedures.[203]

The synthesis of the 4,6-dioxo-TCO derivative is based on the established method by Jendrella, with the addition of an extra glycol handle for further conjugation. The synthesis is based on stereoconversion and started from dioxepin which underwent a reaction with methyl diazoacetate in the presence of catalytic $Rh_2(OAc)_4$ to furnish cyclopropyl carboxylate (2.19). This intermediate is subsequently hydrolyzed and transformed into urea (2.21) using the Curtius rearrangement. Nitrosation of urea is then followed by the ring opening to afford the dioxo-TCO (2.23, Scheme 2.5).[226]

Kinetic studies of DO-TCO with benzylamino tetrazine in PBS at 37°C showed a second-order rate constant of k_2 = 332 ± 3 $M^{-1}s^{-1}$. Notably, this value is two orders of magnitude lower than the corresponding rate constant measured for TCO-OH (33,585 ± 326 $M^{-1}s^{-1}$). Despite the anticipated higher internal strain in DO-TCO, the authors postulated that the decreased reactivity can be attributed to additional steric constraints introduced by the glycol moiety adjacent to the *trans*

double bond. Remarkably, when stored at -20°C, no degradation or isomerization of DO-TCO was observed for up to six months. Slow isomerization of the compound was observed over 5 days at 37°C in D_2O. In the presence of cysteine, DO-TCO isomerized rapidly to *cis*, with no *trans* isomer present after 6 hours. However, in the presence of mercaptoethanol, isomerization occurred along with decomposition, with about 70% remaining at a 25h time point.[226]

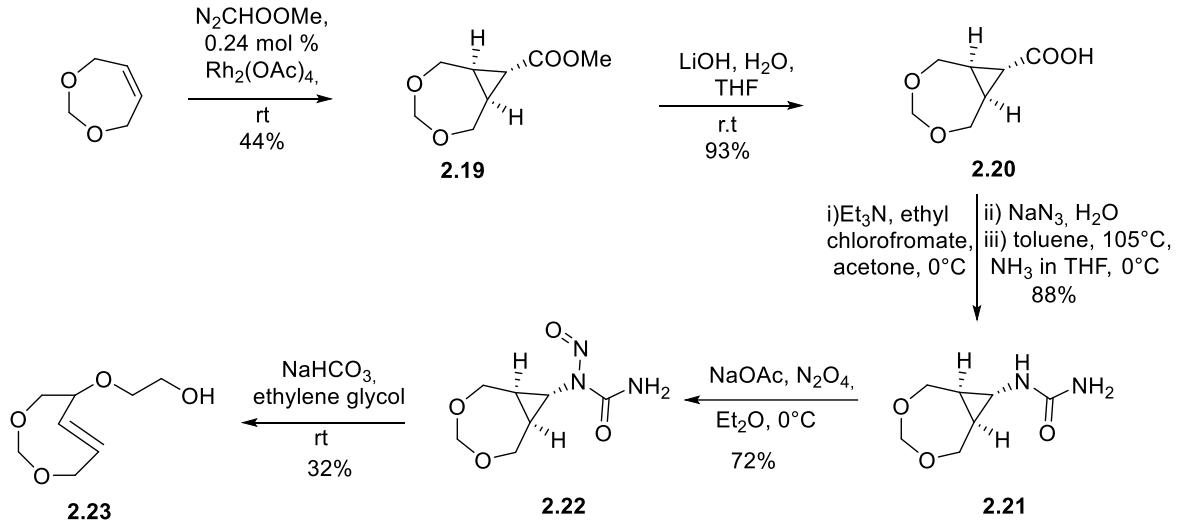

Scheme 2.5 *Synthesis of 4,6-dioxo-TCO (DO-TCO).*

2.5.8 *trans*-5-oxocene (oxoTCO)

To expand the biorthogonal toolbox with small, hydrophilic, and reactive TCO derivatives, Lambert *et al* designed two oxygen-containing isomers, namely trans-5-oxocene and trans-4-oxocene dienophiles.[167] Computational predictions indicated that the short C-O bonds in the backbone of the eight-membered ring would increase strain on the double bond. Indeed, the calculated C–C=C–C dihedral angle for *trans*-5-oxocene (134.6°) and *trans*-4-oxocene (134.4°) was significantly shorter than that for TCO (137.7°). Additionally, the energy barriers for the IEDDA reaction with 3,6-diphenyl-s-tetrazine were significantly lower for *trans*-5-oxocene (ΔΔE‡ –1.23 kcal/mol, ΔE‡(ZPE) –1.54 kcal/mol, and ΔH‡ –1.44 kcal/mol) relative to *trans*-cyclooct-4-enol, while *trans*-4-oxocene exhibited similar energy barriers to *trans*-cyclooct-4-enol. These computational DFT transition state calculations suggested that *trans*-5-oxocene would be thus more reactive than *trans*-4-oxocene. The higher ring strain in *trans*-4-oxocene was counteracted by the electron-withdrawing effect of the allylic oxygen, which deactivated the alkene through hyperconjugation.[167]

Based on these computational predictions, an alcohol-functionalized *trans*-5-oxocene (2.25) was synthesized. Photoisomerization of the *cis*-oxocene (2.24) resulted in a 2.2:1 diastereomeric mixture of *trans*-oxocenes with equatorial isomer as the major product (Scheme 2.6). Notably, the separation of these diastereomers using silica gel chromatography was unsuccessful, and preparative supercritical fluid chromatography was challenging, leading to the use of the diastereomeric mixture in subsequent experiments.

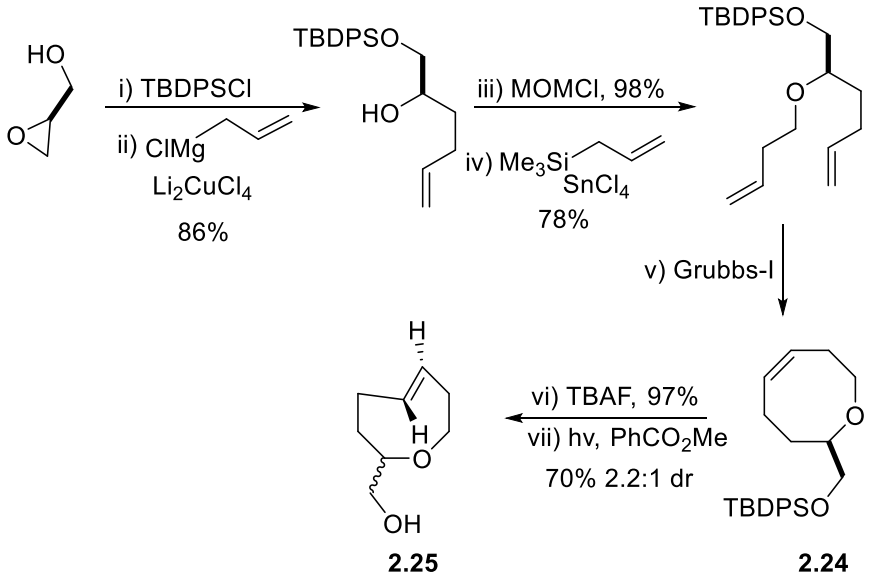

Scheme 2.6 *Synthesis of trans-5-oxocene (oxo-TCO).*

The diastereomerically pure equatorial isomer of oxo-TCO exhibited a rate constant of 44,100 ± 2600 M^{-1} s^{-1} in PBS at 25 °C with 3,6-dipyridyl-s-tetrazine. As the isolation of a diastereomerically pure sample of the axial diastereomer, was not successful, the rate constant was calculated to be 310,000 M^{-1} s^{-1} based on the rates observed for the diastereomer mixture and the pure equatorial isomer. The 7-fold rate acceleration for the axial isomer of oxo-TCO is consistent with prior reports for the axial isomer of *trans*-cyclooc-4-enol. The diastereomeric mixture of oxo-TCO showed fast kinetics when reacted with a succinic acid derivative of 3,6-dipyridyl-s-tetrazine with a second-order rate constant (k_2) of 94,600 ± 5,700 M^{-1} s^{-1} in PBS at 25°C. Although faster than the *trans*-cyclooct-4-enol isomers, the reaction remained approximately 4-fold slower than conformationally strained d-TCO under comparable conditions (366,000 M^{-1} s^{-1}).

The logP value was experimentally determined (logP 0.51), indicating improved hydrophilicity compared to equatorial *trans*-cyclooct-4-enol (logP 1.11) and d-TCO (logP 0.94).[73] The major equatorial diastereomer of *trans*-5-oxocene showed less than 10% degradation after 1 week in

deuterated PBS. In contrast, the more reactive axial (minor) diastereomer was prone to degradation with a half-life of 36 hours in PBS and complete degradation after 9 days. The compound showed higher isomerization in the presence of mercaptoethanol in buffered solutions (92%) when compared to organic solvents (8%). Cell imaging with a GFP encoded Tz containing ncAAs and oxo-TCO resulted in rapid and quantitative labeling both in solution and in bacteria cells.

2.5.9 Other heteroatoms containing TCOs

Other endocyclic heteroatoms containing *trans*-cyclooctenes have been described. Toomoka reported the synthesis of *trans*-dialkoxysilane from (*E*)-2-pentene-1,5-diol and commercially available dichlorosilanes in the presence of $AgNO_3$ yielding the eight-membered ring which was followed by photoisomerization. In an alternative approach, ring-closing metathesis in the presence of Grubbs catalyst also yielded the ring. The obtained alkene was reported to be highly reactive in Diels-Alder reactions.[169] Similarly, Woerpel also described a diastereoselective synthesis of functionalized *trans*-dioxasilacyclooctenes through the insertion of silyenes into vinyl epoxides followed by the subsequent allylations of aldehydes.[230] Finally, sulfur and nitrogen-containing TCOs have also been described but are mostly studied in the fields of transannular cyclization (Figure 2.9).[231, 232]

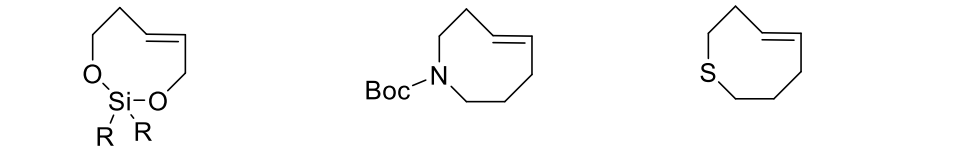

Trans-dialkoxysilane **2.26** | 5-aza-trans-cyclooctene **2.27** | 5-thia-trans-cyclooctene **2.28**

Figure 2.9 *Structures of endocyclic heteroatom containing TCOs.*

2.6 Applications of trans-cyclooctenes in nuclear medicine

Nuclear imaging techniques rely on the use of radiolabeled targeted biological vectors or small molecules, known as radiotracers, to image cellular functions or pathological processes by single-photon emission computed tomography (SPECT) or positron emission tomography (PET). The high sensitivity of nuclear imaging techniques allows for the visualization of the accumulation of radiotracers in biochemical processes at low nanomolar to micromolar concentrations. The use of TCO-Tz ligation in radiochemistry has increased over the years due to the fast kinetics and

biocompatibility. TCOs in particular have found use as a radiolabeling strategy or as an *in vivo* labeling method through a pretargeting strategy for imaging and therapy.

2.6.1 ^{18}F-labelled TCO as radioligand

TCO as a radioligand was first explored by Fox *et al.* in 2010, where [^{18}F]FTCO was demonstrated to react with 3,6-dipyridyl-s-tetrazine within seconds in an excellent radiochemical yield (RCY) of 98% at low micromolar concentrations.[233] [^{18}F]FTCO was first used *in vivo* as a radiolabeling method for a Tz-conjugated RGD (Arg-Gly-Asp) peptide for PET imaging of $\alpha_v\beta_3$ integrins. The labeling of the RGD peptide with ^{18}F using IEDDA was achieved in 5 min with efficient conjugation (RCY = 90%) at low concentrations of Tz precursor molecule. PET imaging of U87MG xenografts, which express $\alpha_v\beta_3$ integrins, showed a tracer accumulation in tumors with uptake values of 2.7 ± 0.5% ID/g. However, the pharmacokinetics of the radiofluorinated tracer were suboptimal. A significant amount of activity accumulated in the liver and abdomen, which is associated with the hydrophobicity of this first-generation TCO-Tz system.[234] In the following studies, bifunctional tetrazine-maleimide partners were introduced for site-specific labeling via cysteine residues on peptides and proteins. Here too, labeling with [^{18}F]FTCO allowed for high RCY > 95% and high specific activity of 111-222 GBq µmol^{-1} for [^{18}F]FTCO-Tz-cRGDyC peptide.[235]

Similarly, TCO-tetrazine ligation has been used to radiolabel exendin-4, a glucagon-like peptide-1-receptor (GLP-1R) agonist with ^{18}[F]FTCO for imaging of islet transplantation models. Notably, the use of TCO-tetrazine ligation for radiolabeling allowed for higher specific activity of the radiotracer when compared to the use of ^{18}F-labelled prosthetic groups (*N*-2-(4-^{18}F-fluorobenzamido)ethylmaleimide ([^{18}F]FBEM) and [^{18}F]fluorobenzaldehyde) which is needed to avoid blocking effects, when the receptor expression is limited.[236, 237] Importantly, the use of ^{18}[F]FTCO as a prosthetic group allows for rapid labeling at room temperature and aqueous conditions which are ideal for labeling peptides. However, the higher lipophilicity of the ligation product formed as well as the formation of dihydropyridazine isomers can potentially hamper the clinical translation.

[^{18}F]FTCO has also been used for radiofluorination of small molecules such as AZD2281, a poly(ADP-ribose)polymerase 1 (PARP1) inhibitor without affecting the affinity of the compound toward its

target.[238] *In vivo,* PET-imaging results in MDA-MB-436 tumor-bearing mice showed an accumulation of ^{18}F-labeled AZD2281 in PARP1-overexpressing cancer cells. [239]

In another study, Fox *et al*. successfully prepared a radiolabeled s-TCO using ^{18}F, via nucleophilic substitution of a tosylated precursor. The exceptionally fast reaction kinetics of [^{18}F]Fs-TCO allowed the use of more stable diphenyl-s-tetrazine conjugated peptides, which improved the *in vivo* stability of the radiolabeled peptides in comparison to peptides conjugated with 3,6-dipyridyl-s-tetrazine. [^{18}F]Fs-TCO remained stable in PBS (pH 7.4) for up to 2 h at 37 °C. After one hour of incubation in fetal bovine serum, [^{18}F]Fs-TCO showed 74% intact tracer. The lower radiochemical stability for PET probe assembly is not an issue, as the IEDDA reaction takes place within a few minutes. Furthermore, [^{18}F]Fs-TCO-DiPhTz-RGDyK demonstrated persistent and prominent uptake in U87MG tumors with tumor uptake values increasing up to 8.9 ± 0.5% ID/g at 4h p.i. This was an improvement when compared to ^{18}F-TCO-labeled 3,6-dipyridyl-s-tetrazine-RGD conjugates, where the tumor uptake decreased over time. Given the increased tumor uptake at later time points, it was hypothesized that [^{18}F]Fs-TCO-DiPhTz-RGDyK possessed a prolonged circulation which contributed to persistent tumor uptake of the labeled peptide. This observation was further translated by Wang *et al.* to improve tumor uptake of different radiolabeled peptides, such as NT20.3, Exendin-4, and bombesin, through enhanced blood circulation afforded by the introduction of the ^{18}F-labeled s-TCO-DiPhTz system in above mentioned peptides.[240] The mechanism of enhanced blood circulation was attributed to the binding of diphenyl tetrazine moiety with plasma protein, specifically with hemopexin and transferrin. Generally, the lipophilicity of the radiolabeled ^{18}F-TCO-Tz ligation product results in modest tumor-to-background contrast. To improve contrast ratios, novel radioligands were constructed using [^{18}F]Fs-TCO and neurotensin conjugates of a more hydrophilic Tz (3,6-di(2-hydroxyethyl)tetrazine). This Tz showed fast kinetics (k_2=11,500 M^{-1} $s^{-}1$) and yielded a PET-imaging probe with less non-specific uptake in the H1299 non-small cell lung carcinoma tumor model.[241]

Recently, Wang *et al.* developed an ^{18}F-labeled *trans*-5-oxocene TCO, which has the advantage of having increased hydrophilicity to enable faster clearance of the tracer from non-target organs. The tracer was found to be 85% intact after 1h of incubation in PBS. The reason for tracer degradation was attributed to radiolysis. In a comparison study, [^{18}F]FoxoTCO, [^{18}F]Fd-TCO, and [^{18}F]Fs-TCO were used as prosthetic groups for rapid ligation with a Tz conjugated to a neurotensin peptide, Lys-

NT20.3. *In vivo,* PET imaging of each tracer was evaluated in neurotensin receptor-positive PC-3 tumor-bearing mice. The [^{18}F]FoxoTCO labeled peptide showed similar tumor uptake when compared with the [^{18}F]Fs-TCO and [^{18}F]Fd-TCO click products. However, the increased hydrophilicity of [^{18}F]FoxoTCO resulted in a significantly higher tumor-to-muscle ratio of 15.8 ± 2.2, compared with 6.5 ± 1.5 and 3.8 ± 0.9 for the s-TCO and d-TCO, respectively, at 30 min p.i. This high ratio (16.2 ± 2.3) was also sustained after 3.5 h and is attributed to lower non-specific uptake of the [^{18}F]FoxoTCO radiolabeled peptide (Figure 2.10) [242]

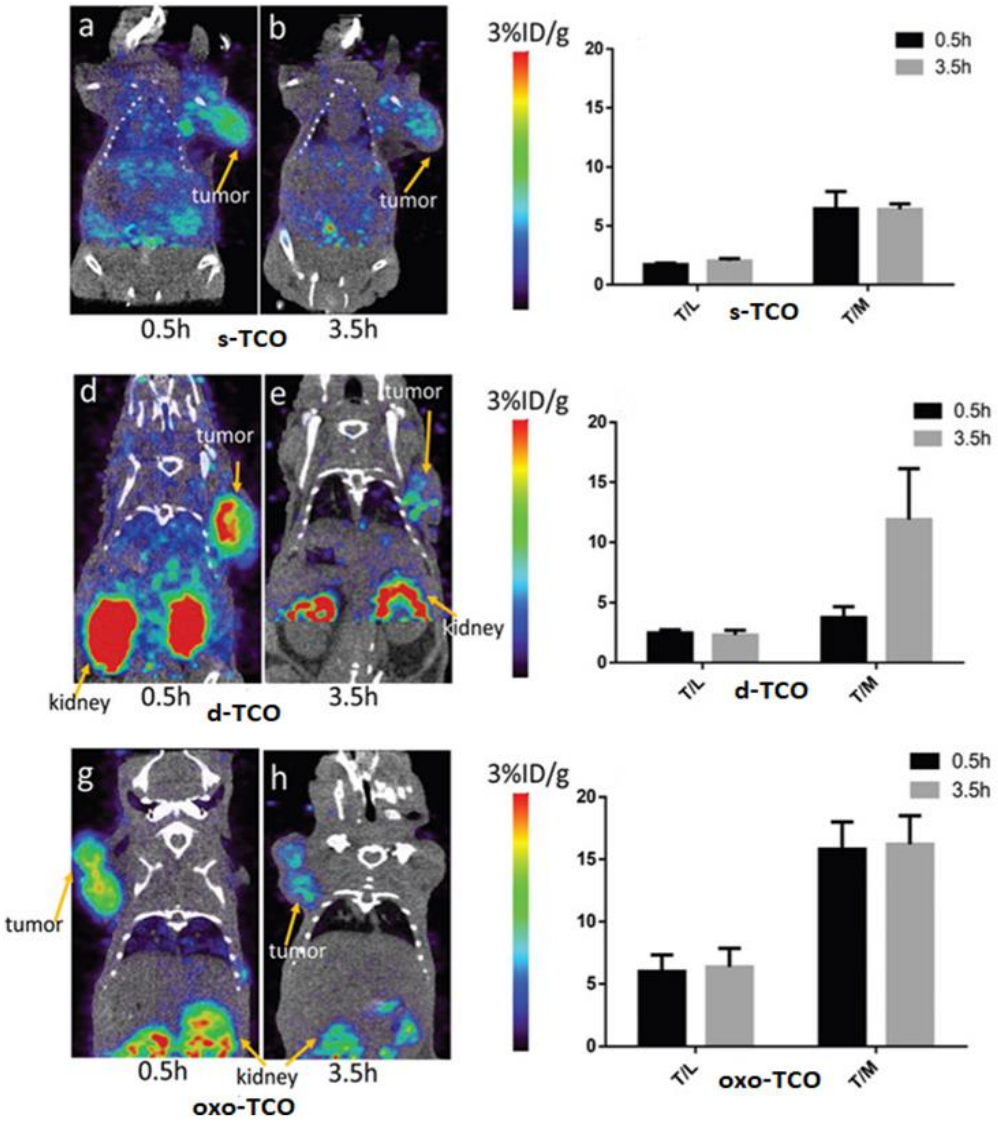

Figure 2.10 *Representative PET/CT images of the PC-3 tumor-bearing mice at 0.5 and 3.5h post-injection with [^{18}F]Fs-TCO, [^{18}F]Fd-TCO, and [^{18}F]FoxoTCO-derived NT-analogs. Image-derived tumor-to-liver ratios (T/L), and tumor-to-muscle (TLM) ratios from the conversion of the region of interest to %ID/g.The grey and black bars represent the uptake ratio at 0.5h and 3.5h respectively. The tumor-to-background ratio is improved by using oxoTCO derived-NT analog. Reproduced from Wang et al. with permission from the Royal Society of Chemistry.*[242]

2.6.2 TCO as a bioorthogonal tag in pretargeted imaging and therapy

Apart from being used as a radiolabeling strategy, TCO-Tz ligation has also been widely used in pretargeted imaging. Pretargeting is an approach used in immuno-PET imaging to overcome the slow clearance associated with directly radiolabeled antibodies. It involves a two-step process where an antitumor antibody conjugated with a bioorthogonal tag is first injected to accumulate in the target site. This is followed by the injection of radiolabeled molecule which specifically binds to the bioorthogonal tag. The unbound fraction of the radiolabeled molecule is rapidly excreted from the body allowing the use of short-lived radioisotopes for imaging.[25] Despite previous investigations into other pretargeting methods, the IEDDA reaction between a TCO and a Tz has emerged as a highly promising approach owing to its exceptionally rapid reaction kinetics; with k_2 up to $10^{6-7} M^{-1} s^{-1}$.[27, 73] While both TCO and Tz can be radiolabeled, most pretargeting studies have utilized a TCO-conjugated mAb as the targeting vector and a Tz-based radioligand.

Pioneering work by Robillard *et al.* demonstrated the potential of TCO-Tz ligation as a pretargeting strategy for imaging tumors *in vivo*.[89] Here, a *trans*-cyclooct-4-enol-modified Ab conjugate (CC49-TCO) was used in combination with a ^{111}In-labeled DOTA-Tz as a radioligand for the SPECT imaging of TAG-72 expressing colorectal cancer xenografts. This approach achieved excellent image contrast with a tumor-to-muscle ratio of 13:1.[89] In subsequent studies, the use of axial isomer of the TCO with a short benzamide linker allowed for a 10-fold increase in reactivity and 1.55-fold improved *in vivo* stability. This allowed for a longer lag time of 72h, between the mAb-TCO and radiolabeled Tz injection without compromising the tumor uptake while significantly increasing the tumor-to-blood ratio.[78] To further enhance the pharmacokinetics of the mAb-TCO conjugate, the linker was modified to an acetamide which further increased the stability of the conjugated TCO through bigger steric hindrance around the TCO tag. This modification resulted in improved tumor accumulation of ^{177}Lu-labeled DOTA-Tz up to 9.35%ID/g (Figure 2.11).[81]

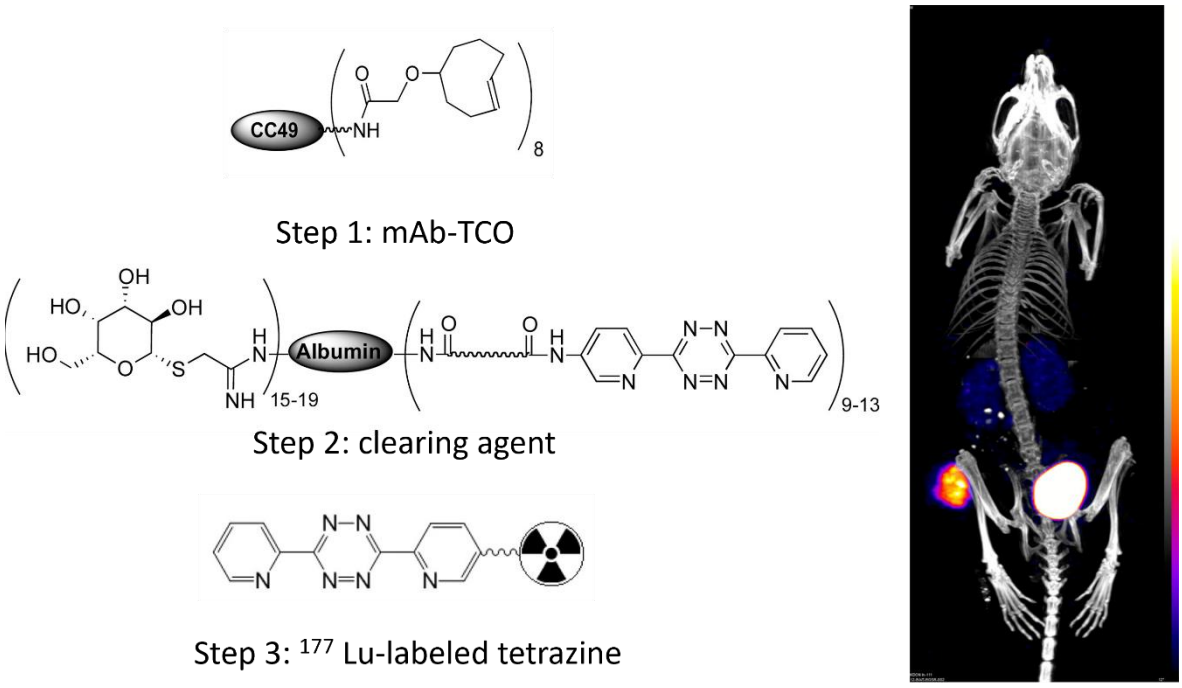

Figure 2.11 *Representative SPECT/CT image of tumor-bearing mice injected with CC49-TCO, followed by two doses of galactose-albumin-tetrazine clearing agent (30 and 48h post-mAb injection) and ^{177}Lu-labeled tetrazine at 50h post-mAb injection. The image shows high radioactivity uptake in the tumor and low uptake in non-target organs. Most of the activity is present in the bladder. Adapted with permission from Rossin et al. Copyright 2014 American Chemical Society.*[81]

Several other groups have since then adopted the strategy to visualize different tumor types with mAb conjugated to TCO in combination with radiolabeled Tzs.[85, 92, 243-245] Additionally, the approach was also successfully applied to delineate tumors in a pancreatic cancer xenograft model, where high antigen circulation and target internalization complicate the *in vivo* targeting process.[82] Early efforts by Zeglis *et al*. already showed the superiority of the pretargeting approach based on TCO-Tz ligation when compared to directly radiolabeled antibodies. Although a higher absolute tumor uptake of 33%ID/g was observed for directly labeled [^{64}Cu]Cu-NOTA-A33 in SW1222 xenografts, a lower effective dose (0.0124 mSv/MBq) was observed without compromising image contrast.[85] It is noteworthy to mention that lower radiotracer uptake can be a disadvantage in a pretargeted therapy setting where a high absorbed dose in the tumor is required. Similar results were observed in a recent study with a TCO-conjugated anti-CD44v6 Chimeric mAb U36 in combination with ^{89}Zr-labeled tetrazine for imaging of head-and-neck squamous cell carcinoma (HNSCC) xenografts. The pretargeted approach resulted in lower absolute tumor uptake when compared to directly labeled mAb (1.5 ± 0.2 vs 17.1 ± 3.0% ID/g at 72 h p.i.) but with comparable tumor-to-non-target tissue ratios and significantly lower absorbed doses.[246] With the recent advancements in direct Tz labeling

procedures, further studies on pretargeting have been conducted with ^{18}F-labeled Tzs in combination with mAb-TCO.[80, 84, 93, 247] Although the absolute tumor uptake values are generally low with ^{18}F-labeled Tzs, studies have shown significant improvements in the tumor-to-muscle ratios up to 20.8 resulting in images with better contrast while reducing the radiation burden.[94, 95]

The use of TCO-Tz ligation has also attracted interest in the field of brain imaging. Recently, bispecific antibodies to transferrin receptor (TfR) were conjugated with TCO either for radiolabeling or for a pre-targeting approach across the blood-brain barrier (BBB). The TfR enables the active transport of antibodies across the BBB via receptor-mediated transcytosis due to its expression in endothelial cells of the BBB and on neurons.[248] Based on this, bispecific antibodies have been used for the visualization of β-amyloid (Aβ) plaques. Sehlin *et al.* labeled bispecific antibody ligands RmAb158-scFv8D3 and Tribody A2 functionalized with TCO and with ^{18}F-labeled Tz. As the conjugates were pre-clicked before injection, the antibody ligands' half-life in blood was too long to optimally match the physical half-life of fluorine-18 ($t_{1/2}$ = 110 min) and no significant uptake differences were observed between a wild type and tg-ArcSwe mouse model with increased Aβ aggregation and production.[249] Recently, a pretargeting approach was applied with a brain-penetrating mAb31 (mAb31-BrainShuttle). mAb31 was functionalized with TCO moieties for pretargeted labeling of Aβ plaques using a tritium-labeled Tz in the PS2APP Alzheimer's disease mouse model. *In vitro* clicked mAb-TCO-Tz was able to pass the BBB of transgenic PS2APP mice and specifically visualize Aβ plaques *ex vivo*. However, no significant labeling of Aβ plaques was observed *in vivo*.[250] In a proof-of-concept study, Shalgunov *et al.* demonstrated the *in vivo* click reaction of ^{18}F-labelled Tz with TCO in the brain. TCO-tagged PeptoBrush polymer was injected in the right striatum of Long-Evans rats followed by the radiolabeled Tz, where the accumulation of the Tz was visible at the point of PeptoBrush injection.[251] However, the study still leaves a gap to image targets beyond BBB as the approach described was based on intracerebral injection of both click components.

Other small molecules and nanoparticles have also been used for pretargeted imaging. One example is TCO-conjugated bisphosphonates in combination with ^{99m}Tc-labeled Tz or ^{177}Lu-labeled Tz either for the imaging or therapy of bone diseases. When assessed *in vivo* the pretargeting approach showed selective and high uptake in the knee (20.07 ± 4.9 %ID/g) and shoulder (16.2 ± 4.8 %ID/g).[252] Recently, Zeglis *et al*. translated the approach to image osteodestructive lesions in

dogs using [^{64}Cu]Cu-SarAr-Tz, demonstrating the feasibility of *in vivo* pretargeting in larger animals with bigger blood volume.[253]

Pretargeting studies in mice injected with mesoporous silica nanoparticles (MSNs) conjugated with TCO and s-TCO, followed by ^{11}C-labeled tetrazine showed a significantly increased activity concentration in the lung.[204] Notably, MSNs conjugated to TCO performed better than with the more reactive s-TCO tag even though both modified MSNs contained similar dienophile-loading. This again highlights the effect of lower stability of s-TCO under *in vivo* conditions. In another study, supramolecular nanoparticles (SNP) encapsulating TCO-grafted molecular building block, which disassembles once the SNPs retain in the tumor via the enhanced permeability and retention (EPR) effect, were used in pair with ^{64}Cu-labeled Tz. Imaging studies in U87MG glioblastoma tumor-bearing mice showed high accumulation and retention of radioactivity mainly in the tumor and liver. Although improved tumor uptake was observed in comparison to the traditional nanoparticle-based platform, high uptake of nanoparticles in the liver remains a disadvantage.[254]

Besides imaging, a pretargeting approach involving TCO-Tz ligation has also been applied in radioligand therapy. Pretargeted radioimmunotherapy (PRIT) is a promising strategy for delivering a therapeutic radiation dose to solid tumors while sparing normal tissues. An initial study by Rossin *et al.* in 2013 used pretargeting with CC49-TCO conjugate to deliver a β-emitter [^{177}Lu]Lu-DOTA-PEG_{11}-Tz in LS174T-tumor-bearing mice. In the study, two doses of a galactose-albumin-based clearing agent were injected at 30 h and 48 h followed two hours later by the injection of [^{177}Lu]Lu-DOTA-PEG_{11}-Tz. This allowed for the clearance of circulating mAb-TCO conjugate from blood. The use of a clearing agent led to a 2-fold increase in tumor uptake and a 125-fold enhancement in the tumor-to-blood ratio compared to the approach without a clearing agent.[79] This is of importance in therapy as it reduces dose-limiting hematotoxicity. Dosimetry calculations suggested that the pretargeting system could allow for an 8-fold higher tumor absorbed dose in mice when compared to the conventional approach.[255] Encouraged by this, several therapeutic radionuclide-labeled tetrazine frameworks based on the pretargeted click chemistry have been developed and evaluated *in vivo*.[252, 256-260] However, only a few studies reported the therapeutic efficacy using PRIT.

Houghton and coworkers demonstrated the use of a TCO-modified 5B1 antibody paired with a ^{177}Lu-labeled Tz for therapy in a murine model of pancreatic cancer. TCO-5B1 was administered first followed 72 h later by the injection of [^{177}Lu]Lu-DOTA-PEG$_7$-Tz in varying doses (400, 800, and 1,200 µCi). At higher doses of radioligand, tumor regression or growth delay was observed when compared to control groups.[257] Membreno *et al*. reported a PRIT study with the same Tz radioligand [^{177}Lu]Lu-DOTA-PEG$_7$-Tz and huA33-TCO on a colorectal cancer model. The study reported found significant differences in survival and tumor growth development between the treatment and control groups.[258] Rondon *et al.* used lutetium-177 for the first time in a disseminated model of peritoneal carcinomatosis. Intraperitoneal injection of 35A7-TCO followed 24h later by [^{177}Lu]Lu-DOTA-PEG$_7$-Tz demonstrated a significant delay in a decrease of tumor growth in the treated mice compared to the control.[261] Poty *et al.* showed the efficacy of ^{225}Ac-PRIT ([^{225}Ac]Ac-DOTA-PEG$_7$-Tz paired with 5B1-TCO) in both subcutaneous and orthotopic models of CA19.9-positive PDAC xenografts. When compared to conventional radioimmunotherapy (RIT), the median survival times of the two administration methods were similar at the highest injected dose, but with a higher incidence of hematotoxicity in cohorts treated with conventional RIT. In contrast, the maximal tolerated dose (MTD) was not reached in PRIT-treated cohorts allowing for higher injected activities in future investigations.[262]

In a pretargeted theranostic approach, Keinänen *et al*. performed a PRIT study using the copper-64 (imaging) and copper-67 (therapy) pair of radioisotopes. Therapy studies were conducted in a murine model of human colorectal carcinoma using a huA33-TCO and [^{67}Cu]Cu-MeCOSar-Tz in varying doses. Studies revealed a dose-dependent therapeutic response, with an increased median survival time for the highest dose (55.5 MBq). Additionally, mice injected with a fractionated dose of [^{67}Cu]Cu-MeCOSar-Tz exhibited less hematological toxicity without sacrificing therapeutic efficacy. Furthermore, a correlation between the tumor uptake of [^{64}Cu]Cu-MeCOSar-Tz and the subsequent therapeutic response to [^{67}Cu]Cu-MeCOSar-Tz was observed highlighting the advantage of theranostic pair in predicting responders and non-responders.[83]

2.6.3 ^{18}F-labeled TCO in pretargeted imaging

In contrast to radiolabeled Tz, radiolabeled TCO has been less explored for pretargeted imaging. Nevertheless, many studies have emerged in the past years. [^{18}F]FTCO was first evaluated *in vivo* as a pretargeted PET imaging agent in the brain by wyffels *et al*.[263] Although the study revealed brain penetration of [^{18}F]FTCO, it was quickly metabolized *in vivo* in plasma and brain with indications of further defluorination at later time points, thus rendering it unsuitable for *in vivo* use.[263] Further efforts from Ruivo *et al.* to improve the stability of the ^{18}F-labeled TCO involved the incorporation of a 1,4,7-triazacyclononane-N,N',N''-triacetic acid (NOTA) chelator which was subsequently radiolabeled by complexation of Al[^{18}F]F (2.29, Figure 2.12). The tracer showed improved *in vivo* stability, with 51.9 ± 5.16% of intact tracer remaining after 60 min. Moreover, *cis*-isomer was identified as the only main radiometabolite and no defluorination was observed. *In vivo,* pretargeted imaging of LS174T colon cancer xenografts in mice treated with Tz conjugated CC49-antibody showed clear delineation of the tumor when compared with the control. However, abdominal activity remained high due to the hydrophobicity of the TCO-core.[264] Recently, radiolabeled d-TCOs have caught the attention in pretargeted imaging due to their fast kinetics, improved stability, and increased hydrophilicity. Billaud *et al*. synthesized a pegylated [^{18}F]Fd-TCO (2.31, Figure 2.12) via nucleophilic substitution of a tosyl precursor with 12% RCY. The resulting [^{18}F]Fd-TCO was shown to be stable, with 94% of intact tracer remaining after 2 h incubation at 37 °C in PBS. In rat plasma, slow isomerization of [^{18}F]Fd-TCO into the corresponding *cis*-isomer was observed, with 52% and 34% of the intact *trans*-compound remaining after 1 and 2 hours of incubation at 37 °C, respectively.[213] The tracer showed favorable *in vitro* stability but due to the suboptimal pharmacokinetics the absolute tumor uptake in the pretargeted approach remained low with prominent abdominal background activity.[87] Subsequently, novel ^{18}F-labelled d-TCO amide derivatives were developed by Ruivo *et al.* of which [^{18}F]MICA-213 (2.30, Figure 2.12) was used in a pretargeting study. *In vitro* the tracer showed improved stability with 79% of intact tracer remaining after 2 h incubation at 37°C in plasma. A pretargeting study in LS174T tumor-bearing mice showed clear visualization of the tumor in the group treated with CC49-Tz conjugate when compared to the control group. Although the probe showed high tumor uptake, the background signal was high, resulting in modest tumor-to-background contrast.[88] In all of the above-mentioned examples, the high background due to abdominal uptake is a common factor that needs to be improved for further translation of radiolabeled TCOs in pretargeted imaging.

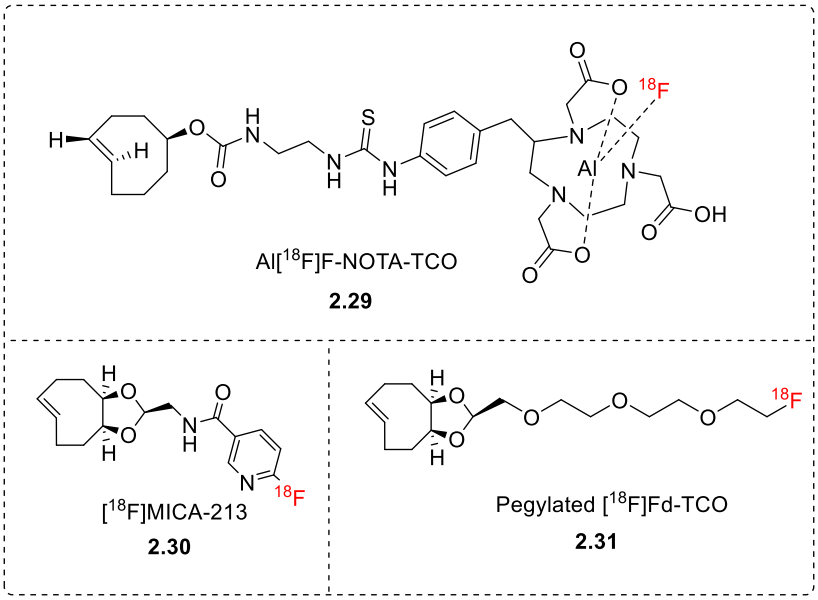

Figure 2.12 *[18]F-labelled TCO and d-TCO derivatives used in pretargeted imaging*

2.7 TCO-Tetrazine – Click-to-release reaction and mechanism

The click-to-release strategy was first introduced by the Robillard group.[218] The IEDDA click-to-release or IEDDA decaging reaction consists of two steps: a cycloaddition followed by an elimination step. It is based on the elimination of a leaving group from the vinyl position of a TCO following the tautomerization of the 4,5- dihydropyridazine to pyridazine (Scheme: 2.7).

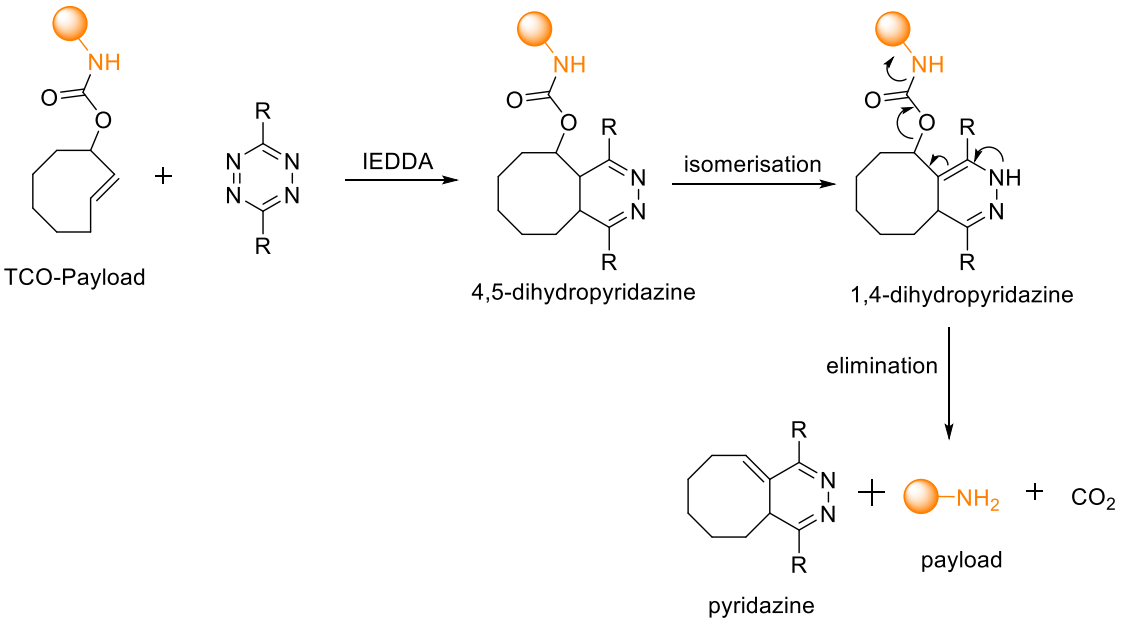

Scheme 2.7 *IEDDA decaging reaction between a TCO-carbamate conjugated to a drug molecule and a tetrazine.*

In their initial study, Robillard *et al.* applied the strategy to activate a prodrug (TCO-carbamate-Doxorubicin *in vitro*. When reacted with 3,6-dipyridyl-s-tetrazine, the reaction rate of the axial diastereomer of the TCO was 16 times faster (k_2 = 57.7 M^{-1} s^{-1} in ACN, than the equatorial (k_2 = 0.37 M^{-1} s^{-1}). Despite the fast cycloaddition rate, only 7% free doxorubicin (Dox) was released after 3 h from the TCO-conjugated prodrug. However, when the prodrug was reacted with dimethyl tetrazine (DMT), a significantly faster release rate was observed, with 79% complete release occurring within 16 minutes, even though the cycloaddition step was slower implying that a faster cycloaddition rate may not be the determining factor in elimination. *In vitro*, experiments involving the caged prodrug (EC_{50} = 3.834 µM) demonstrated a notable reduction in toxicity in A431 tumor cells compared to the parent drug (EC_{50} = 0.037 µM). Furthermore, the combination of the prodrug and DMT resulted in an almost complete restoration of cytotoxicity of Dox (EC_{50} = 0.049 µM).[218]

As the initial studies showed that a slower-reacting DMT led to higher drug release when compared to faster-reacting 3,6-dipyridyl-s-tetrazine, Chen and coworkers conducted a comprehensive investigation on the impact of Tz substituents on the elimination rates. Their findings revealed a significant release enhancement for asymmetric Tz when compared to their symmetric counterparts. Notably, the presence of EWGs was observed to promote the rate of cycloaddition but hinder the rate of elimination due to the formation of a stable cycloaddition intermediate (Figure 2.13). Tzs incorporating a single EWG along with a small and relatively electron-neutral group were studied and exhibited an impressive release of up to 90% within 4 min in living cells.[265]

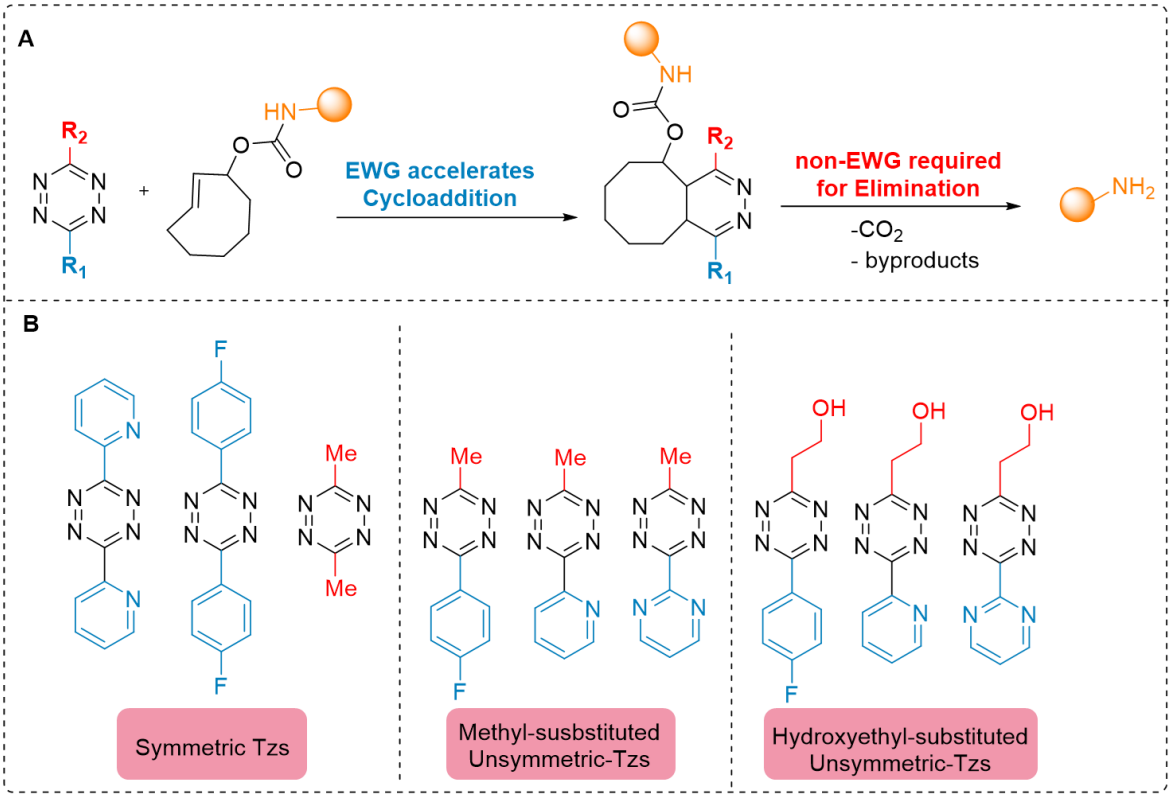

Figure 2.13 *A) Unsymmetric Tzs containing EWG and a non-EWG on the other side promote the elimination efficiency. B) Releasing efficiency of symmetric and unsymmetric tetrazines in increasing order. Unsymmetric tetrazines Tzs exhibit superior releasing efficiency in comparison to symmetric counterparts. Hydroxyethyl-substituted Tzs showed higher releasing efficiency than methyl-substituted Tzs. Adapted with permission from Chen et al.*[265] *Copyright 2016 Wiley-VCH Verlag GmbH & Co. KGaA, Weinheim.*

The TCO-Tz click-to-release reaction often leads to the incomplete release of the payload. Studies by the Weissleder group revealed that the incomplete release results from the formation of a dead-end tricyclic product, resulting from the cyclization of the carbamate amine onto Tz after the cycloaddition (Scheme 2.8). To circumvent this pathway, the use of tertiary amines was proposed. However, as the amine linker originates from the drug, it may not always be the most desirable modification. Moreover, the investigations also demonstrated that the release is pH-dependent, with higher release rates observed under acidic conditions. Introducing carboxylic acid functionalized tetrazines, which contain a nearby proton to accelerate the tautomerization rate, was shown to be an alternative to lowering the pH of the reaction medium. Notably, this approach resulted in the complete release as rapid tautomerization disfavors the dead-end cyclization product.[266]

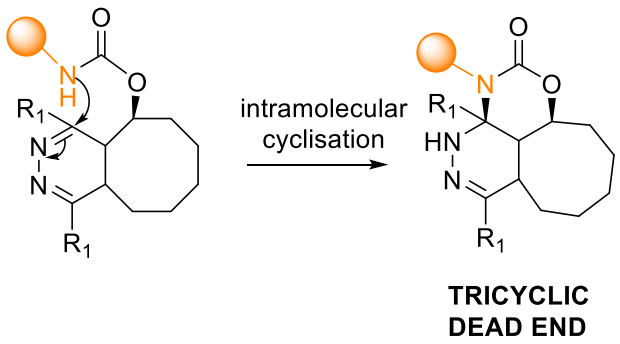

Scheme 2.8 *Formation of Tricyclic dead-end product via intramolecular cyclization of carbamate amine on to tetrazine resulting in incomplete release.*

In terms of reactivity with functionalized TCOs, asymmetric Tzs were shown to react in two possible orientations: head-to-head or head-to-tail. The study demonstrated that the head-to-head isomer preferentially forms the releasing isomer due to assisted H-transfer from the vicinal carboxylic acid. Conversely, the head-to-tail isomer favored the formation of the non-releasing isomer (Scheme 2.9).[266]

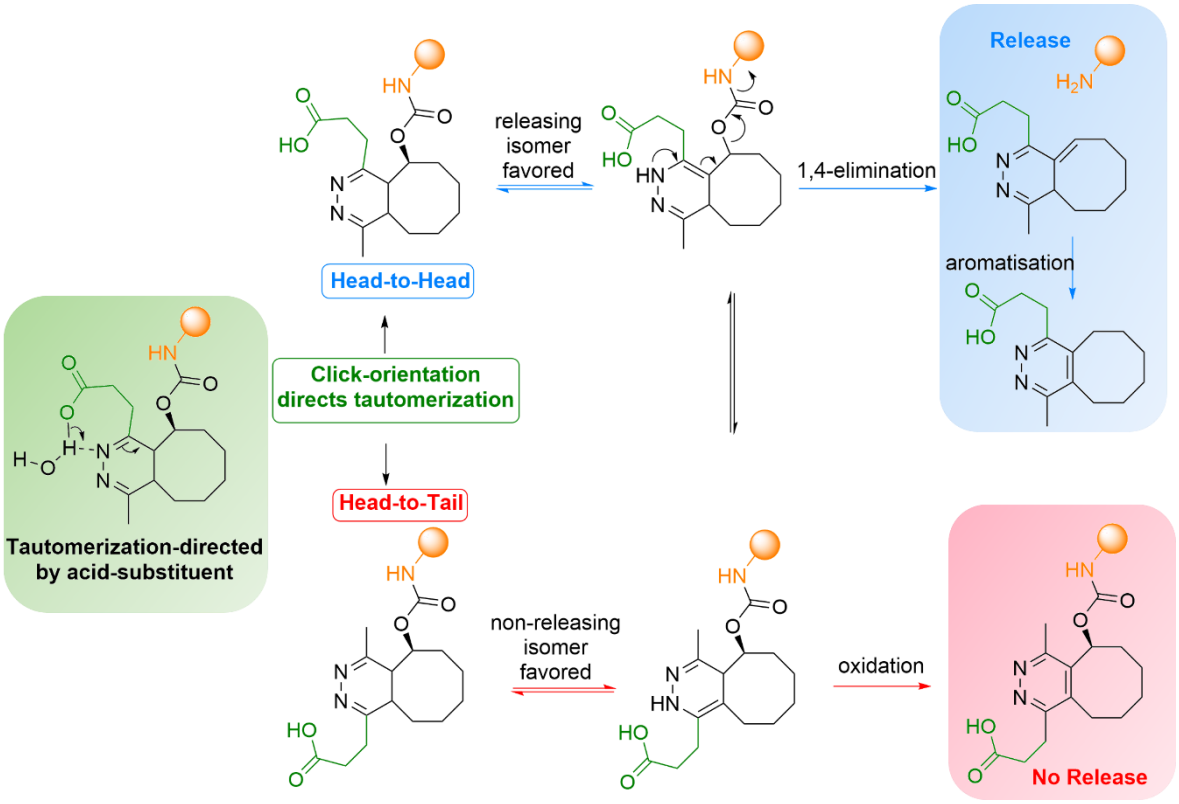

Scheme 2.9 *Tautomerization enhancement by acid-functionalized tetrazines through acid-assisted H-transfer. Click orientation of the substituted tetrazine determines the pH-dependent drug release. A Head-to-Head orientation favors the formation of a releasing isomer whereas, a Head-to-Tail orientation favors the formation of a non-releasing isomer.*

The group of van Kasteren also reported a novel class of amino-ethyl functionalized Tzs that enable rapid and pH-independent release. The amino-ethyl group is protonated in a biologically relevant pH range (pH 3.5-7.5), which then acts as an intramolecular proton donor, thereby accelerating the tautomerization rate. Furthermore, it plays a catalytic role in the elimination reaction through proximity to either the dihydropyridazine or the carbamate. The incorporation of cationic ammonium functionality resulted in a 4-fold increase in elimination rate when compared to the carboxylic acid group, which could be further enhanced by introducing EWGs onto the Tz scaffold.[267]

Later on, mechanistic investigations conducted by Robillard *et al.* revealed that the formation of 1,4-dihydropyridazine tautomer is the key releasing factor. 1,4-dihydropyridazine tautomer promptly liberates CO_2 and amine upon its formation. Consequently, the rate of 1,4-dihydropyridazine formation becomes a limiting factor influencing the overall elimination yield. In contrast, the 2,5-dihydropyridazine tautomer oxidizes slowly to pyridazine without releasing the payload, leading to a limited overall elimination yield (< 40%). The research group also expanded the scope of release to encompass other functional groups such as aromatic carbonates, aromatic and aliphatic esters, as well as aromatic, benzylic, and aliphatic ethers.[193] However, it should be noted that ester and carbonates are not stable in plasma or cellular environments, rendering them unsuitable for biological applications. Subsequently, Davies *et al.* reported the release of carboxylic acids and alcohols from a TCO-carbamate conjugate employing a self-immolative benzyl ether linker.[268, 269]

Robillard *et al.* also presented a reverse strategy in which the TCO acts as the activator and the tetrazine serves as the linker for the prodrug. In this approach, the TCO does not require allylic substitution, allowing for the use of faster-reacting TCOs. In a pretargeting strategy, the targeting moiety must be stable, which prevents the use of more reactive s-TCO derivatives. Since the trigger has a shorter exposure to *in vivo* conditions, the stability requirements are not as strict. Therefore, it was proposed that by using TCO as the trigger, the reaction rate could be increased using more reactive TCOs. The study demonstrated that depending on the TCO used, an increase in reactivity (6-800 fold) and high elimination yields ranging from 67% to 93% through the 1,4-elimination of the carbamate substituted to a tetrazine (Scheme 2.10). However, it should be noted that the TCO-triggered pyridazine elimination has only been demonstrated to work effectively with secondary amines, indicating a limited scope of leaving groups. Although this limitation can be partially

overcome by employing a self-immolative linker based on an alkylated amine, further exploration of the chemical scope is needed.[270] Additionally, a pretargeting strategie often requires a large excess of the activator. However, the reverse approach allows the use of lower doses due to the faster kinetics. Moreover, Tz linkers are relatively easier to synthesize than TCO linkers and show greater stability *in vivo* conditions, which makes this strategy more widely applicable. TCO-triggered cleavage holds great potential and may offer improved cycloaddition kinetics and antibody-drug conjugates (ADC) stability compared to TCO-conjugated ADC.

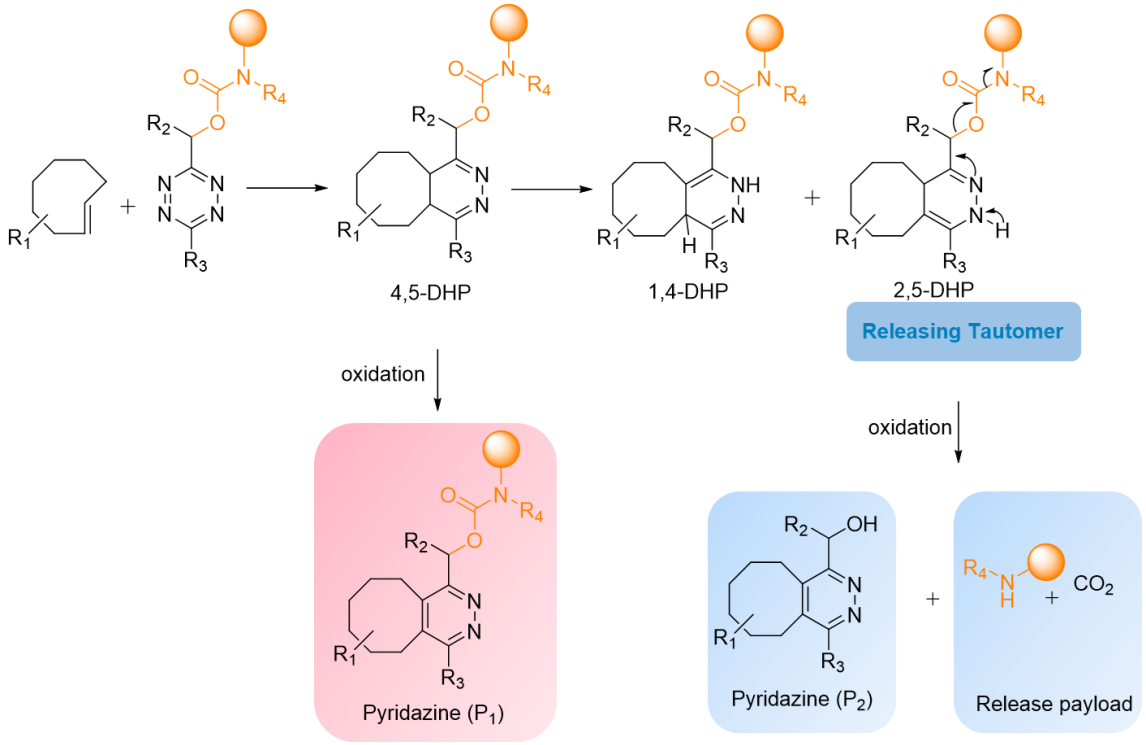

Scheme 2.10 *Schematic representation of mechanistic studies of a reaction of TCO with model tetrazine, affording 4,5-DHP and then 1,4-DHP and 2,5-DHP, of which one liberates dimethylamine, in conjunction with the formation of pyridazines P_1 and P_2.*

Since the discovery of the click-to-release strategy different derivatives of releasing TCOs have been developed. The reported compounds are discussed in the following section.

2.7.1 *Trans*-cyclooct-2-en-1-yl carbamate (r-TCO)

The r-TCO contains a carbamate substituent in the allylic position of TCO for the release of the payload. Upon reaction of r-TCO with Tz, a subsequent post-click tautomerization, and 1,4-elimination occurs, resulting in the cleavage of the carbamate and subsequent elimination of CO_2 and free amine.[218] The synthesis of r-TCO involves an initial epoxidation of cycloheptene, followed

by ring expansion to obtain *cis*-cyclooct-2-enol (2.32, Scheme 2.11). This compound is then subjected to photoisomerization, resulting in the formation of two isomers of *trans*-cyclooct-2-enol (2.33, Scheme 2.11) that can be further derivatized.[217] Notably, the allylic substituent leads to a 20-fold decrease in reactivity of the axial r-TCO (k_2 = 57.7 $M^{-1}s^{-1}$) when compared to *trans*-cyclooct-4-enol (k_2 = 1140 $M^{-1}s^{-1}$) in ACN at 20°C.[218] An unexpectedly larger difference in reactivity, with 156-fold lower reactivity, was measured for the equatorial hydroxyl-derived carbamate when compared to the axial substitution. This discrepancy in reactivity was attributed to steric hindrance, as well as potential electronic effects. With a half-life of 20 days, r-TCO showed comparable stability to *trans*-cyclooct-4-enol derivatives commonly used for IEDDA-based click ligation. Notably, r-TCO contains only one functional group that allows for chemical modification. Nevertheless, it has found utility as a click-removable tag, frequently employed in the design of caged drugs, enzymes, and proteins, and nanoparticle-based prodrug activation.[271-273]

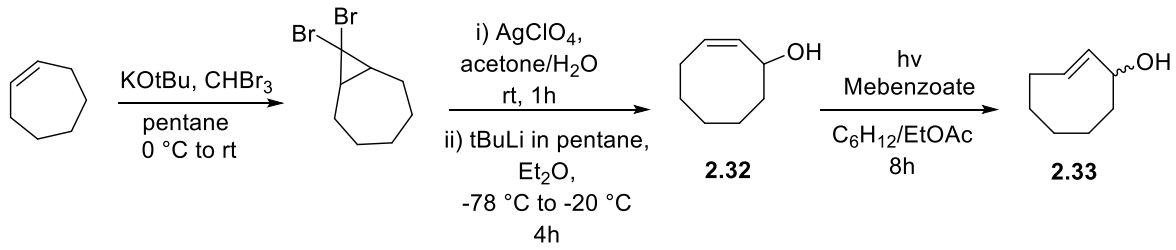

Scheme 2.11 *Synthesis of r-TCO.*

2.7.2 Click-cleavable TCO (cTCO)

In an attempt to develop bioorthogonally activatable ADC, Robillard and coworkers designed a click-cleavable TCO with an additional site for functionalization. This enabled a chemically controlled drug release through an *in vivo* reaction between a Tz and cTCO-linked ADC, which was pretargeted to a non-internalizing cell surface receptor.[274] The introduction of an additional functional group on the eight-membered ring offered the possibility to fine-tune the pharmacokinetics of the TCO by attaching a hydrophilic moiety. This approach was also employed to design prodrugs with improved solubility and reduced lipophilicity.[271, 275]

The synthesis of cTCO (2.37, Scheme 2.12) involved a lengthy 9-step procedure, starting from 1,4-cyclooctadiene. This included an iodolactonization of 4-cyclooctene-1-carboxylic acid, followed by hydrogen iodide elimination and lactone hydrolysis to stereoselectively install the hydroxyl in the allylic position while maintaining the *cis* configuration of the CO_2Me moiety. The installation of a

methyl group in the α-position was crucial to prevent undesired epimerization during lactone hydrolysis and to enable regioselective conjugation of cTCO (Scheme 2.12). Although it provides access to the single CCO diastereomer (as a racemic mixture), the preparation of cTCO demands a substantially higher effort. cTCO exhibited an exceptionally long shelf-life, with a half-life of 2.6 years for the *trans* isomer in a PBS stock solution at 4°C. In serum, the *trans* isomer demonstrated a stability half-life of 5 days, showing only a decrease in reactivity towards Tz without any payload release.[274]

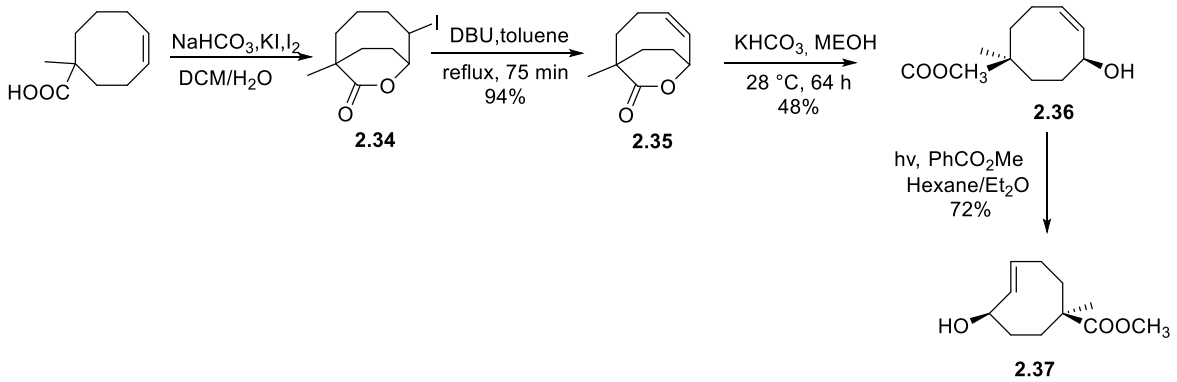

2.34 **2.35** **2.36** **2.37**

Scheme 2.12 *Synthesis of cTCO.*

2.7.3 Cleavable C_2-Symmetric *trans*-Cyclooctene (C_2TCO)

Mikula *et al.* developed a C_2-symmetric *trans*-cyclooctene (C_2TCO) with leaving groups at each of the two allylic positions of TCO with the axial configuration. Starting from 1,3-cyclooctadiene, the desired C_2TCO-diol (bis-axial) was prepared in three steps (Scheme 2.13). Flow-photoisomerization of the bis-diol (2.38) using TAg silica gel yielded bis-axial-TCO (47%) and bis-equatorial-TCO (30%). Second-order rate constants for the initial click reaction of up to 400 $M^{-1}s^{-1}$ were measured followed by instantaneous release. Complete cleavage (>99%) of C_2TCO conjugates was achieved within minutes even at low µM concentrations of both reactants. When bis sarcosinyl modified-C_2TCO was incubated in cell growth media (10% FBS) at 37 °C, more than 97% of C_2TCO remained stable for up to 48 h.[172]

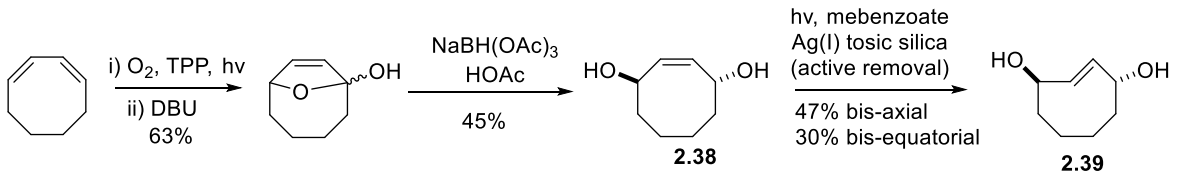

2.38 **2.39**

Scheme 2.13 *Synthesis of C_2-TCO.*

The C_2TCO conjugated to mAb and AF594 fluorophore was applied in a bioorthogonal *turn-off* strategy for extracellular and intracellular cleavage of fluorophore. Following the addition of 3-(1,2,4,5-tetrazin-3-yl)propanoic acid (HPA-Tz) a rapid cleavage of the fluorophore with a dramatic reduction in brightness and the near-complete elimination of the signal within 6 min of Tz addition was observed. Although fast and complete disassembly can be achieved with C_2TCO, one cannot control which one of the two groups is released, which could be an obstacle when controlled delivery of molecular cargo is required.[172]

2.7.4 Dioxolane-fused cleavable TCO (dcTCO)

Mikula *et al*. also developed a synthetic approach to enhance the accessibility of release TCOs through oxidative desymmetrization of a symmetric precursor.[173] This approach limited the number of possible isomers produced compared to allylic oxidation of non-symmetrical precursors, which can lead to a mixture of regio and stereoisomers, complicating the further synthesis. The diastereoselective synthesis involved oxidative desymmetrization of the TIPS-protected dioxolane-fused cis-cyclooctene (2.40) mediated by diphenyl diselenide. This process altered the position of the double bond in relation to the fused dioxolane. Subsequent photoisomerization allowed for the isolation of both equatorial and axial isomers (Scheme 2.14). By shifting the fused dioxolane from 5'/6' (d-TCO) to the 4'/5' position (dcTCO), the double bond adopted a less strained crown conformation, thereby increasing the stability while decreasing reactivity compared to d-TCO. The axial dcTCO derivative showed similar reactivity to r-TCO-PEG_4 with k_2 values of 74 $M^{-1}s^{-1}$ and 80 $M^{-1}s^{-1}$ respectively when reacted with DMT. On the other hand, the equatorial dcTCO demonstrated considerably lower reactivity, with a 30-fold decrease compared to the axial isomer, attributed to the increased steric demand of the carbamate in the transition state at the equatorial release position.

Incubation of axial dcTCO in PBS at 37 °C showed good stability, with 99% intact dcTCO remaining after 96 h, surpassing the high stability of rTCO. Additionally, logP calculations for a range of derivatives indicated a significantly reduced lipophilicity of dcTCO compared to r-TCO with an average difference in $c\log P_{7.4}$ value of −1.74. Cell experiments demonstrated over 1000-fold reduction in cytotoxicity for the dcTCO conjugated prodrug of CA4 in comparison to native CA4. The activity of the prodrug was fully restored upon Tz-triggered bioorthogonal cleavage of the dcTCO linker.[173]

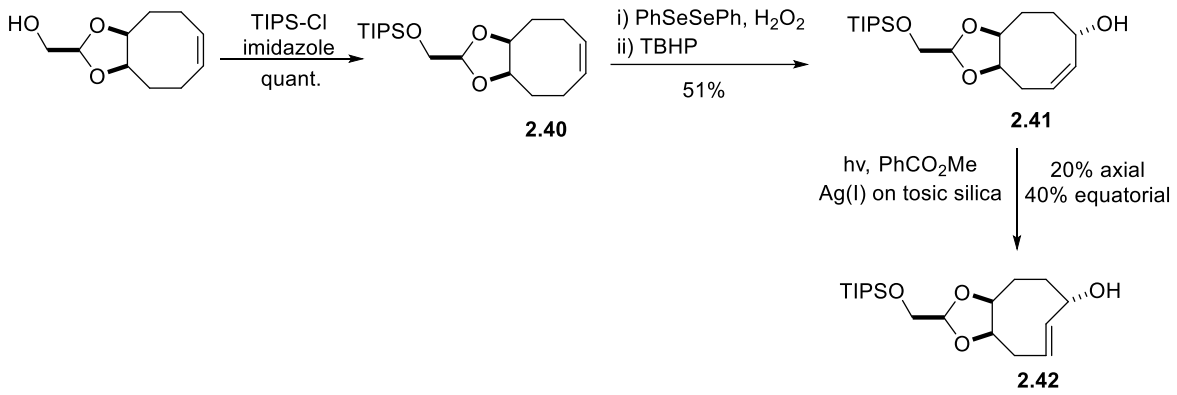

Scheme 2.14 *Synthesis of dcTCO.*

2.7.5 Cleavable s-TCO

The reactivity of release TCOs with allylic substitution is lower than the parent TCO, necessitating a higher dose of the tetrazine activator for efficient release. An increase in reaction rate is desired *in vivo* as this enables the use of a lower activator dose.[218] Based on the reactivity enhancement of TCO through the *cis* fusion of a cyclopropane ring, Robillard and coworkers envisioned developing a cleavable s-TCO with a syn-positioned carboxylic acid substituent on the fused cyclopropane of a BCN. Two different approaches were described starting from 1,3-cyclooctadiene or 1,5-cyclooctadiene (Scheme 2.15 A and B). In both cases, two *trans*-cyclooctene isomers with the hydroxyl groups at the axial and equatorial positions were generated.[174]

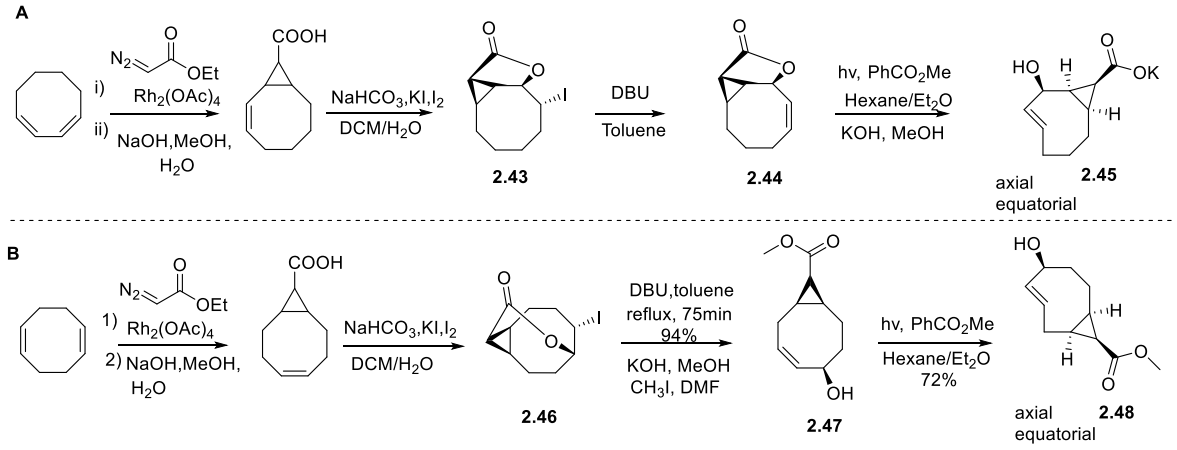

Scheme 2.15 *A): Synthesis of difunctionalized s-TCO derivative starting from 1,3-cyclooctadiene B) Synthesis of difunctionalized s-TCO derivative starting from 1,5-cyclooctadiene.*

When studied for their reactivity, the equatorial isomers of both s-TCOs were slower in comparison to the axial isomers. The s-TCO cleavable linkers derivatized with *N*-methyl benzylamine demonstrated higher reactivity with DMT in ACN when compared to the parent r-TCO (0.54 $M^{-1}s^{-1}$)

with similar allylic benzylamine substituent.[218, 274] 1,3-s-TCO (2.45) showed a 15-fold increase in rate with a k_2 of 8.0 $M^{-1}s^{-1}$, whereas 1,5-s-TCO (2.48) gained a 5-fold increase in reactivity with a k_2 of 2.9 $M^{-1}s^{-1}$.[274] *In vitro,* studies investigating payload release upon treatment with DMT revealed a complete release within 30 min for both s-TCOs. Stability evaluation of s-TCO conjugates with CC49 in PBS at 4°C revealed good stability for up to 1 year for 1,5-sTCO (2.48). On the other hand, 1,3-s-TCO (2.45) showed deactivation within a few days making it unsuitable for release applications. *In vivo*, 1,5-s-TCO (2.48) showed a deactivation half-life of 5.6 days, which is comparable to that of the state-of-the-art TCO linker with a similar allylic benzylamine substituent.[274, 276]

Similarly, Rutjes and coworkers also developed a synthetic pathway to obtain the strained difunctionalized releasing TCO. The novel synthetic pathway allowed for the installation of the two orthogonal handles in only four steps.[175] The monocyclopropanation of 1,5-cyclooctadiene with ethyl diazoacetate afforded a mixture of the *exo*- and *endo*-diastereomers in a 2:1 ratio, respectively. The *endo*- and exo-diastereomers were then separately activated by *N*-iodosuccinimide (NIS) in the presence of sodium acetate and acetic acid, generating the acetylated iodohydrin (2.50) in a single step.[277] Subsequent dehydroiodination reaction resulted in the difunctionalized *cis*-cyclooctene (2.51) which was photoisomerized into the TCO derivative, yielding both axial and equatorial isomers (Scheme 2.16). In contrast to the diastereomers formed through the *exo*-pathway, the diastereomers from the *endo*-pathway remained inseparable.

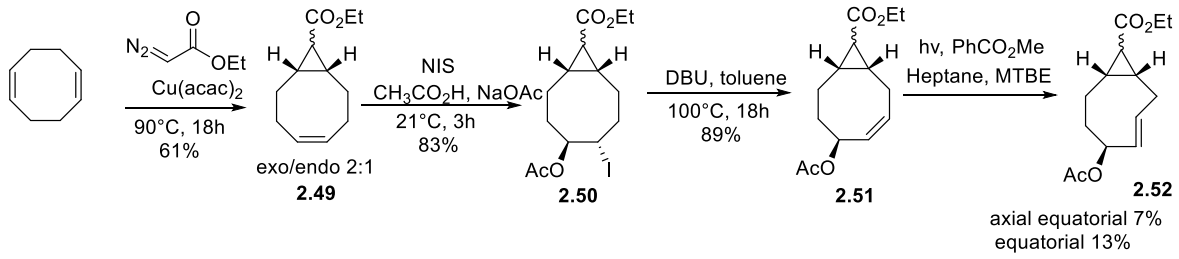

Scheme 2.16 *Synthesis of difunctionalized s-TCO derivative starting from 1,5-cyclooctadiene.*

The click kinetics of the axial *exo*-TCO demonstrated second-order rate constants in ACN at room temperature with k_2 values of 594.0 $M^{-1}s^{-1}$ and 0.8589 $M^{-1}s^{-1}$ with 3,6-dipyridyl-s tetrazine and DMT, respectively. *In vitro* experiments showed that over 50% of the payload was released when the *exo*-axial TCO was reacted with DMT. The stability of the releasing axial TCO was investigated in both PBS and mouse serum at 37 °C. The free carboxylic derivative of axial TCO remained stable after seven days in PBS and up to 4 h in mouse serum. Although no isomerization was observed, the

compound showed degradation over time in mouse serum (16h).[175] The *exo*-derivative of difunctionalized cleavable s-TCO linker was modified with Dox at the allylic alcohol. When evaluated in Hela cells, the s-TCO caged Dox showed a 21-fold increase in cytotoxicity following the addition of DMT, when compared to prodrug alone. The improved synthetic pathways and kinetics of these release TCOs open possibilities to further fine-tune the parameters of the *in vivo* cleavage reactions.

2.8 Applications of TCO in targeted drug delivery

The click-to-release strategy holds great potential for enabling targeted drug delivery to cancerous tissues, offering an alternative approach to traditional antitumor drugs with their associated toxic effects and limited efficacy. By utilizing the locally triggered click-to-release mechanism, antitumor drugs can be specifically delivered or activated at the tumor sites, potentially reducing toxicity and enhancing therapeutic outcomes.

2.8.1 Tetrazine triggered drug cleavage from TCO conjugates

The Robillard group was the first to validate the use of click-to-release *in vivo*. Following their initial study with r-TCO, the group demonstrated the use of a bifunctional click cleavable TCO-linker (cTCO), which could be conjugated with an antibody and a payload for targeted drug release in mice.[274] The cTCO-Dox prodrug was conjugated to the CC49 antibody which targets TAG72 antigen. The ADC exhibited good *in vivo* stability with only a negligible amount of TCO-deactivation (10% over 26h) In an LS174T tumor-bearing mouse model, the ^{125}I-labeled ADC showed a high tumor uptake of 30–40% ID/g at 30 h after injection. Although the ADC could be selectively activated by Tz, the release yields of Dox were rather unsatisfactory likely due to the rapid clearance of the trigger, DMT. However, modification of DMT with dextran resulted in the release of up to 51.3% of Dox 24 hours after injection, emphasizing the importance of selecting a Tz that persists longer in circulation.[274]

Following this, the Robillard group reported the use of the ADC approach utilizing diabody conjugates (Figure 2.14). Monomethyl auristatin E (MMAE) caged by a bifunctional cTCO was conjugated to diabody through maleimide conjugation. The ^{125}I-labeled ADC showed fast clearance and selective uptake in the LS174T tumor with an uptake value of 29 %ID/g matching the uptake value of CC49 mAb in the same tumor model. Additionally, the group replaced the DMT-dextran

with a 3,6-bisalkyl-Tz-DOTA as a decaging activator. The introduction of a DOTA chelator on the Tz reduced the clearance rate and increased the decaging yield. The on-tumor reaction between the cTCO-ADC and the DOTA-Tz, examined through a blocking study revealed no tumor uptake of [^{177}Lu]Lu-3,6-bispyridyl-DOTA-Tz in group where 3,6-bisalkyl-DOTA-Tz was administered as a blocking agent before the radiotracer. In contrast, in the control group where no Tz-activator was injected, a high tumor uptake of [^{177}Lu]Lu-3,6-bispyridyl-DOTA-Tz was observed.

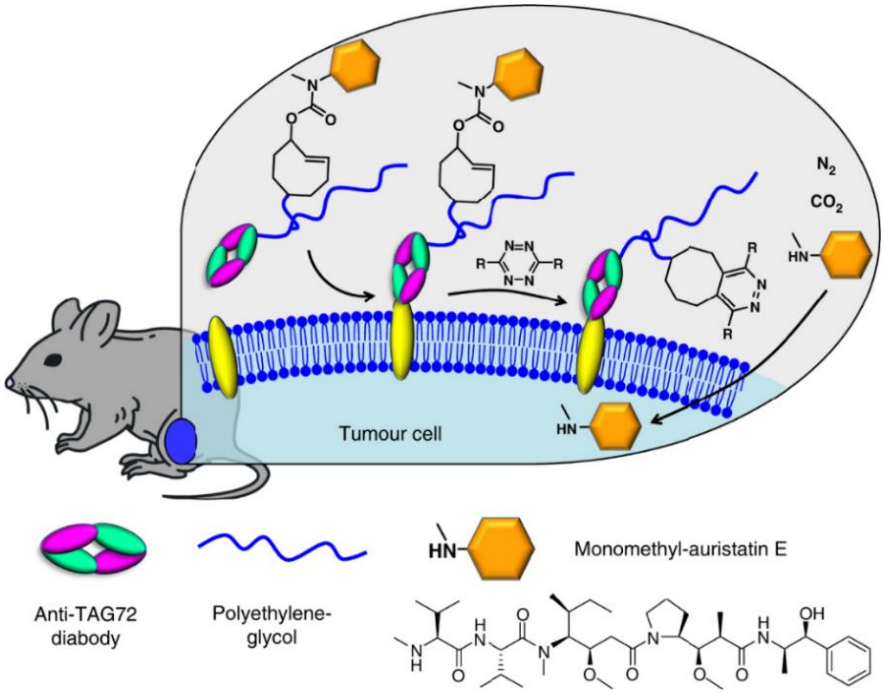

Figure 2.14 *Schematic representation of on-tumor liberation of a cell-permeable drug (monomethyl auristatin E, MMAE) from a trans-cyclooctene-linked ADC following systemic administration of a tetrazine activator. Reprinted from Rossin et al.[276] Published by Springer Nature and distributed under the Creative Common Attribution License 4.0 (CC BY).*

When examined for drug release levels in tumor vs other tissues, a 100-fold lower MMAE level was observed in the liver and plasma in comparison to tumor in the group treated with cTCO-ADC followed by 3,6-bisalkyl-DOTA-Tz. Notably, a potent therapeutic effect was observed in two mouse xenograft models, LS174T, and OVCAR-3 treated with cTCO-ADC conjugate and 3,6-bisalkyl-DOTA-Tz.[276] The multi-dose study with four cycles of the ADC-and Tz trigger resulted in tumor regression and survival of mice until the end of the study. The study highlights the potential of small molecule-triggered decaging reactions for therapeutic purposes.

Mejia-Oneto *et al* reported a “catch and release” strategy for controlled tissue-specific drug release in mice with soft tissue sarcoma. They used a TCO-carbamate-Dox prodrug with 75 times lower

cytotoxic activity against HT1080 cells compared to Dox. Initially, a tetrazine-modified hydrogel was injected at the tumor site, followed by intravenous injection of the TCO-prodrug, the bioorthogonal reaction (the 'catch' step) occurred as the prodrug circulated and reached the target site, leading to its concentration at the tumor site. Subsequent tautomerization and release of the active drug resulted in improved antitumor efficacy and reduced myelosuppression compared to a control group treated with free Dox.[271]

Czuban and co-workers also applied a similar approach to concentrate and activate systemically administered antibiotic prodrugs using a hydrogel platform containing multiple Tzs. This enabled the activation of multiple dosages of the prodrug, efficiently inhibiting the planktonic and biofilm growth of bacteria.[278]

Following this, Rozyen and coworkers introduced the click-activated protodrugs against cancer (CAPAC) platform, termed SQ3370 (Figure 2.15). A tetrazine-modified hyaluronate-based biopolymer (SQL70) was injected at the tumor site followed by the systemic administration of a TCO-modified prodrug with attenuated activity. Here too, the use of a bifunctional cTCO allowed for its modification with a cytotoxic payload on one end and a hydrophilic group on the other, improving the pharmacokinetics of the prodrug. The lead candidate SQP33, consisting of a TCO functionalized with Dox and glycine, showed improved aqueous solubility and 83 times lower cytotoxicity than the parent compound. In mice, the maximum tolerated dose (MTD) of SQP33 in combination with locally injected SQL70 was determined to be 19.1 times the MTD of free Dox. Pharmacokinetics studies in rats show that a single injection of SQL70 efficiently captures multiple SQP33 protodrug doses given cumulatively at 10.8 times the MTD of conventional doxorubicin, with significantly reduced systemic toxicity. Moreover, combined treatment with SQL70 and SQP33 showed significantly slowed down tumor growth, and prolonged overall survival in a syngeneic tumor mice model with MC38 flank tumors.[275] This approach holds great promise as it allows the concentration and local activation of cytotoxic drugs at the tumor site allowing larger therapeutic doses under a better safety profile. A first-in-human Phase II clinical trial of SQ3370 in patients with advanced solid tumors is ongoing.[279] It should be noted, however, that injectable hydrogel-based activation is primarily limited to the treatment of resectable tumors due to the requirement for hydrogel installation at the target site.

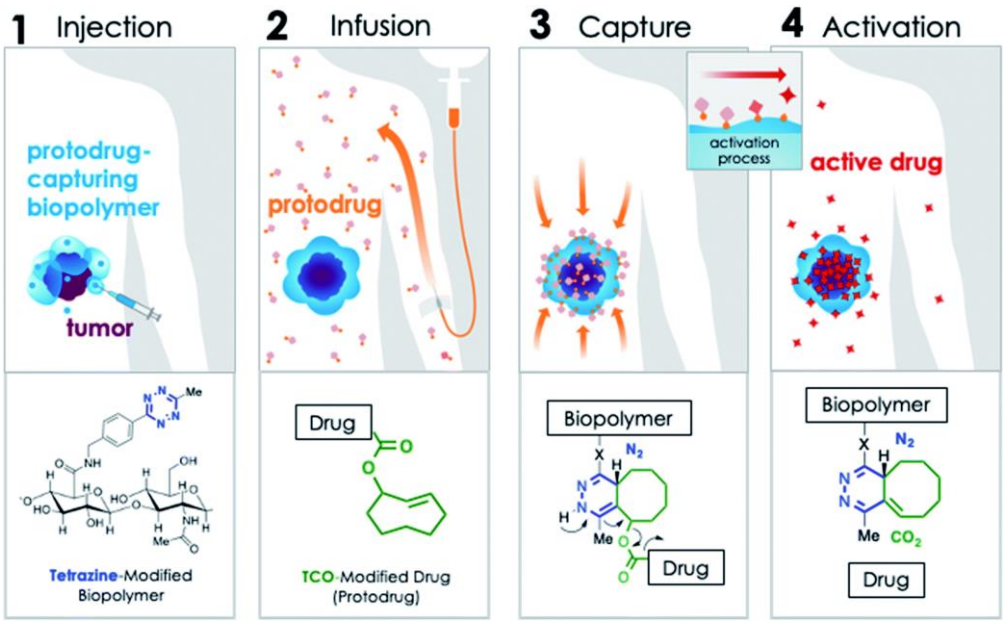

Figure 2.15 *Mechanism of CAPAC platform. 1) Tz-modified biopolymer is locally injected at the pathological site. (2) A TCO-modified drug (protodrug) is infused systemically. (3) The protodrug is captured by the biopolymer at the desired site through a rapid covalent reaction between Tz and TCO moieties, followed by (4) chemical rearrangement to release the active drug. Reprinted from Royzen et al.*[275] *with permission from the Royal Society of Chemistry.*

The applications of Tz-triggered release have been explored in various contexts to achieve spatiotemporally controlled prodrug activation. Chen *et al* conjugated a tetrazine to a phosphorylated self-assembly tri-peptide motif, KYF. In response to the upregulation of phosphatase in cancer cells, enzyme-instructed supramolecular self-assembly (EISA) was triggered, resulting in the specific accumulation of Tz-KYF inside cancer cells. Upon treatment with a TCO-Dox prodrug, tumor inhibition, and selectivity for cancer over non-cancer cells were observed.[280]

In another example, image-guided prodrug activation was achieved using fluorescently labeled magnetic iron oxide nanoparticles. These nanoparticles were modified with both a Tz and a fluorophore. Fluorescent imaging confirmed the accumulation of the nanoparticles specifically inside MDA-MB-231 breast cancer cells. Subsequent addition of TCO-Dox prodrug led to an efficient release of the active Dox.[281]

In another study, TCO-Dox prodrug and tetrazine were separately encapsulated into micelles that are sensitive to low pH and matrix metalloproteinase 2 (MMP-2), conditions characteristic of the tumor microenvironment (TME). Upon systemic administration in mice with 4T1 tumors, the nanoparticles dissociated specifically in the tumor cells, leading to the selective activation of the

prodrug in TME and inhibition of tumor development, while demonstrating lower toxicity in non-target tissues.[282]

In another example, the controlled activation of cytotoxic T-cells was demonstrated both *in vitro* and *in vivo*. Epitopes essential for T-cell activation were caged by modifying a key lysine residue with TCO-protecting groups. Upon the addition of a Tz, T-cell receptor activation was restored. The use of a cTCO-protecting group containing an additional polar group resulted in enhanced solubility and decaging yield. This approach was successfully implemented in two different epitopes, indicating its potential as a generic application to lysine-sensitive T-cell receptors.[194] In another case, siRNA molecules were inactivated through conjugation to nanoparticles using a bifunctional TCO. After accumulation in cells, the introduction of a tetrazine resulted in linker cleavage and activation of siRNA. This led to RNA interference and subsequent gene silencing in the targeted cells.[283] These examples highlight the versatility of the TCO-tetrazine reaction in controlling cellular processes and modulating biological functions.

Alternative applications include cell-selective proteome labeling.[284] A mAb-tetrazine conjugate (cetuximab-Tz) was used to target cells overexpressing EGFR, followed by the addition of a modified nucleoside, TCO-puromycin. Upon IEDDA decaging at the target site, the TCO-protecting group is removed, enabling the incorporation of puromycin into protein synthesis. This strategy allowed for selective labeling even in heterogeneous co-cultured cells with labeling observed exclusively in cells expressing the antigen.

The click-to-release reaction has also been applied to enable High-Performance Liquid Chromatography (HPLC)-free synthesis of RNA.[285] A cleavable TCO linker was coupled to the RNA strand in the final coupling step. Subsequently, the TCO-coupled RNA strand was treated with agarose modified with 3,6-dipyridyl-s-tetrazine, facilitating the selective trapping of the product onto Tz-modified agarose. By employing a Tz that undergoes slow elimination, all by-products can be filtered from the resin before the TCO group is cleaved, thereby generating the desired product without contaminants. Finally, a TCO thiocarbamate has also been described for the release of carbonyl sulfide, which is converted to H_2S by carbonic anhydrase.[286]

2.9 Future perspectives

Trans-cyclooctenes (TCOs) have emerged as an indispensable tool in the field of chemical biology and nuclear medicine. With their rapid kinetics and high selectivity towards tetrazines, the TCO-Tz ligation has become a cutting-edge approach in various chemical transformations, labeling of biomolecules and for the release of bioactive compounds. In our review, we explored different types of TCOs and discussed recent advancements in the synthesis of their derivatives, as well as their reactivity and stability profiles. We showcased the versatility of TCOs through examples of their applications in ligation and release chemistry, where they have proven to be powerful tools for targeted imaging and drug delivery platforms.

While recent developments are promising, several key challenges must be addressed in the future. Although many TCOs have been developed and efforts have been made to establish more feasible synthetic pathways, functionalized TCOs remain relatively inaccessible compared to their tetrazine counterparts. Often, the synthetic routes are lengthy and result in low yields, and some derivatives suffer from inseparable diastereomer formation. For instance, the more hydrophilic oxo-TCO is used as a diastereomeric mixture. Although flow-photoisomerization has facilitated the synthesis of different TCOs, upscalability and ease of purification of the produced diastereomers remain challenging.

Additionally, stability poses another challenge for the use of TCOs. A slow isomerization *in vivo* is acceptable considering its fast kinetics. Moreover, non-crystalline derivatives of strained TCOs tend to isomerize during prolonged storage. However, storing these derivatives as stable silver(I) (Ag(I)) metal complexes can extend their shelf-life, which can be readily dissociated upon the addition of NaCl.[222] Storing TCOs as Ag(I)-TCO complexes might offer a solution for long-term storage.

Moreover, different stability requirements are necessary for bioorthogonal partners. Bioorthogonal tags require higher stability as they reside in biological environment throughout the entire duration of an experiment, whereas reporter probes only need to be stable during the labeling phase. Consequently, *trans*-cyclooct-4-enol has often been the bioorthogonal tag of choice for *in vivo* applications, as it is less prone to isomerization than s-TCO and d-TCO. For live cell applications, faster-reacting s-TCO and d-TCO are highly valuable as reporting probes, as only a short incubation times is required owing to their rapid kinetics. Several studies have utilized these probes for cellular

and *in vivo* experiments. However, the hydrophobicity of TCO and s-TCO probes has also led to significant nonspecific labeling, necessitating intensive washing steps. Novel *trans*-5-oxocene and a-TCO have shown improvement due to their increased hydrophilicity, but only a few studies have been reported to date using these compounds. Overall, there is a need to develop TCO derivatives with enhanced stability and increased hydrophilicity while still displaying rapid kinetics under cellular or *in vivo* conditions.

In the field of radiochemistry, radiolabeled TCOs have functioned as prosthetic groups and facilitated the labeling of proteins and peptides at physiological and mild conditions, enabling the imaging of diverse molecular targets. Similarly, the use of TCO-Tz ligation has revolutionized the field of pretargeted imaging, resulting in specific tumor uptake in tumor tissue and higher image contrast, ultimately leading to improved patient outcomes with reduced radiation burden and toxicity. Several preclinical studies have employed this approach. Nonetheless, the clinical translation of the pretargeting approach based on IEDDA is still lacking. A noteworthy milestone is the recently FDA-approved human clinical trial for the PET imaging of pancreatic cancer patients, using [^{64}Cu]Cu-Tz-SarAr and hu5B1-TCO through a pretargeting approach.[86]

The reverse approach, where a tetrazine is conjugated to a biological vector, enables the use of fast-reacting TCOs when rapid reaction kinetics are paramount. Although a few examples of pretargeted strategies with TCO and d-TCO derivatives are available, substantial improvements in tumor-to-background ratios are required. The inherent hydrophobic core of these probes often leads to high abdominal uptake, compromising the image contrast. Therefore, the challenge lies in developing stable and hydrophilic TCOs with high reactivity and functional handles that allow the modulation of pharmacokinetics to reduce nonspecific accumulation. Additionally, pretargeted radiotherapy through TCO-Tz ligation is an emerging field with significant therapeutic potential.

Similarly, decaging reactions using TCO-cleavable linkers have shown great potential in targeted drug delivery. This approach expands the range of targets for antibody-drug conjugate (ADC) therapy beyond those relying on existing intracellular activation mechanisms. Studies aimed at expanding the number of functional groups that can be decaged from TCO have been conducted. This enables the decaging of a variety of functional groups, expanding the scope for unmasking of drugs, amino acid residues, proteins and other biomolecules. These applications demonstrate the

broad utility of the TCO-tetrazine reaction beyond bioorthogonal chemistry, paving the way for innovative strategies in cell labeling, RNA synthesis, and controlled release of bioactive compounds. A human clinical trial with hydrogel-based platform SQ3370 for the release of a cytotoxic drug has already moved towards phase II. Furthermore, studies aiming to optimize the therapeutic effect of ADCs have been reported for pretargeted tumor treatment. In brief, the utilization of TCO as a reactant in inverse-electron-demand Diels-Alder (IEDDA) reactions holds immense potential and bears substantial implications for the progress of individualized therapy.

OBJECTIVES AND OUTLINE

Objectives and Outline

Pretargeted imaging through inverse electron-demand Diels-Alder (IEDDA) reaction enables the combination of specificity of antibodies with the use of short-lived radioisotopes such as Fluorine-18 for PET imaging. This facilitates the early visualization of molecular targets with the potential of improving target-to-background ratios while minimizing radiation exposure to the patients. Moreover, the versatility of the strategy allows it to be adapted to study diverse molecular targets.

Current pretargeting studies often suffer from low tumor-to-blood ratios leading to high background signals due to unfavorable pharmacokinetics or *in vivo* instability of the radiolabeled compounds. To ensure successful clinical translation, it is crucial to improve the stability and pharmacokinetics of small molecules to achieve high target-to-non-target radioactivity concentrations, shortly after the radiotracer administration. For this, the tracer should accumulate rapidly at the target site while displaying short residence times at off-target sites. Given the need for selective accumulation and reactivity of the two components at the desired tissue, the reagent stability, as well as the reaction kinetics of the reagents must be exceptionally high. Furthermore, the reagents should be easy to synthesize to enable the reaction's widespread use. Overall, there is a need for further investigation to refine the pharmacokinetics of the IEDDA reaction partners to enhance the applicability of this strategy.

Most pretargeting studies are based on the use of TCO-mAb conjugates and radiolabeled tetrazines. However, TCO is known to isomerize to *cis*-cyclooctene when exposed to Cu-bound serum proteins, making it several orders of magnitude less reactive with tetrazines. Moreover, TCO also tends to bury inside the protein core, leaving only a few reactive tags for the *in vivo* reaction with tetrazine. To circumvent this issue, we aimed to replace the TCO moieties conjugated to the targeting vector with more stable tetrazines. The replacement of TCO with stable tetrazines is expected to address both the physiological deactivation and hydrophobic burying of the tags. Moreover, recent advancements have led to the development of faster-reacting strained TCO derivatives, such as *cis*-dioxolane-fused TCO (d-TCO). The combination of these faster-reacting radiolabeled TCOs with stable tetrazines holds the potential to enhance the *in vivo* ligation in the pretargeting approach. Therefore, the objective of this doctoral dissertation was to develop novel radiofluorinated

derivatives of TCO and *cis*-dioxolane fused trans-cyclooctene (d-TCO) with the overarching aim of improving the *in vivo* pretargeting efficacy (Figure 1). Subsequently, their potential as PET probes was evaluated in a bioorthogonal pretargeted imaging setting. Additionally, a fluorescence-based cell permeability assay was developed to assess the cellular permeability of the d-TCOs and their ability to react in intracellular compartments for the visualization of internalizing targets.

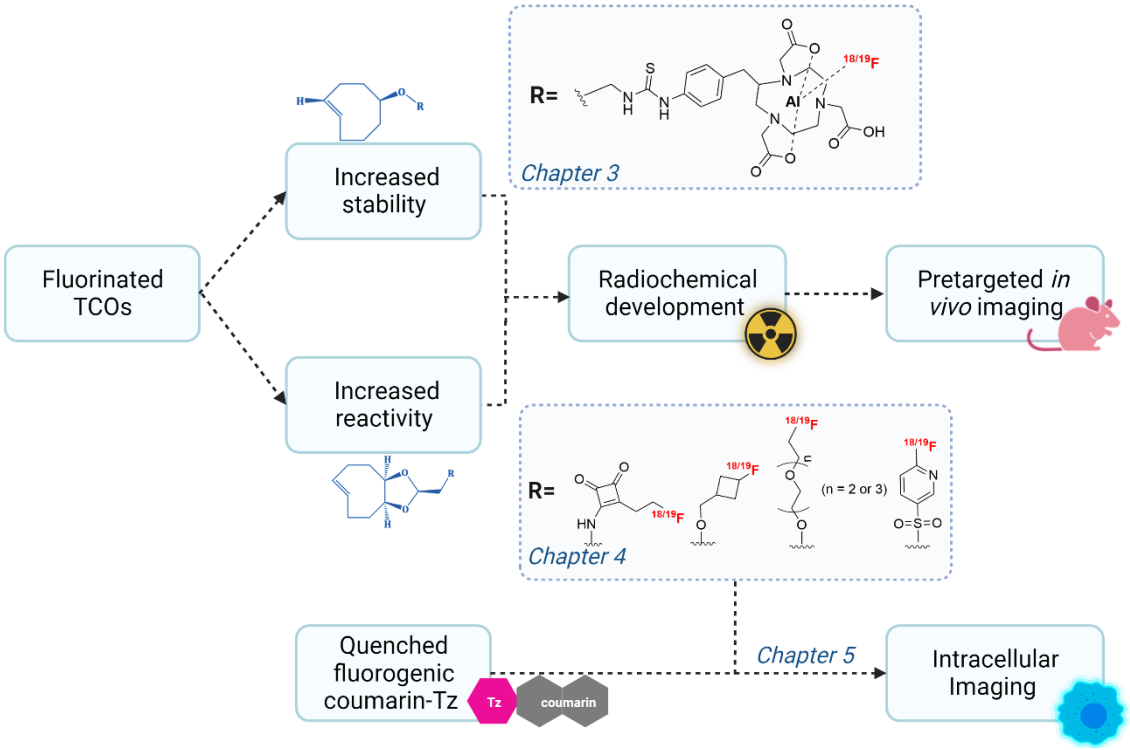

Figure 1 *Schematic overview of the objectives of the doctoral dissertation. The synthesized TCO-and d-TCO derivatives are evaluated in a pretargeted imaging setting. Chapter 3 describes the development and evaluation of a stable TCO-NOTA derivative. Chapter 4 focuses on the development and evaluation of d-TCO derivatives. Chapter 5 explores the cell-permeability and intracellular click-liagtion ability of d-TCO derivatives for imaging of intracellular targets using fluoroscence quenched coumarin-tetrazine probes.*

Chapter 1 serves as an introductory chapter, with a general introduction to immuno-PET and the pretargeting approach. It outlines the fundamental concepts of bioorthogonal chemistry and the use of ^{18}F-radiolabelling methodologies, to create the framework for the following chapters.

Chapter 2 provides an overview of the IEDDA reaction mechanism and the factors that influence the kinetics followed by an extensive overview on TCO. The chapter describes the recent development in the discovery of novel TCOs and derivatives, their synthesis, reactivity, stability, and biomedical applications.

Chapter 3 describes the development of [^{18}F]AlF-labeled 5-hydroxy-TCO-NOTA derivative as a radiotracer with improved metabolic stability and its evaluation as a counterpart for IEDDA reaction with a tetrazine-tagged antibody. The biodistribution and *in vivo* stability of this novel ^{18}F-labeled 5-hydroxy-TCO were studied. Its potential for pretargeting PET imaging was evaluated in LS174T tumor-bearing mice pre-treated with a tetrazine-modified anti-TAG-72 monoclonal antibody (CC49).

Given the relatively slow reaction kinetics of 5-hydroxy-TCO, Chapter 4 shifts toward the use of faster-reacting highly strained d-TCO derivatives. Chapter 4 reports on the development and *in vivo* evaluation of fluorinated d-TCO derivatives. A small series of d-TCO derivatives with structurally diverse linkers was synthesized. The linkers incorporated were chosen to improve the pharmacokinetics of the derivatives as well as to increase the metabolic stability of the synthesized compounds. The newly synthesized derivatives were assessed for their reaction kinetics and the *in vivo* ligation capability with mAb-bound tetrazines in a pretargeted blocking experiment. From the assay, the two most promising compounds were further radiochemically developed and evaluated for their pharmacokinetics and stability *in vivo*. [^{18}F]MICA-214 with a squaramide linker showed higher *in vivo* stability and favorable pharmacokinetics. Therefore, [^{18}F]MICA-214 was selected for *in vivo* pretargeted PET imaging in LS174T colorectal tumor-bearing mice pretreated with a tetrazine-modified anti TAG-72 monoclonal antibody (CC49).

Beyond the cell surface targets, Chapter 5 explores the possibility of visualization of intracellular or internalizing targets. We envisaged that the intrinsic hydrophobicity of the d-TCO compounds could facilitate membrane permeation, enabling the visualization of intracellular targets. To test the hypothesis, a cell permeability assay was used to evaluate the d-TCO derivatives developed in Chapter 4 employing the turn-on fluorescence properties of tetrazine-conjugated fluorophore. The chapter describes the synthesis of Coumarin-tetrazine derivatives conjugated with Ibrutinib. The conjugate was used in a cell fluorescence assay to evaluate the ability of the fluorinated d-TCO compounds to cross the cell membrane.

Finally, Chapter 6 provides the general discussion of this dissertation, offering insights into the prospects for the development of TCOs as radiotracers and their potential applications in pretargeted imaging and therapy.

CHAPTER 3

Improved stability of a novel fluorine-18 labeled TCO analogue for pretargeted PET imaging

Based on the publication:

Eduardo Ruivo, Karuna Adhikari, Filipe Elvas, Jens Fissers, Christel Vangestel, Steven Staelens, Sigrid Stroobants, Pieter Van der Veken, Leonie Wyffels, Koen Augustyns

Improved stability of a novel Fluorine-18 labeled TCO analogue for pretargeted PET imaging. *Nucl Med Biol.* **2019**;76-77:36-42.

doi:10.1016/j.nucmedbio.2019.11.001

Contribution:

Synthesis of intermediates, cold-reference, and precursor for radiolabeling, development of radiolabeling procedure, *ex vivo* biodistribution

Chapter 3 Improved stability of a novel fluorine-18 labeled TCO analog for pretargeted PET imaging

3.1 Abstract

Introduction: Biorthogonal pretargeted imaging using the inverse electron demand Diels Alder (IEDDA) reaction between tetrazine (Tz) and *trans*-cyclooctene (TCO) is one of the most attractive strategies in molecular imaging. It allows the use of short-lived radioisotopes such as fluorine-18 for imaging of long circulating vectors with improved imaging contrast and reduced radiation dose. Here we aim to develop a novel ^{18}F-labeled trans-cyclooctene (TCO) with improved metabolic stability and assess its potential usefulness in a pretargeted PET imaging approach.

Results: The radiotracer was obtained with a radiochemical yield (RCY) of 12.8 ± 2.8% and a radiochemical purity (RCP) of ≥95%. It also showed a promising *in vivo* stability with 51.9 ± 5.16% of radiotracer remaining intact after 1h. The biodistribution in healthy mice demonstrated mixed hepatobiliary and renal clearance, with a rapid blood clearance and low uptake in other tissues. The low bone uptake indicated lack of tracer defluorination. Interestingly, a pretargeted PET imaging experiment showed a significantly increased radiotracer uptake (0.67±0.16 %ID/g, $p<0.001$) in the tumors of mice pre-treated with CC49-tetrazine compared to the CC49 alone (0.16±0.08 %ID/g).

Conclusions: [^{18}F]MICA-205 represents a large improvement in *in vivo* metabolic stability compared to previous reported ^{18}F-labeled TCOs, allowing a clear visualization of tumor tissue in a small-animal pretargeted PET imaging experiment. Despite the favorable *in vivo* stability and image contrast obtained with [^{18}F]MICA-205, the development of next-generation derivatives with increased absolute tumor uptake is warranted for future pretargeting applications.

3.2 Introduction

Positron emission tomography (PET) is a non-invasive imaging modality with the capacity to track radiolabeled (bio)molecules *in vivo*. Of the common radionuclides used in PET, Fluorine-18 is the most broadly utilized radionuclide due to its high positron efficiency, high specific radioactivity and clinically attractive half-life (~110 min).[287] These properties minimize the toxic effects of radiation exposure to the patient while increasing the imaging resolution. However, the relatively slow pharmacokinetics of radiolabeled monoclonal antibodies (mAbs) require the radioactive half-life of the isotope to be compatible with the long biologic half-life of the mAbs. For this reason, mAbs are often labeled with isotopes with long physical half-lives (e.g. ^{89}Zr, $t_{1/2}$ = 78 h). Long-lived isotopes allow time for the mAbs to accumulate at the target site while simultaneously preventing the premature decay of their radioactive payload. However, this combination of long biologic and physical half-lives gives rise to a critical limiting complication: high activity concentrations and radiation doses to non-target organs.[288] To circumvent this problem, considerable attention has been dedicated to the development of targeting methodologies that combine the specificity of mAbs with the pharmacokinetics of smaller molecules. One particularly appealing method of achieving this balance while still using intact mAbs is termed pretargeting. This method involves 4 steps: the injection into the bloodstream of a bivalent mAb with the ability to bind both an antigen and a radioligand; the slow accumulation of the mAb at the target and concomitant clearance of the mAb from the blood and non-target tissues; the injection into the bloodstream of the small-molecule radioligand; and the binding of the radioligand to the mAb, followed by the rapid clearance of excess radioactivity. The fast blood clearance and distribution of the small-molecule ligands not only reduces background radiation dose to non-target organs but also facilitates the use of radioisotopes with short half-lives such as Fluorine-18 that would normally be incompatible with mAb-based imaging. In recent years, biorthogonal chemistry emerged as a potential tool to aid in the creation of novel, mAb-based pretargeting systems.[85, 89] Regarding bioorthogonal chemistry, inverse-electron-demand Diels-Alder (IEDDA) reaction between tetrazine and *trans*-cyclooctene (TCO) appears to be the most suitable of all reactions tested so far for pretargeting due to its biocompatibility and relatively fast reaction kinetics. Nonetheless, the kinetics and *in vivo* stability of IEDDA ligands still need further improvement to become truly applicable in a broad range of pretargeting applications. This could be achieved, for example, by introducing suitable modifications either on the TCO or on the tetrazine moieties.[39]

Bifunctional chelators can provide an efficient method for radiolabeling different chemical moieties and biomolecules with ^{18}F via $Al^{18}F$ chelation in aqueous medium. The hexadentate ligand 1,4,7-triazacyclonanne-1,4,7-triacetic acid (NOTA) is a macrocyclic chelator with promising properties for radiolabeling of peptides and small molecules with Fluorine-18. Zeglis *et al.* performed a proof-of-concept study with Al[^{18}F]F-NOTA labeled tetrazine showing this strategy to be a stable and synthetically efficient methodology for *in vivo* biorthogonal chemistry. They have also shown that the structural modifications could increase the excretion of the radiotracer *via* the renal system improving the tumor-to-background ratios at early time points.[289] However, this approach has a few shortcomings related to the long-term instability of TCO bound to mAbs in physiological conditions and hydrophobic burying of the TCO-tag within the target molecule.[78, 290] As an alternative to the conventional approach, in 2016 our group reported the inverse strategy where tetrazines were studied as tags for antibody modification and radiolabeled TCOs as imaging probes in order to overcome the limitations of the previous approach. The usefulness of this approach was demonstrated in a pretargeted live-cell fluorescent imaging experiment resulting in a selective and rapid labeling of cells. The obtained results suggested the translation of this approach for *in vivo* pretargeted PET imaging applications.[201] In a first study, our group performed the ^{18}F-labeling of a TCO and its biodistribution. However, its fast metabolization with non-specific accumulation in bone made its utility limited for pretargeted imaging.[291] In the current study, AlF-NOTA labeling was applied for the radiofluorination of TCO in an attempt to circumvent the above-mentioned issue.

We report the development and *in vivo* evaluation of a novel $Al^{18}F$-NOTA labeled TCO radioligand ([^{18}F]MICA-205) as a potential counterpart for IEDDA reaction with a tetrazine-tagged antibody (Figure 3.1). The biodistribution of this novel tracer and its potential for pretargeting approach is investigated. In this proof of concept study, we used the CC49 antibody, a murine monoclonal antibody that is directed against tumor associated glycoprotein 72 (TAG-72), expressed by the majority of human adenocarcinomas.[292] A mice model was established with colorectal cancer cell line (LS147T) xenografts expressing the antigen TAG-72.[293] The CC49 mAb for pretargeting was covalently modified with a methyl-tetrazine-NHS as a biorthogonal reactive moiety and a NOTA modified TCO was synthesized and labeled with fluorine-18. To the best of our knowledge, no studies have been performed so far with Al[^{18}F]F-NOTA labeled TCO.

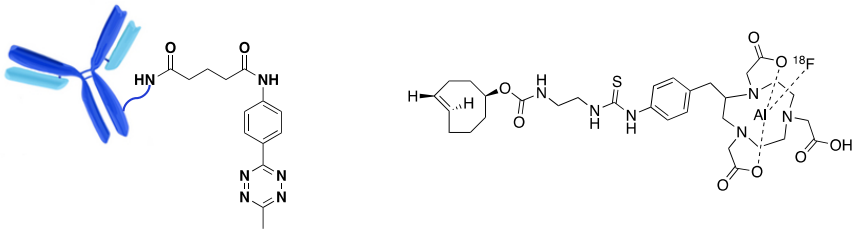

Figure 3.1 *Bioorthogonal ligands for in vivo pretargeted PET imaging.*

3.3 Materials and methods

3.3.1 General

All chemical reagents were obtained from commercial sources and used without further purification. Characterization of all compounds was done with ^{1}H NMR, ^{13}C NMR, and mass spectrometry. ^{1}H NMR and ^{13}C NMR spectra were recorded on a 400 MHz Bruker Avance III nanobay spectrometer, where necessary flash purification was performed by silica gel column chromatography using Biotage ® SNAP cartridges (silica gel cartridge size: 10–100 g; flow rate 10–50 mL/min) on a Biotage ® ISOLERA One flash system equipped with an internal variable dual-wavelength diode array detector (200–400 nm). Positive ion mode accurate mass spectra (HRMS) were acquired using a Q-TOF II instrument (Waters, Manchester, United Kingdom). No carrier-added [^{18}F]F− was produced in a Siemens Eclipse HP cyclotron by bombardment of [^{18}O]H_2O (Rotem Industries, Israel) by the ^{18}O(p,n)^{18}F reaction. Radiosynthesis of [^{18}F]TCO was carried out on an automated synthesis module (Fluorsynthon III, Veenstra Instruments, The Netherlands) specifically adapted to this radiosynthesis. Radiochemical yields were calculated from the theoretical initial amount of [^{18}F]F− and decay corrected to end of bombardment (EOB). Purification of [^{18}F]MICA-205 following radiosynthesis was done by semi-preparative HPLC using a Knauer HPLC pump and a Smartline UV detector (λ = 254 nm) in line with a Hi-Rad 1000-CD-X CdWO4 scintillation detector (Scionix, The Netherlands). Radiochemical and chemical purity was determined by analytical reversed-phase HPLC using a Shimadzu LC-20AT HPLC pump equipped with an SPD-20A UV/VIS detector (λ = 244 nm, Shimadzu, Japan) in series with a NaI-scintillation detector for radiation detection (Raytest, Germany). The recorded data were processed by the GINA-Star 5 software (Raytest, Germany). Radioactivity in samples from animal studies was measured in a Wizard2 2480

automatic gamma counter (Perkin Elmer, Finland). Full body PET/CT acquisitions were acquired on an Inveon microPET/CT scanner (Siemens Preclinical Solutions Inc., USA).

3.3.2 Synthesis

2,2',2''-(2-(4-(3-(2-((((S,E)-cyclooct-4-en-1-yloxy)carbonyl)amino)ethyl)thioureido)benzyl)-1,4,7-triazonane-1,4,7-triyl)triacetic acid (NOTA-TCO, 3.2): (S,E)-cyclooct-4-en-1-yl (2-aminoethyl)carbamate (47.1 mg, 0.222 mmol) was dissolved in DMF (1.5 mL) under argon. 2,2',2''-(2-(4-isothiocyanatobenzyl)-1,4,7-triazonane-1,4,7-triyl)triacetic acid (p-SCN-Bn-NOTA) (100 mg, 0.222 mmol) dissolved in DMF (1.5 mL) and triethylamine (0.118 mL, 0.888 mmol) were added to the solution. The reaction mixture was stirred at room temperature for 45 min. After completion of the reaction (monitored by UPLC) the product was purified using preparative HPLC (gradient: 5% - 65%, ACN 0.1% TFA/H_2O 0.1%TFA in 25 min, Rt = 16 min). This yielded TCO-NOTA **3.2** (100 mg, 68%) as a white solid. ^{1}H-NMR ($CDCl_3$, 400MHz): δ 9.65 (s, 3H), 7.77 (d, *J* = 7.5Hz, 2H), 7.35 (d, *J* = 7.5 Hz, 2H), 7.26 (s, 1H), 7.19 (s, 1H), 5.75 – 5.53 (m, 2H), 4.77-4.73 (m, 1H), 4.07 (t, 2H), 3.55 (t, 2H), 3.36 (s, 6H), 3.27-3.21 (m, 1H), 3.08–1.97 (m, 12H), 1.90 – 1.72 (m, 4H), 1.67-1.47 (m, 6H). ^{13}C-NMR (101 MHz, $CDCl_3$): δ 179.50, 177.41, 177.40, 173.14, 173.10, 155.92, 135.81, 134.02, 130.14, 130.11, 128.44, 128.42, 126.62, 126.41, 79.84, 66.24, 60.81, 60.53, 60.11, 59.54, 55.54, 55.51, 55.21, 53.00, 46.21, 40.81, 37.74, 35.21, 31.40, 25.41, 25.12, 22.44. HRMS (ESI+): *m/z* = 663.3171 $[M+H]^+$. Calcd for C31H46N6O8S 663.3181.

Aluminumfluoride-2,2',2''-(2-(4-(3-(2-((((S,E)-cyclooct-4-en-1-yloxy)carbonyl)amino)ethyl)thioureido)benzyl)-1,4,7-triazonane-1,4,7-triyl)triacetic acid (MICA-205, 3.3): $AlCl_3.6H_2O$ (1.46 mg) was mixed with KF (1.16 mg) in 0.5ml of NaOAc 0.2 M pH 4.0. To this solution was added TCO-NOTA (5 mg in 0.5 mL of ACN). The mixture was reacted for 15 min at 100 ˚C. The reaction was checked by analytic HPLC (Phenomenex kinetex EVO C18, 150 × 4.6 mm, 5 µm, 0.05 M NaOAc buffer pH 5.5/0.1%TFA in CH_3CN, 80:20, 1 mL/min, 244 nm). The product TCO-NOTA-AlF was purified by semi-PREP HPLC (Phenomenex Luna C18(2), 250 × 10 mm, 10 µm; NaOAc 0.05M pH 5.5/ACN (70:30, V:V), 3 mL/min, 244 min). UPLC MS (ESI+): *m/z* = 729.3 $[M+Na]^+$.

3.3.3 CC49 Antibody modification with Tetrazine-NHS

Typically, 2 mg of CC49 (5 mg/mL solution) was reacted with 30 molar eq. of tetrazine-NHS (4.8 µL in DMSO) in a total volume of 500 µL PBS. [201] The pH was adjusted to 9 with 1 M sodium carbonate buffer pH4. The reactions were carried out for 45 min at RT in the dark. The resulting mAb conjugates were purified *via* size exclusion chromatography (PD-10 column, GE Healthcare), concentrated using vivaspin2 centrifugal devices, and stored in PBS at 4 °C. The MW increase resulting from the tetrazine conjugation was not detectable by SDS-PAGE so mass spectrometry using a Q-TOF instrument was used to determine the average number of tetrazine molecules per antibody, as described before.[201] This procedure afforded an average of 8 tetrazine groups per antibody, as determined by mass spectrometry.

3.3.4 Stop-flow kinetic analysis

The reaction between MICA-205 and methyl-tetrazine-NHS was measured under pseudo-first order conditions in water: methanol 50:50 by following the exponential decay of the tetrazine at 298 nm over time using an SX20 stoppedflow spectrophotometer (Applied Photophysics Ltd.). The average of all runs was automatically fitted using the software Pro-data SX. Solutions of TCO in methanol: water 50:50 were prepared in concentrations of 0.1, 1, 2 and 3 mM and of tetrazine in water in concentration of 0.05 mM. The solutions were thermostatted in the syringes of the spectrophotometer before measuring. An equal volume of each was mixed by the stopped flow device and 400 data points were recorded over a period of 10 seconds, and performed in quadruplicate at 298 K. The k_{obs} was determined by nonlinear regression analysis of the data points using Prism software (v. 6.00, GraphPad Software Inc).

3.3.5 Radiochemistry

Radiosynthesis of [^{18}F]MICA-205 was performed by cyclotron production of [^{18}F]F^- solution that was transferred to the hotcell and passed over a preconditioned QMA Sep-Pak Light cartridge (Waters) (5mL trace-select H_20, dried with compressed air) to recover the [^{18}O]H_2O. The fixed [^{18}F]F^- was eluted from the QMA cartridge using 400 µL 0.9% NaCl solution. The eluate was added to a reaction vial containing 475 µl 2 mM $AlCl_3$ in 0.1 M NaOAc buffer (pH 4). This reaction was left to stir for 15min at room temperature followed by addition of 0.7 mg of TCO-NOTA precursor in 1 mL absolute EtOH. The reaction mixture was heated at 90 °C for 10 min. After cooling the reaction to 75 °C, 1

mL of H_2O was added. The reaction mixture was passed over a preconditioned Alumina N Light cartridge (Waters) before injection on the HPLC. The reaction mixture was purified by semi-preparative HPLC (Phenomenex Kinetex EVO C18, 150 × 100 mm, 5 µm) using a mixture of NaOAc 0.05 M pH 5.5/ethanol (70:30, V:V) as mobile phase at a flow rate of 3 mL/min. The fraction containing Al[^{18}F]-MICA-205 (t_R = 18.5 min) was collected, sterile filtered (Pall Acrodisc syringe filter, 13mm, 0.2µm Supor membrane) and diluted with 0.9% NaCl to reduce the EtOH concentration to < 10% in the final formulation. To evaluate the chemical and radiochemical purity reversed phase analytical HPLC analysis (Phenomenex Kinetex EVO C18, 150 × 4.6 mm, 5 µm) was performed using an isocratic elution of 0.05 M NaOAc buffer pH 5.5/0.1% TFA in ACN (80:20, V:V) at a flow rate of 1 mL/min. The recorded data were processed by the GINA-Star 5 software (Raytest). RCY were calculated from the theoretical initial amount of [^{18}F]F^- and decay corrected to end of bombardment (EOB).

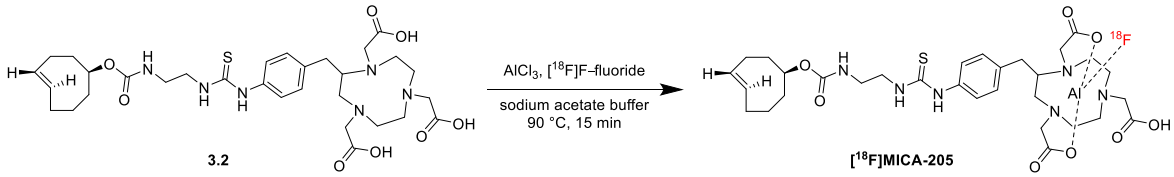

Scheme 3.1 *Radiosynthesis of [^{18}F]MICA-205.*

3.3.6 Partition coefficient determination

The partition coefficient (log *D*) of [^{18}F]MICA-205 was measured using the 'shake-flask' method.[294] Briefly, approximately 74 kBq of Al[^{18}F]-MICA-205 was added to a test tube containing a mixture of 2 mL n-octanol and 2 mL PBS (0.01 M, pH 7.4). The mixture was shaken well, vortexed for 2 min and centrifuged at 3000 rpm for 10 min. After separation of the layers, a 0.5 mL aliquot of both layers was taken into separate tubes and counted for radioactivity in an automatic gamma- (γ) counter (Wizard2 2480, Perkin Elmer). Corrections were made for differences in mass and density between the two phases. The octanol-water partition coefficients were obtained by dividing the octanol containing radioactivity by the PBS containing radioactivity and the log10 of this ratio was calculated. The reported log *D* value represents the mean of three determinations and is expressed as mean ± standard deviation (SD).

3.3.7 Animal experiments

The *in vivo* experiments were performed in tumor-free or tumor-bearing female nude Balb/C mice (20−25 g), Charles River Laboratories). Mice were kept under environmentally controlled conditions (12-h light/dark cycle, 20 – 24 °C and 40 – 70 % relative humidity) in IVC cages with food and water *ad libitum*. The human colon cancer cell line LS174T (ATCC CL-188) was obtained from the ATCC and maintained in Eagle's Minimal Essential Medium (Sigma) supplemented with 10% fetal bovine serum, 2 mM L-glutamine, 1 mM sodium pyruvate, and 1% penicillin-streptomycin (Invitrogen) at 37 °C and 5% CO_2. Mice were inoculated subcutaneously with 5×10^6 viable cells in 100 µL of sterile PBS and were used 7−10 days after tumor inoculation, when the tumors reached a size of approximately 70−200 mm^3. At the end of each experiment, the mice were euthanized by cervical dislocation. Experimental procedures and protocols were performed in accordance with European Directive 86/609/EEC Welfare and Treatment of Animals and were approved by the local ethical commission (2017-10, University of Antwerp, Belgium).

3.3.8 *In vitro* stability evaluation

The in vitro stability of [^{18}F]MICA-205 was evaluated in 0.9% NaCl saline solution at 37 °C for up to 2 h. Approximately, 185-370 kBq of [^{18}F]MICA-205 was incubated in 200 µL of 0.9% NaCl saline solution. At selected timepoints up to 2 h, samples were withdrawn and analyzed by analytical radio-HPLC.

3.3.9 *In vivo* metabolite analysis and ex vivo biodistribution

Female nude Balb/C healthy and LST174 tumor bearing mice were intravenously administered with [^{18}F]MICA-205 (9.25 MBq per mouse, n=3/time point) *via* the lateral tail vein. At 5, 15,30 and 60 min, post-radiotracer injection (p.i.), blood was collected through cardiac puncture in EDTA-coated tubes and used to evaluate the *in vivo* plasma stability of [^{18}F]MICA-205 (n=3/time point). The plasma fraction was obtained by centrifugation at 4000g for 7 min, and mixed (200 µL) with an equal volume of cold ACN to enable sample deproteination. After vigorously vortexing and γ-counting, the samples were centrifuged at 4000g for 4 min, and the supernatant and the pellet were γ-counted separately to determine the amount of recovered radioactivity in the organic phase. The radioactive contents of the supernatant (100 µL) were analyzed by analytical radio-HPLC using the method described above. Fractions were collected every 30 s and counted for

radioactivity in an automated γ-counter. The selected organs and tissues were harvested, weighed, and blotted dry. The sample radioactivity was counted in a γ-counter (Wizard2 2480, PerkinElmer) and the uptake of radiotracer reported as injected dose per gram (%ID/g).

3.3.10 *In vivo* µPET imaging studies

For the pretargeting experiment female healthy Balb/C mice (n= 5) and LS174T tumor bearing (n= 5) mice were injected with Tz-CC49 (200 µg in 200 µl of saline) 24h prior to the administration of Al[^{18}F]-MICA-205. Then, after sufficient time for target accumulation and clearance of the non-bounded antibody CC49 (24 h pretargeting step), mice were anesthetized using isoflurane (5% for induction, 2% for maintenance), placed on the animal bed in the scanner and intravenously (i.v.) injected via lateral tail vein with [^{18}F]MICA-205 (5.94 ± 0.03 MBq).[89] Static µPET imaging followed by *ex vivo* biodistribution was performed 1h p.i. As a control experiment, mice were treated with wild type CC49 antibody (200 µg in 200 µl of saline) and after 24h were injected with the same dose of radiotracer. Static whole-body PET images were acquired after 60 min p.i. using an Inveon small animal PET-CT scanner (Siemens). After each PET acquisition, a whole-body CT scan was acquired to obtain anatomic information for segmentation and attenuation/scatter correction. Throughout the entire PET-CT scanning procedure, the mice were maintained at constant body temperature by using a heating pad. For quantitative analysis, PET data were reconstructed using 3-dimensional ordered subset expectation maximization (OSEM3D, 16 subsets and 2 iterations) and 18 maximum a posteriori (MAP) iterations including single scatter stimulation (SSS) and attenuation correction. The PET images were reconstructed on a 128 x 128 x 159 matrix with a voxel size of 0.776 x 0.776 x 0.776 mm.

3.3.11 Data analysis

Data are expressed as mean ± SD. Statistical analysis was performed using Prism (version 6.01; GraphPad Software). Statistical significance between two data sets was evaluated by the unpaired two-tailed Student t-test. Differences between groups were considered statistically significant if the p value was < 0.05.

3.4 Results and Discussion

3.4.1 Synthesis

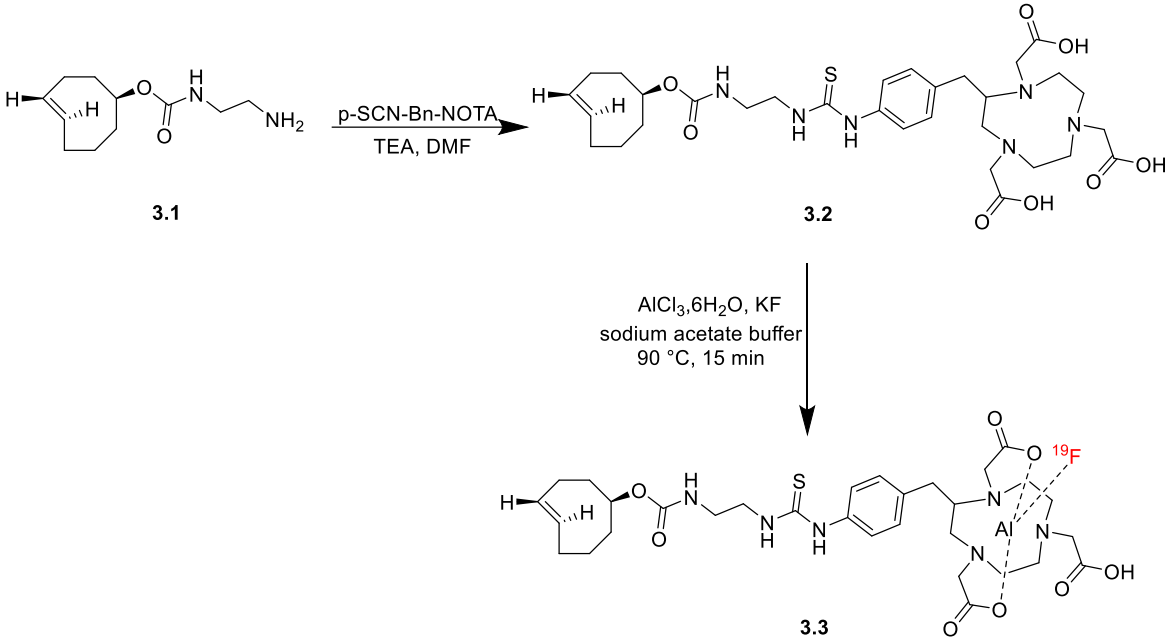

Scheme 3.2 *Synthesis of TCO-NOTA precursor and cold reference.*

With the aim to improve the stability of the TCO, we investigated the insertion of a NOTA ligand into the TCO for the posterior radiolabeling with fluoride-18. The precursor for radiolabeling (**3.2**) was obtained from reaction of compound (**3.1**), previously reported by our group, with the chelator p-SCN-Bn-NOTA (Scheme 3.2).[201] Since formation of cis-cyclooctene was observed, purification of this compound was performed in order to afford the pure *trans*-cyclooctene precursor **3.2** (68%). In order to obtain the cold reference **3.3**, chelation with $AlCl_3$ at low pH (4.0) with addition of KF was performed. The product was purified by semi-preparative HPLC to afford **3.3**.

3.4.2 Stop-flow kinetic analysis

The kinetic rate constant between compound **3.3** and methyl-tetrazine-NHS was evaluated by UV-spectrophotometry at 290 nm under pseudo-first order conditions in 50:50 methanol: water. A rate constant of 568 $M^{-1}s^{-1}$ was determined, which is significantly lower when compared to the new TCO generations with increased ring strain.[73, 78, 213, 288] It is also described that methyl-tetrazines present slower kinetic rates compared to other tetrazines, however the methyl-tetrazine was used due to

its favorable balance between stability and reactivity, as previously reported.[201] Nevertheless, the obtained reaction rate is in accordance to the ones reported for the first TCO generations.[73]

3.4.3 Radiosynthesis

The ^{18}F-labeled [^{18}F]MICA-205 was obtained with a decay corrected RCY of 12.8 ± 2.8% and a RCP of ≥ 96%. The pH of the Al[^{18}F]-NOTA complexation reaction and the use of metal-free solvents proved to be crucial factors in the radiochemical yields. Although high purity was achieved, the purification of [^{18}F]MICA-205 (Rt = 13.18 min) was complex due to the presence of its isomer, cis-cyclooctene, which is the main impurity observed (Rt = 15.00 min), as observed in Figure 3.2. The identity of the tracer could be confirmed by co-elution with MICA-205 cold reference. The radiotracer showed a moderate lipophilicity with a log *D* value of 2.23 ± 0.01. The *in vitro* stability showed that [^{18}F]MICA-205 remained stable in 0.9% NaCl saline solution at 37 °C for 2h. Only minor decomposition under the form of isomerization to cis-TCO was observed after 2 h, with 90.3 ± 4.4% of the intact radiotracer remaining.

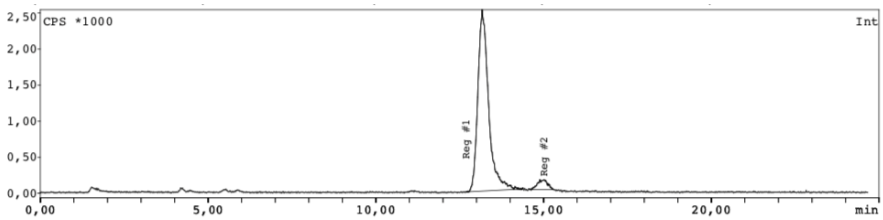

Figure 3.2 *Analytical HPLC radiochromatogram of [^{18}F]MICA-205 after semi-preparative HPLC purification.*

3.4.4 *In vivo* metabolites and biodistribution studies in non-tumor bearing mice

In order to study the stability and pharmacokinetic properties, [^{18}F]MICA-205 was injected in healthy Balb/C nude mice.The metabolite analysis showed favorable *in vivo* plasma stability with 67.7 ± 0.43 % of intact [^{18}F]MICA-205 remaining at 15 min p.i. We could mainly observe some isomerization from *trans* to *cis*-cyclooctene (Figure 3.3A). Since most of the radiotracer remained intact at this early time point, we decided to also evaluate stability at later time points. One hour after [^{18}F]MICA-205 injection 51.9 ± 5.16% of the radiotracer remained intact. The main radiometabolite at later time points was the *cis* isomer indicating high stability of the side chain and chelating complex. Since the *in vivo* click reaction with a tetrazine-modified mAb should occur within minutes after injection, the slow cis-isomerization should not compromise a pretargeting experiment. This result is a significant improvement compared to the first Fluorine-18 labeled TCO in our group which showed essentially two polar metabolites with no intact radiotracer after 30

min.[291] Furthermore, it also displays significantly higher stability than previously reported TCO analogs.[288 78 213 73]

The distribution of radioactivity in various tissues as a function of time following *i.v.* administration of [^{18}F]MICA-205 is presented in Figure 3.3B. The biodistribution study demonstrates a mixed hepatobiliary and renal excretion of the tracer with a fast washout through the liver (7.09 ± 3.01%ID/g at 15 min to 3.77 ± 0.71%ID/g at 1 h p.i.) and kidneys (8.46 ± 0.33%ID/g at 15 min to 0.36 ± 0.37%ID/g at 1 h p.i.), which was expected due to the moderate lipophilic character of the radiotracer. However, some retention of activity was observed in the small intestines at 60 min pi, as observed in Figure 3.3B. Comparing this result with recently published data revealed similar trends, where an Al[^{18}F]-NOTA radiotracer showed predominantly excretion *via* the liver with highest accumulation in the intestines and only low kidney uptake.[260] On the other hand, the tracer shows a rather slow clearance from the blood with 1.22 ± 0.18%ID/g at 15 min to 0.98 ± 0.59%ID/g at 1 h p.i. The uptake in all other healthy tissues remained relatively low. Low uptake of radioactivity in the bone (0.42 ± 0.19 %ID/g at 1 h p.i.), demonstrates the high stability of the chelating complex as was also demonstrated in the metabolite study. This result confirms other studies that also indicate high stability for other radiotracers labeled with Al[^{18}F]F-NOTA complex.[295-297]

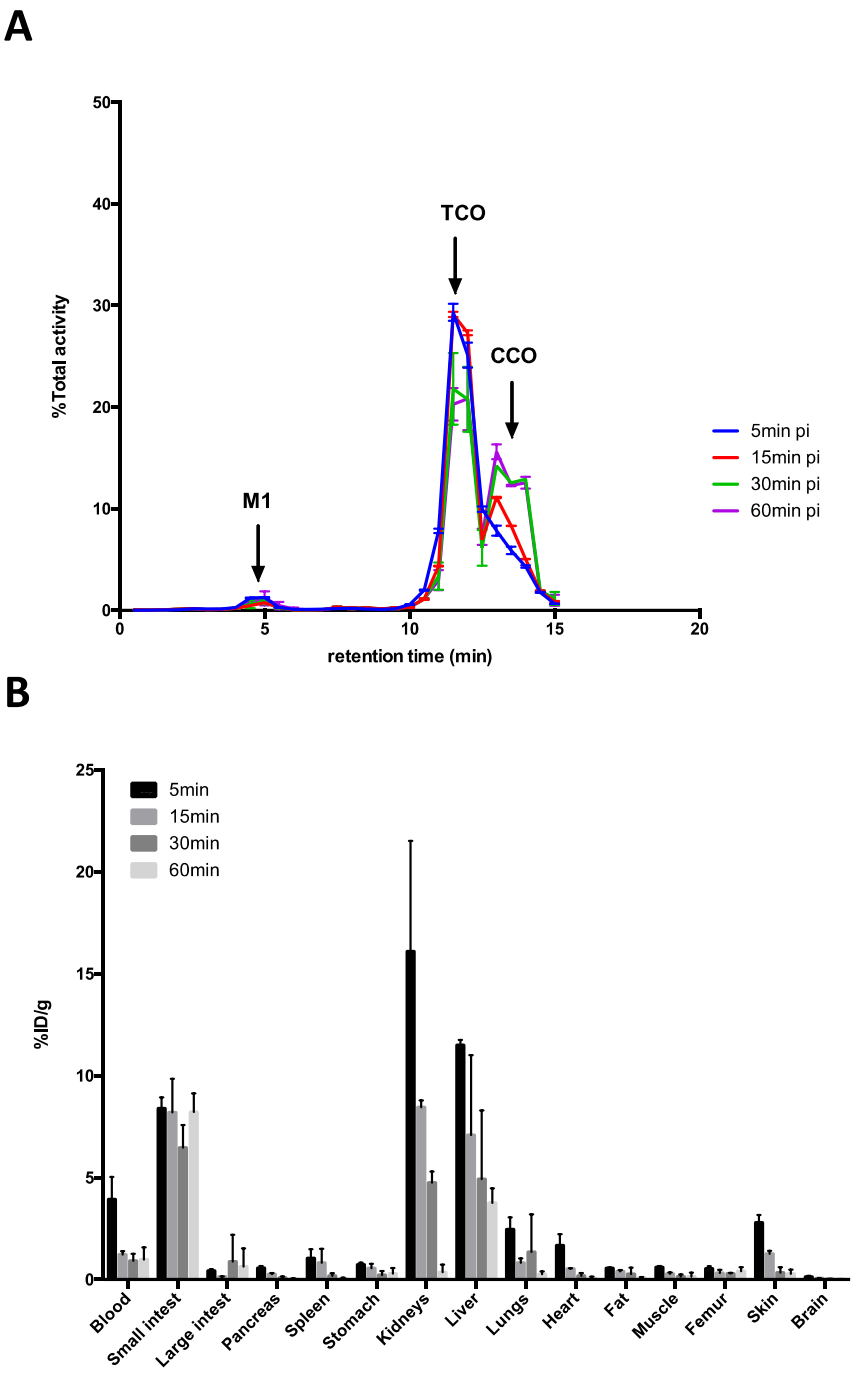

Figure 3.3 *(A) In vivo plasma metabolites (n=3) and (B) Ex vivo tissue distribution at different time points (n=3) post injection of [^{18}F]MICA-205 in healthy Balb/C nude mice.*

3.4.5 *In vivo* pretargeted µPET imaging in tumor-bearing mice

To investigate the potential use of [^{18}F]MICA-205 for *in vivo* pretargeting µPET imaging, LS174T tumor-bearing mice were pre-treated with the anti-TAG-72 mAb CC49 conjugated with an in house developed stable methyl-tetrazine 24h prior to injection of [^{18}F]MICA-205.[201] Micro-PET imaging was performed at 1h p.i., based on the aforementioned relatively low image background observed in the biodistribution results (Figure 3.3B). As demonstrated by the µPET images (Figure 3.4A) tumor tissue could be clearly visualized in the mice pre-treated with CC49-Tz while this was not the case for the control mice pre-treated with CC49. As was also demonstrated in the *ex vivo* biodistribution study in healthy mice, high abdominal uptake was observed, which may hamper imaging of the abdominal region in future applications. To quantify more accurately the *in vivo* behavior of [^{18}F]MICA-205 in a pretargeting set-up , an *ex vivo* biodistribution was performed. The data (Figure 3.4B) revealed a significant higher tumor uptake (0.67 ± 0.16 %ID/g, $p<0.001$) compared to controls (0.16±0.08 %ID/g). In accordance with the biodistribution performed in heathy mice, the uptake in other organs remained generally low. However, a higher accumulation in small intestines (22.± 3.8 %ID/g) were observed in pretargeted mice. This high uptake in small intestines together with moderate uptake in liver (2.9 ± 2.3 %ID/g), large intestines (0.9 ± 1.3 %ID/g) and the lower kidney uptake (0.59 ± 0.1 %ID/g) suggest that this tracer has a preference for the hepatobiliary excretion route. Furthermore, the low tumor uptake is most likely linked to the slow blood elimination of this probe. Based on recent studies introduction of a PEG linker between the TCO and NOTA chelator may lead to an increased renal excretion and accelerated intestinal excretion, thus translating into higher tumor uptake.[260] This would overcome the abdominal background in future imaging experiments. Moreover, the use of clearing agents can also be useful to further increase tumor-to-blood ratios and maximize tumor dose in pretargeting approaches.

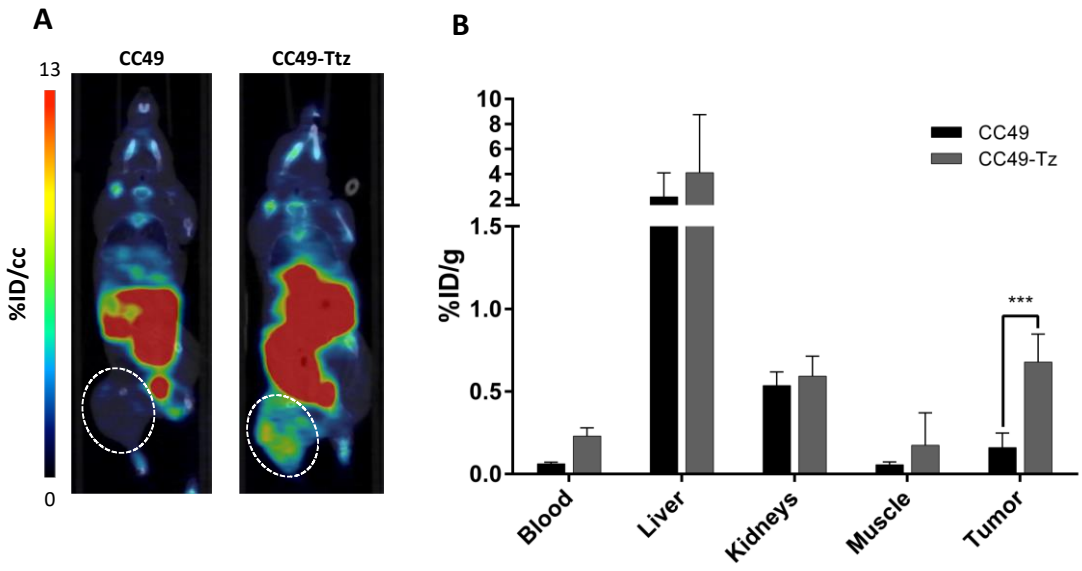

Figure 3.4 *(A): representative µPET images of LS174T tumor-bearing mice injected with [^{18}F]MICA-205 24h after injection of CC49 or CC49-Tz. Static images were acquired 1 h post tracer injection. The white dashed line encircles the tumor region; (B): Pretargeting ex vivo biodistribution of LS174T tumor-bearing mice 60 min post tracer injection (n=5/group, p<0.001).*

3.5 Conclusions

A TCO analogue containing a NOTA chelator was developed to allow radiolabeling by chelation with aluminum fluoride. MICA-205 showed a moderate *in vitro* reactivity towards methyl-tetrazine, yet in a pretargeting PET imaging experiment, [^{18}F]MICA-205 was able to visualize LS174T tumor xenografts with significantly higher tumor uptake in mice pre-treated with CC49-Tz compared to control animals pre-treated with CC49 24h prior to tracer injection. [^{18}F]MICA-205 proved to be stable with >50% of the tracer remaining intact at 1 h p.i. These results suggest a high stability of the side chain and chelating complex. Despite the encouraging results, further studies must be performed to further improve the tumor uptake and decrease the background activity in the abdominal cavity.

CHAPTER 4

Characterization of Structurally diverse ^{18}F-Labeled d-TCO Derivatives as a PET Probe for Bioorthogonal Pretargeted Imaging

Published as:

Karuna Adhikari, Jonatan Dewulf, Christel Vangestel, Pieter Van der Veken, Sigrid Stroobants, Filipe Elvas, and Koen Augustyns

Characterization of Structurally Diverse ^{18}F-Labeled d-TCO Derivatives as a PET Probe for Bioorthogonal Pretargeted Imaging. ACS Omega **2023** 8 (41), 38252-38262

DOI: 10.1021/acsomega.3c04597

Contribution: Design and synthesis of cold-references, precursors for radiolabeling, radiochemical development, *in vitro* and *in vivo* experiments, data acquisition, analysis and writing manuscript.

Chapter 4 Characterization of Structurally diverse ^{18}F-Labeled d-TCO derivatives as a PET probe for bioorthogonal pretargeted imaging

4.1 Abstract

Introduction: The pretargeted imaging strategy using inverse electron demand Diels-Alder (IEDDA) cycloaddition between a *trans*-cyclooctene (TCO) and tetrazine (Tz) has emerged and rapidly grown as a promising concept to improve radionuclide imaging and therapy in oncology. This strategy has mostly relied on the use of radiolabeled Tz together with TCO-modified targeting vectors leading to a rapid growth of the number of available radiolabeled tetrazines, while only a few radiolabeled TCOs are currently reported. Here, we aim to develop novel and structurally diverse ^{18}F-labeled *cis*-dioxolane fused-TCO (d-TCO) derivatives to further expand the bioorthogonal toolbox for *in vivo* ligation and evaluate their potential for positron emission tomography (PET) pretargeted imaging.

Results: A small series of d-TCO derivatives were synthesized and tested for their reactivity against tetrazines, with all compounds showing fast reaction kinetics with tetrazines. A fluorescence-based pretargeted blocking study was developed to investigate the *in vivo* ligation of these compounds without a labor-intensive prior radiochemical development. Two compounds showed excellent *in vivo* ligation results with blocking efficiency of 95 and 97%. Two novel ^{18}F-labeled d-TCO radiotracers were developed, from which **[^{18}F]MICA-214** showed good *in vitro* stability, favorable pharmacokinetics, and moderate *in vivo* stability. Micro-PET pretargeted imaging with **[^{18}F]MICA-214** in mice-bearing LS174T tumors treated with tetrazine-modified CC49 monoclonal antibody (mAb) (CC49-Tz) showed significantly higher uptake in tumor tissue in the pretargeted group (CC49-Tz 2.16 ± 0.08% ID / mL) when compared to the control group with non-modified mAb (CC49 1.34 ± 0.07% ID / mL).

Conclusions: A diverse series of fast-reacting fluorinated d-TCOs were synthesized. A pretargeted blocking approach in tumor-bearing mice allowed the choice of a lead compound with fast reaction kinetics with Tz. A novel ^{18}F-labeled d-TCO tracer was developed and used in a pretargeted PET

imaging approach, allowing specific tumor visualization in a mouse model of colorectal cancer. Although further optimization of the radiotracer is needed to enhance the tumor-to-background ratios for pretargeted imaging, we anticipate that the ^{18}F-labeled d-TCO will find use in studies where increased hydrophilicity and fast bioconjugation are required.

4.2 Introduction

Bioorthogonal chemistry for pretargeted imaging through inverse electron demand Diels-Alder (IEDDA) reaction between a 1,2,4,5-tetrazine (Tz) and a *trans*-cyclooctene (TCO) with its ultrafast kinetics and selectivity has attracted considerable interest in the field of targeted delivery of radionuclides and molecular imaging.[41, 298, 299] Immuno-positron emission tomography (Immuno-PET) is an imaging technique that combines the selectivity and affinity of monoclonal antibodies (mAbs) with the high resolution and sensitivity of PET to visualize and quantify specific biomolecules or cells *in vivo*.[10] However, the slow pharmacokinetics of antibodies requires the use of long-lived radioisotopes leading to high radiation exposure in nontarget organs. A pretargeted immuno-PET imaging through an IEDDA reaction between a TCO and Tz uses the specificity of antigen-mAb interaction and has the advantage of enabling the use of short-lived radioisotopes in a multistep approach.[92] Briefly, an antibody is injected first and accumulates in the target before a small radiolabeled molecule is administered after a few days of clearance of the long-circulating antibody. These two moieties react *in vivo* through biorthogonal chemistry. The unbound fraction of the radiolabeled molecule is then rapidly excreted from circulation.[27] The temporal separation of the antibody from the radioactivity administration allows the use of short-lived radioisotopes such as fluorine-18 [^{18}F]F$^-$ ($t_{1/2}$ =110 min) with favorable decay properties (97% β^+ emission, 634 keV maximum β^+ energy) and short β^+ trajectory in tissues (<2.3 mm) for high-resolution PET imaging.[101] The use of short-lived isotopes also leads to lower radiation burden to the patient during the imaging and improved tumor-to-background ratios resulting in high-contrast PET images.

Considerable research has been devoted to the pretargeted imaging approach with [^{18}F]F$^-$ using biorthogonal chemistry where TCO-Tz ligation has become the gold standard.[92, 300] Apart from its selectivity and biorthogonality, TCO-Tz ligation shows ultrafast kinetics with the first-order rate constant up to $10^{6\text{-}7}$ $M^{-1}s^{-1}$. The exceptionally fast reaction kinetics plays a pivotal role in the feasibility of *in vivo* pretargeted imaging.[73] With the advances in the field of bioorthogonal

chemistry and tetrazine labeling, numerous studies have been reported where the ligation between a mAb conjugated to TCO and ^{18}F-radiolabeled-Tz pair was used for pretargeted tumor imaging.[80, 93-95, 247] Although lower absolute tumor uptake values were observed, improved tumor-to-background ratios have been obtained using ^{18}F labeled-Tz when compared to the "state-of-the-art" chelator-based radiolabeled tetrazines.[301, 302] In principle, both tetrazines and TCO can be radiolabeled. However, the inverse approach, where the TCO is radiolabeled and the tetrazine is conjugated to mAb, is still less explored. Nevertheless, it has been shown that TCO directly conjugated to mAb tends to bury within the protein core, leaving only a few reactive tags available. This could be circumvented by extending the distance between the targeting and the reactive moiety, by introducing, for example, hydrophilic PEG linkers.[290] Moreover, TCO also isomerizes to its less reactive *cis*-form in circulation.[78] Furthermore, the polarity of radiolabeled tetrazines restricts the imaging of noninternalizing and peripheral targets. Thus, the replacement of the TCO tags with tetrazines could offer an alternative to circumvent the prolonged exposure of TCO to physiological conditions and enable the visualization of internalizing targets, owing to the increased cell permeability of TCOs. [^{18}F]FTCO, initially developed as an ^{18}F-labeling strategy for pre-assembled [^{18}F]FTCO-Tz targeting molecules, showed poor metabolic stability *in vivo* for pretargeted imaging.[233, 263] Later, a more stable TCO-NOTA derivative was successfully radiolabeled through chelation with Al[^{18}F]F and used to visualize LS174T tumor xenografts.[264] In recent years, new generations of faster and more stable conformationally strained cyclopropane-fused TCO (sTCO) and cis-dioxolane fused TCO (d-TCO) have been described. These are often employed to track and image fast biological processes and as labeling agents for the assembly of PET probes.[73, 152, 213, 288] The use of d-TCOs may improve the *in vivo* ligation due to their improved kinetics, stability, and increased aqueous solubility. However, only a few ^{18}F-labeled d-TCO's have been used for pretargeting applications. In 2017, Billaud *et al.* reported on the initial use of an ^{18}F-labeled d-TCO probe in a pretargeted imaging setting. The tracer showed favorable *in vitro* stability and pharmacokinetics, while the absolute tumor uptake in the pretargeted approach remained low with substantial abdominal background activity.[87] In 2020, a new d-TCO amide derivative was successfully used by our group in a pretargeting study in LS174T tumor-bearing mice.[88] Despite improved tumor uptake values being achieved, the tumor-to-background ratio could yet be optimized. These findings highlight the need for the development of more diverse and improved TCO structures with improved stability, reactivity, and pharmacokinetic profile, which are critical

for understanding the role of different variables in pretargeted imaging via bioorthogonal TCO-Tz ligation and steering its future as a powerful diagnostic tool.

Here, we report the synthesis of a small series of fluorinated d-TCO derivatives and the initial screening of their *in vivo* reactivity through a pretargeted blocking study. The d-TCO core was modified with sulfonyl fluoropyridine, short poly(ethylene glycol) (PEG) chains, cyclobutyl ring, and squaramide as linkers. These linkers were chosen to modulate the lipophilicity of the d-TCO core to minimize the nonspecific tracer accumulation while also impacting the overall metabolic stability of the radiotracer in vivo.[303-306] The probe that yielded the highest blocking signal was selected for further radiochemical development and pharmacokinetics studies. Finally, a pretargeted µPET imaging experiment was performed in mice bearing LS174T human colorectal tumors pretreated with a tetrazine-modified anti-TAG-72 monoclonal antibody (CC49) to visualize the tumor.

4.3 Materials and Methods

4.3.1 General

All chemicals, reagents, and solvents were purchased from commercial suppliers (Sigma-Aldrich, Acros, TCI-Europe, FluoroChem, BioRad, and Jena Bioscience) and used without further purification. Phosphate-buffered saline (PBS, 0.01 M, pH 7.4) solutions were obtained from diluting a 0.5 M stock purchased from Gentest Life technology.

NMR spectra were recorded on a Bruker Avance DRX 400 MHz spectrometer. ^{1}H and ^{13}C spectra are referenced to residual solvent peaks, coupling constants are given in Hertz. HRMS analyses were performed using a Q-TOF II instrument (Waters, Manchester, UK). UPLC-MS analyses were performed on a Waters Acquity UPLC system coupled to a Waters TQD ESI mass spectrometer and TUV detector. Kinetics were performed on an SX-20 stopped-flow system (Applied Photophysics). log *D* values were calculated with Collaborative Drug Vault. Chromatographic purifications were performed with a Biotage ISOLERA One flash system equipped with an internal variable dual-wavelength diode array detector (200-400 nm).

4.3.2 Stopped-flow kinetics

The reaction between d-TCOs and the tetrazines was measured under pseudo-first-order conditions in water/methanol 50:50 with excess TCO by following the exponential decay of the MeBA-Tz at 264 nm and $2Pyr_2$-Tz at 300 nm over time using an SX 20 stopped-flow spectrophotometer (Applied Photophysics Ltd.). The solutions were thermostatted in the syringes of the spectrophotometer before measuring. An equal volume of each was mixed by the stopped-flow device, and 4000 data points were recorded over a period of 20 seconds and performed in quadruplicate at 37 °C. Data were analyzed by fitting an exponential decay using GraphPad Prism version 9.3.1 (RRID: SCR_002798), and the obtained kobs were plotted vs TCO concentration using nonlinear regression to afford the second order constant (k_2), based on the equation kobs=[TCO] k_2 for MeBA (Figure S4.1). For $2Pyr_2$ pseudo-first-order rate constants were divided by the TCO concentration to calculate the second-order rate constants (Table S4.1).

4.3.3 Blocking studies

4.3.3.1 *Animal model*

The *in vivo* experiments were performed in tumor-bearing female nude Balb/C mice (6-8 weeks old, Charles River Laboratories). Mice were kept under environmentally controlled conditions (12-h light/dark cycle, 20-24°C, and 40-70% relative humidity) in IVC cages with food and water ad libitum. The human colon cancer cell line LS174T (ATCC CL-188) was obtained from the ATCC. Cells were maintained in DMEM (Sigma) supplemented with 10% fetal bovine serum, 2 mM L-glutamine, 1 mM sodium pyruvate, and 1% penicillin-streptomycin (Invitrogen) at 37 °C and 5% CO_2.

The xenograft model was generated by subcutaneous injection of LS174T (5×10^6 viable cells in 100 µL of Dulbecco phosphate-buffered saline, DPBS) tumor cells into the right hind flank of 6- to 8-week-old female Balb/C nude mice. After tumor inoculation, tumor dimensions were measured using a digital caliper three times over a week. Tumor volumes were calculated according to the formula (length x $width^2$)/2. At the end of each experiment, the mice were euthanized by cervical dislocation. All experimental procedures and protocols were performed following European Directive 86/609/EEC Welfare and Treatment of Animals and were approved by the local ethical commission (2018-87, University of Antwerp, Belgium).

4.3.3.2 *In vivo fluorescence imaging*

For the positive and negative control group, nude female Balb/C LS174T tumor-bearing mice (n=4) were either injected with CC49-Tz (100 µg/ 100 µL, 0.67 nmol) or CC49 (100 µg/ 100 µL, 0.67 nmol) 72 h before TCO-Cy5 (40 nmol/ 100 µL) injection. Mice in the blocked group were injected with CC49-Tz 72h before the unlabeled d-TCO derivatives (40 nmol/100 µL) followed by TCO-Cy5 (40 nmol/100 µL) after 1h (Figure 4.1A). The mice were anesthetized with 2.5% isoflurane (IsoFlo, Zoetis) for 3 min in an induction chamber. Upon induction, mice were transferred to the IVIS Spectrum *in vivo* Imaging System (PerkinElmer) and imaged. Image sequences were acquired with the same exposure time, binning, and F-stop values. Images were analyzed and the tumor uptake of TCO-Cy5 was quantified by drawing the region of interest (ROI) using Aura V3.2 (Spectral Instruments Imaging). The uptake value of the positive control group was used as a reference value (100% tumor uptake). The uptake value of the negative group was used to determine the background signal (0% tumor uptake). These reference values were used to normalize the observed tumor uptake in groups with a blocking experiment. Tumor uptake of the blocked group is presented as a percentage normalized mean efficiency (Figure 4.1).

4.3.4 **Radiochemistry**

The radiosynthesis was carried out in an automated AllinOne synthesis module (TRASIS, Ans, Belgium) with an integrated HPLC system with a UV detector and radioactivity detector. No-carrier added aqueous [^{18}F] fluoride was produced in an Eclipse HP cyclotron (Siemens) using the ^{18}O(p,n)^{18}F reaction by proton bombardment of [^{18}O]H_2O (Rotem Industries) and passed through an ion exchange resin (Sep-Pak Accell Plus QMA Light cartridge (Waters)). [^{18}F]F- was eluted from the resin in the reactor vial with 1 mL of a mixture of 0.025 M K_2CO_3/0.1 M kryptofix$_{2.2.2}$ in CH_3CN/H_2O (95:5 (v/v)) for [^{18}F]MICA-214 and 0.01 M tetraethylammonium bicarbonate (TEAB) in CH_3CN/H_2O (90:10 (v/v)) for [^{18}F]MICA-215 and evaporated to dryness. For [^{18}F]MICA-214, a tosylate precursor solution (6 mg) in dry DMF was added and reacted for 10 min at 100 °C and for [^{18}F]MICA-215 a tosylate precursor (5 mg) in dry ACN was added and reacted for 10 min at 70 °C. After cooling down to 50 °C, 1 mL of buffer was added and the mixture was passed through a Sep-Pak Alumina N Light cartridge (Waters) (preconditioned with 10 mL of water), before injection on the HPLC. [^{18}F]MICA-214 was purified using a Waters X-Bridge C18 250 x 10 mm (5 µm) HPLC column using a mobile phase consisting of NaOAc 0.05 M pH 5.5/EtOH (70:30 (v/v)) at a flow rate of 3 mL/min ([^{18}F]MICA-214 t_R = 18 min). [^{18}F]MICA-215 was purified using a Phenomenex Luna C18 250 x 10 mm (5µm)

HPLC column using a mobile phase NaOAc 0.05M pH 5.5/ EtOH (60:40 (v/v)) at a flow rate of 3 mL/min ([^{18}F]MICA-215 t_R = 28 min). Radiotracers were sterile-filtered and diluted with 0.9% NaCl to reduce ethanol concentration to < 10% in the final formulation. Radiochemical purity was determined by analytical reversed-phase HPLC using a Phenomenex Kinetex EVO C18 150 x 4.6 mm (5 µm) with an isocratic elution of H_2O + 0.1% TFA /CH_3CN + 0.1% TFA (72:28) over 10 min for [^{18}F]MICA-214; and H_2O + 0.1% TFA /CH_3CN + 0.1% TFA (70:30) over 15 min for [^{18}F]MICA-215, with a flow rate of 1 mL/min (Figure S4.4). The recorded data were processed by the GINA-Star 5 software (Raytest). Radiochemical yields (RCY) were calculated from the theoretical initial amount of [^{18}F]F^- and decay corrected to the end of bombardment (EOB).

4.3.5 Partition coefficient determination

The partition coefficient (log $D_{\text{n-octanol/PBS pH 7.4}}$) of [^{18}F]MICA-214 and [^{18}F]MICA-215 was measured using the "shake-flask" method. Briefly, approximately 74 kBq of [^{18}F]MICA-214 or [^{18}F]MICA-215 was added to a test tube containing a mixture of 2 mL n-octanol and 2 mL PBS (0.01 M, pH 7.4). The mixture was shaken well, vortexed for 2 min, and centrifuged at 3000 rpm for 10 min. After the separation of the layers, a 0.5 mL aliquot of both layers was taken into separate tubes and counted for radioactivity in an automatic gamma- (γ) counter (Wizard2 2480, Perkin Elmer). Corrections were made for differences in mass and density between the two phases. The octanol-water partition coefficients were obtained by dividing the octanol-containing radioactivity by the PBS-containing radioactivity and the log10 of this ratio was calculated. Reported log *D* values represent the mean of three determinations and were expressed as mean ± standard deviation (SD).

4.3.6 *In vitro* stability evaluation

The stability of [^{18}F]MICA-214 and [^{18}F]MICA-215 were evaluated in PBS (0.01 M, pH 7.4) and mouse plasma at 37°C for up to 120 min. Approximately, 185-370 kBq of [^{18}F]MICA-214 or [^{18}F]MICA-215 was incubated in 100 µL PBS or mouse plasma. The incubation was quenched by adding ice-cold ACN (100 µL), followed by vortexing and centrifugation (5 min, 4000g) to remove the proteins from samples in plasma. The radioactive contents of the supernatant (100 µL) were analyzed by analytical radio-HPLC. The HPLC eluate was collected in fractions of 15 s, and the radioactivity was counted in an automated γ-counter.

4.3.7 *Ex vivo* biodistribution studies

Female nude Balb/C healthy and LST174 tumor-bearing mice were intravenously administered with [^{18}F]MICA-214 or [^{18}F]MICA-215 approximately 5 MBq per mouse, *n*=3/time point via the lateral tail vein. At 5, 15, 30, and 60 min post-radiotracer injection (p.i.), the blood was collected through cardiac puncture and the mice were euthanized by cervical dislocation. The selected organs and tissues were harvested, weighed, and blotted dry. The sample radioactivity was counted in a γ-counter (Wizard^2 2480, PerkinElmer) and the uptake of radiotracer is presented as injected dose per gram (%ID/g).

4.3.8 *In vivo* metabolite analysis

The blood from the *ex vivo* biodistribution studies was collected in EDTA-coated tubes. The plasma fraction was obtained by centrifugation at 4000g for 7 min and mixed (200 µL) with an equal volume of ice-cold ACN to enable deproteination. The samples were centrifuged at 4000g for 4 min, and the supernatant and pellet were γ-counted separately. The radioactive contents of the supernatant (100 µL) were analyzed by analytical radio-HPLC. The HPLC eluate was collected in fractions of 15 s, and the radioactivity was counted in an automated γ-counter.

4.3.9 *In vivo* µPET imaging studies

Nude female Balb/C mice bearing LS174T tumors (n=4) were anesthetized using isoflurane (5% for induction, 2% for maintenance), placed on the animal bed in the scanner, and i.v. injected via lateral tail vein with 8-9 MBq of [^{18}F]MICA-214. Dynamic whole-body PET images were acquired for 60 min (12x10 s, 3x20 s, 3x30 s, 3x60 s, 3x150 s, and 9x300 s frames), using an Inveon small animal PET-CT scanner (Siemens). After each PET acquisition, a whole-body CT scan was performed to obtain anatomic information for segmentation. The mice were maintained at constant body temperature throughout the PET-CT scanning procedure using a heating pad. For quantitative analysis, PET data were reconstructed using a list-mode iterative reconstruction with proprietary spatially variant resolution modeling in 8 iterations and 16 subsets of the 3D ordered subset expectation maximization (OSEM 3D) algorithm.[307] The PET images were additionally reconstructed on a 128 x 128 x 159 matrix with a voxel size of 0.776 x 0.776 x 0.776 mm. CT-based attenuation and single scatter stimulation (SSS) scatter corrections were applied to the PET data. For the dynamic scans, volumes of interest (VOIs) were manually drawn on the PET/CT images using PMOD (version 3.6;

PMOD Technologies) to delineate the regions with distinct PET time-activity patterns: heart, liver, kidney, bladder, muscle, brain, bone, and tumor. The average organ activity per volume was obtained from the coregistered PET images and the decay-corrected time-activity curves (TACs) were extracted for each target organ. For an absolute measure of tracer uptake in the tissue, normalized images were scaled according to the percent-injected dose (%ID/mL = tissue uptake from the scanner [kBq/mL]/injected dose [kBq] x 100).

4.3.10 Data analysis

Data were expressed as mean ± SD. Statistical analysis was performed using GraphPad Prism version 9.3.1 (RRID: SCR_002798). Statistical significance between the two data sets was evaluated by the unpaired two-tailed Student *t*-test. Differences between groups were considered statistically significant if the p-value was less than 0.05.

4.4 Results

4.4.1 Synthesis of d-TCO derivatives

Five d-TCOs with structurally diverse linkers were synthesized. The d-TCO-amide derivatives were synthesized from the d-TCO-amine scaffold, as previously described.[88] **UAMC-4129** was synthesized in two steps by reacting the d-TCO-amine **4.8** with diethylsquarate followed by nucleophilic substitution with a 2-fluoroethylamine (Scheme 4.1). Similarly, the nucleophilic substitution of 6-fluropyridine-3-sulfonyl chloride with the d-TCO-amine afforded sulfonamide **UAMC-3725** (Scheme 4.1). Compound **4.2** (syn diastereomer) was obtained following a previously reported procedure.[73] In parallel, the cyclobutyl intermediate **4.26** was prepared in four steps starting from the reduction of 3-(benzyloxy)cyclobutane-1-carboxylic acid. The obtained alcohol was tosylated, followed by the removal of the benzyl-protecting group through hydrogenation on Pd/C. The alcohol was fluorinated with perfluoro-1-butanesulfonyl fluoride (PBSF) to afford **4.26**. Compound **4.2** was deprotonated with sodium hydride followed by nucleophilic substitution of the tosyl group on **4.26** to afford **4.27** which was finally photoisomerized in a closed-loop flow photoreactor to afford the desired reference compound **UAMC-3933** (Scheme 4.1). The synthesis of **UAMC-3711** and **UAMC-3724** was carried out through modification of a reported procedure.[213] Starting from diethylene or triethylene glycol, PEG synthons **4.14** and **4.19** were prepared in two steps by first protecting one of the hydroxyl groups with benzoyl chloride (BzCl). In the second step, the other hydroxyl was

oxidized to an aldehyde in the presence of the Dess–Martin periodinane reagent. In parallel, the oxidation of 1,5-cyclooctadiene into diol **4.1** was carried out using OsO_4. Diol **4.1** was acetalized with **4.14** or **4.19** affording the dioxolane **4.15** and **4.20**, respectively, with syn diastereomer as the major product. After deprotection using LiOH, the hydroxyl group was fluorinated with PBSF to afford **4.17** or **4.22**, and finally, the *trans*-for-*cis* photoisomerization gave the references **UAMC-3711** and **UAMC-3724** (Scheme 4.1).

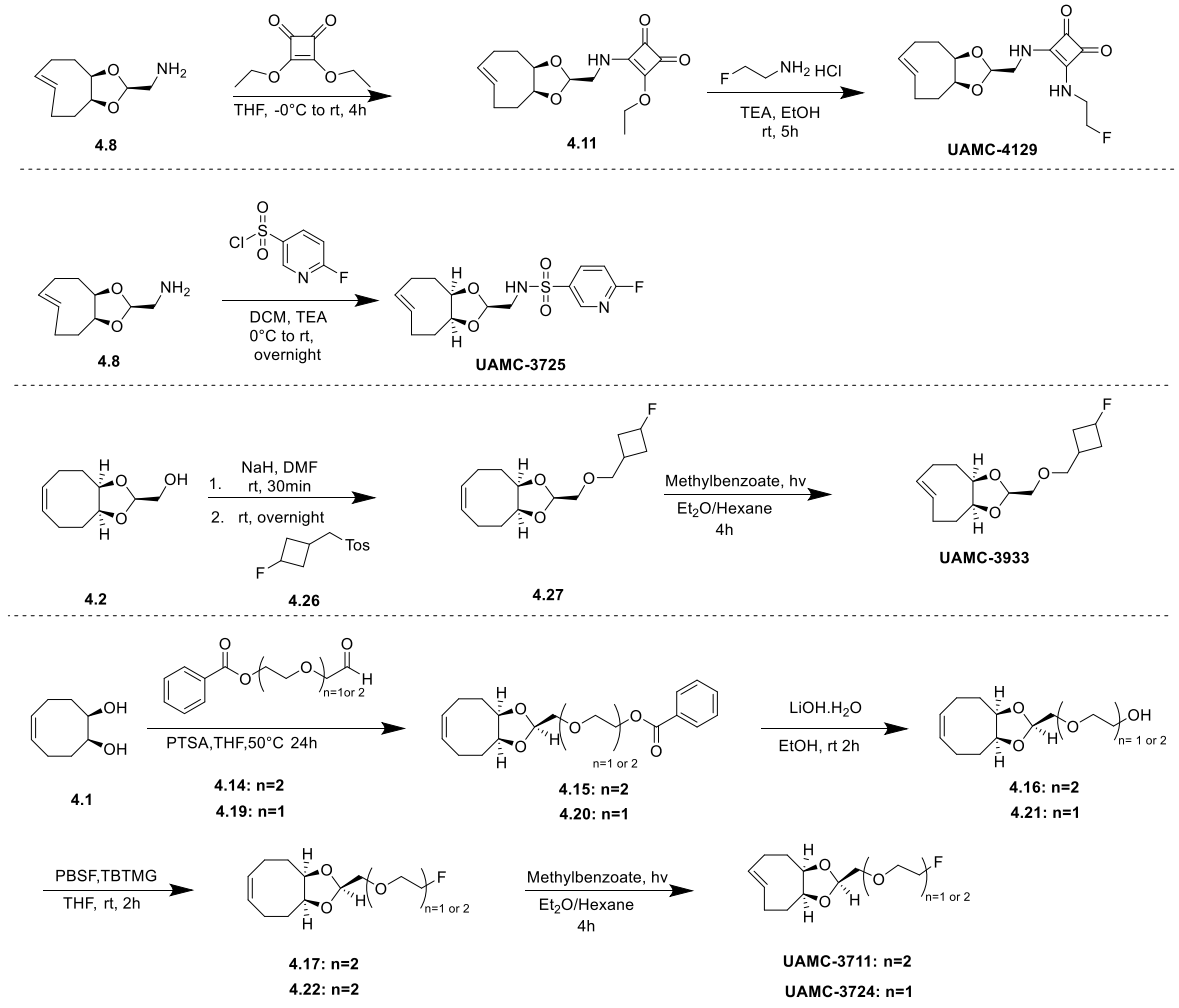

Scheme 4.1 *Synthesis of d-TCO derivatives.*

4.4.2 Reaction Kinetics of d-TCOs with Tetrazine

Second-order rate constants for the reaction of the synthesized d-TCOs with tetrazines were determined by pseudo-first-order measurements in a stopped-flow photometer at 37 °C in a solvent system consisting of MeOH/H_2O 50:50 (v/v). With 6-Methyl benzyl amine tetrazine (MeBA), the rate constants measured were in the range of 2067-4802 $M^{-1}s^{-1}$ (Table 4.1; Figure S4.1). To

compare the results with the literature, the d-TCOs were also reacted with 3,6-di-2-pyridyl-1,2,4,5-tetrazine ($2Pyr_2$) showing a remarkable rate constant in the range of 87265-184892 $M^{-1}s^{-1}$ (Table 4.1; Table S4.1) which is in the similar range as previously reported d-TCO compounds.[73]

Table 4.1 *Calculated log D and Rate constants of synthesized d-TCOs with MeBA and $2Pyr_2$ in $MeOH/H_2O$ at 37 °C*

TCO	Log *D*	k_2 ($M^{-1}s^{-1}$) MeBA	k_2 ($M^{-1}s^{-1}$) $2Pyr_2$
UAMC-4129	0.76	4802 ± 693	184892 ± 312
UAMC-3933	2.96	3735 ± 323	87265 ± 133
UAMC-3711	1.58	2067 ± 224	91460 ± 77
UAMC-3724	1.71	4240 ± 102	146200 ± 91
UAMC-3725	1.92	3506 ± 311	142626 ± 107

4.4.3 Pretargeted Blocking

A pretargeted blocking assay was established to assess the *in vivo* ligation performance of the unlabeled d-TCO derivatives with Tz-modified antibodies (mAb-Tz) in tumor-bearing mice. The assay is based on the pretargeted blocking of ^{111}In-labeled-Tz as reported by Stéen *et al.* to identify the key parameters to obtain optimal Tz-based radiotracers.[80] Here, a Cy5-fluorophore-conjugated TCO was used together with a Tz-modified CC49 Ab (CC49-Tz) as a standard model for *in vivo* ligation. CC49 is a noninternalizing mAb that targets the tumor-associated glycoprotein-72 (TAG-72) which is overexpressed in a wide range of solid tumors, making it a perfect candidate for pretargeting. Based on previous reports, a pretargeting interval of 72 h was selected to maximize the clearance of unbound CC49-Tz from the circulation and to ensure lower background during imaging.[78] CC49 was modified with MeBA-NHS ester following a previously reported procedure yielding average of 8-Tz bound to CC49 (Figure S4.2).[89] A binding assay was performed to confirm the conservation of the binding affinity of the mAb-Tz conjugate to the TAG-72 antigen when compared to the native CC49 Ab. CC49 (K_d = 11.70 nM; 95% CI 9.91 -13.49) and CC49-Tz (K_d = 17.68 nM; 95% CI 8.42-26.94) both showed similar binding affinity towards human TAG-72 (Figure S4.3).

Through the blocking assay, the *in vivo* ligation efficiency of the unlabeled d-TCO derivatives can be inversely correlated to the uptake of TCO-Cy5 in the tumor (Figure 4.1A, B). The highest blocking efficiencies of 93 and 95% *in vivo* were observed for the d-TCO derivates **UAMC-3711** and **UAMC-4129** with the lowest uptake values of TCO-Cy5 in tumor 7 ± 3% (n=4) and 5 ± 2% (n=4), respectively. The *ex vivo* analysis also validated the findings from *in vivo* fluorescence measurements (Figure 4.1C). **UAMC-3724** showed moderate blocking efficiency with 17 ± 9% (n=4) of TCO-Cy5 uptake in the tumor, whereas **UAMC-3725** and **UAMC-3933** showed poor *in vivo* ligation performance with, respectively, higher TCO-Cy5 uptake values in tumor of 50 ± 20 % (n=4) and 53 ± 20% (n=4). Given their high *in vivo* ligation efficiency, *UAMC-4129* and *UAMC-3711* were chosen for further radiochemical development and evaluation.

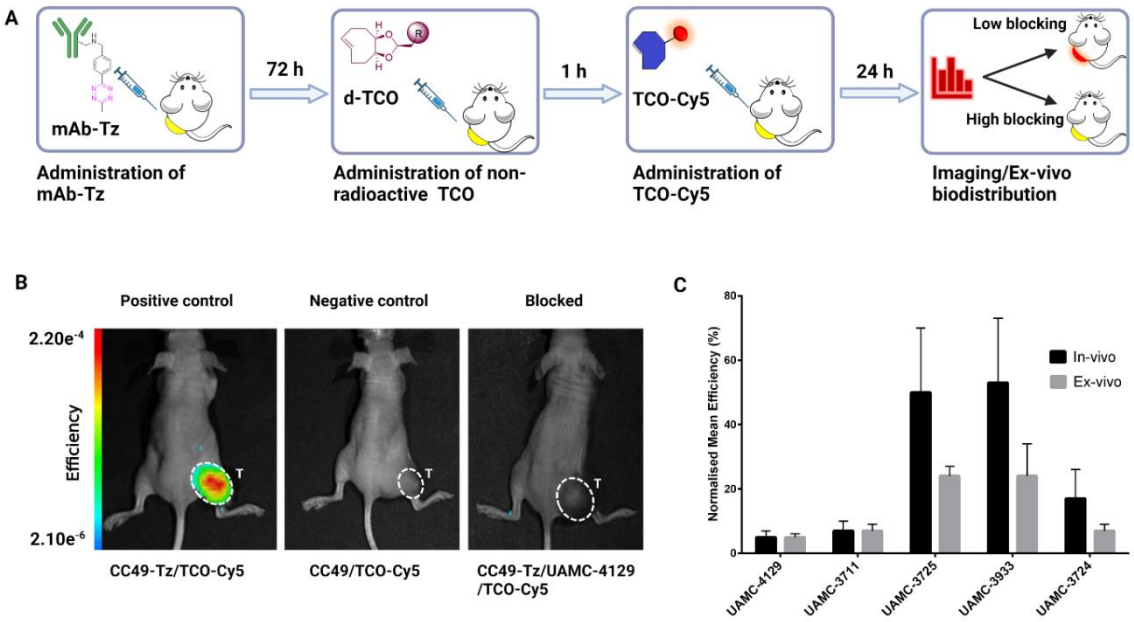

Figure 4.1 *(A) Procedure followed for the in vivo pretargeted blocking approach. (B) In vivo representative fluorescence image of TCO-Cy5 uptake in LS174T tumor-bearing mice. Images were acquired 24 h post-TCO-Cy5 injection and the fluorescence signal was quantified as total efficiency. The white dashed line encircles the tumor. (C) Tumor uptake of TCO-Cy5 in vivo and ex vivo was expressed as total efficiency in the blocked group. Data normalized to TCO-Cy5 uptake in positive and negative control groups. (mean ± SD, n=4/group)*

4.4.4 Radiochemistry

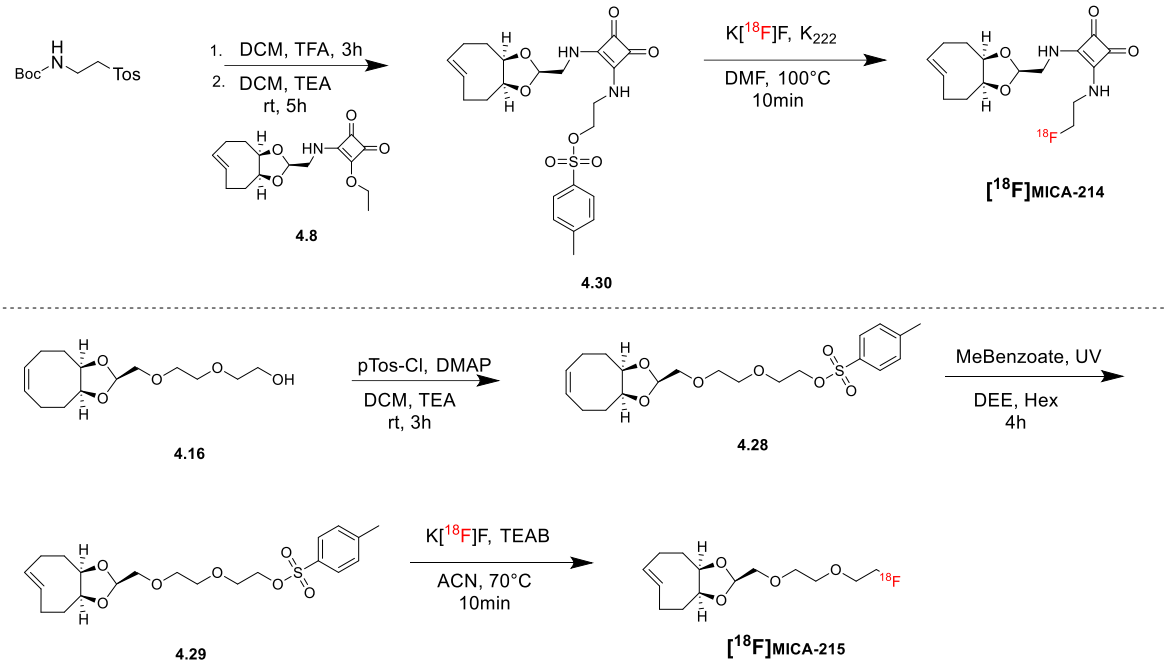

Scheme 4.2 *Precursor synthesis and radiosynthesis of [^{18}F]MICA-214 and [^{18}F]MICA-215.*

For the synthesis of **MICA-214** precursor, 2-((tert-butoxycarbonyl)amino)ethyl 4-methylbenzenesulfonate was first deprotected with trifluoroacetic acid (TFA) followed by the addition of **4.8** afforded the tosylate precursor **4.30**. Precursor **4.30** (6 mg) was reacted with K[^{18}F]F in DMF for 10 min at 100°C to afford the radiolabeled product [^{18}F]MICA-214 (Scheme 2) in 5.2 ± 0.6% isolated radiochemical yield (RCY) decay corrected to end of bombardment (EOB) with >98% radiochemical purity (RCP) and molar activity (A_m) -between 36 and 50 GBq/µmol and a total synthesis time of 60 min. **MICA-215** precursor was obtained by first tosylating **4.16** followed by the isomerization to trans-precursor **4.29**, which was reacted with K[^{18}F]F in acetonitrile for 10 min at 100°C to afford the radiolabeled product **[^{18}F]MICA-215** (Scheme 4.2) in 11.2 ± 0.4% isolated RCY (decay corrected to EOB), with >98% RCP and Am ≥ 7.34 GBq/µmol and a total synthesis time of 72 min. The identity of both tracers was confirmed by coinjection and coelution of the isolated radiotracers with the nonradiolabeled references **UAMC-4129** and **UAMC-3711** (Figure S4.4). Both radiotracers showed moderate lipophilicity with log *D* values of 0.62 ± 0.09 (n=3) for [^{18}F]MICA-214 and 1.25 ± 0.10 (n =3) for [^{18}F]MICA-215. The *in vitro* stability of both radiotracers was investigated by incubating the tracer in PBS at room temperature and mouse plasma at 37°C. Both tracers showed excellent stability in PBS at 2 h with 93 ± 1.6% for **[^{18}F]MICA-214**, and 100% intact tracer

for **[^{18}F]MICA-215** (Figure S4.5). In plasma, 42 ± 2.9% (n=3) of **[^{18}F]MICA-214** was available at 2 h (Figure S4.5), with the formation of one polar radiolabeled metabolite and a gradual increase of cis-isomer formation. In contrast, **[^{18}F]MICA-215** showed very good stability in plasma, with 94 ± 2.4% (n = 3) of intact radiotracer present at 2 h (Figure S4.5), and only a small amount of radiometabolites formation observed.

4.4.5 *Ex vivo* biodistribution and in vivo stability studies in non-tumor-bearing mice

Next, the pharmacokinetic profile and *in vivo* stability of the new d-TCO PET probes were evaluated in healthy mice (Figure 4.2; Tables S4.2 and S4.3; Figure S4.6). The *ex vivo* biodistribution of **[^{18}F]MICA-214** and **[^{18}F]MICA-215** showed mixed hepatobiliary and renal clearance of the radiotracer. For both tracers, the majority of the activity cleared through kidneys (**[^{18}F]MICA-214** 2.2 ± 0.5% ID/g at 60 min; **[^{18}F]MICA-215** 4.4 ± 0.2% ID/g at 60 min) followed by accumulation in the bladder and excretion in the urine (**[^{18}F]MICA-214** 59.7 ± 15.1% ID/g at 60 min; **[^{18}F]MICA-215** 606.3 ± 252.4 %ID/g at 60 min). A smaller fraction of the **[^{18}F]MICA-214** cleared through the liver (**[^{18}F]MICA-214** (4.0 ± 0.8% ID/g) at 60 min) with the highest accumulation in the small intestines (**[^{18}F]MICA-214** (17.8 ± 4.7% ID/g) at 60 min). In contrast, the uptake of **[^{18}F]MICA-215** in small intestine remained lower (**[^{18}F]MICA-215** (5.2 ± 0.1% ID/g at 60 min)). Importantly, both tracers showed an absence of *in vivo* defluorination, with no significant increase in bone uptake (**[^{18}F]MICA-214** (2.8 ± 1.3% ID/g) at 60 min; **[^{18}F]MICA-215** 2.7 ± 0.2 %ID/g at 60 min). Overall, **[^{18}F]MICA-214** showed lower accumulation in remaining organs at 1 h p.i. compared to **[^{18}F]MICA-215** (Figure 4.2, Table S4.2 and S4.3) and better renal clearance in comparison to previously reported d-TCO radiotracers.[88, 213]

Both tracers were rapidly metabolized *in vivo* with 24.6 ± 2.4% (n=3) of tracer remaining intact at 5 min and 10.8 ± 0.57% (n=3) at 15 min for **[^{18}F]MICA-214**. For **[^{18}F]MICA-215**, 7.9 ± 2.3% (n=3) and 2.1 ± 0.4% (n=3) of radiotracer were intact at 5 and 15 min, respectively (Figure S4.6). In both cases, one prominent polar radiometabolite peak was observed, increasing over time up to 1 h p.i. (92.0 ± 1.7% for **[^{18}F]MICA-214** and 95.1 ± 0.3% for **[^{18}F]MICA-215**). Although the radiotracer is relatively rapidly metabolized *in vivo*, studies have shown that this only has a limited effect on the *in vivo* ligation due to the fast kinetics of the TCO-Tz reaction.[80] Nonetheless, the intact radiotracer must accumulate at the target site in sufficient quantities and react with the Tz-Ab conjugate to visualize the target. Due to the overall higher accumulation of **[^{18}F]MICA-215** combined with the faster *in vivo* metabolization of **[^{18}F]MICA-215** at earlier time points, its use *in vivo* is limited. Therefore, only **[^{18}F]MICA-214** was chosen for further pretargeted imaging studies in a tumor model.

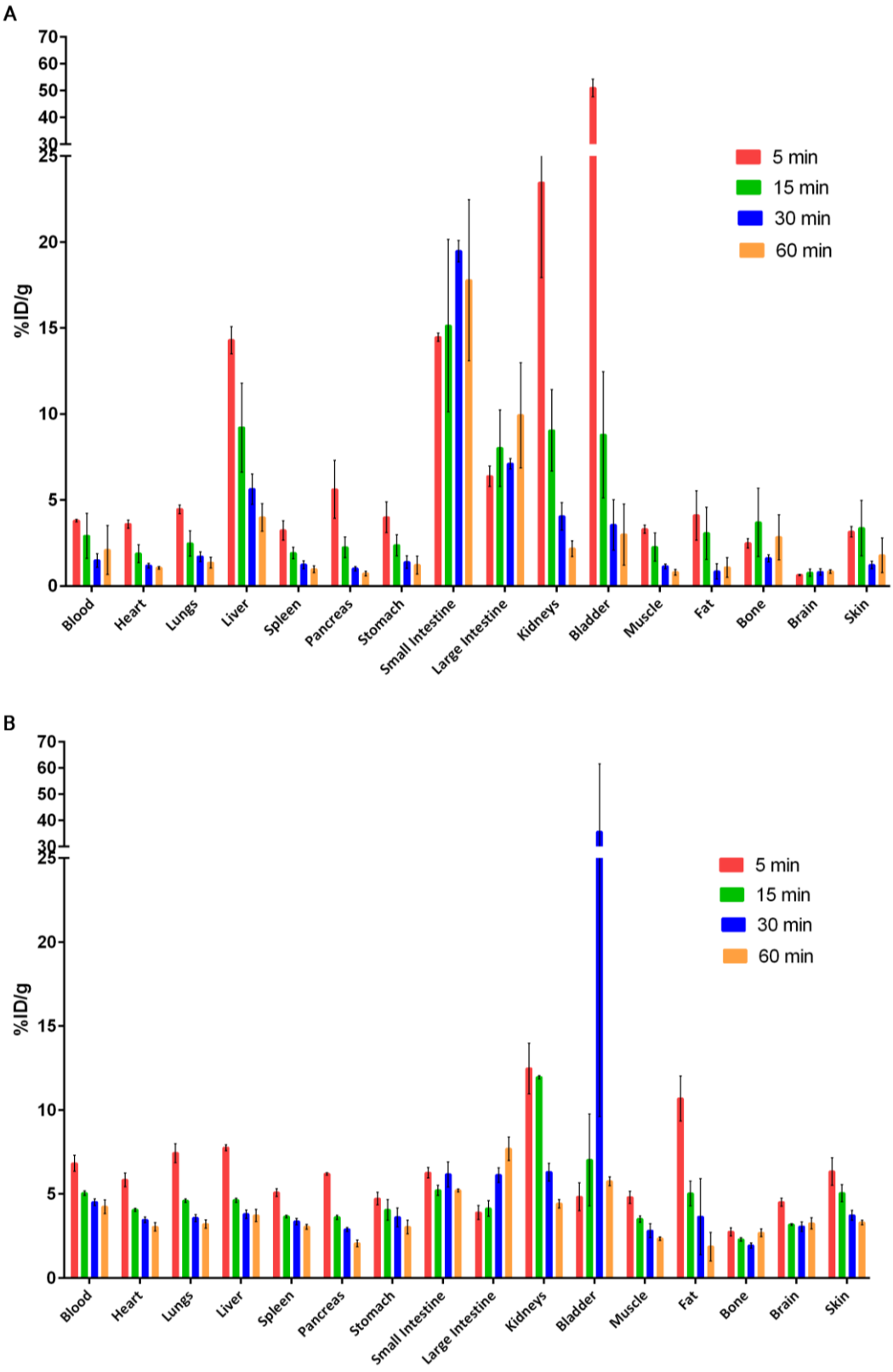

Figure 4.2 *Biodistribution of (A)* ***[^{18}F]MICA-214*** *and (B)* ***[^{18}F]MICA-215*** *in naïve BALB/c nude mice (mean ± SD, n=3/group)*

4.4.6 *In vivo* pretargeted µPET imaging

Given the tracer's fast clearance, *in vivo* stability, low nonspecific tissue accumulation, and excellent *in vivo* ligation properties, we proceeded with pretargeted imaging in a tumor model using **[^{18}F]MICA-214**. *In vivo*, pretargeted µPET imaging was performed in LS174T tumor-bearing mice pre-treated with either CC49-Tz or CC49 (control group) 72 h before injection of **[^{18}F]MICA-214.** The µPET images demonstrated an increased activity accumulation in the tumor in the group injected with CC49-Tz (2.16 ± 0.08% ID/mL). In contrast, in the control group, the activity remained significantly lower (1.34 ± 0.07 %ID/mL; $p < 0.0001$), which is consistent with the fact that there was no Tz tag present in the Ab (Figure 4.3A and 4.3B). In accordance with the biodistribution studies in healthy mice, there were no differences in the uptake of radioactivity in other tissues between groups, indicating that CC49-Tz has been cleared from all nontarget tissues. *Ex vivo* biodistribution studies validated the *in vivo* results with significantly higher tumor uptake of **[^{18}F]MICA-214** in mice injected with CC49-Tz (1.73 ± 0.37 %ID/g) than in the control group (1.08 ± 0.10 %ID/g; $p = 0.0144$), as shown in Figure 4.3C (Table S4.4).

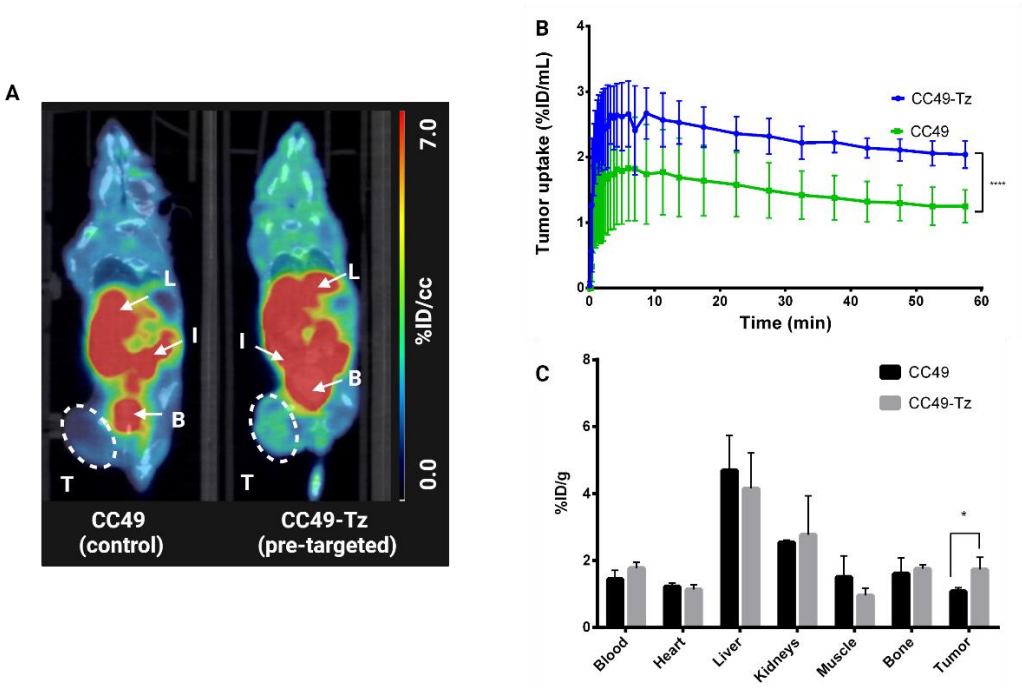

Figure 4.3 *(A) In vivo representative coronal µPET/CT image of LS174T tumor-bearing mice injected with [^{18}F]MICA-214 72 h post-CC49 (control) or CC49-Tz (pre-targeted) injection. PET images represent averaged tracer distribution from the dynamic scans (0-60 min). The white dashed lines encircle the tumor region, and arrows represent the bladder (B), intestines (I), and liver (L). (B) Time-activity curve of tumor uptake of [^{18}F]MICA-214 in groups injected with CC49-Tz and control group injected with CC49 (0 to 60 min) (mean ± SD, n=4/group). (C) Ex vivo biodistribution of LS174T tumor-bearing mice 60 min post tracer injection.*

4.5 Discussion

In vivo, pretargeted imaging relies highly on the stability and fast reaction kinetics between the reaction partners TCO and Tz. The d-TCO scaffold was selected due to its fast kinetics and enhanced stability compared to other strained TCO structures.[73] Compounds derivatized with short ethylene glycol chains were designed to increase hydrophilicity. A squaramide linker was chosen to impact both the hydrophilicity and stability of the tracer. However, sulfonylamide and cyclopropyl linkers were chosen to impact the ^{18}F-C bond stability.[306] For the synthesis of the d-TCO derivatives, mild reaction conditions were opted to avoid trans to cis isomerization during synthesis. Where possible the compounds were isomerized at the final stage of synthesis.

The synthesized compounds were tested for reactivity against tetrazine. As we inverted the functionalities, the stability of the Tz conjugated to mAb rather than just the ultrafast kinetics plays a significant role. 6-Methylated tetrazines are known to be more stable in exposure to physiological conditions.[140] Hence, MeBA was selected as the model Tz for *in vivo* ligation based on literature regarding its use in biological applications, stability, and commercial availability. MeBA with its remarkable stability and moderate kinetics is currently, to our best knowledge, the only tetrazine in use in a human clinical trial for pretargeted drug delivery.[275, 279] Only slight differences in the reactivity of d-TCOs with different linkers were observed, as the linkers are distant from the reaction center of the dienophile. Compounds with more hydrophilic linkers exhibited slightly faster kinetics. The kinetics of the synthesized d-TCOs are also comparable to previously reported d-TCO derivatives.[88, 213] The overall reactivity remained similar to the parent d-TCO compound with k_2 of 167000 ± 7000 $M^{-1}s^{-1}$ in similar reaction conditions.

To assess the *in vivo* ligation of the synthesized compounds, a pretargeted blocking assay was developed. This screening assay allowed to have an earlier readout of the TCO reactivity towards Ab-modified Tz, avoiding the need for time-consuming radiochemical development of each TCO derivative. Compounds **UAMC-3711** and **UAMC-4129** containing polar linkers (squaramide and PEG chain) showed excellent blocking efficiency. In contrast, compounds containing more lipophilic cyclobutyl fluoride and 6-fluoro-3-sulfonylpyridine linkers and with higher log *D* values showed poor blocking efficiency. Nonetheless, bigger compound libraries are required to establish a more profound correlation.

The radiolabeling conditions differed slightly for both tracers. In the case of **[^{18}F]MICA-214** better radiochemical conversion (RCC) was achieved with Kryptofix$_{2.2.2}$ ($K_{2.2.2}$) when compared to that with tetraethylammonium bicarbonate (TEAB). On the other hand, TEAB provided sufficient RCC for **[^{18}F]MICA-215**. TCOs are known to isomerize at higher temperatures.[308] Here, a larger disparity in temperature tolerance was observed. Only a negligible amount of trans-to-cis isomerization was observed for **[^{18}F]MICA-214** up to 100°C. However, only the cis-isomer of **[^{18}F]MICA-215** was isolated at temperatures above 80°C. Also, the choice of solvent played a role. In both cases, only cis isomers were observed when reactions were performed in DMSO. The RCC for both tracers was satisfactory, and isolated RCY of both tracers remained relatively low due to some trans-to-cis isomerization of both precursors and products during radiosynthesis. Nonetheless, the reported RCYs are comparable to previously reported 18F-labeled d-TCOs.[88, 213, 264]

In vitro, **[^{18}F]MICA-215** exhibited superior stability compared to **[^{18}F]MICA-214**. However, the situation was reversed *in vivo*, with **[^{18}F]MICA-214** demonstrating a higher stability than **[^{18}F]MICA-215**. This finding emphasizes the importance of conducting *in vivo* stability assessments rather than relying solely on extrapolating data from plasma stability screenings.

In biodistribution studies, both tracers displayed mixed renal and hepatobiliary clearance resulting in high abdominal activity as observed for previously described d-TCO radiotracers.[88, 213] **[^{18}F]MICA-214** showed faster renal clearance when compared to **[^{18}F]MICA-215** with higher radioactivity accumulation in kidneys and bladder at earlier time points (Figure 4.2). Higher radioactivity accumulation in intestines is observed with **[^{18}F]MICA-214** (17.8 ± 4.7% ID/g at 60min) compared to **[^{18}F]MICA-215** (5.2 ± 0.01% ID/g at 60 min), indicating that the accumulation might be associated with linker dependent metabolization of the compound. Thus, further fine-tuning of the linker with polar groups to decrease liver clearance could reduce abdominal activity. Furthermore, the *in vivo* stability assessment of **[^{18}F]MICA-214** and **[^{18}F]MICA-215** showed substantial metabolization of the radiotracers (Figure S4.6). Thus, the higher accumulation of radioactivity can also be attributed to the accumulation of the radiometabolites in these organs. In both instances, the HPLC analysis revealed the presence of a polar radiometabolite. Among the potential metabolites that may be formed *in vivo*, one could be the free aldehyde with an ^{18}F-label on the linker, resulting from the hydrolysis of the dioxolane ring of the d-TCO. Several strategies have been proposed in the literature to stabilize the acetal group *in vivo*, such as the introduction of proximal electron-

withdrawing groups, basic amines, heteroaryl rings, or the implementation of steric and strain effects.[309] Nevertheless, further detailed analysis and investigations are imperative to substantiate this hypothesis. During the pretargeted imaging study, the radioactivity in the blood remained similar to the biodistribution studies, suggesting the **[^{18}F]MICA-214** is primarily reacting with CC49-Tz at the tumor site rather than with mAb still circulating in the blood implying a good pretargeting interval between the mAb-Tz and the radiotracer injection.[80, 95] Both *in vivo* PET/CT data and *ex vivo* analysis showed a significantly higher tumor uptake compared to control group confirming the *in vivo* d-TCO-Tz ligation. The main obstacle remains the high abdominal uptake as seen with previously developed d-TCO derivatives.[87, 88] When compared with ^{18}F-labeled-Tzs, a low tumor-to-muscle (T/M) ratio of 1.8 was observed (Table S4.4). However, with a tumor-to-blood (T/B) ratio of 0.9 and tumor-to-liver ratio of 0.4 (Table S4.4), the target-to-background contrast remained comparable to previously reported studies with ^{18}F-labeled-Tzs.[93-95] This emphasizes the general need to improve the tumor-to-background ratios in pretargeted imaging studies. Further optimization of the tracer with more polar linkers containing longer PEG-chains or introduction of diacetic acid or sugar molecules could increase the TCO's polarity enhancing the real clearance while decreasing nonspecific uptake. Additionally, the use of more hydrophilic-TCO variants, like oxo-TCO could offer an alternative.[242] Finally, the identification of metabolites could guide the design of TCOs towards more metabolically stable compounds. These combined factors might decrease the uptake of the tracer in nontarget tissues to reduce the background signal, which led to low tumor-to-background ratios.

4.6 Conclusion

Pretargeted PET imaging is a promising approach for the development of precision and highly efficient tools for the personalized diagnostics and safe radionuclide therapy treatment of patients. Despite recent progress in the field, the development and availability of radiolabeled compounds for *in vivo* use remains quite limited. Bigger libraries of the compound and systematic studies are needed to gain further insight into the pretargeting approach to pave the way toward clinical translation. In an effort to expand the bioorthogonal toolbox, we have developed a diverse series of d-TCO probes with excellent reactivity toward tetrazines and evaluated their *in vivo* ligation ability through a pretargeted blocking approach. From the series, the best-performing compounds were selected for further radiochemical development, pharmacokinetics, and *in vivo* stability

evaluation. Finally, the radiotracer **[^{18}F]MICA-214** was used in pretargeted PET imaging in mice-bearing tumors. Although higher activity accumulation of the radiotracer was achieved in the mice injected with CC49-Tz compared with the control group, further optimization of the radiotracer is needed to reduce background uptake, and thus enhance tumor contrast in future studies. Nevertheless, this work creates a base for further development and evaluation of d-TCO-based radiotracers for pretargeted PET imaging.

4.7 Supplemental data

4.7.1 Chemical Synthesis and Characterization

(1R,2S,Z)-cyclooct-5-ene-1,2-diol (4.1)

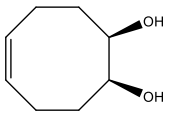

Synthesized according to a modified protocol from Darko *et al*.[310]. Cyclooctadiene (22.25 mL, 181 mmol) was added dropwise to a stirring solution of Osmium tetroxide (1.85 mL, 4% wt. in H_2O 0.29 mmol) and *N*-Methylmorpholine-*N*-oxide monohydrate (20.5 mL, 50% wt. in H_2O, 85.5 mmol) in THF:acetone: H_2O (1:1:1, 450 mL) at 0°C. After the addition was complete, the mixture was stirred at room temperature for 48 h. Sodium metabisulfite (0.76 g) and Florisil (9.84 g) slurried in water (66 mL) were added and stirred for 30 minutes, and the mixture was filtered through a pad of celite. The filtrate was neutralized with 1N H_2SO_4 and concentrated to remove all organics. The resulting aqueous solution was adjusted to pH 2 with 1N H_2SO_4 and extracted with EtOAc (3 x 400mL). The combined organic phases were washed with brine, dried over Na_2SO_4, and concentrated into a white solid. The product was purified by silica gel flash chromatography (50-80% EtOAc in Heptane) to provide diol 4.1 as a white solid (3.95g, 15%). ^{1}HNMR spectra are in accordance with previously reported data.[310] ^{1}H NMR (400 MHz, $CDCl_3$) δ = 5.73 – 5.61 (m, 2H), 4.04 – 3.94 (m, 2H), 2.58 – 2.42 (m, 2H), 2.13 – 1.95 (m, 4H), 1.87 – 1.73 (m, 2H).^{13}C NMR (101 MHz, $CDCl_3$) δ = 130.1, 75.2, 32.1, 23.1.

((2s,3aR,9aS,Z)-3a,4,5,8,9,9a-hexahydrocycloocta[d][1,3]dioxol-2-yl)methanol (4.2)

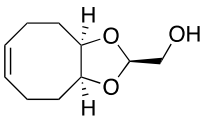

Synthesized according to a modified protocol from Darko *et al*.[310] p-Toluenesulfonicacidmonohydrate (0.51 g, 2.67 mmol) was added to a solution of **4.1** (1.90 g, 13.36 mmol), and 2,5-Dihydroxy-1,4-dioxane (1.44 g, 12.03 mmol) in THF (100 mL) and stirred at room temperature for 48 hours. The mixture was diluted with $CHCl_3$ (100 mL) and washed with saturated $NaHCO_3$ (100 mL). The organics were separated, washed with brine (50 mL), dried over Na_2SO_4, filtered, and concentrated. The crude oil was purified by silica gel flash chromatography (0-30% EtOAc in Heptane) to afford a colorless oil (1.64 g, 67%). ^{1}H NMR (400 MHz, $CDCl_3$) δ = 5.65-5.57 (m, 2H), 4.93 (t, *J* = 3.2 Hz, 1H), 4.23 – 4.18 (m, 2H), 3.66 (d, *J* = 3.2 Hz, 2H), 2.55 – 2.44 (m, 2H), 2.15 – 2.03 (m, 6H), 2.01 – 1.95 (m, 2H).^{13}C NMR (101 MHz, $CDCl_3$) δ = 129.0, 101.2, 79.4, 63.4, 28.6, 23.6.

((2s,3aR,9aS,Z)-3a,4,5,8,9,9a-hexahydrocycloocta[d][1,3]dioxol-2-yl)methyl methanesulfonate (4.3)

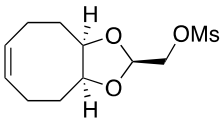

Synthesized as previously reported by Ruivo et.al. [88] To a solution of **4.2** (1.6 g, 8.60 mmol), *N*, *N*-Di-iso-propylethylamine (3.30 ml, 18.93 mmol), and 4-Dimethylaminopyridine (0.11 g, 0.86 mmol) in dry Dichloromethane (25 mL) was added Methanesulfonylchloride (0.80 ml, 10.32 mmol) under N_2 atmosphere. The reaction mixture was stirred at RT for 1 h and then washed with a saturated solution of $NaHCO_3$ (20mL). The organic layers were combined, washed with brine (10 mL), dried over $Na2SO_4$, filtered, and evaporated under reduced pressure. The product was purified by silica gel flash chromatography (0-30% EtOAc in Heptane) to afford a pale-yellow oil (2.03 g, 90%). ^{1}H NMR (400 MHz, CDCl3) δ = 5.66 – 5.54 (m, 2H), 5.06 (t, *J* = 3.7 Hz, 1H), 4.23 (d, *J* = 3.7 Hz, 2H), 3.07 (s, 3H), 2.57 – 2.44 (m, 2H), 2.15 – 2.02 (m, 4H), 2.00 – 1.91 (m, 2H). ^{13}C NMR (101 MHz, $CDCl_3$) δ = 129.2, 98.8, 79.7, 69.5, 38.0, 28.4, 23.5.

(2s,3aR,9aS,Z)-2-(azidomethyl)-3a,4,5,8,9,9a-hexahydrocycloocta[d][1,3]dioxole (4.4)

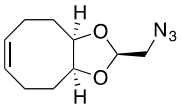

To a solution of **4.3** (1.2 g, 4.44 mmol) in dry DMF (15 mL) was added Triethylamine (1.24 ml, 8.88 mmol) and sodium azide (0.72 g, 11.10 mmol) under N_2 atmosphere and refluxed overnight. The mixture was cooled down to RT and diluted with EtOAc (100mL) and washed with ice-cold water (100 mL). The organic phase was separated, and the aqueous phase was extracted with EtOAc (2 x 50 mL). The organics were combined, washed with brine (50 mL), dried over Na_2SO_4, filtered, and evaporated under reduced pressure. The product was purified by silica gel flash chromatography (0-30% EtOAc in Heptane) to afford a colorless oil (0.53 g, 61%). ^{1}H NMR (400 MHz, $CDCl_3$) δ = 5.68 – 5.55 (m, 2H), 4.99 (t, *J* = 3.6 Hz, 1H), 4.27 – 4.15 (m, 2H), 3.34 (d, *J* = 3.6 Hz, 2H), 2.60 – 2.43 (m, 2H), 2.20 – 2.06 (m, 4H), 2.05 – 1.95 (m, 2H).^{13}C NMR (101 MHz, $CDCl_3$) δ = 129.4, 100.4, 79.7, 53.2, 28.6, 23.5.

((2s,3aR,9aS,Z)-3a,4,5,8,9,9a-hexahydrocycloocta[d][1,3]dioxol-2-yl)methanamine (4.5)

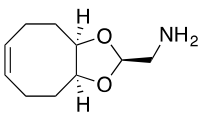

Lithium aluminum hydride 2.4M in THF (2.21 mL, 5.31 mmol) was added to a dry flask and cooled at 0°C. Then, dry THF (10 mL) was added. To this slurry, and at 0°C, **4.4** (550 mg, 2.60 mmol) dissolved in dry THF (5 mL) was added dropwise. The reaction was heated to reflux for 30 min, then cooled to 0ºC. The mixture was diluted with diethyl ether (30 mL). NaOH (10% wt, 2mL) was added dropwise until gas evolution stopped. Water

(15 mL) was added, and the mixture was stirred further at 0°C for 30min. The salts were filtered, and the organics were separated from the aqueous phase and washed with water (30 mL) and brine (20 mL), dried with Na_2SO_4, filtered, and evaporated under reduced pressure to afford a colorless oil. The compound was used in the next step without further purification. ^{1}H NMR (400 MHz, $CDCl_3$) δ = 5.63 – 5.55 (m, 2H), 4.78 (t, *J* = 3.2 Hz, 1H), 4.18 – 4.11 (m, 2H), 2.80 (d, *J* = 3.3 Hz, 2H), 2.50 – 2.42 (m, 2H), 2.09 – 2.01 (m, 4H), 1.97 – 1.90 (m, 2H). ^{13}C NMR (101 MHz, $CDCl_3$) δ = 129.5, 102.6, 79.2, 44.8, 28.8, 23.5.

2,2,2-trifluoro-N-(((2s,3aR,9aS,Z)-3a,4,5,8,9,9a-hexahydrocycloocta[d][1,3]dioxol-2-yl)methyl)acetamide (4.6)

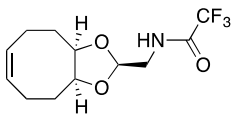

To a solution of **4.5** (656 mg, 3.58 mmol) and Pyridine (0.43 ml, 5.37 mmol), in DCM (30 mL) under N_2 at 0 °C, Trifluoroacetic anhydride (0.60 ml, 4.30 mmol) was added dropwise. The ice bath was removed, and the reaction mixture was stirred at rt for 2 h. The reaction mixture was quenched with water (20 mL) and extracted with DCM (40 mL). The organic phases were combined, washed with brine (20 mL), dried with Na_2SO_4, filtered, and evaporated under reduced pressure. The compound was used in the next step without further purification. ^{1}H NMR (400 MHz, $CDCl_3$) δ = 6.53 (s, 1H), 5.69 – 5.55 (m, 2H), 4.96 (t, *J* = 3.1 Hz, 1H), 4.30 – 4.14 (m, 2H), 3.58 (dd, *J* = 5.8, 3.1 Hz, 2H), 2.57 – 2.41 (m, 2H), 2.17 – 1.88 (m, 6H). ^{13}C NMR (101 MHz, $CDCl_3$) δ = 157.5 (q, $^2J_{C,F}$ = 36.9 Hz), 129.6, 114.5 (q, $^1J_{C,F}$ = 288.9 Hz), 98.7, 79.6, 41.7, 28.7, 23.3.

2,2,2-trifluoro-N-(((2s,3aR,9aS,E)-3a,4,5,8,9,9a-hexahydrocycloocta[d][1,3]dioxol-2-yl)methyl)acetamide (4.7)

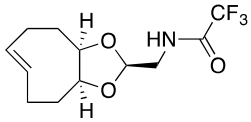

The flow photoisomerization procedure was followed using **4.6** (997 mg, 3.57 mmol) in ether/hexanes (300 mL) and Methyl benzoate (0.90 mL, 7.14 mmol) in a quartz tube.[310] A 25 g Biotage SNAP column was filled with silica gel (6 cm) and the remaining space was packed with 10% silver-impregnated silica (5.70 g). The column was connected to a pump and flushed with 1:1 ether/hexanes (200 mL). Irradiation was carried out at 254 nm for 4 h. The column was flushed with EtOAc (150 mL) and dried under airflow. The silica was placed into a flask and stirred in ammonium hydroxide solution (25% wt., 200 mL) and DCM (200 mL) for 10 min. The silica was filtered and washed with additional ammonium hydroxide (100 mL) and dichloromethane (100 mL). The phases were separated, and the aqueous

layer was extracted an additional three times with DCM (3 x 50 mL). The combined organic layers were washed with water (2 x 150 mL) and brine (100 mL), dried over Na_2SO_4, filtered, and concentrated under reduced pressure. The product was purified by silica gel flash chromatography (DCM 100%) to afford a colorless oil (285 mg, 29%). ^{1}H NMR (400 MHz, $CDCl_3$) δ = 6.45 (s, 1H), 5.67 – 5.57 (m, 1H), 5.55 – 5.44 (m, 1H), 4.91 (t, *J* = 2.8 Hz, 1H), 4.05 – 3.86 (m, 2H), 3.63 – 3.50 (m, 2H), 2.47 – 2.37 (m, 1H), 2.33 – 2.25 (m, 1H), 2.23 – 2.09 (m, 2H), 1.95 – 1.78 (m, 2H), 1.72 – 1.61 (m, 1H), 1.53 – 1.40 (m, 1H). ^{13}C NMR (101 MHz, $CDCl_3$) δ = 157.4 (q, $^2J_{C,F}$ = 37.1 Hz), 136.4, 131.2, 115.8 (q, $^1J_{C,F}$ = 310.6 Hz) 98.1, 83.0, 80.9, 41.2, 38.6, 33.6, 31.3, 25.5.

((2s,3aR,9aS,E)-3a,4,5,8,9,9a-hexahydrocycloocta[d][1,3]dioxol-2-yl)methanamine (4.8)

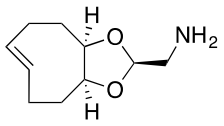

Compound **4.7** (280 mg, 0.286 mmol) was dissolved in MeOH (2 mL) and Sodium hydroxide (115 mg, 2.86 mmol) in H_2O (0.67 mL) was added. The mixture was heated to reflux for 90 min. The mixture was cooled down to room temperature, evaporated and the residue was diluted in water (20 mL) and extracted with DCM (2 x 20mL). The compound was used in the next step without further purification. ^{1}H NMR (400 MHz, $CDCl_3$) δ = 5.67 – 5.57 (m, 1H), 5.56 – 5.46 (m, 1H), 4.74 (t, *J* = 3.1 Hz, 1H), 4.03 – 3.85 (m, 2H), 2.80 (t, *J* = 2.8 Hz, 2H), 2.46 – 2.34 (m, 1H), 2.31 – 2.24 (m, 1H), 2.22 – 2.09 (m, 2H), 1.93 – 1.79 (m, 2H), 1.74 – 1.49 (m, 2H). ^{13}C NMR (101 MHz, $CDCl_3$) δ = 136.3, 131.2, 101.6, 82.7, 80.6, 44.2, 38.7, 33.9, 31.3, 25.7.

3-ethoxy-4-((((2s,3aR,9aS,Z)-3a,4,5,8,9,9a-hexahydrocycloocta[d][1,3]dioxol-2-yl)methyl) amino)cyclobut-3-ene-1,2-dione (4.9)

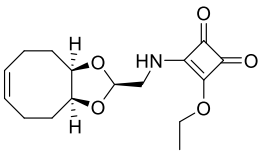

Compound **4.5** (200 mg, 1.09 mmol) was dissolved in anhydrous THF (10 mL) under an N_2 atmosphere. The solution was cooled down to 0°C followed by a dropwise addition of Diethylsquarate (0.13 mL, 0.87 mmol). The reaction was stirred at room temperature for 4h. The reaction mixture was evaporated under reduced pressure and used in the next step without further purification. ^{1}H NMR (400 MHz, $CDCl_3$) δ = 5.91 (s, 1H), 5.67 – 5.54 (m, 2H), 4.96 (t, *J* = 2.8 Hz), 4.82 – 4.72 (m, 2H), 4.28 – 4.14 (m, 2H), 3.65 – 3.58 (m, 2H), 2.56 – 2.41 (m, 2H), 2.16 – 1.87 (m, 6H), 1.45 (t, *J*=7.1 Hz, 3H). ^{13}C NMR (101 MHz, $CDCl_3$) δ 188.8, 183.7, 177.8, 173.6, 128.7, 99.4, 79.7, 69.9, 46.5, 28.6, 23.4. UPLC/MS (ESI+): *m/z* = 308.2 [M+H]+.

3-((2-fluoroethyl)amino)-4-((((2s,3aR,9aS,Z)-3a,4,5,8,9,9a -hexahydrocycloocta[d][1,3] dioxol-2-yl)methyl)amino)cyclobut-3-ene-1,2-dione (4.10)

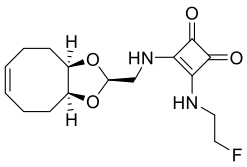

Compound **4.9** (370 mg, 1.20 mmol) was dissolved in EtOH (10 mL). Triethylamine (1.68 ml, 12.04 mmol) and 2-Fluoroethylamine hydrochloride (359 mg, 3.61 mmol) were added and stirred at room temperature for 5h. The mixture was concentrated under reduced pressure and the crude product was purified by silica gel flash chromatography (0-3% MeOH in DCM) to afford **4.10** as a white powder (123 mg, 32%). ^{1}H NMR (400 MHz, DMSO) δ = 7.63 (s, 1H), 7.49 (s, 1H), 5.64 – 5.54 (m, 2H), 4.87 (t, *J*=3.5 Hz, 1H), 4.53 (dt, *J*=47.0 Hz, 4.9 Hz, 2H), 4.16 – 4.07 (m, 2H), 3.89 – 3.74 (m, 2H), 3.69 (s, 2H), 2.47 – 2.34 (m, 2H), 2.08 – 1.93 (m, 4H), 1.91 – 1.77 (m, 2H). ^{13}C NMR (101 MHz, DMSO) δ = 182.9, 182.7, 168.5, 167.7, 129.3, 99.9, 83.4 (d, $^{1}J_{C,F}$ =165.5 Hz), 78.6, 45.8, 43.6 (d, $^{2}J_{C,}$F =19.8 Hz), 28.1, 22.8. UPLC/MS (ESI+): *m/z* = 325.1 [M+H]+.

3-ethoxy-4-((((2s,3aR,9aS,E)-3a,4,5,8,9,9a-hexahydrocycloocta[d][1,3]dioxol-2yl)methyl)amino) cyclobut-3-ene-1,2-dione (4.11)

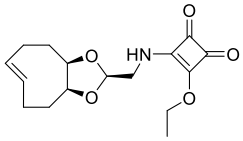

Compound **4.8** (194 mg, 1.06 mmol) was dissolved in dry THF (15 mL) under N_2. Diethylsquarate (0.16 mL, 1.06 mmol) was added dropwise at 0°C and stirred further at room temperature for 4h. The solvents were evaporated, and the crude mixture was purified by silica gel flash chromatography (0-5% MeOH in DCM) to afford **4.11** as a white powder (265 mg, 81%). ^{1}H NMR (400 MHz, $CDCl_3$) δ = 5.90 (s, 1H), 5.63 – 5.41 (m, 2H), 4.90 (t, *J*=2.6 Hz, 1H), 4.78 – 4.69 (m, 2H), 4.02 – 3.88 (m, 2H), 3.62 – 3.56 (m, 2H), 2.46 – 2.34 (m, 1H), 2.31 – 2.21 (m, 1H), 2.20 – 2.06 (m, 2H), 1.93 – 1.82 (m, 1H), 1.80 – 1.68 (m, 1H), 1.69 – 1.51 (m, 1H), 1.45 (t, *J*=7.1 Hz, 4H). ^{13}C NMR (101 MHz, CDCl3) δ 188.8, 183.7, 177.8, 173.7, 136.5, 131.1, 98.9, 83.3, 81.1, 69.8, 46.1, 38.8, 33.7, 31.4, 25.6, 16.0. UPLC/MS (ESI+): *m/z* = 308.1 [M+H]+.

3-((2-fluoroethyl)amino)-4-((((2s,3aR,9aS,E)-3a,4,5,8,9,9a-hexahydrocycloocta[d][1,3]dioxol-2-yl)methyl)amino)cyclobut-3-ene-1,2-dione (UAMC-4129)

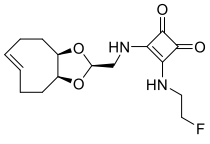

Compound **4.11** (48 mg, 0.16 mmol) was dissolved in EtOH (2.5 mL). Triethylamine (0.22 ml, 1.56 mmol) and 2-Fluoroethylaminehydrochloride (46.60 mg, 0.47 mmol) were added and stirred at room temperature for 4h. The mixture was concentrated under reduced pressure and the crude product was purified by silica gel flash chromatography (1-8% MeOH in DCM) to afford UAMC-4129 as a white fluffy powder (41 mg,

81%). ^{1}H NMR (400 MHz, DMSO) δ = 7.61 (s, 1H), 7.42 (s, 1H), 5.64 – 5.47 (m, 2H), 4.80 (t, *J*=3.4 Hz, 1H), 4.53 (dt, *J*=47.5 Hz, 4.9 Hz, 2H), 4.06 – 3.88 (m, 2H), 3.87 – 3.81 (m, 1H), 3.80 – 3.75 (m, 1H), 3.69 (s, 1H), 3.63 (s, 1H), 2.34 – 2.26 (m, 1H), 2.20 – 2.04 (m, 3H), 1.89 – 1.77 (m, 1H), 1.66 – 1.52 (m, 2H), 1.50 – 1.42 (m, 1H). ^{13}C NMR (101 MHz, DMSO) δ = 182.8, 182.7, 168.5, 167.7, 136.0, 131.3, 99.3, 83.0 (d, $^{1}J_{C,F}$ =165.8 Hz), 81.9, 79.9, 45.4, 43.6 (d, $^{2}J_{C,}$F =19.6 Hz), 38.2, 33.1, 30.7, 25.1. HRMS/ESI: *m/z* $[M+H]^+$ = 325.1552 (calculated for $C_{16}H_{21}N_2O_4F_1$: 325.1558).

6-fluoro-N-(((2s,3aR,9aS,Z)-3a,4,5,8,9,9a-hexahydrocycloocta[d][1,3]dioxol-2-yl)methyl)pyridine -3-sulfonamide (4.12)

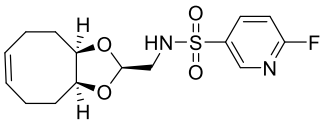

Compound **4.6** (150 mg, 0.82 mmol) was dissolved in dry Dichloromethane (8 ml) and cooled down to 0°C. Triethylamine (0.11 mL, 0.82 mmol) was added followed by slow addition of 6-fluoropyridine-3-sulfonyl chloride (0.10 mL, 0.82 mmol) and stirred at room temperature overnight. The mixture was diluted with DCM (40 mL) and Water (20 mL), and the organic phase was separated. The aqueous phase was extracted DCM (2 x 40 mL), washed brine (30 mL), dried with Na_2SO_4, filtered, and evaporated. The crude product was purified by silica gel flash chromatography (5-30% EtOAc in Heptane) to give white solids (140 mg, 50%). ^{1}H NMR (400 MHz, CDCl3) δ = 8.76 – 8.70 (m, 1H), 8.29-8.21 (m, 1H), 7.06 (dd, *J*=8.6 Hz, 2.8 Hz, 1H), 5.65 – 5.51 (m, 2H), 4.89 (t, *J*=6.1 Hz, 1H), 4.82 (t, *J*=3.3 Hz, 1H), 4.16 – 4.03 (m, 2H), 3.28 (dd, *J*=6.1 Hz, 3.2 Hz, 2H), 2.52 – 2.37 (m, 2H), 2.10 – 1.78 (m, 6H). ^{13}C NMR (101 MHz, CDCl3) δ = 165.2 (d, $^{1}J_{C,F}$ =257.5 Hz), 147.8 (d, $^{3}J_{C,F}$ =16.9 Hz), 140.5 (d, $^{3}J_{C,F}$ =9.2 Hz), 135.3 (d, $^{4}J_{C,F}$ =4.7 Hz), 129.3, 110.1 (d, $^{2}J_{C,F}$ =37.9 Hz), 98.9, 79.4, 45.3, 28.5, 23.2. UPLC/MS (ESI+): *m/z* = 343.1 [M+H]+.

6-fluoro-N-(((2s,3aR,9aS,E)-3a,4,5,8,9,9a-hexahydrocycloocta[d][1,3]dioxol-2yl)methyl)pyridine -3-sulfonamide (UAMC-3725)

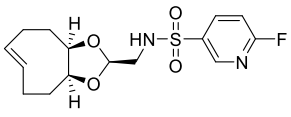

Compound **4.8** (75 mg, 0.41 mmol) was dissolved in anhydrous DCM (4 mL) and cooled down to -40°C. Triethylamine (0.06 mL, 0.41 mmol) was added followed by a slow addition of 6-fluoropyridine-3-sulfonyl chloride (0.05 mL, 0.41 mmol) dissolved in (4mL) DCM and stirred overnight at room temperature. Water (10 mL) was added, and the organic phase was separated. The aqueous phase was extracted with DCM (2 x 20mL). The organic phases were combined, washed with brine (20 mL), dried with Na_2SO_4, filtered, and evaporated. The product was purified by silica gel flash chromatography (5-

50% EtOAc in Heptane) to give white solids (70mg, 50%). ^{1}H NMR (400 MHz, CDCl3) δ = 8.75 – 8.69 (m, 1H), 8.26 – 8.20 (m, 1H), 7.10 – 7.02 (m, 1H), 5.62 – 5.38 (m, 2H), 4.92 – 4.83 (m, 1H), 4.76 (t, *J*=3.1 Hz, 1H), 4.01 – 3.72 (m, 2H), 3.34 – 3.18 (m, 2H), 2.42 – 2.32 (m, 1H), 2.30 – 2.21 (m, 1H), 2.19 – 1.98 (m, 2H), 1.90 – 1.77 (m, 1H), 1.75 – 1.66 (m, 1H), 1.56 – 1.30 (m, 2H). ^{13}C NMR (101 MHz, $CDCl_3$) δ = 165.3 (d, $^{1}J_{C,F}$ =246.7 Hz), 147.9 (d, $^{3}J_{C,F}$ =16.8 Hz), 140.6 (d, $^{3}J_{C,F}$ =9.4 Hz), 136.5, 135.4 (d, $^{4}J_{C,F}$ =4.8 Hz), 131.3, 110.2 (d, $^{2}J_{C,F}$ =38.0 Hz), 98.5, 83.1, 80.9, 45.0, 38.7, 33.8, 31.3, 25.7. HRMS/ESI *m/z* $[M+H]^+$ = 343.1122 (calculated for $C_{15}H_{19}N_2O_4F_1$:343.1050).

2-(2-(2-hydroxyethoxy)ethoxy)ethyl benzoate (4.13)

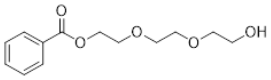

To a solution of Triethyleneglycol (3.06 mL, 22.79 mmol) in anhydrous DCM (120 mL) were successively added *N*, *N*-Di-iso-propylethylamine (3.72 mL, 21.36 mmol), and 4-Dimethylaminopyridine (0.17g, 1.42 mmol) under N_2 atmosphere. Benzoyl chloride (1.65 mL, 14.23 mmol) dissolved in anhydrous DCM (15 mL) was added dropwise to the mixture and stirred at room temperature overnight. The mixture was then poured into water (200 mL). The organic layer was separated, and the aqueous phase was extracted with DCM (3 x 100mL). The organic layers were combined, washed with brine (100mL), dried over Na_2SO_4, and evaporated under reduced pressure. The product was purified by silica gel flash chromatography (50-80% EtOAc in Heptane) to give a colorless oil (2.02g, 56%). ^{1}H NMR (400 MHz, $CDCl_3$) δ = 8.09 – 8.04 (m, 2H), 7.59 – 7.53 (m, 1H), 7.48 – 7.40 (m, 2H), 4.52 – 4.47 (m, 2H), 3.87 – 3.82 (m, 2H), 3.74 – 3.67 (m, 6H), 3.63 – 3.58 (m, 2H). ^{13}C NMR (101 MHz, $CDCl_3$) δ = 166.7, 133.2, 130.1, 129.8, 128.5, 72.6, 70.9, 70.6, 69.4, 64.1, 61.9. UPLC/MS (ESI+): *m/z* = 343.1 [M+H]+.

2-(2-(2-oxoethoxy)ethoxy)ethyl benzoate (4.14)

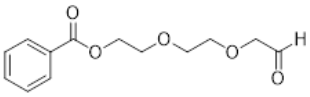

To a solution of **4.13** (1.7 g, 6.69 mmol) in DCM (50 mL) under an N_2 atmosphere was added Dess-Martinperiodinane (3.40 g, 8.02 mmol) and stirred at room temperature for 3h. The reaction was quenched with Sodiumthiosulfate (3,98 g, 16,05 mmol) in a saturated solution of $NaHCO_3$ (50 mL) and stirred for 1 hour. The mixture was filtered, and the organic phase was separated. The aqueous phase was extracted with DCM (2 x 50mL). The organic phases were combined, washed with brine (50 mL), dried over Na_2SO_4, filtered, and evaporated under reduced pressure to give a colorless oil. The crude product was used further without purification.

2-(2-(((2s,3aR,9aS,Z)-3a,4,5,8,9,9a-hexahydrocycloocta[d][1,3]dioxol-2-yl)methoxy) ethoxy) ethyl benzoate (4.15)

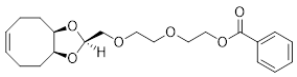

To a solution of **4.14** (577 mg, 2.29 mmol) in anhydrous THF (50 ml) under an N_2 atmosphere were successively added diol **4.1** (0.90 g, 6.4 mmol) and p-toluene sulfonic acid monohydrate (0.60 g, 3.17 mmol). The reaction mixture was heated at 50°C for 24h. The mixture was cooled to room temperature and diluted with EtOAc (25 mL) and a saturated aqueous solution of $NaHCO_3$ (50 mL). After the separation of the organic phase, the water phase was extracted with EtOAc (2 x 25 mL), washed with brine (50 mL), dried with Na_2SO_4, filtered, and evaporated under reduced pressure. The product was purified by silica gel flash chromatography (0-60% EtOAc in Heptane) to afford a colorless oil (480.4 mg, 56%). ^{1}H NMR (400 MHz, $CDCl_3$) δ = 8.08 – 8.03 (m, 2H), 7.59 – 7.53 (m, 1H), 7.47 – 7.40 (m, 2H), 5.63 – 5.54 (m, 2H), 4.97 (t, *J* = 4.3 Hz, 1H), 4.50 – 4.44 (m, 2H), 4.17 – 4.10 (m, 2H), 3.86 – 3.81 (m, 2H), 3.72 (s, 4H), 3.59 (d, *J* = 4.2 Hz, 2H), 2.55 – 2.43 (m, 2H), 2.13 – 1.88 (m, 6H). ^{13}C NMR (101 MHz, $CDCl_3$) δ 166.7, 133.1, 130.2, 129.8, 129.3, 128.5, 100.7, 79.2, 77.4, 73.2, 71.3, 70.8, 69.4, 64.3, 28.6, 23.6.

2-(2-(((2s,3aR,9aS,Z)-3a,4,5,8,9,9a-hexahydrocycloocta[d][1,3]dioxol-2-yl)methoxy) ethoxy) ethan-1-ol (4.16)

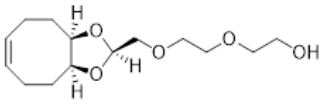

To a solution of **4.15** (1.2 g, 3.19 mmol) in Ethanol (15 mL) was added Lithium hydrate (0.20 g, 4.78 mmol). The mixture was stirred at room temperature for 2 h. The mixture was quenched with a mixture of a saturated solution of sodium chloride (100 mL), water (30 mL), and a 5% aqueous solution of sodium carbonate (10 mL). DCM (20 mL) was added to the mixture and the organic phase was separated. The aqueous phase was extracted with DCM (2 x 40 mL), washed with brine (30 mL), dried with Na_2SO_4, filtered, and evaporated under reduced pressure. The product was purified by silica gel flash chromatography (10-80% EtOAc in Heptane) to afford a colorless oil (842 mg, 97%). ^{1}H NMR (400 MHz, $CDCl_3$) δ = 5.64 – 5.55 (m, 2H), 4.99 (t, *J* = 4.2 Hz, 1H), 4.20 – 4.12 (m, 2H), 3.74 – 3.65 (m, 6H), 3.62 – 3.57 (m, 4H), 2.56 – 2.43 (m, 2H), 2.15 – 2.01 (m, 4H), 2.00 – 1.90 (m, 2H). ^{13}C NMR (101 MHz, $CDCl_3$) δ = 129.3, 100.7, 79.3, 73.1, 72.6, 71.2, 70.4, 61.9, 28.6, 23.6.

(2s,3aR,9aS,Z)-2-((2-(2-fluoroethoxy)ethoxy)methyl)-3a,4,5,8,9,9a-hexahydrocycloocta [d][1,3] dioxole (4.17)

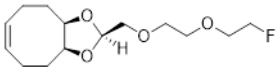

To a solution of **4.16** (500 mg, 1.84 mmol) in anhydrous THF (10 mL), Perfluoro-1-butanesulfonyl fluoride (0.73 mL, 4.04 mmol) and 2-(tert-butyl)-1,1,3,3-tetramethylguanidine (0.41 mL, 2.02 mmol) were added and stirred 1h at room temperature. The mixture was diluted with DCM (20 mL) and water (20 mL). The organic phase was separated, and the aqueous phase was extracted with DCM (2 x 20 mL). The organic phases were combined, washed with brine (30 mL), dried with Na_2SO_4, filtered, and evaporated under reduced pressure. The product was purified by silica gel flash chromatography (0-50% EtOAc in Heptane) to give a colorless oil (280.9 mg, 56%). ^{1}H NMR (400 MHz, $CDCl_3$) δ = 5.66 – 5.54 (m, 2H), 4.98 (t, *J*=4.2 Hz, 1H), 4.66 – 4.58 (m, 1H), 4.54 – 4.47 (m, 1H), 4.21 – 4.11 (m, 2H), 3.82 – 3.75 (m, 1H), 3.75 – 3.65 (m, 5H), 3.59 (d, *J*=4.2 Hz, 2H), 2.57 – 2.44 (m, 2H), 2.15 – 2.02 (m, 4H), 2.00 – 1.90 (m, 2H). ^{13}C NMR (101 MHz, $CDCl_3$) δ 129.3, 100.8, 83.3 (d, $^1J_{C,F}$ = 170.5 Hz), 79.3, 73.2, 71.3, 70.9, 70.6 (d, $^2J_{C,F}$ = 20.3 Hz), 70.5, 28.6, 23.6. UPLC/MS (ESI+): *m/z* =275.2 [M+H]+.

(2s,3aR,9aS,E)-2-((2-(2-fluoroethoxy)ethoxy)methyl)-3a,4,5,8,9,9a-hexahydrocycloocta [d][1,3] dioxole (UAMC-3711)

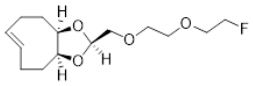

A solution of **4.17** (375 mg, 1.37 mmol) in ether/hexane (300 mL) and Methyl benzoate (0.35 mL, 2,73 mmol) was irradiated at 254 nm for 4 h. Afterwards, the column was flushed with ethyl acetate (150 mL) and dried under airflow. The silica of the column was poured into a flask and stirred in ammonium hydroxide (75 mL) and dichloromethane (75 mL) for 10 min. The silica was filtered and washed with additional ammonium hydroxide (30 mL) and dichloromethane (30 mL). The phases were separated, and the aqueous layer was extracted with DCM (2 x 200 mL). The combined organic layers were washed with water (2 x 100 mL), dried over Na_2SO_4, filtered, and evaporated under reduced pressure. The product was purified by silica gel flash chromatography (0-50% EtOAc in Heptane). ^{1}H NMR (400 MHz, $CDCl_3$) δ = 5.67 – 5.45 (m, 2H), 4.90 (t, *J*=4.2 Hz, 1H), 4.64 – 4.58 (m, 1H), 4.52 – 4.47 (m, 1H), 3.98 – 3.85 (m, 2H), 3.79 – 3.75 (m, 1H), 3.73 – 3.65 (m, 5H), 3.61 – 3.51 (m, 2H), 2.45 – 2.34 (m, 1H), 2.32 – 2.18 (m, 2H), 2.18 – 2.07 (m, 1H), 1.93 – 1.77 (m, 2H), 1.74 – 1.61 (m, 1H), 1.60 – 1.47 (m, 1H). ^{13}C NMR (101 MHz, $CDCl_3$) δ = 136.5, 131.3, 100.4, 83.3 (d, $^1J_{C,F}$=167.6 Hz), 82.7, 80.7, 72.8, 71.3, 70.8, 70.5 (d, $^2J_{C,F}$ =19.0 Hz), 38.8, 33.9, 31.5, 25.8. HRMS/ESI: *m/z* $[M+Na]^+$ = 297.1467 (calculated for $C_{14}H_{23}O_4F_1Na$: 297.1473).

2-(2-hydroxyethoxy)ethyl benzoate (4.18)

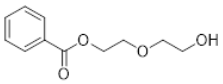

To a solution of Diethyleneglycol (1.79 mL, 18.85 mmol) in anhydrous DCM (100 mL) were successively added *N*, *N*-Di-iso-propylethylamine (4.92 mL, 28.3 mmol), and 4-Dimethylaminopyridine (0.23 g, 1.89 mmol) under N_2 atmosphere. Benzoyl chloride (1.97 mL, 16.96 mmol) was added dropwise, and the mixture was stirred at room temperature for 3h. The mixture was poured into water (100mL). The organic layer was separated, and the aqueous phase was extracted with DCM (3 x 100mL). The organic layers were combined, washed with brine (100 mL), dried over Na_2SO4, filtered, and evaporated under reduced pressure. The product was purified by silica gel flash chromatography (0-80% EtOAc in Heptane) to give a colorless oil (1.70 g, 43%). ^{1}H NMR (400 MHz, $CDCl_3$) δ = 8.10 – 8.02 (m, 2H), 7.61 – 7.52 (m, 1H), 7.50 – 7.40 (m, 2H), 4.53 – 4.46 (m, 2H), 3.88 – 3.81 (m, 2H), 3.80 – 3.72 (m, 2H), 3.69 – 3.62 (m, 2H). ^{13}C NMR (101 MHz, $CDCl_3$) δ = 166.7, 133.2, 130.1, 129.8, 128.5, 72.5, 69.4, 64.2, 61.9. UPLC/MS (ESI+): *m/z* =233.2 [M+Na]+.

2-(2-oxoethoxy)ethyl benzoate (4.19)

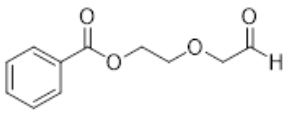

To a solution of **4.18** (0.92 g, 4.40 mmol) in DCM (40 mL) was added Dess-Martinperiodinane (2.24 g, 5.27 mmol) under N_2 atmosphere and stirred at rt for 2.5 h. The reaction was quenched with Sodium thiosulfate (2.62 g, 10.55 mmol) and a saturated NaHCO3 (50 mL) solution and stirred for 1.5 h. The mixture was separated, and the aqueous phase was extracted with DCM (2 x 50mL). The organic layers were combined, and washed with brine (30mL), dried over Na_2SO_4, filtered, and evaporated under reduced pressure. The crude product was used further without purification.

2-(((2s,3aR,9aS,Z)-3a,4,5,8,9,9a-hexahydrocycloocta[d][1,3]dioxol-2-yl)methoxy)ethyl benzoate (4.20)

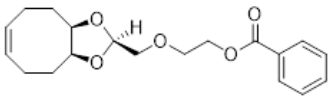

To a solution of **4.19** (895 mg, 4.30 mmol), in anhydrous THF (80 mL) under an N_2 atmosphere were successively added diol (611 mg, 4.30 mmol) and p-toluene sulfonic acid monohydrate (409 mg, 2.15 mmol). The reaction mixture was heated at 50°C for 24h. The mixture was cooled to rt and diluted with EtOAc (25 mL) and with a saturated aqueous solution of $NaHCO_3$ (50 mL). After separation, the aqueous phase was extracted with EtOAc (2 x 50 mL). The organic phases were combined, washed with brine (50mL), dried over Na_2SO_4, and evaporated under reduced pressure. The product was purified by silica gel flash

chromatography (0-50% EtOAc in Heptane) to give a colorless oil (755 mg, 53%). ^{1}H NMR (400 MHz, $CDCl_3$) δ = 8.09 – 8.04 (m, 2H), 7.59 – 7.53 (m, 1H), 7.47 – 7.40 (m, 2H), 5.64 – 5.54 (m, 2H), 4.99 (t, *J*=4.1, 1H), 4.51 – 4.46 (m, 2H), 4.19 – 4.12 (m, 2H), 3.92 – 3.86 (m, 2H), 3.64 (d, *J*=4.1 Hz, 2H), 2.57 – 2.43 (m, 2H), 2.17 – 1.89 (m, 6H). ^{13}C NMR (101 MHz, $CDCl_3$) δ = 166.6, 133.0, 129.7, 129.2, 128.3, 100.7, 79.2, 77.2, 72.9, 69.8, 64.2, 28.5, 23.5. UPLC/MS (ESI+): *m/z* =355.1 [M+Na]+.

2-(((2s,3aR,9aS,Z)-3a,4,5,8,9,9a-hexahydrocycloocta[d][1,3]dioxol-2-yl)methoxy)ethan-1-ol (4.21)

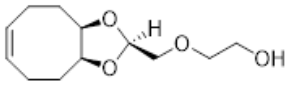

To a solution of **4.20** (755 mg, 2.27 mmol) in Ethanol (10 mL) was added Lithium hydrate (143 mg, 3.41 mmol). The mixture was stirred at room temperature for 2h. The mixture was quenched with a mixture of a saturated solution of sodium chloride (20 mL), water (6 mL), and a 5% aqueous solution of sodium carbonate (2 mL). DCM (20 mL) was added to the mixture and the organic phase was separated. The aqueous phase was extracted with DCM (2 x 40 mL), washed with brine (30 mL), dried with anhydrous Na_2SO_4, filtered, and evaporated under reduced pressure. The product was purified by silica gel flash chromatography (10-80% EtOAc in Heptane) to afford a colorless oil (505 mg, 97%). ^{1}H NMR (400 MHz, $CDCl_3$) δ = 5.65 – 5.55 (m, 2H), 4.98 (t, *J*=4.0 Hz, 1H), 4.22 – 4.13 (m, 2H), 3.77 – 3.70 (m, 2H), 3.69 – 3.63 (m, 2H), 3.61 (d, *J*=4.0 Hz, 2H), 2.61 – 2.41 (m, 3H), 2.18 – 1.90 (m, 6H). ^{13}C NMR (101 MHz, $CDCl_3$) δ = 129.3, 100.6, 79.3, 73.3, 72.7, 61.9, 28.6, 23.6. UPLC/MS (ESI+): *m/z* =251.1 [M+Na]+

(2s,3aR,9aS,Z)-2-((2-fluoroethoxy)methyl)-3a,4,5,8,9,9a-hexahydrocycloocta [d][1,3]dioxole (4.22)

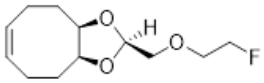

To a solution of **4.21** (498 mg, 2.18 mmol) dissolved in anhydrous THF (10 mL), PBSF (0.86 mL, 4.80 mmol) and TBTMG (0.48 mL, 2.40 mmol) were added and stirred for 1h at room temperature. The mixture was diluted with DCM (30 mL) and water (30 mL). The organic phase was separated, and the aqueous phase was extracted with DCM (2 x 20 mL). The organic phases were combined, washed with brine (30 mL), dried with Na_2SO_4, filtered, and evaporated under reduced pressure. The product was purified by silica gel flash chromatography (20-60% EtOAc in Heptane) to give a colorless oil (420 mg, 84%). ^{1}H NMR (400 MHz, $CDCl_3$) δ = 5.67 – 5.54 (m, 2H), 4.99 (t, *J*=4.2 Hz, 1H), 4.57 (dt, *J*=4.2 Hz, $^{2}J_{H\text{-}F}$ = 48.0 Hz, 2H), 4.22 – 4.12 (m, 2H), 3.79 (dt, *J*=4.2 Hz, 2H, $^{3}J_{H\text{-}F}$ = 29.8 Hz, 2H), 3.61 (d, *J*=4.2 Hz, 2H), 2.59 – 2.43 (m,

2H), 2.18– 1.90 (m, 6H). ^{13}C NMR (101 MHz, $CDCl_3$) δ = 129.3, 100.7, 83.2 (d, $^1J_{C,F}$ = 166 Hz), 79.3, 73.2, 71.1(d, $^2J_{C,F}$ =20 Hz), 28.6, 23.6.

(2s,3aR,9aS,E)-2-((2-fluoroethoxy)methyl)-3a,4,5,8,9,9a-hexahydrocycloocta[d][1,3] dioxole (UAMC-3724)

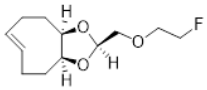

A solution of **4.22** (100 mg, 0.43 mmol) and Methyl benzoate (0.11 mL, 0,87 mmol) dissolved in ether/hexane (200 mL) was irradiated at 254 nm for 4.5 h. Afterwards, the column was flushed with ethyl acetate (75 mL) and dried under airflow. The silica of the column was poured into a flask and stirred in ammonium hydroxide (75 mL) and dichloromethane (75 mL) for 10 min. The silica was filtered and washed with additional ammonium hydroxide (30 mL) and dichloromethane (30 mL). The phases were separated, and the aqueous layer was extracted with DCM (2 x 50 mL). The combined organic layers were washed with water (2 x 500 mL), dried over Na_2SO_4, filtered, and evaporated under reduced pressure. The product was purified by silica gel flash chromatography (0-50% EtOAc in Heptane) to give a colorless oil (58 mg, 58%). ^{1}H NMR (400 MHz, $CDCl_3$) δ = 5.69 – 5.46 (m, 2H), 4.91 (t, *J*=4.2 Hz, 1H), 4.57 (dt, *J*=4.0 Hz, $^2J_{H-F}$ = 47.5 Hz, 2H), 4.00 – 3.88 (m, 2H), 3.79 (dt, *J*= 4.0 Hz, $^2J_{H-F}$ = 29.7 Hz, 2H), 3.64 – 3.55 (m, 2H), 2.47 – 2.08 (m, 4H), 1.94 – 1.79 (m, 2H), 1.76 – 1.48 (m, 2H). ^{13}C NMR (101 MHz, $CDCl_3$) δ = 136.5, 131.4, 100.3, 83.2.0 (d, $^1J_{C,F}$ =169.0 Hz), 82.8, 80.8, 72.8, 71.1 (d, $^2J_{C,F}$ =19.8 Hz), 38.9, 33.9, 31.5, 25.8. HRMS/ESI: *m/z* $[M+Na]^+$ = 253.1201 (calculated for $C_{12}H_{19}O_3F_1Na$: 253.1210).

(3-(benzyloxy)cyclobutyl)methanol (4.23)

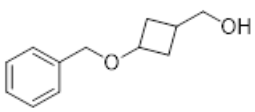

To a solution of 3-(benzyloxy)cyclobutane-1-carboxylic acid as a mixture of diastereoisomers (5.0 g, 24.24 mmol) in THF (50 mL) under N_2 atmosphere at 0°C was added Lithiumaluminumhydride (20.20 mL, 48.5 mmol in THF 2,4 M) dropwise and the solution was stirred 2h at RT. The mixture was diluted with diethyl ether (50 mL), cooled to 0°C, and quenched by a dropwise addition of 10% NaOH solution (5 mL). Additional water (10 mL) was added, and the mixture was stirred 30min at RT. The salts were there filtered, and the organic phase was separated, washed with water (2 x 40 mL) and brine (30 mL, dried with Na_2SO_4, and evaporated under reduced pressure. The product was purified by silica gel flash chromatography (0-50% EtOAc in Heptane) to give a colorless oil (4.6g, 99%). ^{1}H NMR (400 MHz, $CDCl_3$) δ = 7.39 – 7.24 (m, 5H), 4.45-4.40 (m, 2H), 4.02 – 3.89 (m, 1H), 3.66 – 3.58 (m, 2H), 2.45 – 2.29 (m, 2H), 2.23 – 1.96 (m, 2H), 1.80 – 1.66 (m, 1H). ^{13}C NMR (101 MHz, $CDCl_3$) mixture of

diastereomers δ = 138.2 (minor), 138.2 (major), 128.4, 127.9 (major), 127.9 (minor), 127.6 (major), 127.6 (minor), 71.8, 70.0 (major), 69.4 (minor), 67.2 (major), 66.7 (minor), 32.9 (major), 31.7 (minor), 29.8 (minor), 28.3 (major). UPLC/MS (ESI+): *m/z* =193.1 [M+H]+

(3-(benzyloxy)cyclobutyl)methyl 4-methylbenzenesulfonate (4.24)

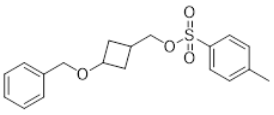

To a solution of **4.23** (4.37 g, 22.73 mmol) in anhydrous DCM (50 mL) under an N_2 atmosphere was added 4-Dimethylaminopyridine (0.56 g, 4.55 mmol), Triethylamine (3.17 mL, 22.73 mmol) and p-Tosylchloride (4.33 g, 22.73 mmol) and stirred overnight at RT. The reaction was quenched with 1M HCL (30 mL) and the organic phase was separated. The aqueous phase was extracted with DCM (2 x 40mL), combined, and washed with water (50 mL) and brine (50 mL), dried with Na_2SO_4, filtered, and evaporated under reduced pressure. The product was purified by silica gel flash chromatography (0-50% EtOAc in Heptane) to give a colorless oil (7.7g, 98%). ^{1}H NMR (400 MHz, $CDCl_3$) δ = 7.82 – 7.75 (m, 2H), 7.39 – 7.23 (m, 7H), 4.37 (s, 2H), 3.98 (d, *J*=6.6 Hz, 2H), 3.98 – 3.85 (m, 1H), 2.45 (s, 3H), 2.39 – 2.27 (m, 2H), 2.23 – 1.99 (m, 1H), 1.74 – 1.60 (m, 2H). ^{13}C NMR (101 MHz, $CDCl_3$) δ = 144.9, 138.1, 133.2, 130.0, 128.5, 128.0, 128.0, 127.8, 74.2, 70.2, 69.2, 33.3, 25.4, 21.8. UPLC/MS (ESI+): *m/z* =369.1 [M+Na]+

(3-hydroxycyclobutyl)methyl 4-methylbenzenesulfonate (4.25)

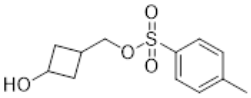

To a solution of **4.24** (7.7 g, 22.23 mmol) MeOH (60 mL) under an N_2 atmosphere was added Palladiumhydroxide (1.56 g, 2.23 mmol), and the reaction was stirred 2h at rt with a positive pressure of H_2. The mixture was filtered over a pad of celite and evaporated under reduced pressure. The product was purified by silica gel flash chromatography (0-50% EtOAc in Heptane) to afford white solids (2.89g, 51%). ^{1}H NMR (400 MHz, $CDCl_3$) δ = 7.83 – 7.74 (m, 2H), 7.38 – 7.31 (m, 2H), 4.21 – 4.07 (m, 1H), 3.98 (d, *J*=6.2 Hz, 2H), 2.45 (s, 3H), 2.45 – 2.33 (m, 2H), 2.17 – 1.99 (m, 1H), 1.68 – 1.55 (m, 2H). ^{13}C NMR (101 MHz, $CDCl_3$) δ = 144.9, 133.2, 130.0, 128.0, 73.9, 63.7, 36.2, 24.7, 21.8. UPLC/MS (ESI+): *m/z* =279.3 [M+Na]+

(3-fluorocyclobutyl)methyl 4-methylbenzenesulfonate (4.26)

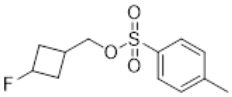

To a solution of **4.25** (2.9 g, 11.31mmol) in THF (20 mL) were added Perfluoro-1-butanesulfonyl fluoride (4.47 mL, 24.89 mmol) and 2-tert-Butyl-1,1,3,3-tetramethylguanidine (2.66 mL, 12.45 mmol) under N2 atmosphere and stirred 6h at rt. The

reaction was quenched with water (20mL) and the organic phase was separated. The aqueous phase was extracted with DCM (2 x 30mL), combined, and washed with water (50 mL) and brine (50 mL), dried with Na_2SO_4, filtered, and evaporated under reduced pressure. The product was purified by silica gel flash chromatography (0-30% EtOAc in Heptane) to afford a colorless liquid (1.27g, 44%). ^{1}H NMR (400 MHz, CDCl3) δ = 7.83 – 7.76 (m, 2H), 7.39 – 7.32 (m, 2H), 5.16-4.89 (m, 1H), 4.04 – 3.97 (m, 2H), 2.70 – 2.57 (m, 1H), 2.46 (s, 3H), 2.44 – 2.27 (m, 2H), 2.25 – 2.02 (m, 2H). ^{13}C NMR (101 MHz, $CDCl_3$) δ = 145.1, 133.0, 130.1, 128.0, 86.7(d, $^1J_{C,F}$ =206.2 Hz), 72.8 (d, $^4J_{C,F}$ =2.5 Hz), 32.7 (d, $^2J_{C,F}$ =22.1 Hz), 26.7 (d, $^3J_{C,F}$ =11.8 Hz), 21.8 UPLC/MS (ESI+): *m/z* = 259.1[M+H]+

(2s,3aR,9aS,Z)-2-(((3-fluorocyclobutyl)methoxy)methyl)3a,4,5,8,9,9a-hexahydrocycloocta [d] [1,3]dioxole (4.27)

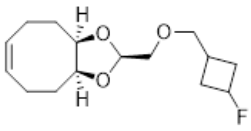

To a solution of **4.2** (793 mg, 4.30 mmol) dissolved in DMF (20 mL) under N_2 was added Sodium hydride (163 mg, 6.46 mmol). The temperature was increased to 30°C and the mixture was stirred for 30 min until no bubbling of H_2 gas out of the mixture. **4.26** (1001 mg, 3.87 mmol) was then added to the mixture and stirred overnight at 30°C. Water (40 mL) was added and the mixture was extracted with EtOAc (3x 50 mL). The EtOAc phases were combined and washed with water (100 mL) followed by brine (50 mL), dried with Na_2SO_4, filtered, and evaporated under reduced pressure. The crude product was purified by silica gel flash chromatography (0-30 % EtOAc in Heptane) to give a colorless oil (545 mg, 47%). ^{1}H NMR (400 MHz, CDCl3) δ = 5.66 – 5.54 (m, 2H), 5.09 (m, 1H), 4.96 (t, *J*=4.1 Hz, 1H), 4.20 – 4.12 (m, 2H), 3.53 (d, *J*=4.1 Hz, 2H), 3.49 (d, *J*=6.7 Hz, 2H), 2.63 – 2.44 (m, 3H), 2.43 – 2.15 (m, 4H), 2.14 – 1.89 (m, 6H). ^{13}C NMR (101 MHz, CDCl3) δ = 129.4, 100.9, 87.6 (d, $^1J_{C,F}$ =206.2 Hz), 79.3, 75.3 (d, $^4J_{C,F}$ =2.2 Hz), 73.0, 33.2 (d, $^2J_{C,F}$ =21.0 Hz), 28.6, 26.9 (d, $^3J_{C,F}$ =12.8 Hz), 23.5.

(2s,3aR,9aS,E)-2-(((3-fluorocyclobutyl)methoxy)methyl)-3a,4,5,8,9,9a-hexahydrocycloocta [d][1,3] dioxole (UAMC-3933)

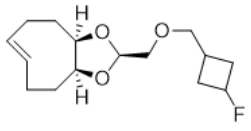

A solution of **4.27** (300 mg, 1.11 mmol) and Methyl benzoate (0.28 mL, 2.22 mmol) dissolved in ether/hexane (300 mL; 1:1/v/v) was irradiated at 254 nm for 4.5 h. Afterward, the column was flushed with ethyl acetate (100 mL) and dried under airflow. The silica of the column was poured into a flask and stirred in ammonium hydroxide (100 mL) and DCM (100 mL) for 10 min. The silica was filtered and washed with additional ammonium hydroxide (75 mL) and DCM (75 mL). The phases were separated, and

the aqueous layer was extracted with DCM (2 x 50 mL). The combined organic layers were washed with water (100 mL) and brine (100 mL), dried over Na_2SO_4, filtered, and evaporated under reduced pressure. The product was purified by silica gel flash chromatography (0-30% EtOAc in Heptane) to give a colorless oil (149 mg, 49%) ^{1}H NMR (400 MHz, CDCl3) δ = 5.69 – 5.45 (m, 2H), 5.21 – 4.98 (m, 1H), 4.88 (t, *J*=4.1 Hz, 1H), 3.98 – 3.86 (m, 2H), 3.53 – 3.49 (m, 2H), 3.49 – 3.46 (m, 2H), 2.63 – 2.47 (m, 1H), 2.46 – 2.07 (m, 8H), 1.94 – 1.78 (m, 2H), 1.76 – 1.60 (m, 1H), 1.60 – 1.47 (m, 1H). ^{13}C NMR (101 MHz, CDCl3) δ = 136.5, 131.4, 100.5, 87.6 (d, $^1J_{C,F}$ =206.2 Hz), 82.7, 80.7, 75.3 (d, $^4J_{C,F}$ =2.1 Hz), 72.5, 38.9, 33.9, 33.3 (d, $^2J_{C,F}$ =21.1 Hz), 31.5, 26.9 (d, $^3J_{C,F}$ =13.1 Hz), 25.8. HRMS/ESI *m/z* $[M+Na]^+$ = 293.1519 (calculated for $C_{15}H_{23}O_3F_1Na$: 293.1523).

2-(2-(((2s,3aR,9aS,Z)-3a,4,5,8,9,9a-hexahydrocycloocta[d][1,3]dioxol-2-yl)methoxy)ethoxy)ethyl 4-methylbenzenesulfonate (4.28)

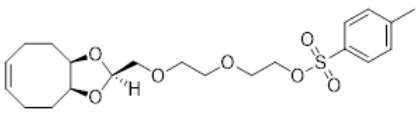

To a solution **4.16** (340 mg, 1.25 mmol) in anhydrous DCM (8 mL) under N_2 was added 4-Dimethylaminopyridine (30.5 mg, 0.25 mmol) and Triethylamine (0.52 mL, 3.75 mmol) and the solution was cooled down to 0°C. p-Tosylchloride (286 mg, 1.50 mmol) was added to the reaction mixture and stirred at 0°C for 3h. The mixture was diluted with DCM (30 mL) and Water (30 mL), and the organics was separated from the aqueous phase. The aqueous phase was extracted with DCM (2 x 30 mL). All organics were combined, dried with Na_2SO_4, filtered, and evaporated under reduced pressure. The crude product was purified by silica gel flash chromatography (0-40 % EtOAc in Heptane) to give a colorless oil. ^{1}H NMR (400 MHz, $CDCl_3$) δ = 7.83 – 7.76 (m, 2H), 7.37 – 7.31 (m, 2H), 5.64 – 5.57 (m, 2H), 4.95 (t, *J*=4.2 Hz, 1H), 4.19 – 4.10 (m, 4H), 3.71 – 3.51 (m, 8H), 2.53 – 2.46 (m, 2H), 2.45 (s, 3H), 2.15 – 1.89 (m, 6H). ^{13}C NMR (101 MHz, $CDCl_3$) δ = 144.9, 133.2, 130.0, 129.4, 128.2, 100.8, 79.3, 73.2, 71.3, 70.8, 69.4, 68.8, 28.7, 23.6, 21.8. UPLC/MS (ESI+): *m/z* =427.2 [M+H]+

2-(2-(((2s,3aR,9aS,E)-3a,4,5,8,9,9a-hexahydrocycloocta[d][1,3]dioxol-2-yl)methoxy)ethoxy)ethyl 4-methyl benzenesulfonate (4.29)

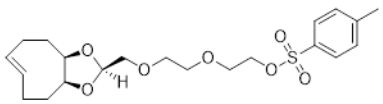

A solution of **4.28** (420 mg, 0.99 mmol) and Methyl benzoate (0.25 mL, 1,97 mmol) dissolved in ether/hexane (300 mL) was irradiated at 254 nm for 4.5 h. Afterward, the column was flushed with ethyl acetate (100 mL) and dried under airflow. The silica of the column was poured into a flask and stirred in ammonium hydroxide (100 mL) and dichloromethane (100 mL) for 10 min. The silica was filtered and washed

with additional ammonium hydroxide (75 mL) and dichloromethane (75 mL). The phases were separated, and the aqueous layer was extracted with DCM (2 x 50 mL). The combined organic layers were washed with water (100 mL) and brine (100 mL), dried over Na_2SO_4, filtered, and evaporated under reduced pressure. The product was purified by silica gel flash chromatography (0-30% EtOAc in Heptane) to give a colorless oil (140mg, 33%). ^{1}H NMR (400 MHz, CDCl3) δ = 7.83 – 7.75 (m, 2H), 7.37 – 7.29 (m, 2H), 5.67 – 5.44 (m, 2H), 4.86 (t, *J*=4.2 Hz, 1H), 4.18 – 4.11 (m, 2H), 4.00 – 3.82 (m, 2H), 3.69 – 3.64 (m, 2H), 3.64 – 3.53 (m, 4H), 3.51 – 3.49 (m, 2H), 2.4 (s, 3H), 2.41 – 2.34 (m, 1H), 2.33 – 2.05 (m, 3H), 1.94 – 1.76 (m, 2H), 1.73 – 1.45 (m, 2H). ^{13}C NMR (101 MHz, CDCl3) δ = 144.9, 136.5, 133.1, 131.3, 129.9, 128.1, 100.3, 82.7, 80.7, 72.8, 71.2, 70.8, 69.3, 68.8, 38.8, 33.9, 31.4, 25.8, 21.8. HRMS/ESI *m/z* $[M+Na]^+$ = 449.1618 (calculated for $C_{21}H_{30}O_7S_1Na$: 449.1604).

2-((2-((((2s,3aR,9aS,E)-3a,4,5,8,9,9a-hexahydrocycloocta[d][1,3]dioxol-2-yl)methyl)amino)-3,4-dioxocyclobut-1-en-1-yl)amino)ethyl 4-methylbenzenesulfonate (4.30)

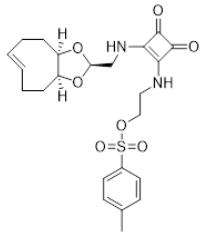

To a solution of 2-((tert-Butoxycarbonyl)amino)ethyl 4-methylbenzenesulfonate (200 mg, 0.61 mmol) in DCM (8 mL) was added TFA (0.73 mL, 9.51 mmol) under N_2 atmosphere. The mixture was stirred for 3h at rt and the solvent was evaporated under reduced pressure. The mixture was redissolved in Ethanol (5 mL) followed by the addition of **4.11** (100 mg, 0.33 mmol) and Triethylamine (0.45 mL, 3.25 mmol) and stirred overnight at rt. The solvent was evaporated, and the crude mixture was purified by silica gel flash chromatography (0-5% MeOH in DCM) to afford a white powder (91 mg, 58%). ^{1}H NMR (400 MHz, CDCl3) δ = 7.79 – 7.72 (m, 2H), 7.38 – 7.32 (m, 2H), 5.72 – 5.37 (m, 2H), 4.91 (t, *J*=2.8 Hz, 1H), 4.18 (t, *J*=4.9 Hz, 2H), 4.06 – 3.86 (m, 6H), 3.70 (s, 2H), 2.44 (s, 3H), 2.42 – 2.33 (m, 1H), 2.29 – 2.21 (m, 1H), 2.20 – 2.04 (m, 2H), 1.93 – 1.79 (m, 1H), 1.79 – 1.72 (m, 1H), 1.71 – 1.59 (m, 1H), 1.56 – 1.43 (m, 1H). ^{13}C NMR (101 MHz, CDCl3) δ = 192.2, 183.3, 177.3, 169.4, 145.6, 136.7, 132.3, 131.1, 130.2, 128.1, 83.4, 81.1, 70.1, 46.2, 43.2, 38.8, 33.6, 31.5, 25.6, 21.9. HRMS/ESI *m/z* $[M+H]^+$ = 477.1705 (calculated for $C_{23}H_{28}N_2O_7S_1Na$: 477.1690).

4.7.2 Reaction Kinetics

Stock solutions of the d-TCOs were prepared in DMSO at a concentration of approximately. 100mM. The exact concentration was determined by absorbance titration with 3,6-Di-2-pyridyl-1,2,4,5-tetrazine ($2Pyr_2$) (extinction coefficient at 520 nm; 433.2 $M^{-1}cm^{-1}$), quantifying the decrease in tetrazine absorbance upon reaction with TCO.[173] d-TCO stock solutions were diluted to the concentrations of 0.5, 1, 2, and 3 mM (water: methanol 50:50 v/v) except for UAMC-4129 (0.25, 0.5, 0.75, and 1mM), and the reaction with (4-(6-methyl-1,2,4,5-tetrazin-3-yl)phenyl)methanamine (MeBA) (0.1 mM, water: methanol 50:50 v/v). For the reaction with $2Pyr_2$, 1 mM of d-TCOs (water: methanol 50:50 v/v) was used with 0.1 mM of $2Pyr_2$ (water: methanol 50:50 v/v).

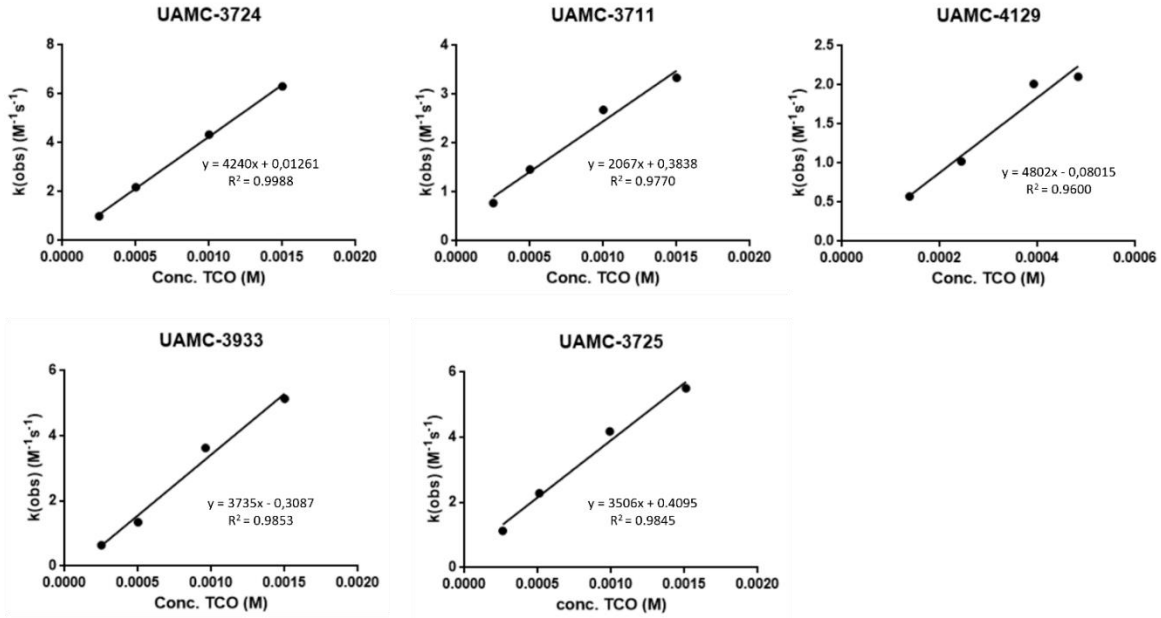

Figure S4.1 *Determination of the bimolecular rate constant k_2 from the stopped-flow reaction of MeBA with d-TCOs. The observed rates k_{obs} of quintuplicate sets of measurements were plotted against the concentration of the d-TCOs to obtain the bimolecular rate constant k_2 from the slope of the plot.*

Table S4.1 *Second-order rate constants (k_2, n=5, mean ± SD) derived from observed rates (k_{obs}) between the d-TCOs and $2Pyr_2$*

TCO	k(obs)	k_2 ($M^{-1}s^{-1}$) $2Pyr_2$
UAMC-4129	43.50 ± 0.31	184892 ± 312
UAMC-3933	43.43 ± 0.13	87265 ± 133
UAMC-3711	45.73 ± 0.08	91460 ± 77
UAMC-3724	73.10 ± 0.09	146200 ± 91
UAMC-3725	73.31 ± 0.11	142626 ± 107

4.7.3 Antibody Production and Conjugation

Hybridoma cells were grown in 15% serum media supplemented with penicillin (10 U/mL) and streptomycin (10 ug/mL). Upon reaching cell confluency, the supernatant media was collected and the CC49 antibody was harvested and purified by protein G affinity chromatography using a MabTrap kit (GE Healthcare) according to the manufacturer's instructions. The purified CC49 was washed with PBS using an Amicon Ultra-15 (Amicon Ultra Merck Life Sciences) centrifugal unit. This method yielded a CC49 solution (5 mg/mL) containing a single band of ~150 kDa, as confirmed by SDS-PAGE .

A CC49 solution (2 mg from a 5 mg/mL solution) reacted with methyl-tetrazine-NHS (20 equiv., 15 µL in dimethyl sulfoxide) in a total volume of 500 µL PBS. Sodium carbonate buffer (1 M, 1.6 µL) was used to adjust the pH to 9, and the reaction was carried out for 45 min at RT in the dark. The purification of the conjugate was performed via size exclusion chromatography (PD-10 column) and concentrated using Vivaspin Turbo 4 (Sartorius) centrifuge tubes to be stored in PBS at 4 °C. To determine the degree of tetrazine conjugation to the antibody, electronspray ionization quadrupole time-of-flight mass spectrometry (ESI-Q-TOF-MS) was used.[201]

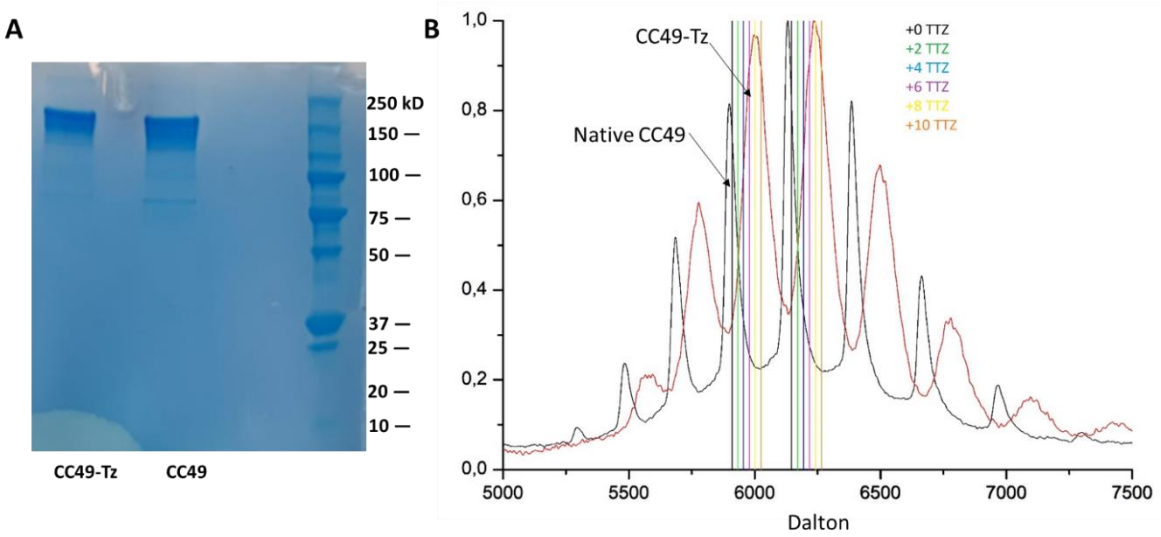

Figure S4.2 *A) SDS-PAGE of purified native CC49 and tetrazine conjugated CC49 (Right Lane: protein MW standard). B) ESI-QTOF deconvoluted mass spectrometry data of bioconjugate CC49-tz showing that the bioconjugation yielded between 6 and 10 tetrazines (dominant peak 8 Tz attached). Black spectra represents the native CC49 and red spectra corresponds to the CC49-Tz conjugate.*

4.7.3.1 *Binding Affinity*

Briefly, Immulon 2HB high-binding 96-well (Thermo Fisher Scientific, Waltham, MA, USA) plates were coated with 100 µL of a human CA72-4 antigen (MW 48 kDa) solution (CA72-4 Cancer Antigen from the human metastatic liver; Lee Biosolutions) at 4°C overnight. Following this, the plates were washed three times with 0.2 % Tween/PBS and then blocked with a 3 % bovine serum albumin (BSA)/PBS solution for 1 h at room temperature to avoid non-specific binding. The blocking solution was subsequently removed, and the wells were washed three times with 0.2 % Tween/PBS. A dilution series was performed in triplicate using unmodified CC49 and CC49-tz conjugate. Samples were added to the first well (160 µg/mL, 150 µL) and 1/5 serial dilution was performed 10 times yielding a concentration range of 160 to 8,2 x 10^{-5} µg/mL. After 1 h incubation at room temperature, the antibody solutions were removed, and the wells were washed three times with 0.2 % Tween/PBS. This was followed by the addition of rabbit anti-human horseradish peroxidase (HRP) secondary antibodies (Abcam, London, UK, Cat# ab6759, RRID: AB_955434) (1/130,000 dilution, 2 mg/mL stock, 100 µL) and incubation for 1 h at room temperature. After washing three times with 0.2 % Tween/PBS, 100 µL HRP substrate (1:1 TMB substrate kit, 100 µL, Thermo Fisher Scientific, Waltham, MA, USA) was added to the wells and incubated for 20 min at room temperature. The color reaction was stopped by adding 100 µL 1 M H_2SO_4 (Sigma Aldrich, Saint Louis, MO, USA)

stopping solution. The plates were read at 450 nm and plotted data were analyzed to determine half-maximal effective concentration values using GraphPad.

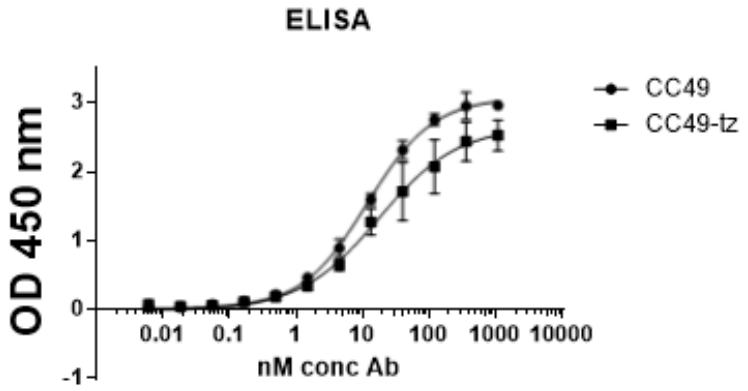

Figure S4.3 *Binding affinity of native CC49 and CC49-Tz.*

4.7.4 Radiochemistry

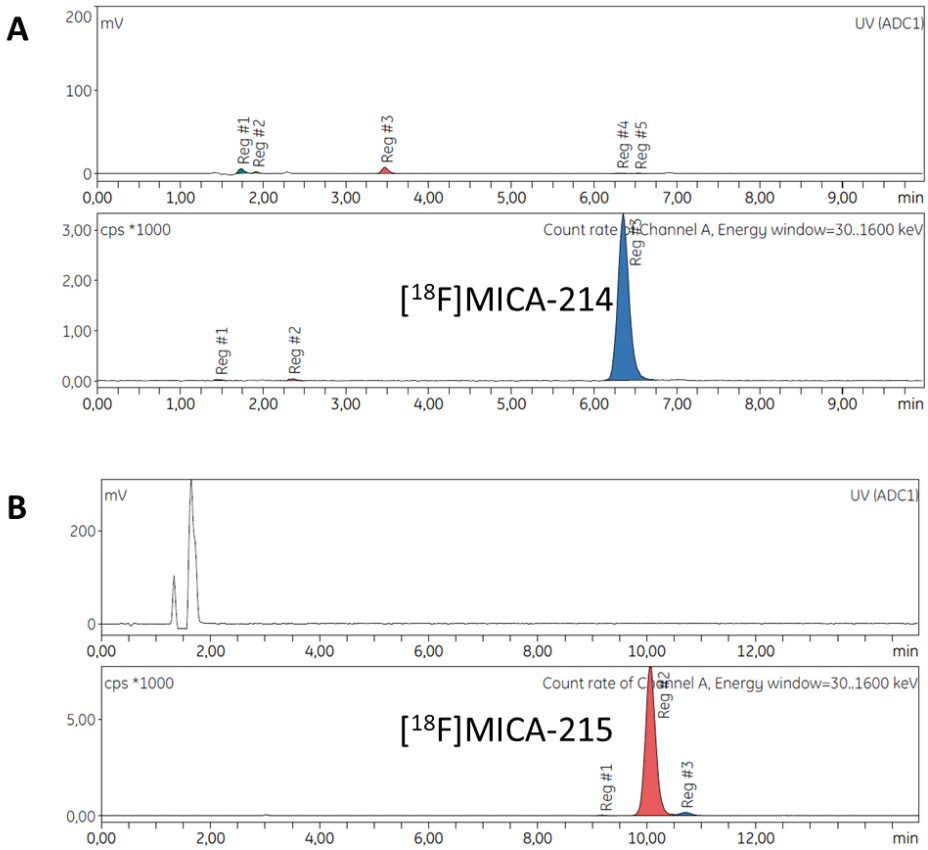

Figure S4.4 *Radiochromatograms of A: [^{18}F]MICA-214 (t_R= 6.42min) and B: [^{18}F]MICA-215 (t_R= 10.07 min) after RP-HPLC purification.*

4.7.5 *In vitro* stability of radiotracers

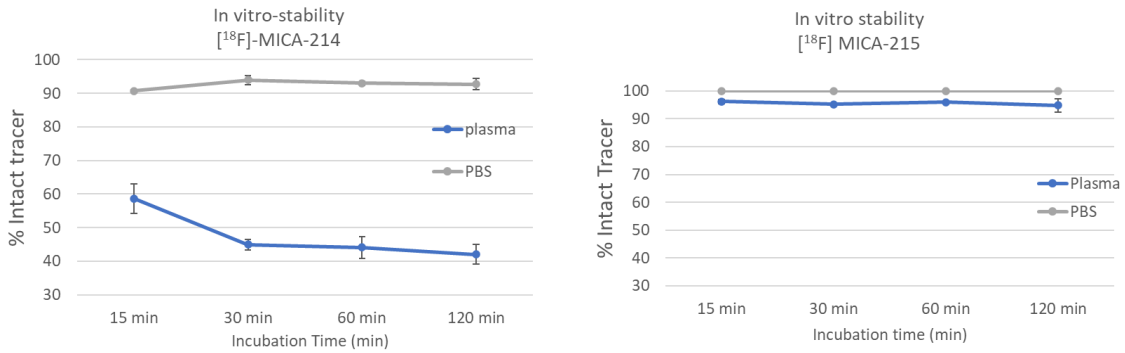

Figure S4.5 *In vitro stability of [^{18}F] MICA-214 and [^{18}F] MICA-215 in PBS at room temperature and in mouse plasma at 37 °C. (n=3, data are represented as mean ± SD)*

4.7.6 *Ex vivo* biodistribution and *in vivo* stability studies

Complete biodistribution and *ex vivo* analysis (%ID/g) was performed for [^{18}F] MICA-214 and [^{18}F] MICA-215 at different time points (5, 15, 30, 60 min).

Table S4.4 *Biodistribution data for [^{18}F]MICA-214 in healthy mice. The data represent the mean % ID/g ± SD (n = 3).*

Organ	5 min	15 min	30 min	60 min
Blood	3.8 ± 0.1	2.9 ± 1.3	1.5 ± 0.4	2.1 ± 1.4
Heart	3.6 ± 0.2	1.9 ± 0.5	1.2 ± 0.1	1.1 ± 0.1
Lungs	4.5 ± 0.2	2.5 ± 0.7	1.7 ± 0.3	1.4 ± 0.3
Liver	14.3 ± 0.8	9.2 ± 2.6	5.6 ± 0.9	4.0 ± 0.8
Spleen	3.2 ± 0.6	1.9 ± 0.3	1.2 ± 0.2	1.0 ± 0.2
Pancreas	5.6 ± 1.7	2.3 ± 0.6	1.0 ± 0.1	0.7 ± 0.1
Stomach	4.0 ± 0.9	2.4 ± 0.6	1.4 ± 0.4	1.2 ± 0.5
Small Intestine	14.5 ± 0.2	15.1 ± 5.0	19.5 ± 0.6	17.8 ± 4.7
Large Intestine	6.4 ± 0.6	8.0 ± 2.2	7.1 ± 0.3	9.9 ± 3.1
Kidneys	23.4 ± 5.5	9.0 ± 2.4	4.0 ± 0.8	2.2 ± 0.5
Bladder	50.9 ± 3.3	8.8 ± 3.7	3.6 ± 1.5	3.0 ± 1.8
Muscle	3.3 ± 0.2	2.3 ± 0.8	1.1 ± 0.1	0.8 ± 0.2
Fat	4.1 ± 1.4	3.1 ± 1.5	0.8 ± 0.4	1.1 ± 0.6
Bone	2.5 ± 0.3	3.7 ± 2.0	1.6 ± 0.2	2.8 ± 1.3
Brain	0.6 ± 0.0	0.8 ± 0.2	0.8 ± 0.2	0.8 ± 0.1
Skin	3.2 ± 0.3	3.4 ± 1.6	1.2 ± 0.2	1.8 ± 1.0
Urine*	5098.7 ± 6595.2	842.7 ± 626.379	637.3 ± 25.1	59.8 ± 15.10

**The values reported constitute a qualitative assesment of clearance tracer or metabolites in urine. The measured values surpassed the upper limit of quantification.*

Table S4.3 *Biodistribution data for [^{18}F]MICA-215 in healthy mice. The data represent the mean % ID/g ± SD (n = 3).*

Organ	5 min	15 min	30 min	60 min
Blood	6.8 ± 0.5	5.0 ± 0.1	4.5 ± 0.2	4.2 ± 0.4
Heart	5.8 ± 0.4	4.1 ± 0.1	3.5 ± 0.2	3.0 ± 0.3
Lungs	7.4 ± 0.6	4.6 ± 0.1	3.6 ± 0.2	3.2 ± 0.2
Liver	7.8 ± 0.2	4.6 ± 0.1	3.8 ± 0.3	3.7 ± 0.4
Spleen	5.1 ± 0.2	3.7 ± 0.1	3.4 ± 0.2	3.0 ± 0.1
Pancreas	6.2 ± 0.1	3.6 ± 0.1	2.9 ± 0.1	2.1 ± 0.2
Stomach	4.7 ± 0.4	4.1 ± 0.6	3.6 ± 0.6	3.0 ± 0.4
Small Intestine	6.3 ± 0.3	5.2 ± 0.3	6.2 ± 0.7	5.2 ± 0.1
Large Intestine	3.9 ± 0.4	4.1 ± 0.5	6.1 ± 0.4	7.7 ± 0.7
Kidneys	12.5 ± 1.5	12.0 ± 0.1	6.3 ± 0.5	4.4 ± 0.2
Bladder	4.8 ± 0.8	7.0 ± 2.7	35.6 ± 25.9	5.8 ± 0.3
Muscle	4.8 ± 0.4	3.5 ± 0.2	2.8 ± 0.4	2.3 ±0.1
Fat	10.7 ± 1.3	5.0 ± 0.7	3.6 ± 2.3	1.9 ± 0.9
Bone	2.7 ± 0.2	2.3 ± 0.1	1.9 ± 0.2	2.7 ± 0.2
Brain	4.5 ± 0.2	3.2 ± 0.1	3.1 ± 0.3	3.3 ± 0.3
Skin	6.3 ± 0.8	5.0 ± 0.5	3.7 ± 0.3	3.3 ± 0.1
Urine*	30.6 ± 4.7	271.8 ± 121.3	850.3 ± 376.3	606.3 ± 252.4

**The values reported constitute a qualitative assesment of clearance tracer or metabolites in urine. The measured values surpassed the upper limit of quantification.*

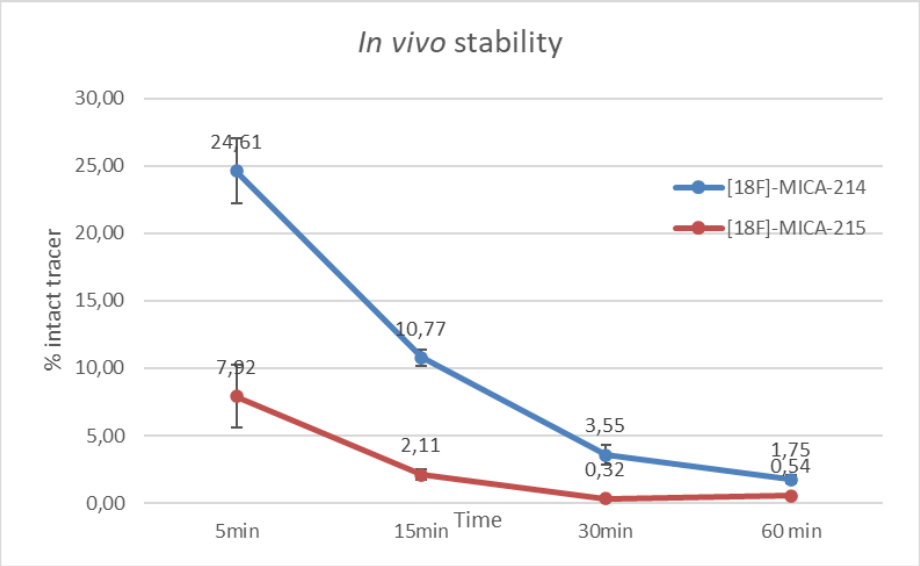

Figure S4.6 *In vivo stability of [^{18}F] MICA-214 and [^{18}F] MICA-215 in BALB/c nude mice (n=3/time point, data are represented as mean ± SD)*

4.7.7 Pretargeted PET-Imaging of [^{18}F]MICA-214 in LS174T xenografts

Table S4 *Ex-vivo biodistribution data and tumor/non-tumor ratios for [^{18}F]MICA-214 in mice bearing LS174T xenografts. The data represent the mean % ID/g ± SD (n = 4).*

Organ	Pretargeting	Control
Blood	2.1 ± 0.6	1.4 ± 0.3
Liver	4.2 ± 1.1	4.7 ± 1.0
Kidneys	2.8 ± 1.2	2.5 ± 0.1
Muscle	1.0 ± 0.2	1.5 ± 0.6
Bone	1.6 ± 0.3	1.6 ± 0.5
Small Intestine	20.6 ±3.8	21.8 ± 1.7
Large Intestine	9.5 ± 0.6	8.8 ± 1.9
Bladder	11.2 ± 6.0	7.1 ± 3.8
Tumor	1.7 ± 0.4	1.1 ± 0.1
Tumor /Blood	0.9 ± 0.4	0.8 ± 0.2
Tumor/Liver	0.4 ± 0.1	0.2 ± 0.1
Tumor/Muscle	1.8 ± 0.3	0.8 ± 0.3
Tumor/Bone	1.0 ± 0.3	0.7 ± 0.2

CHAPTER 5

Synthesis of turn-on tetrazines and their application in studying the cell permeability of TCOs

Proof of Concept Study: Unpublished data

Research internship (01/10/2021-24/12/2021) performed at the Department of Molecular Chemistry and Chemical Biology-Technical University of Vienna

Karuna Adhikari, Patrick Keppel, Andreas Löffler, Barbara Sohr, Hannes Mikula

Contribution:

Synthesis of Coumarin-tetrazine probes and *in vitro* evaluation, data acquisition, analysis and writing

Chapter 5 Synthesis of turn-on tetrazines and their application in studying the cell permeability of TCOs

5.1 Abstract

Introduction: Pretargeted imaging through inverse electron-demand Diels-Alder reaction combines the high target specificity and affinity of monoclonal antibodies (mAbs) while enabling the use of short-lived radioisotopes to acquire high contrast images. However, intracellular imaging of tumor biomarkers with mAb based agents has proven difficult as most antibodies internalize following their binding to their targes at the cell surface. This leads to a reduction of available bioorthogonal tags for the binding of reporter molecule. To address this challenge, we propose utilizing the enhanced cell permeability afforded by the more lipophilic profile of d-TCO derivatives. In this present study, a proof of concept fluorescence-based cell assay has been developed. This assay employs a fluorinated d-TCO in combination with a quenched fluorogenic coumarin-tetrazine conjugated to an internalizing Bruton's tyrosine kinase inhibitor, Ibrutinib. The coumarin-tetrazine probe generates a turn-on fluorescence effect upon reaction with d-TCOs. This approach allows for the investigation of cell permeability and intracellular click ligation of unmodified d-TCO derivatives, thereby enabling the visualization of intracellular targets or targets located beyond the blood-brain barrier.

Results: Based on the turn-on quenched fluorogenic properties, coumarin-tetrazines probes with azetidine or amine substitution and a acid handle were synthesized. The reaction kinetics between a model azetidine substituted tetrazine showed fast kinetics with d-TCOs, with rate constants ranging from 11,098 to 13,183 $M^{-1}s^{-1}$. The azetidine substituted tetrazine probe was conjugated to Ibrutinib as an intracelluar targeting vector, which binds to Bruton's tyrosine kinase in the cytoplasm. In a cell permeability assay, a bright turn-on fluorescence was observed for a d-TCO derivative (UAMC-3933) with the lipophilic linker in the cytoplasm colocalizing with the BTK-mCherry signal.

Conclusion: Two quenched fluorogenic coumarin-tetrazine probes were synthesized with excellent turn-on effect. An azetidine susbtituted probe was conjugated to Ibrutinib and applied in a cell-

fluorescence assay for a targeted intracellular imaging of BTK. The proof-of-concept study demonstrated a bright turn-on fluoresence in the cytoplasm with the d-TCO derivative UAMC-3933. This approach can be translated to antibodies to study the pretargeted imaging with internalizing antibodies.

5.2 Introduction

Pretargeted imaging represents a promising approach to address challenges associated with the slow pharmacokinetics of mAbs in the field of nuclear imaging and therapy.[27] It combines the high target specificity and affinity of mAbs with the use of short-lived radioisotopes, enabling the acquisition of high contrast images within a shorter time frame post radiotracer injection, while minimizing the radiation exposure for patients. It is a widely studied topic in nuclear imaging with applications in both diagnostics and therapy.

Nevertheless, an obstacle in the pretargeting strategy is the internalization of mAbs after binding to their target.[40] Following the binding of a mAb to its antigen or receptor, all mAbs internalize via endocytosis of the mAb-receptor complex, albeit at different rates. Following endocytosis and subsequent catabolism of the mAb-receptor complex, cell membrane receptors are either recycled back to the cell surface or routed to the lysosomes for degradation. This internalization process of mAbs is a desirable feature for targeted therapeutic applications, such as ADC or radiolabeled mabs, facilitating specific payload delivery to cells overexpressing the target while reducing systemic toxicity.[311] However, it can pose challenges in the context of pretargeted imaging. This challenge arises from the potential reduction in the availability of mAb-TCO construct for reaction with Tz-radiotracers. Tz-radiotracers have been radiolabeled via chelation chemistry due to their instability in direct radiolabeling conditions. Given the high molecular weights of macrocyclic chelators and the charge, Tzs conjugated to these chelators do not pass the cell membrane. Depending on the internalization kinetics, the receptor-mAb-Tz complex can be present on the cell surface, or after internalization intracellularly in endosomes, or lysosomes which complicates the pretargeting approach.[82] However, a more lipophilic, small molecular-weight radiotracer could cross the cell membrane and react with internalized targets within these cellular compartments.

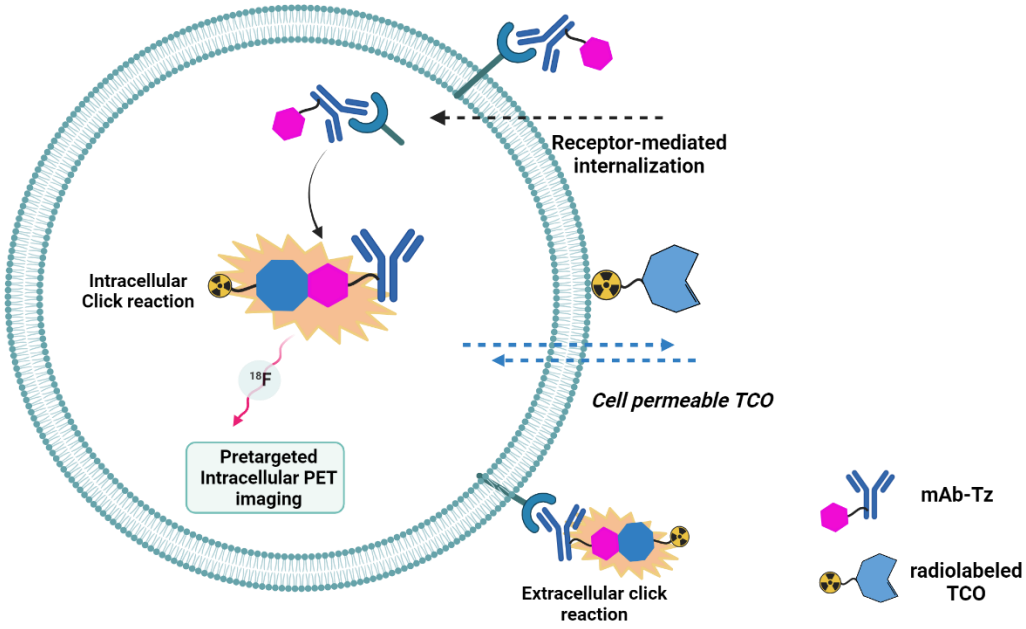

Figure 5.1 *Schematic representation of a pretargeted intracellular imaging approach using cell-permeable TCOs. A mAb-Tz construct can be located either at extracellular surface or be internalized. The use of a cell-permeable TCO allows for the click-reaction at both the cell surface and with internalized mAb-Tz conjugates.*

One of the underlying motivations behind the introduction of the inverse approach described in this thesis was to exploit the enhanced cell permeability afforded by the more lipophilic profile of TCOs, opening up the possibility to visualize intracellular targets or targets beyond the blood-brain barrier. A cell-permeable radiolabeled TCO that is stable and reactive towards the mAb-Tz tag in intracellular conditions could allow the intracellular imaging of internalizing targets. This on the other hand opens up possibilities of studying intracellualr biomarkers that were previously considered challenging to access due to their cellular location. To support the hypothesis that TCOs can be used for imaging of internalizing targets in the context of pretargeted imaging, the cell permeability of unmodified TCO was investigated. To demonstrate this, we have performed a proof-of-concept study, using an assay based on the turn-on fluorescence property of tetrazine-conjugated fluorophores. Weissleder *et al*. first reported the ability of tetrazines to quench the fluorescence of certain fluorophores which could be turned on following the addition of the dienophile reaction partner.[312] Different fluorophores have been conjugated to tetrazines to quench the fluorogenic properties and to subsequently induce the turn-on effect to visualize biological targets, where extensive washing of the excess fluorogenic compound is not needed. Three different mechanisms have been proposed through which the quenching of fluorescence of

tetrazine-modified dyes are observed, FRET (Förster resonance energy transfer), TBET (through-bond energy transfer), or PeT (photoinduced electron transfer).

For FRET-based quenching, an overlap between the emission wavelength of the attached fluorophore and the absorption range of the tetrazine (typically between 520-540 nm) is essential and the fluorescent core is linked to the tetrazine through a flexible linker. In contrast, TBET does not require spectral overlapping and the probes are conjugated to tetrazines via an electronically decoupled rigid linker.[313] Notably, TBET-based quenching provides significantly improved fluorescence "turn-on" response with up to 10,000-fold enhancement. Specifically, the coumarin-based tetrazines, also known as HELIOS probes, are one example of the TBET-based probes. These probes have displayed an exceptional turn-on ratio and they span the visible-light spectrum from blue to green. The use of the HELIOS probe in a no-wash fluorogenic imaging of mitochondria within OVCAR-429 cells, where mitochondria were tagged with RFP, exhibited an excellent colocalization following the sequential addition of anti-mitochondria-TCO antibodies and the HELIOS probe.[314]

Inspired by this, Galeta *et al.* conducted further analysis of the influence of various substituents on the photophysical properties of the coumarin-tetrazine dyes. The study revealed that azetidine-substitution in combination with a pyridinyl spacer provided a higher turn-on ratio. However, the synthesis of pyridinyl spacer was challenging during the oxidation of dihydro tetrazine intermediate. In contrast, the preparation of compounds incorporating phenyl spacer appeared more amenable.[315]

Considering these findings, this chapter describes the design and synthesis of coumarin-tetrazine derivatives containing functional groups amenable to further modification for subsequent conjugation with a targeting moiety. This was done with the overarching objective of establishing a cell permeability assay, tailored for the assessment of unmodified-d-TCO compounds reported in Chapter 3.

The assay was based on the selective covalent binding of the drug ibrutinib to Bruton tyrosine kinase (BTK), a non-receptor kinase located within the cellular cytoplasm. Therefore, we have synthesized a coumarin-based turn-on tetrazine modified with ibrutinib. Subsequently, this modified probe was used in HT1080 cells transfected with BTK-mCherry to visualize the turn-on

click reaction of the quenched fluorogenic probe, following the addition of d-TCO compounds. This approach enables a qualitative assessment of the capability of d-TCOs compound to react within an intracellular environment.

5.3 Materials and Methods:

5.3.1 General

All chemicals and reagents were purchased from commercial suppliers (Sigma-Aldrich, Acros, TCI-Europe, FluoroChem, BLD Pharmatech) and used without further purification. Phosphate-buffered saline (PBS, 0.01 M, pH 7.4) solutions were obtained from diluting a 0.5 M stock purchased from Gentest Life technology. Solvents used for column chromatography were purchased from Donau Chemie AG. DCM, THF, and diethyl ether were dried using PURESOLV-columns (Inert Corporation). Dry DMF was obtained from ACROS Organics and stored under argon.

Thin layer chromatography was performed using TLC plates on aluminum support (Merck, silica gel 60, fluorescent indicator 254). Column chromatography was performed using a BUCHI Sepacore Flash System (2 x BUCHI Pump Module C-605, BUCHI Pump Manager C-615, BUCHI UV Photometer C-635, and BUCHI Fraction Collector C-660) and a Reveleris X2 Purification System (BUCHI). Silica gel 60 (40-63 µm) was obtained from Merck. Kinetex AXIA LC columns (C18 or C8; 5 µm, 100 Å, 100 x 30.0 mm, Phenomenex) were used for preparative HPLC. HPLC grade solvents were purchased from VWR (USA).

NMR spectra were recorded on a Bruker Avance UltraShield 400 MHz spectrometer at 20 °C. ^{1}H and ^{13}C spectra are referenced to residual solvent peaks, coupling constants are given in Hz.

HPLC-MS (LCMS) analysis was performed on a Nexera X2 system (Shimadzu) comprised of LC-30AD pumps, a SIL-30AC autosampler, a CTO-20AC column oven, and a DGU-20A5/3 degasser module. Detection was done using an SPD-M20A photodiode array, an RF-20Axs fluorescence detector, an ELS-2041 evaporative light scattering detector (JASCO), and an LCMS-2020 mass spectrometer (ESI/APCI). If not stated otherwise, all separations were performed using a Waters XSelect CSH™ C18 2.5 µm (3.0 x 50 mm) column XP at 40 °C and a flowrate of 1.7 mL/min with 0.1% aqueous formic acid or ammonium formate buffer (2.5 mM, pH 8.4) and acetonitrile (gradient elution).

Acidic HPLC conditions (acetonitrile/0.1% formic acid) 0 min: 5%, 0.15 min: 5 %, 2.20 min: 98%, 2.50 min: 98%; Buffered HPLC conditions (acetonitrile/2.5 mM ammonium formate buffer, pH 8.4) 0 min: 5%, 0.15 min: 5%, 2.20 min: 98%, 2.50 min: 98%. Kinetics were performed on a SX20-LED stopped-flow system (Applied Photophysics). All data obtained from kinetic measurements were analyzed with GraphPad Prism version 9.3.1 (RRID: SCR_002798).

5.3.2 Synthesis

4-methyl-2-oxo-2H-chromen-7-yl trifluoromethane sulfonate (5.2)

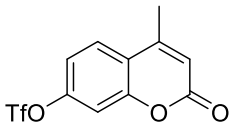

7-Hydroxy-4-methyl coumarin (5.1) (9.5 g, 54.0 mmol) and 4-Dimethylaminopyridine (3.3 g, 27.0 mmol) were dissolved in anhydrous DCM (100 ml) under Argon. The suspension was cooled down to -10°C. *N, N*-Di-iso-propylethylamine (13.8 mL, 81 mmol) was added slowly after which the suspension turned into a yellowish-clear solution. Triflic anhydride (10 mL, 59 mmol) was added dropwise over 30 (turned dark orange) and stirred further 30 min at 0°C. A saturated solution of $NaHCO_3$ (240 mL) was added and the organic phase was separated from the aqueous phase. The aqueous phase was extracted with DCM (2 x 40 mL). The organic phases were combined, dried with Na_2SO_4, filtered, and evaporated. The product was purified by silica gel flash chromatography (0-25% EtOAc in PE) to afford white solids (9.7 g, 58%). ^{1}H NMR (400 MHz, CD2Cl2) δ 7.73 (d, *J* = 8.7 Hz, 1H), 7.33 – 7.22 (m, 2H), 6.33 (q, *J* = 1.3 Hz, 1H), 2.45 (d, *J* = 1.4 Hz, 3H).

7-(azetidin-1-yl)-4-methyl-2H-chromen-2-one (5.3)

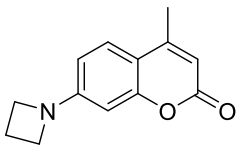

Triflate **5.2** (1.079 g 3.5 mmol), RuPhos (163 mg, 0.35 mmol), RuPhosPdG3 (293 mg, 0.35 mmol), Cs_2CO_3 (2.851 g, 8.75 mmol) and azetidine hydrochloride (360 mg, 3.85 mmol) were added in a round bottom flask with a Schlenk tube. The flask was evacuated and backfilled with argon 3 times. Then, anhydrous toluene (20mL) was added, and the reaction mixture was stirred under an argon atmosphere for 18h at 80°C. The mixture was cooled down to rt and the solvents were evaporated. The product was purified by silica gel flash chromatography (0-30% EtOAc in DCM) to give yellow solids (630 mg, 84%). ^{1}H NMR (400 MHz, CDCl3) δ 7.38 (d, *J* = 8.7 Hz, 1H), 6.30 (dd, *J* = 8.6, 2.3 Hz, 1H), 6.22 (d, *J* = 2.3 Hz, 1H), 6.00 – 5.95 (m, 1H), 3.99 (t, 4H), 2.49 – 2.38 (m, 2H), 2.34 (d, *J* = 1.1 Hz, 3H).

7-(azetidin-1-yl)-3-bromo-4-methyl-2H-chromen-2-one (5.4)

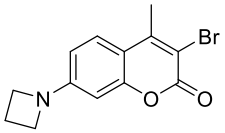

Compound **5.3** (395 mg, 1.84 mmol) was dissolved in Acetonitrile (40 mL) and N-Bromosuccinimide (327 mg, 1,85 mmol) was added at room temperature. The reaction was stirred at rt for 1h and the solvent was evaporated. The product was purified by silica gel flash chromatography (100% DCM) to give yellow solids (515mg, 95%). ^{1}H NMR (400 MHz, $CDCl_3$) δ 7.42 (d, *J* = 8.8 Hz, 1H), 6.31 (dd, *J* = 8.8, 2.3 Hz, 1H), 6.19 (d, *J* = 2.3 Hz, 1H), 4.04 – 3.96 (m, 4H), 2.53 (s, 3H), 2.47 – 2.39 (m, 2H).

3-(7-(azetidin-1-yl)-4-methyl-2-oxo-2H-chromen-3-yl)benzonitrile (5.5)

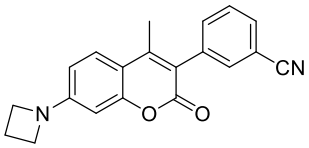

Compound 5.4 (500 mg, 1.70 mmol), 3-Cyanophenylboronicacid (500 mg, 3.40 mmol), $PdCl_2$(dppf) (119 mg, 0.170 mmol) and Potassium carbonate (470 mg, 3.40 mmol) were suspended in 1,4-Dioxane (18 mL) and Water (6,00 mL) mixture and stirred at 100°C for 1.5 hours. The mixture was cooled to rt, extracted with DCM (3x 40 mL), dried with Na_2SO_4, filtered, and evaporated. The product was purified by silica gel flash chromatography (0-2% EtOAc in DCM) to afford the desired product as a bright yellow solid (496 mg, 92%). ^{1}H NMR (400 MHz, $CDCl_3$) δ 7.68 – 7.63 (m, 1H), 7.61 – 7.59 (m, 1H), 7.56 – 7.55 (m, 2H), 7.47 (d, *J* = 8.7 Hz, 1H), 6.35 (dd, *J* = 8.7, 2.3 Hz, 1H), 6.26 (d, *J* = 2.3 Hz, 1H), 4.07 – 3.95 (m, 4H), 2.52 – 2.39 (m, 2H), 2.23 (s, 3H).

3-(7-amino-4-methyl-2-oxo-2H-chromen-3-yl)benzonitrile (5.8)

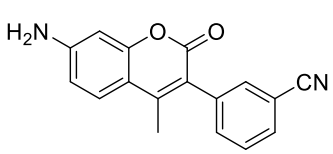

To compound 5.7 (500 mg, 1.97 mmol) in Dioxane (18 mL)/Water (6 mL) was added 3-Cyanophenylboronicacid (578 mg, 3.94 mmol), $PdCl_2$(dppf) (138 mg, 0.20 mmol) and Potassium carbonate (544 mg, 3.94 mmol). The reaction mixture was refluxed for 2 hours after which it was concentrated. The crude mixture was diluted with water and DCM and extracted with DCM (3x 80 mL), dried with Na_2SO_4, filtered, and evaporated. The product was purified by silica gel flash chromatography (0-2% MeOH in DCM) to afford white solids (456 mg, 84%) ^{1}H NMR (400 MHz, DMSO) δ 7.86 – 7.81 (m, 1H), 7.78 (m, 1H), 7.65 – 7.62 (m, 2H), 7.52 (d, *J* = 8.7 Hz, 1H), 6.61 (dd, *J* = 8.7, 2.2 Hz, 1H), 6.46 (d, *J* = 2.2 Hz, 1H), 6.19 (s, 2H), 2.16 (s, 3H).

3-(6-(3-(7-(azetidin-1-yl)-4-methyl-2-oxo-2H-chromen-3-yl)phenyl)-1,2,4,5-tetrazin-3-yl)propanoic acid (5.6)

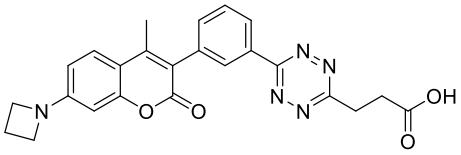

Compound 5.5 (100 mg, 0.32 mmol), 3-Cyanopropanoic acid (470 mg, 4.74 mmol), $Zn(OTf)_2$ (57.5 mg, 0.16 mmol), Dioxane (0.25 ml), and hydrazine hydrate (1.53 mL, 31 mmol) were added in a microwave vial under argon atmosphere and stirred at 65°C for 24h. The mixture was cooled to room temperature, $NaNO_2$ (20 equiv.) in H_2O (5 mL) was added and this mixture was cooled to 0°C. 2M HCl was then carefully added dropwise (gas evolution!) till pH≈3. The crude product was extracted with DCM (3×10 mL), and collected organics were dried over Na_2SO4, filtered, and evaporated. The desired product was obtained by first subjecting the crude to reversed-phase column chromatography (ACN (+ 0.1% FA) in H_2O (+0.1 %FA) 5-50% followed by preparative column chromatography to obtain the product as orange solids (4.8 mg, 4%). ^{1}H NMR (600 MHz, DMSO) δ = 8.49 – 8.45 (m, 1H), 8.39 – 8.35 (m, 1H), 7.77 – 7.71 (m, 1H), 7.65 (d, *J*=8.7, 1H), 7.63 – 7.61 (m, 1H), 6.45 (dd, *J*=8.7, 2.3, 1H), 6.32 (d, *J*=2.3, 1H), 4.00 – 3.97 (m, 4H), 2.63 – 2.59 (m, 2H), 2.52 – 2.52 (m, 2H), 2.40 – 2.37 (m, 2H), 2.26 (s, 3H). LC/MS (ESI +): *m/z* = 444.0 [M+H]+

3-(6-(3-(7-amino-4-methyl-2-oxo-2H-chromen-3-yl)phenyl)-1,2,4,5-tetrazin-3-yl)propanoic acid (5.9)

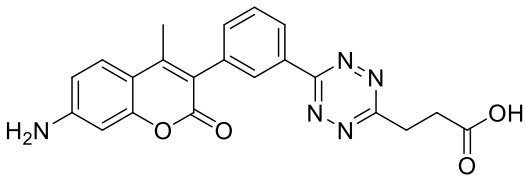

Compound 5.8 (100 mg, 0.36 mmol), 3-Cyano propanoic acid (179 mg, 1.80 mmol), $Zn(OTf)_2$ (65.6 mg, 0.18 mmol), Dioxane (0.25 mL) and hydrazine hydrate (1.76 mL, 3 mmol) were added to a microwave vial under argon atmosphere and stirred at 65°C for 24h. The mixture was cooled to room temperature, $NaNO_2$ (20 equiv.) in H_2O (5 mL) was added and this mixture was cooled to 0°C. 2M HCl was then carefully added dropwise (gas evolution!) till pH≈3. The crude product was extracted with DCM (3×10 mL), and collected organics were dried over Na_2SO_4, filtered, and evaporated. The desired product was obtained by first subjecting the crude to reversed-phase column chromatography (ACN (+ 0.1% FA) in H_2O (+0.1 %FA) 5-50% followed by preparative column chromatography to obtain the mixture of product and starting material. After several attempts, no separation of the product and the starting material was achieved.

Ethyl (E)-4-((tert-butoxycarbonyl)amino)but-2-enoate (5.11)

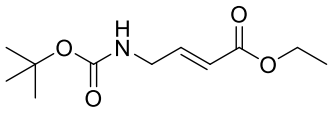

To a solution of NaH in THF (25 mL) at 0°C was added dropwise Triethylphosphonoacetate (3.74 mL, 18.85 mmol). After warming up to room temperature, a solution of N-Boc-2-aminoacetaldehyde (6.10) (1 g, 6.28 mmol) in THF (15 mL) was added to the mixture and stirred at rt for 4h. The solvent was evaporated, and the concentrated mixture was diluted with water (50mL) and extracted with EtOAc (3 x 50mL). The organic phases were combined dried over Na_2SO_4, filtered, and evaporated. The crude mixture was purified by silica gel flash chromatography (EtOAc in PE 0-20%) to afford a clear oil. ^{1}H NMR (400 MHz, CDCl3) δ 6.90 (dt, *J* = 15.7, 4.9 Hz, 1H), 5.93 (dt, *J* = 15.7, 1.9 Hz, 1H), 4.69 (s, 1H), 4.19 (q, *J* = 7.1 Hz, 2H), 3.92 (s, 2H), 1.45 (s, 9H), 1.28 (t, *J* = 7.2 Hz, 3H).

(E)-4-((tert-butoxy carbonyl)amino)but-2-enoic acid (5.12)

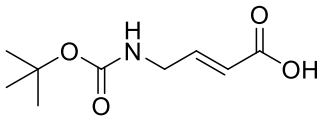

A solution of 5.11 (258 mg, 1.13 mmol) and lithium hydroxide hydrate (236 mg, 5.63 mmol) in THF (6.8 mL) and water (4.5 mL) was stirred overnight at rt. THF was evaporated and the resulting aq. solution was acidified with 1N HCl to pH 3. The aqueous phase was extracted with DCM (3 x 30mL). The organic phases were combined dried over Na_2SO_4, filtered, and evaporated to give white solids. The product was used in the next step without further purification. ^{1}H NMR (400 MHz, CDCl3) δ 7.01 (dt, *J* = 15.7, 4.9 Hz, 1H), 5.95 (dt, *J* = 15.7, 1.9 Hz, 1H), 4.73 (s, 1H), 3.95 (s, 2H), 1.46 (s, 9H).

tert-butyl(R,E)-(4-(3-(4-amino-3-(4-phenoxyphenyl)-1H-pyrazolo[3,4-d]pyrimidin-1-yl)piperidin-1-yl)-4-oxobut-2-en-1-yl)carbamate (5.14)

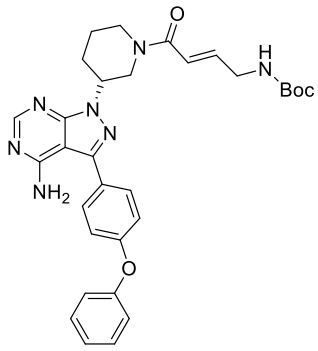

The precursor 5.13 (275 mg, 0.400 mmol) (provided by the host institution) was deprotected by stirring with TFA (20%) in DCM (5mL) at rt for 3.5 hours. After reaction completion, the solvent and excess TFA were evaporated. Compound 5.12 (89 mg, 0.44 mmol) was dissolved in anhydrous DMF (3 mL), and HBTU (167 mg, 0.440 mmol), HOBt (67.4 mg, 0.440 mmol), and $NaHCO_3$ (168 mg, 2.00 mmol) were added. The reaction mixture was stirred at rt for 15 min. A solution of deprotected Ib-precursor in anhydrous DMF (3 mL) was added to the activated acid. The reaction was stirred at RT for 2 days. The solvent was evaporated, and the residue was redissolved in DMF (0.8 mL) and water (0,6 mL). Reversed-phase column chromatography (H_2O/MeCN gradient elution,

0.1% formic acid) gave the product as a sticky yellow solid (186 mg, 82%). ^{1}H NMR (400 MHz, $CDCl_3$) δ = 8.36 (d, *J*=14.4, 1H), 7.68 – 7.60 (m, 2H), 7.44 – 7.34 (m, 1H), 7.22 – 7.12 (m, 3H), 7.10 – 7.06 (m, 2H), 6.81 – 6.68 (m, 1H), 6.44 – 6.30 (m, 1H), 5.68 (s, 2H), 4.87 – 4.83 (m, 2H), 4.72 – 4.68 (m, 1H), 4.59 – 4.55 (m, 0.5 H), 4.17 (d, *J*=13.5, 0.5 H), 3.94 – 3.83 (m, 2H), 3.79 – 3.66 (m, 0.5H), 3.39 – 3.35 (m, 0.5 H), 3.23 – 3.11 (m, 1 H), 2.90 – 2.83 (m, 1H), 2.41 – 2.29 (m, 1H), 2.29 – 2.24 (m, 1H), 1.99 (d, *J*=13.4, 1H), 1.79 – 1.65 (m, 1H), 1.50 – 1.36 (m, 9H). LC/MS (ESI+): *m/z* = $[M+H]^+$ = 570.20

(S,E)-N-(4-(3-(4-amino-3-(4-phenoxyphenyl)-1H-pyrazolo[3,4-d]pyrimidin-1-yl)piperidin-1-yl)-4-oxobut-2-en-1-yl)-3-(6-(3-(7-(azetidin-1-yl)-4-methyl-2-oxo-2H-chromen-3-yl)phenyl)-1,2,4,5-tetrazin-3-yl)propanamide (5.15)

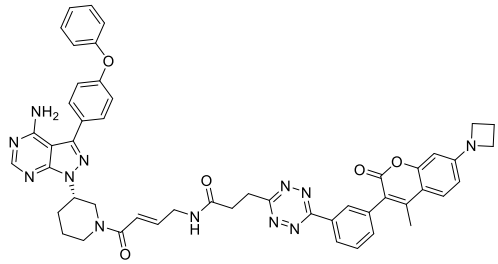

Compound 5.14 (6.42 mg, 0.01 mmol) was dissolved in DCM (500 µL) and TFA (125 µL) was added and stirred for 1h until completion of deprotection. The mixture was then evaporated to dryness. To a solution of 5.6 (5.0 mg, 0.01 mmol) dissolved in DMSO (1 mL) was added *N,N*-Di-iso-propylethylamine (5.89 µL, 0.03 mmol), HOBt (6.41 mg, 0.02 mmol) and HBTU (1.68 mg, 0.012 mmol) and stirred for 15 min. Then the deprotected 5.14 was dissolved in DMSO (100 µL) and added to the activated mixture. LC-MS at 2 h showed complete conversion of the acid. The desired product was obtained by preparative column chromatography (ACN (+ 0.1% FA) in H_2O (+0.1 %FA) 5-50% to obtain the product as pink solids (0.9 mg, 9%) (Figure 5.2). LC/MS (ESI+): *m/z* = $[M+H]^+$ = 895.37

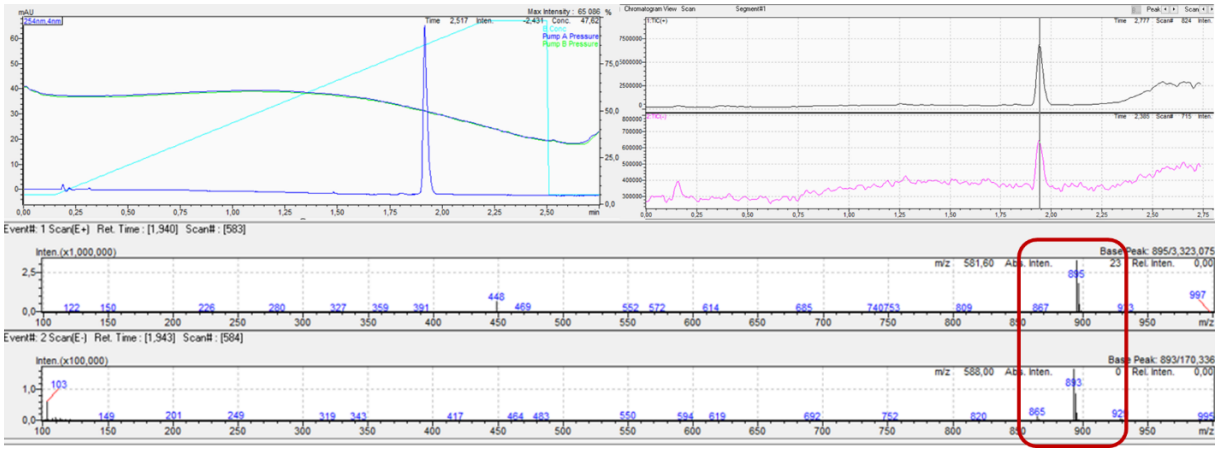

Figure 5.2 *UV-Chromatogram and LC-MS spectra (positive and negative ion-mode) of the purified compound 5.15.*

5.3.3 Reaction kinetics

Stock solutions of the d-TCOs were prepared in DMSO at a concentration of approx. 100mM. The exact concentration was determined by absorbance titration with $2Pyr_2$ (extinction coefficient at 520 nm; 433.2 $M^{-1}cm^{-1}$), quantifying the decrease in tetrazine absorbance upon reaction with TCO.[173] d-TCO stock solutions were diluted to the concentration of 50 µM in PBS (pH 7.4).

The reaction between d-TCOs and the tetrazines was measured under pseudo-first-order conditions in PBS (pH 7.4) at 37 °C with excess TCO (50 µM) by following the fluorescence enhancement of the AzMC-PA-Tz (0.5 µM) at 360 nm over time using an SX 20 stopped-flow spectrophotometer (Applied Photophysics Ltd.). The solutions were thermostatted in the syringes of the spectrophotometer before measuring. An equal volume of each was mixed by the stopped-flow device and 4000 data points were recorded over 25 seconds, and performed in quadruplicate at 37 °C. Data was analyzed by fitting an exponential one-phase association using GraphPad Prism version 9.3.1 (RRID: SCR_002798) (Figure 5.3), and the obtained kobs were divided by the TCO concentration to calculate the second-order rate constants, based on the equation $kobs=[TCO]k_2$.

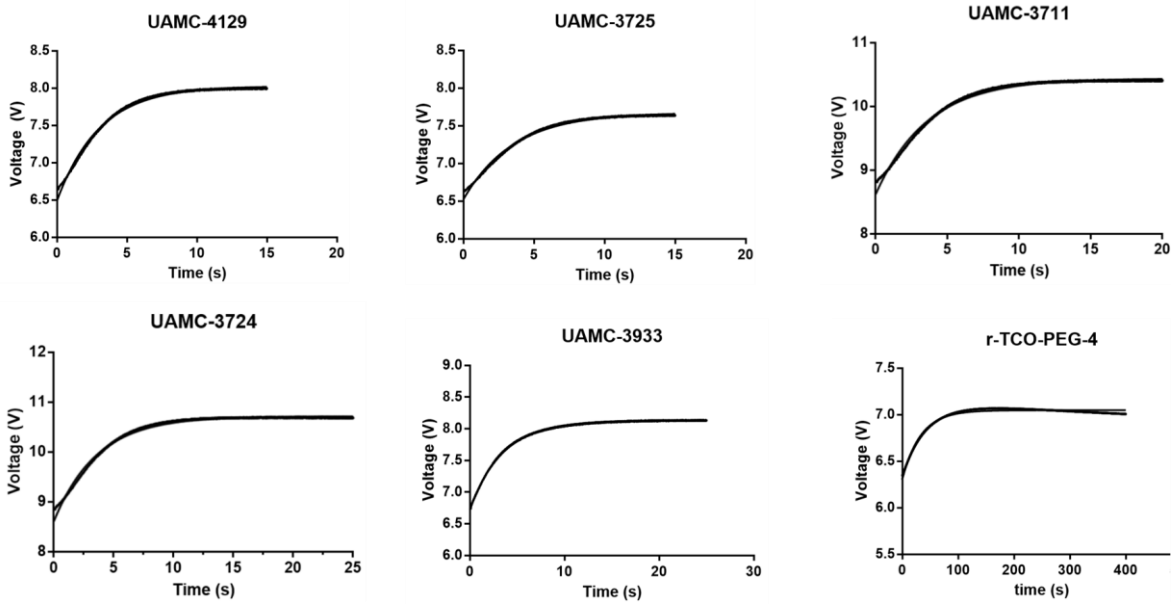

Figure 5.3 *Stopped-flow fluorescence kinetics between d-TCOs and AzMC-PA-Tz.*

5.3.4 Cell viability assay

HT1080 human fibrosarcoma cells (ATCC) were cultivated in EMEM (Minimum Essential Medium Eagle, with Earle's salts, l-glutamine, and sodium bicarbonate; Sigma Aldrich) supplemented with 10 % fetal bovine serum and 1 % antibiotic/antimycotic solution (100X, Sigma-Aldrich) at 37 °C and 5 % CO_2. HT1080 cells were seeded into 96-well plates (triplicates for each group) at 10,000 cells per well and allowed to grow overnight. The medium was removed and a dilution series of Ib-AzMC-PA-Tz, and the d-TCOs in growth medium (50 µM, 10 µM, 2 µM, 0.4 µM, 0.08 µM, 0.016 µM, 0.032 µM, 0.00064 µM, 0.000128µM) was added to the cells (0.1 % final DMSO concentration). Incubation was carried out for 72 hours. Cell viability was assessed by the addition of 10 µl of the MTT labeling reagent (final concentration 0.5 mg/ml) followed by incubation for 4 h at 37 °C and the addition of 100µL of solubilization solution post-incubation. Read-out of absorbance signal was carried out at 570 nm using a PerkinElmer EnSpire Multimode Plate Reader and data processing was done in GraphPad Prism version 9.3.1 (RRID: SCR_002798) (Figure 5.4).

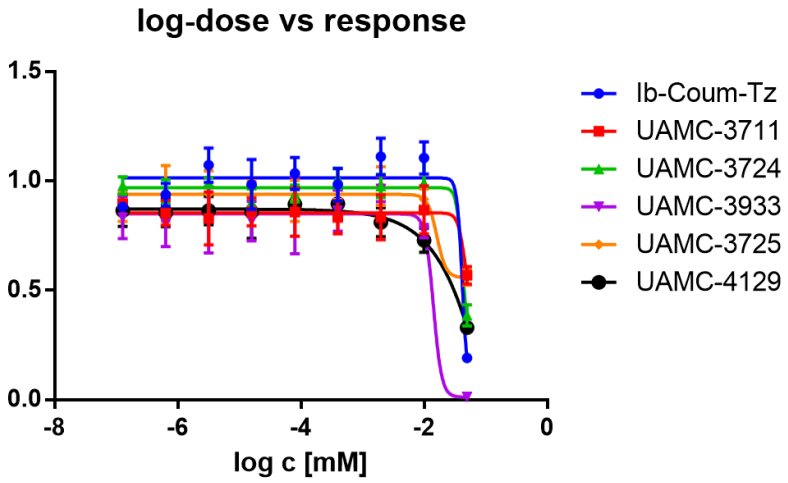

Figure 5.4 *Cell viability in the presence of d-TCOs and Ib-coumarin-Tz probe.*

5.3.5 Cell imaging- Fluorescence microscopy

A transgenic cell line expressing a BTK-mCherry fusion protein in HT1080 human fibrosarcoma cells (HT1080-BTK-mCherry) was seeded into a 96-well plate at 10,000 cells per well and allowed to grow overnight. The medium was removed, and the cells were treated with a 5 µM solution of Ib-Tz in media (100 µL/well) or control 0.1% DMSO, at 37 °C and incubated for 2 h. Cells were washed with medium (3 x 10 mins). TCOs 1 µM in medium (100 µL/well) was added and incubation was carried out for 1h. Subsequently, the medium was removed, and cells were stained with NucRed Live 647

nuclear dye (Invitrogen, 2 drops/mL growth medium) for 15 minutes and washed twice with PBS. Multichannel imaging of the cells was carried out in FluoroBrite DMEM medium (200 µL/well) (Gibco) on an Olympus IX82 microscope.

5.4 Results and Discussion

5.4.1 Synthesis of coumarin-tetrazines and Ib-conjugates

Based on the studies by Galeta *et al.* two Coumarin-tetrazine probes with azetidine **5.6** or amine **5.9** substitution on coumarin core and propanoic acid linker on tetrazine were designed. For the azetidine substitution on the coumarin core, first triflate **5.1** was prepared. The triflate was reacted with azetidine hydrochloride via Buchwald-Hartwig cross-coupling reaction to afford the azetidine-substituted coumarin **5.3**. This was followed by bromination with NBS in MeCN to afford the brominated intermediate **5.4**. Brominated intermediate **5.7** was kindly provided by TU Wien. The brominated intermediates were further reacted with a 3-Cyano-phenyl boronic acid in a Suzuki coupling reaction to afford the nitriles **5.5** and **5.8**. Coumarins **5.5** and **5.8** were then reacted with 3-cyanopropanoic acid in the presence of $Zn(OTf)_2$ and an excess of hydrazine monohydrate at 65°C to afford the tetrazines **5.6** and **5.9** (Scheme 5.1).

In general, the reactions performed for the formation of tetrazine with the corresponding nitriles were very low-yielding (3-4 %). LC-MS measurements during the reaction at different time points only showed small amounts of dihydro tetrazine intermediates, which then were oxidized to tetrazine. For azetidine-substituted tetrazine derivate, the product was only found when the reaction was performed in ethanol. For compound **5.9** product was found when reacted in dioxane as solvent however, nitrile **5.9** showed poor solubility in dioxane and led to the formation of precipitates. Unfortunately, the yield did not improve for both reactions when performed in various other solvents, temperature, or reaction times. Oxidation of dihydro tetrazines was attempted with either sodium nitrite in the presence of HCl or with (Diacetoxyiodo)benzene in the presence of acetic acid. Only oxidation with sodium nitrite led to the formation of tetrazine. Also, the purification of the products from starting nitrile proved to be extremely challenging with traces of nitrile still present after a preparative column chromatography for compound **5.9**. Compound **5.6** was further modified with an Ibrutinib for a proof-of-concept study.

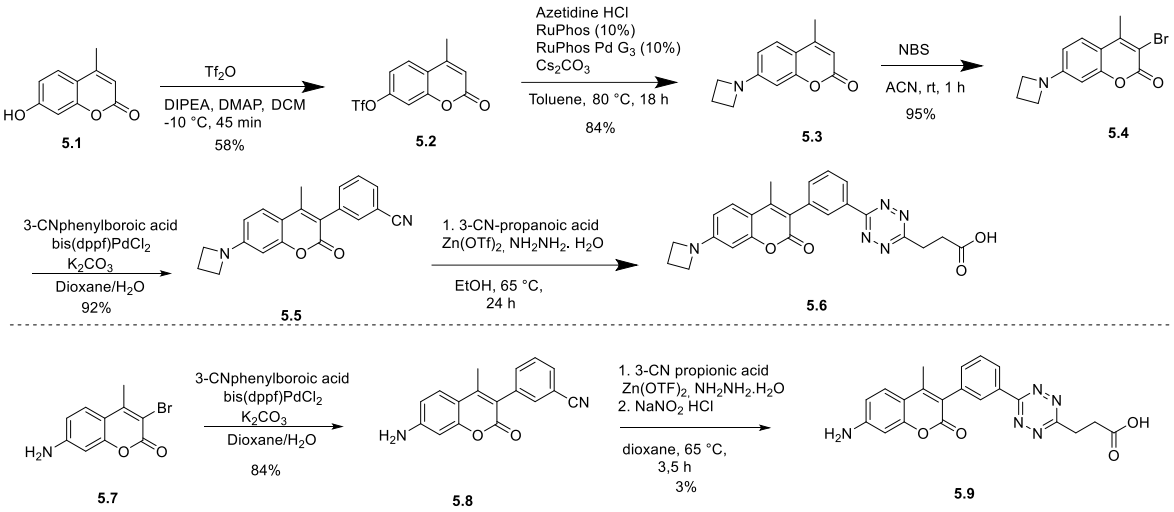

Scheme 5.1 *Synthesis of coumarin-tetrazines.*

Based on the study by Turetsky *et al.*, Ibrutinib (Ib) was modified with a linker containing a Michael acceptor for the conjugation with a coumarin-tetrazine probe (**5.6**). The Michael acceptor is required to preserve the parent drug's selectivity and irreversible binding affinity.[316] The linker was synthesized by reacting N-Boc-2-aminoacetaldehyde with deprotonated triethylphosphonoacetate to afford the alkene **5.10**. Deprotection of the ester provided the free acid **5.11**. The Boc-protected Ib-precursor was provided by TU Wien. The Ib-precursor was deprotected in acidic conditions, and the linker was introduced to the Ib-core by an amide coupling with compound **5.11** to afford compound **5.12**. Coupling of the crude Boc-deprotected compound **5.12** with Coumarin-tetrazine **5.6** finalized the synthetic steps to afford the Ibrutinib conjugated to coumarin-tetrazine probe **5.15** (Ib-coum-Tz, Scheme 5.2).

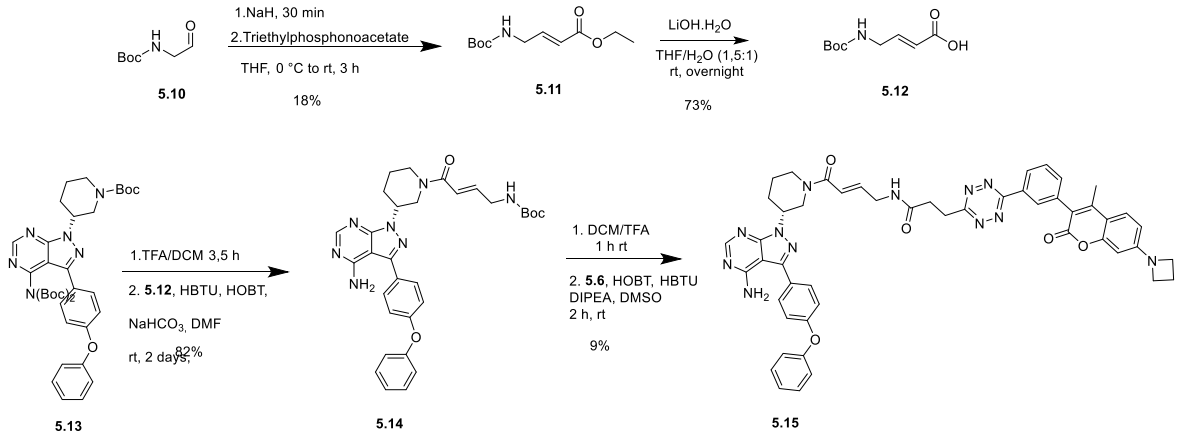

Scheme 5.2 *Synthesis of Ib-coumarin-Tz conjugate 5.15.*

5.4.2 Reaction Kinetics

The reaction kinetics of the synthesized coumarin-tetrazine probe with d-TCOs was studied by monitoring the increase in fluorescence of the coumarin-tetrazine probe upon reaction with TCO. For comparison, the rate constants of the reactions of r-TCO-PEG-4 with a coumarin-tetrazine probe were also determined. As expected, measured second-order rate constants for the ligation were in the range of 11,098 to 13,183 $M^{-1}s^{-1}$ (Figure 5.5) with the d-TCOs and far exceeded the rate constant with the r-TCO (1,184 $M^{-1}s^{-1}$). The measurements are in line with reported values for similar compounds.

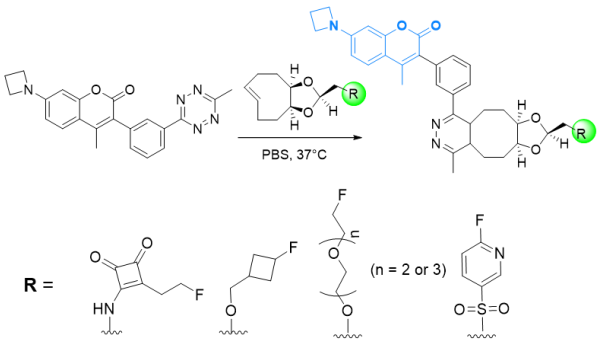

TCO	k(obs)	k_2 ($M^{-1}s^{-1}$)
UAMC-4129	0.330 ± 0.00042	13183 ± 42
UAMC-3933	0.293 ± 0.00036	11730 ± 36
UAMC-3711	0.277 ± 0.00106	11098 ± 106
UAMC-3724	0.279 ± 0.00032	11153 ± 32
UAMC-3725	0.284 ± 0.00053	11342 ± 53
r-TCO-PEG-4	0.031 ± 0.00026	1184 ± 26

Figure 5.5 *Turn-on fluorescence of coumarin-tetrazine post-reaction with TCO and measured rate constants in PBS at 37°C.*

5.4.3 Proof-of-concept cell assay

The Ib-coumarin-Tz probe and d-TCO were first tested for their toxicity in HT1080 cells. Both d-TCOs and Ib-coumarin-Tz probes were not toxic up to 50µM. Next, the probes were used in a cell fluorescence assay, to assess the ability of the d-TCO compounds to pass the cell membrane and react with the Ib-coumarin-Tz bound to BTK in the cytoplasm. To visualize the co-localization between the imaging probe and BTK at the subcellular level, a stable transgenic cell line expressing a BTK-mCherry fusion protein in HT1080 human fibrosarcoma cells was used. The cells were treated with a solution of Ib-coumarin-Tz (**5.15**, 5 µM in cell media) and incubated for 2h. Subsequently, cells were washed and d-TCOs (1µM) were added and incubated for 1h. After incubation, the cell nucleus was stained with NucRed Live 647 nuclear dye, and the cells were imaged using a confocal microscope (Figure 5.6).

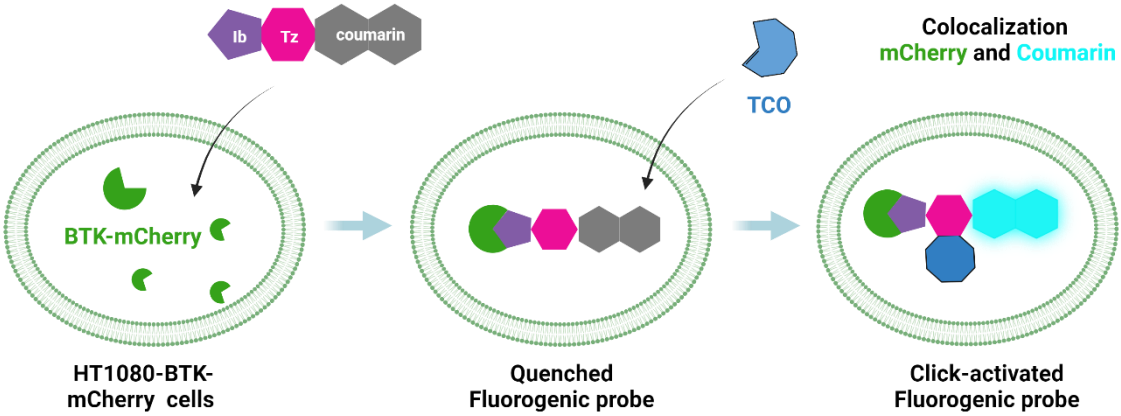

Figure 5.6 *Scheme of cellular uptake and binding to BTK of the Ibrutinib modified with quenched fluorogenic coumarin-tetrazine probe in HT1080-BTK-mCherry cells and subsequent turn-on fluorescence of coumarin-tetrazine upon treatment with TCO.*

This preliminary assay revealed a strong turn-on fluorescence for compound UAMC-3933 in cytoplasm colocalizing with the BTK-mCherry signal. Accordingly, UAMC-3933 was the most lipophilic compound of the series with a clog *D* of 2.96, whereas UAMC-4129 with the lowest clog *D* value of 0.76 showed no fluorescence turn-on despite its fast reaction kinetics. The increased polarity of the compound potentially limits its cell permeability and thus precludes the intracellular click reaction. Compound UAMC-3711 (clog *D* 1.58) and compound UAMC-3725 (clog *D* 1.92) also showed a minimal turn-on effect however fluorescence signal observed remained low (Figure 5.7). As a control, the cells were treated with Ib-modified tetrazine in the absence of d-TCO compounds. Importantly, a low background signal is also observed in the control cells. This might be due to traces of impurities present in the Ib-coumarin-Tz conjugate or due to the formation of degradation products where the coumarin is released from tetrazine in a biological environment. Previous studies with turn-on tetrazines have also highlighted the effect of trace impurities in fluorescence-turn-on ratios.[314, 315] These impurities can produce fluorescence signals and cause high background signals. Nevertheless, the Ib-coumarin-Tz was freshly purified by preparative HPLC before cell assay. This additional purification step before its use in cell assays complicates the use of these ultra-fluorogenic probes. Nevertheless, optimization of incubation times post-TCO addition and optimization of probe concentration is necessary to acquire further data.

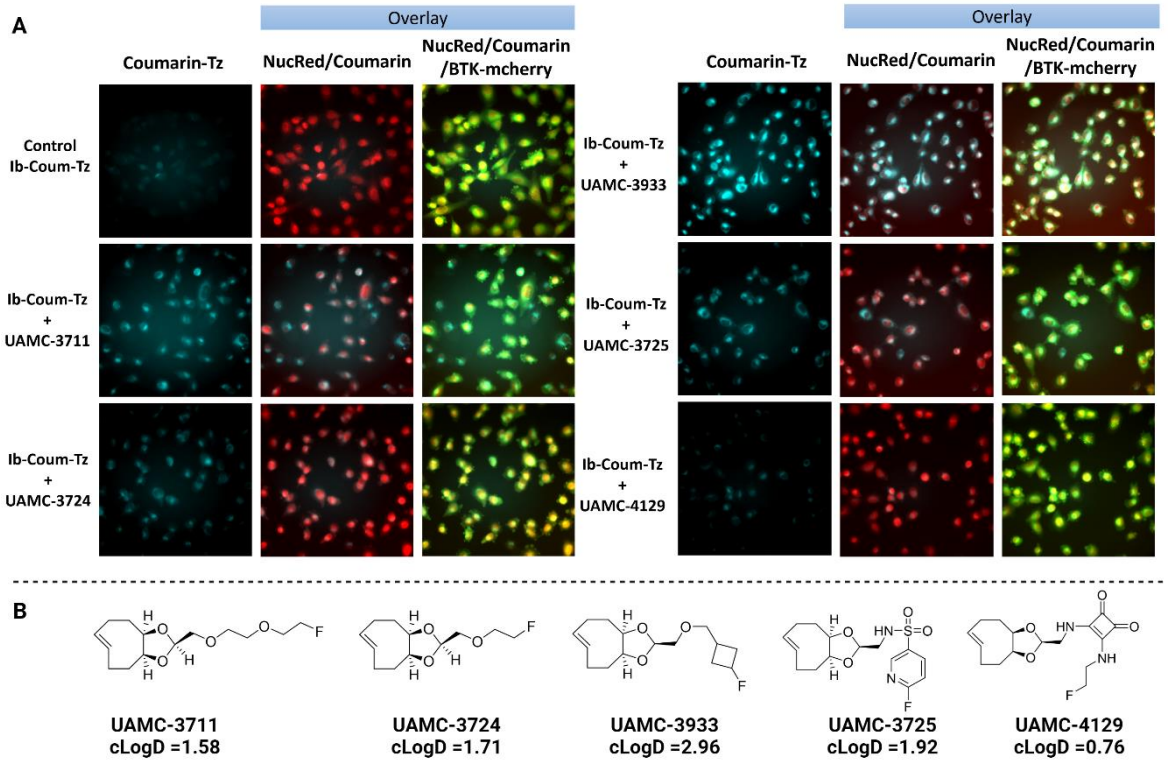

Figure 5.7 *(A) Fluorescence microscopy imaging showing the turn-on fluorescence of Ib-coumarin-tetrazine probe (5µM) after the addition of d-TCO (1µM) in HT1080-BTK-mCherry cells. The turn-on fluorescence of the Ib-coumarin tetrazine probe is shown in Cyan, the nuclear staining in Red, and the cytoplasmic mCherry in green. The brightest turn-on fluorescence signal from the coumarin-tetrazine probe after click reaction with TCO is seen with compound UAMC 3933 (Cyan) together with colocalization with the m-Cherry signal (Green). (B) Chemical structures and respective calculated log D values of d-TCO compounds were evaluated in the assay.*

5.5 Conclusion

Here we described the synthesis of a quenched fluorogenic coumarin probe with an excellent turn-on effect. The probe was successfully conjugated with Ibrutinib for a targeted intracellular imaging of BTK. This conjugate was then used in a cell fluorescence assay to test the ability of d-TCO compounds to pass the cell membrane and react with the tetrazine bound to BTK, where compound UAMC-3933 showed the best cell permeability. Although further optimization of the assay and probes is required for the development of a robust method, this preliminary proof of concept assay shows the potential of bioorthogonal-turn on probes in an intracellular imaging approach.

CHAPTER 6

General Discussion and Future Perspectives

Chapter 6 General Discussion and Future Perspectives

6.1 General Discussion

Immuno-PET has paved the way towards personalized medicine in oncology. Immuno-PET as companion diagnostic tool is a valuable tool and the growing clinical evidence suggests that it can provide patient-tailored treatment to improve patient outcomes. Acquiring the knowledge of the tumor biomarkers and their expression in the tumor microenvironment within a treatment plan is crucial for treatment evaluation and patient stratification. The conventional method to characterize the tumor involves invasive tumor biopsies. However, this method has limitations, as it often fails to provide a representative picture and suffers from sample variability and intra-patient tumor heterogeneity. Additionally, biopsies are not always feasible and are associated with higher patient stress.[317] Alternatively, less invasive liquid biopsies have generated great interest in the past decade. Yet, these techniques, while promising, lack the specificity and sensitivity for a reliable early-stage detection. Furthermore, liquid biopsy samples may not fully reflect the heterogeneity present at the primary tumor site.[318] In contrast, immuno-PET allows for a longitudinal assessment of whole-body biomarker distribution and tumor heterogeneity in a non-invasive manner, providing crucial information for predicting and assessing response to targeted therapies.[10] However, one of the limitations of this approach is the intrinsic long blood circulation half-life of the radiolabeled antibodies, leading to high radiation exposure to patients and longer intervals for imaging. This is where pretargeting plays a very important role, by decoupling the radioactivity from targeting antibodies. This enables the use of shorter-lived radioisotopes reducing the radiation exposure to patients.[25] This on the other hand allows for shorter waiting intervals before imaging. Additionally, applying the pretargeting approach for radionuclide therapy can decrease the dose limiting hematotoxicity and enhance the therapeutic efficacy.[32, 319] Several pretargeting strategies involving conventional strategies were studied in the past but only a few have advanced to clinical trial stages, due to their inherent shortcomings.[27]

Among the different pretargeting approaches, pretargeting through an IEDDA reaction between a TCO and tetrazine has been positioned as one of the most promising approaches. This preference is supported by several key attributes: the TCO-Tz ligation exhibits ultra-fast reaction kinetics, a

prerequisite for *in vivo* applications. Furthermore, it is a biocompatible reaction with very high selectivity and thus tolerates a broad spectrum of functional groups typically present in peptides and proteins. In a two-step bioorthogonal pretargeting approach, the mAb can be modified either with a TCO or Tz and injected in the living subject to bind to its target and clear from non-target tissues. Subsequently, either a radiolabeled Tz or a TCO can be administered after a predetermined time interval, followed by selective and covalent binding to the respective tag on the mAb. This two-step approach offers a robust and versatile methodology to achieve targeted imaging and therapy with improved tumor-to-non-tumor ratios and reduced off-target effects.[27, 40, 41] The added value of a pretargeting approach through IEDDA is a single platform that can be functionalized with different target recoginition vectors and imaging markers or therapeutic agent allowing for its application in diagnostic and/or thernaostic approach.

The traditional approach for bioorthogonal pretargeting consists of an initial injection of a mAb conjugated TCO, followed by the administration of a radiolabeled tetrazine. However, TCO tags conjugated to mAbs are known to undergo deactivation to their unreactive cis-isomer when exposed to Cu-bound serum proteins. Additionally, hydrophobic burying of the TCO tags within the protein core has also been reported. To circumvent these issues, we proposed to replace the TCO tags with stable tetrazines and invert the roles of the two bioorthogonal reaction partners. Consequently, the less stable radiolabeled TCOs would only be exposed to *in vivo* conditions for a shorter period. In this thesis, TCO derivatives were synthesized and radiolabeled with ^{18}F and their usefulness for *in vivo* pretargeted imaging was evaluated in a mouse model of human colorectal cancer.

Radiolabeling of TCO with Fluorine-18 was first described by Fox and co-workers. [^{18}F]FTCO was initially developed as an ^{18}F-labeling strategy for Tz-conjugated targeting molecules. When applied *in vivo* as a pretargeted PET-imaging probe by our group, the tracer showed poor metabolic stability, with the formation of radiometabolites in the plasma as well as in the brain with extensive defluorination at later time points (120 min and 240 min).[263] The proposed hypothesis towards the metabolization of [^{18}F]FTCO was the CYP-mediated O-deethylation of the [^{18}F]fluoroethyl group, which after subsequent modification can lead to defluorination.[263] Therefore, we replaced the fluoroethyl linker of [^{18}F]FTCO with a NOTA-chelator as a linker as well as a radiolabeling moiety (Figure 6.1). The introduced carbamate bond is expected to improve the overall metabolic stability

of the radiotracer. ^{18}F-radiolabeling often requires harsh alkaline conditions followed by lengthy purifications. The chelation of metal ^{18}[F](AlF)$^{2+}$ complex provides a feasible and efficient synthetic strategy for labeling both biomolecules and small molecules.[105] Aluminum (Al^{3+}) forms the strongest metal bonds with fluoride and the $(AlF)^{2+}$ complex is known to bind to chelators.[320] Several studies have demonstrated the versatility of this system to radiolabel molecules using chelators.[92, 105, 111, 321] When compared to different chelators, NOTA is shown to provide the best *in vivo* stability of the chelation complex where the Al^{18}F complex is held in place by the 3 nitrogens and 2 of the carboxyl groups of NOTA.[105] The labeling can be achieved either by adding a preformed Al^{18}F complex to the chelator or through an ^{18}F addition to a preloaded chelator-Al complex. Given, the simplicity and mild labeling procedure, the NOTA-conjugates with preloaded Al^{3+} can also be developed as a lyophilized kit for an easier, faster, and reproducible labeling method.[107, 321]

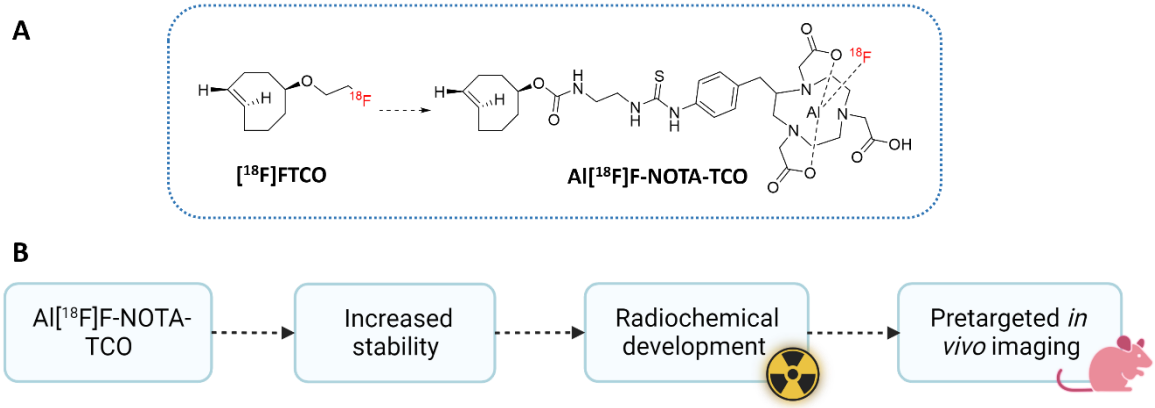

Figure 6.1 *(A) Structures of [^{18}F]FTCO and Al[^{18}F]F-NOTA-TCO (B) Schematic representation of objectives described in Chapter 3.*

The developed TCO-derivative with NOTA-chelator as a linker, **[^{18}F]MICA-205**, showed improved *in vivo* stability with more than 50% of the radiotracer remaining intact after 1h. The main radiometabolite present was the cis-isomer, and the low bone uptake suggested a high stability of the radiolabeled Al^{18}F-NOTA complex.[78, 213, 295-297] Biodistribution studies revealed a fast clearance of tracer from the blood (0.98 ± 0.59 %ID/g at 1 h pi) and a mixed hepatobiliary and renal excretion. Given the moderate lipophilic character of the tracer, radioactivity accumulation was observed in the small intestines at 1 h pi. These findings are in accordance with previous studies with Al^{18}F-NOTA-labeled tracers which also demonstrated predominant excretion via the liver with high intestinal accumulation.[105, 107] All the other non-target tissues displayed a relatively low uptake. In a pretargeted imaging approach, **[^{18}F]MICA-205** demonstrated significantly higher tumor uptake of radiotracer in mice pretreated with CC49-Tz when compared to the control group. However, the

absolute tumor uptake remained low (0.67 ± 0.16 %ID/g) when compared to ^{18}F-labeled Tzs.[93-95] The low absolute tumor uptake in combination with the high abdominal background owing to hepatobiliary clearance of the tracer is not optimal for the imaging approach and requires further optimization. Introduction of PEG linkers between the TCO and the NOTA-chelator could increase the renal excretion and decrease the liver clearance as shown with Tz-radiotracers.[260, 322] In a study by Zeglis *et al.* [^{64}Cu]Cu-Tz-NOTA with a predominant gastrointestinal clearance, shifted the excretion partly to urinary tract when a PEG_7 linker was added ([^{64}Cu]Cu-Tz-PEG_7-NOTA). However, when the NOTA chelator was replaced with a sarcophagine-based chelator (SarAr), the [^{64}Cu]Cu-Tz-SarAr excreted exclusively and rapidly from the renal system. Notably, [^{64}Cu]Cu-Tz-SarAr (logD = −2.08 ± 0.06) was the least hydrophilic compound when compared to [^{64}Cu]Cu-Tz-NOTA (logD = −2.54 ± 0.1) and [^{64}Cu]Cu-Tz-PEG_7-NOTA (logD = −2.44 ± 0.08). The authors concluded that the shift in pharmacokinetics may lie in the change in chelator and the change in overall net charge of radioligands from -1 for NOTA to +2 for SarAr.[322] Similarly, further studies with incorporation of positively charged amino acids or compounds with overall net charge showed faster renal clearance in comparison to compounds with no net charge.[323]

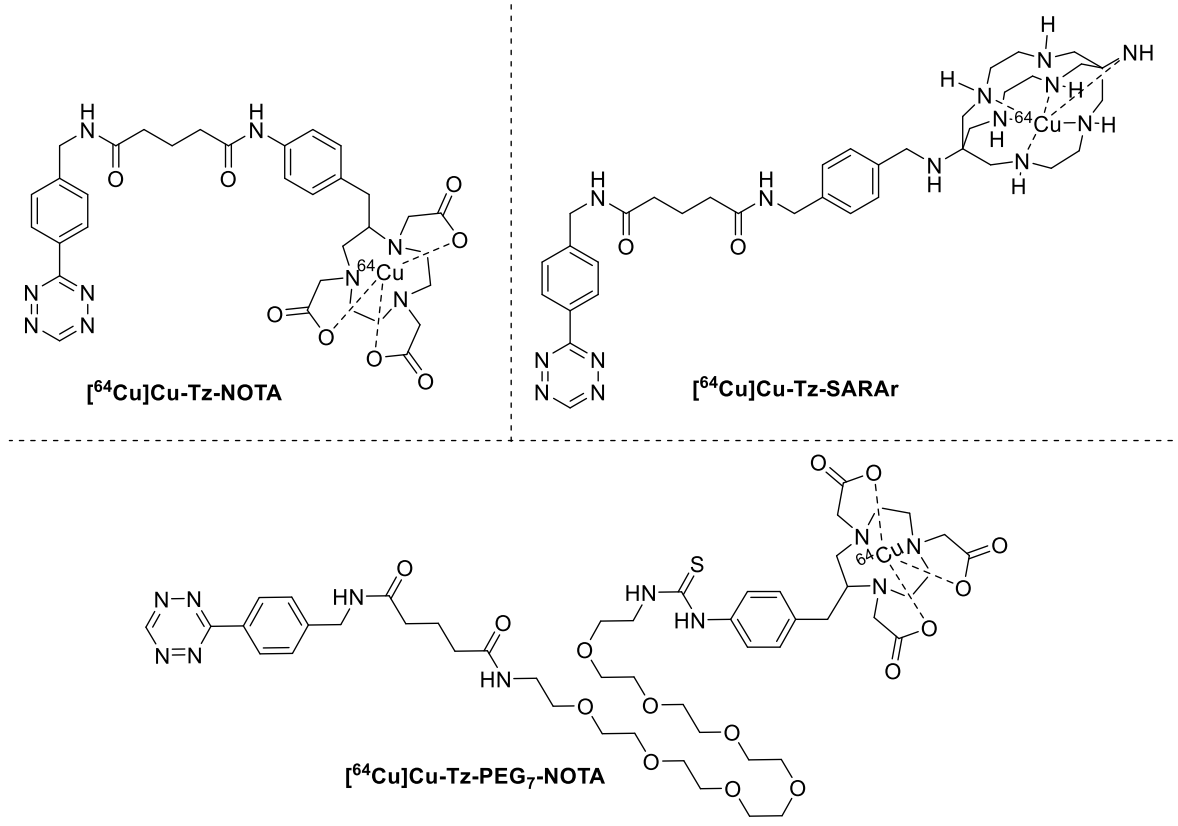

Figure 6.2: *Structures of ^{64}Cu-labeled tetrazines.*

Additionally, further optimization of the pretargeting set-up could also improve the overall image contrast. In the pretargeting study, the TCO-NOTA was used in combination with a stable methyl-tetrazine, previously developed by our group.[201] As the functionalities were inversed, we envisaged that the stability of the tetrazine needs to be high in the physiological conditions. However, the measured reaction constant of the TCO and methyl-Tz pair used in this study was significantly lower (568 $M^{-1}s^{-1}$) when compared to the kinetics of IEDDA pairs used in previously reported pretargeting studies.[78, 81, 89, 213] Thus the use of faster-reacting tetrazines with similar stability profiles could improve the tumor uptake. Furthermore, increasing the pretargeting interval from 24 h to 72 h could further decrease the blood radioactivity and enhance the image contrast.

Given the slower reaction kinetics of MICA-205 and a low absolute tumor uptake, we shifted our focus toward the development of d-TCO derivatives. d-TCO with its increased ring strain is highly reactive towards tetrazine, is more stable compared to highly strained s-TCO, and is less hydrophobic compared to 5-hydroxy TCO.[73] We aimed to study the effect of structurally diverse linkers on the stability and reactivity of the d-TCOs and their overall potential for specific tumor imaging in a pretargeting approach. For this, the d-TCO core was modified with polyethylene glycol, sulfonamide, cyclobutane, and squaramide linkers to study their impact on the probe pharmacokinetics, stability, and the feasibility for direct ^{18}F-radiolabeling (Figure 6.3).[303, 305, 324] Shorter-polyethylene glycol was introduced to increase the hydrophilicity and general stability of the tracers.[304] Similarly, squaramides are also known to increase the general stability and overall hydrophilicity of the compound.[305] Furthermore, sulfonamide and cyclobutane are known for their increased C-F bond stability.[306]

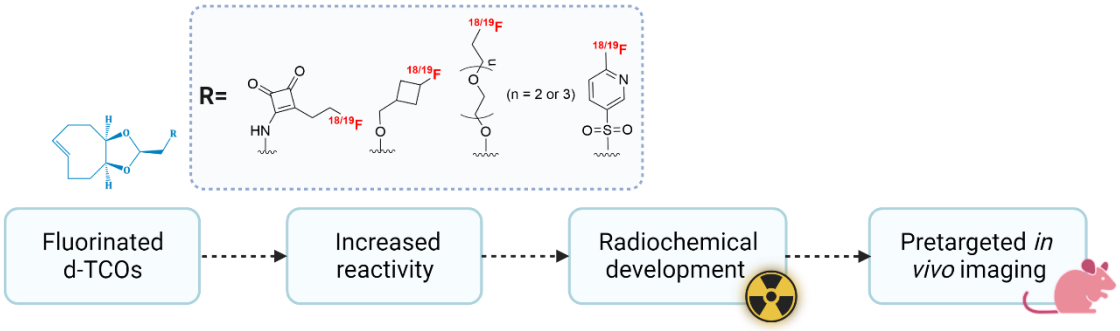

Figure 6.3 *Schematic representation of objectives described Chapter 4.*

All synthesized compounds showed excellent reactivity towards the tetrazines. As expected, the linker modification did not impact the kinetics of the d-TCO core, and the reactivity remained similar

compared to the unmodified d-TCO compound. This indicated that the modification of the d-TCO core with different linker types can be performed in the future for creating bigger libraries of compounds, necessary for a more systematic study and rational design of compounds.

Next, we developed a pretargeted blocking assay to assess the *in vivo* ligation performance of the unlabeled d-TCO derivatives. The assay was based on the work by Steen *et al.* which described the assessment of unlabeled Tz-derivatives.[80] In their original work, a ^{111}In-labeled Tz was used with TCO-modified CC49 as a benchmark for *in vivo* ligation.[80] Here, we opted for the use of a TCO modified with a fluorophore in combination with a tetrazine-modified CC49. Fluorogenic TCO-Cy5 was selected as there are no benchmark radiolabeled TCO's available but also to simplify the workflow in the pre-selection phase. The pre-selection of compounds with the blocking assay avoided the need for time-consuming precursor synthesis for each d-TCO compound as well as the development of radiolabeling procedures. Through the blocking assay, the *in vivo* ligation efficiency of the unlabeled d-TCO derivatives can be inversely correlated to the uptake of TCO-Cy5 in the tumor. The highest blocking efficiencies of 93 and 95% *in vivo* were observed for the d-TCO derivates **UAMC-3711** and **UAMC-4129** with the lowest uptake values of TCO-Cy5 in tumor 7 ± 3% (n=4) and 5 ± 2% (n=4) respectively. Given the small sample size, a statistical correlation was not established. However, the compounds with low calculated log D values showed the highest blocking efficiency. Similar results have also been reported by Steen *et al.* in pretargeted imaging studies using radiolabeled tetrazines.[80] The study showed a distinct relationship between low clog$D_{7.4}$ values and blocking effect when comparing tetrazines with similar reactivities. Lipophilic compounds show higher binding to plasma proteins and are also prone to extensive metabolism due to their higher affinity for metabolic enzymes.[325] This might lead to lower bioavailability and limit the amount of compound reaching the target.

Subsequently, tosylated precursors of **UAMC-3711** and **UAMC-4129** were prepared for the direct ^{18}F-labeling and *in vitro* assessment of the radiotracers **[^{18}F]MICA-215** and **[^{18}F]MICA-214** respectively. Tosylated precursors were chosen due to their effectiveness as a leaving group in a nucleophilic substitution reaction, while also demonstrating stability during synthesis and storage. Moreover, the synthesis of tosylated precursors require mild reaction conditions which offers the additional benefit of easy handling and storage.

Both radiotracers showed excellent stability in PBS. In plasma, **[^{18}F]MICA-214** showed a gradual increase in the formation of the cis isomer over time, whereas **[^{18}F]MICA-215** remained stable with 94 ± 2.4% (n = 3) of intact radiotracer present at 2 h. As expected, the rate of radiotracer metabolism was considerably higher under *in vivo* conditions compared to *in vitro* conditions for both tracers (24.6 ± 2.4% of intact **[^{18}F]MICA-214** and 7.9 ± 2.3% of **[^{18}F]MICA-215** at 5 min). Furthermore, both radiotracers displayed a similar metabolite profile *in vivo* characterized by similar retention times as observed in plasma studies but to a higher extent. In both cases, a prominent polar metabolite peak was observed. The d-TCO core contains a dioxolane ring (an acetal) fused to the eight-membered hydrocarbon framework. Literature suggests that acetals are labile in acidic conditions, where they hydrolyze to their corresponding aldehyde and diol. Potentially, the free aldehyde that liberates from the cyclooctene core corresponds to one of the polar metabolites observed. However, there are drugs approved by the FDA that contain acetals that are orally bioavailable and stable *in vivo*. Itraconazole, topiramate and doxofylline are some of the examples of marketed orally bioavailabe drugs containing cyclic acetals which are widely used for patient treatment.[326] Nevertheless, some strategies can be applied to stabilize acetals *in vivo*. For instance, acetals and ketals are stabilized through the introduction of proximal electron-withdrawing groups, basic amines or heteroaryl rings, or the careful implementation of steric and strain effects.[309] Unfortunately, the identification of the metabolites was not feasible during our studies. However, possible identification of acetal hydrolysis could help guide towards improved synthetic strategies to stabilize the acetal in the d-TCO ring. Interestingly, the metabolites study demonstrated a higher *in vivo* stability for **[^{18}F]MICA-214** than **[^{18}F]MICA-215** which is in contradiction to the *in vitro* plasma studies. This observation suggests that **[^{18}F]MICA-215** might have undergone extensive enzymatic degradation not apparent in the *in vitro* plasma studies. Consequently, extrapolating *in vitro* plasma study results to predict *in vivo* behavior of radiotracers may not be a generally applicable approach, a trend that is often seen in studies with radiotracer development. Conducting an *in vivo* stability investigation offers valuable insights to ensure the appropriate interpretation of behavior and its possible use in further studies.

Similar to previously reported studies with ^{18}F-labeled d-TCOs, biodistribution studies revealed a mixed renal and hepatobiliary clearance resulting in high abdominal activity.[88, 213] Although a faster renal clearance was observed for **[^{18}F]MICA-214** when compared to **[^{18}F]MICA-215**, higher radioactivity accumulation in intestines is observed at later time points for **[^{18}F]MICA-214**.

[^{18}F]MICA-214 contains a squaramide linker which increases the hydrophilicity of the radiotracer (log *D* = 0.62 ± 0.09) contributing to its faster renal clearance. Whereas **[^{18}F]MICA-215** with a short PEG linker showed a moderate log *D* of 1.25 ± 0.10 and a slower renal clearance as seen in the biodistribution studies. This indicates that the higher intestinal accumulation might be associated with linker-dependent metabolization and clearance from the liver. Moreover, substantial metabolization of both radiotracers was also observed *in vivo*. Thus, the higher accumulation of radioactivity can also be attributed to the accumulation of the radiometabolites in the gastrointestinal system. Overall, both tracers showed elevated radiotracer uptake in the gastrointestinal (GI) system. To address this, one potential solution could involve enhancing the renal clearance of the tracer by incorporating longer PEG chains (7-11 units).[323] PEG chains have previously been shown to increase the renal clearance of tetrazine-based radiotracer without affecting the plasma half-lives.[323] Similarly, the incorporation of hydrophilic amino acids such as glutamine and glutamic acid or carbohydrate moieties on the radiotracer has led to decreased liver uptake and increased renal clearance of fibroblast-activating protein inhibitors or prostate-specific membrane antigen ligands.[327, 328]

In addition to these approaches, employing more hydrophilic-TCO variants, like oxo-TCO, holds promise for reducing background interference due to their increased hydrophilicity. Notably, recent studies have demonstrated that the use of oxo-TCO resulted in a higher tumor-to-background ratio compared to d-TCO and s-TCO conjugated peptides.[242] However, it is crucial to acknowledge a challenge associated with oxo-TCO usage. The isomeric mixtures of oxo-TCO must be employed since the separation of the equatorial (major) and axial isomers (2.2:1 diastereomeric mixture) has proven to be difficult.[167] This issue may have implications in pretargeting studies, as the equatorial diastereomer exhibits slower kinetics, potentially affecting the overall effectiveness of the procedure.

Given the extensive metabolization and in general higher background of **[^{18}F]MICA-215**, only **[^{18}F]MICA-214** was further used in a pretargeted imaging study. *In vivo,* PET/CT pretargeted imaging data and *ex vivo* analysis showed a significantly higher tumor uptake of **[^{18}F]MICA-214** in mice pretreated with CC49-Tz compared to the control group, confirming the *in vivo* d-TCO-Tz ligation. Again, the main limitation remained the high abdominal uptake of the radiotracer as seen with previously developed d-TCO/TCO derivatives.[87, 88]

When compared to ^{18}F-labeled Tzs, **[^{18}F]MICA-214** showed only a low tumor-to-muscle (T/M) ratio of 1.8. With the recent advancements in tetrazine labeling, T/M ratios up to 20 have already been achieved for imaging with ^{18}F-labeled Tz (**^{18}[F]5**).[94] This ratio is significantly higher when compared to radiometal-based ^{111}In or ^{64}Cu-labeled tetrazine. Although the absolute tumor uptake was low (1.87± 0.31), tetrazine **^{18}[F]5** exhibited a good clearance profile leading to a lower background. Notably, **^{18}[F]5** contains a diacetic moiety which allowed for a rapid clearance of the radiotracer due to its high polarity (clog *D* = - 6.93). When comparing tumor-to-blood (T/B) ratios, **[^{18}F]MICA-214** showed a low ratio of 0.9, which is similar to the T/B ratio reported for ^{18}F-labeled Tzs.[93-95] This emphasizes the general need to improve the tumor-to-background ratios in pretargeted imaging studies. Although µPET imaging demonstrated the visualization of tumors following the IEDDA ligation, further optimization is needed to reduce the uptake of radiotracer in non-target tissues.

The pretargeted imaging studies conducted in this thesis were carried out using an LS174T colorectal carcinoma model overexpressing a tumor-associated glycoprotein-72 (TAG-72) antigen. The TAG-72 antigen was selected due to its limited shedding and internalization following the binding of the mAb CC49.[293, 329] One of the critical aspects of pretargeting is the non-internalization or at lower rate requirement of the antibody, as an internalized fraction of the mAb becomes less accessible to the subsequently injected radiotracer, resulting in reduced radiotracer uptake at the target site. However, most antibodies internalize through receptor-mediated endocytosis after binding to their cell surface receptors, albeit at varying rates.[311] The rate of internalization together with the clearance profile of mAb, in turn, dictates the interval between the mAb conjugate and radiotracer injections. A slowly internalizing mAb allows for a longer interval, which leads to better tumor-to-background ratios due to the clearance of the antibody from the circulation.

It is also worth noting that many of the known biomarkers of cancer exist within the intracellular compartment. Therefore, research efforts to enhance the cell permeability of the radiolabeled probes are needed to further expand the generalizability of the approach. So far, only a few studies have shown the pretargeting of internalizing antibodies.[82, 84] In the past, tetrazines have often been labeled with radiometals using chelation strategy, which hampers their cell permeability due to the polar nature and high molecular weights and the negative charge of the conjugated chelator molecule. The inversion of functionalities proposed in this thesis could overcome this issue, using the intrinsic hydrophobicity of the TCOs. To assess if the TCOs could efficiently pass the cell

membrane and react with intracellularly bound tetrazines, we designed a proof-of-concept cell fluorescence assay.

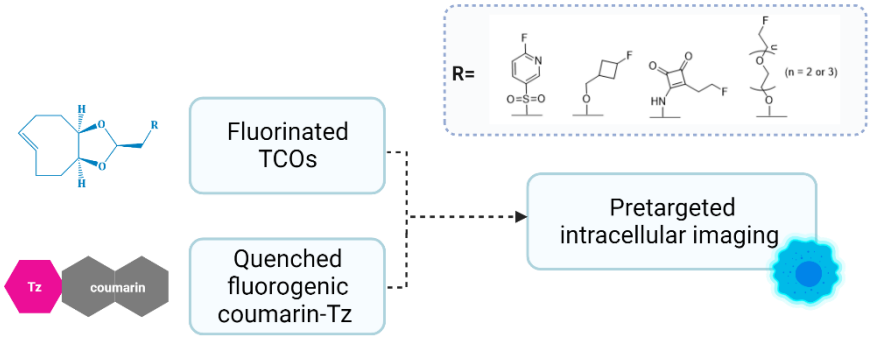

Figure 6.4 *Schematic representation of objectives described in Chapter 5*

A turn-on fluorescence assay was developed using Ibrutinib modified with a coumarin tetrazine probe, taking advantage of the covalent and selective binding of Ibrutinib. In this proof-of-concept study, the addition of **UAMC-3933** revealed a strong turn-on fluorescence of the coumarin in the cytoplasm, which colocalized with the BTK-mCherry signal. Notably, compound **UAMC-3933** is the most apolar compound from the series with a calculated log *D* value of 2.96. In contrast, compound **UAMC-4129** with the lowest log *D* value showed no fluorescence turn-on despite its fast kinetics and its promising extracellular click binding capability, as shown by the blocking assay in Chapter 4. Although further optimization of the assay is required for the quantification, the study already reveals the importance of achieving appropriate balance in probe lipophilicity when designing probes for intracellular imaging. A very polar compound may not pass the cell membrane as seen with **UAMC-4129** and thus not react with the intracellular target. Conversely, a more lipophilic compound shows higher non-specific uptake and is susceptible to extensive liver metabolization as seen with more lipophilic d-TCO radiotracers.

An ideal radiotracer for pretargeting should possess good reactivity, stability, and favorable pharmacokinetic properties. In this thesis two different radiotracers were evaluated in a pretargeting approach. **MICA-205** with relatively slower reaction kinetics toward tetrazine, showed higher stability with intact tracer persisting longer *in vivo*. Conversely, **MICA-214** demonstrated faster reaction kinetics but had a shorter half-life in serum. Based on the kinetic model proposed by Devaraj *et al.,* the *in vivo* labeling efficiency is strongly dependent on the reaction kinetics and the clearance profile of the radiotracer. The model predicted that for a reaction to reach completion *in vivo*, second-order rate constants of k_2 ~ 10^3-10^4 $M^{-1}s^{-1}$ combined with a prolonged circulation

time of several minutes (AUC ≥ 10^3 μM.s) are necessary.[300] Notably, both tracers reported in this thesis allowed the visualization of the tumor. We hypothesize that the availability of intact **MICA-205** (50% intact tracer at 1h) even at later time point in blood compensated for the comparatively slower kinetics of the TCO-Tz pair used. On the other hand, despite having faster reaction kinetics, the lower availability of intact **MICA-214** in blood (25% intact tracer at 5 min) even at earlier time points limited a higher accumulation at target site. Thus, enhancing the *in vivo* stability while maintaining a favorable clearance profile of d-TCO based radiotracer could further improve the *in vivo* ligation efficiency. Although the radiotracers described in the thesis did not show optimal target-to-background ratios, we have successfully confirmed the *in vivo* ligation.

Antibody pretargeting using bioorthogonal click reactions, in comparison to directly radiolabeled antibodies, remains a complex approach. Fine tuning the pharmacokinetics of the small molecule radiotracer for optimal image contrast while retaining a high reactivity towards the bioorthogonal tag and high accumulation at the tumor remains a goal to be pursued. Additionally, it also requires careful optimization of different parameters such as the functional density of the bioorthogonal tag on mAb, the dose of antibody conjugate, the radiotracer dose, antibody internalization, and the interval between the two injections.[330] Additionally, clearing agent or masking agents can be used to enhance the clearance or by quenching the tag on the circulating antibody conjugate to improve target to background ratio by decreasing the blood radioactivity levels. However, this increases the complexity of the overall process as the timing and dosage of the clearing agent can influence the number of targets available at the tumor site.[79, 330] A three-step process also makes it more difficult for clinical translation.

In an effort to optimize the tumor-to-non-target ratio, a two-step pretargeted theranostic approach based on bispecific antibodies has been reported. A bispecific antibody designed against ganglioside GD2 and DOTA was fused with a Self-Assembling and DisAssembling (SADA) domains for pretargeted radioimmunotherapy (SADA-PRIT) using ^{177}Lu to target GD2-positive solid tumors.[36] The fused SADA domains enabled the self-assembly of BsAbs into stable tetramers, but also disassembling into small monomers and dimers in circulation, allowing rapid renal clearance of unbound BsAbs before radiotracer administration.This resulted in a targeted delivery of radiation to the tumor while lowering the dose-limiting toxicity to nontarget organs compared to other two-step PRIT strategies. Given the self-disassembly of BsAb into its monomers and dimers with fast

clearance, the use of a clearing agent is not required, which is logistically preferred over a three-step PRIT. A Phase 1 clinical trial based on this platform is currently ongoing.[334, 335] Such platforms could offer a solution to issues associated with the long circulation half-life of antibodies. However, designing BsAbs for different tumor targets and obtaining their clinical approval remains a lengthy and complex process.

Moreover, successful clinical translation of bioorthogonal pretargeting necessitates careful consideration of diverse parameters. For instance, the random conjugation method for the production of mAb-Tz conjugate is a drawback for a clinical transfer. Clinical use requires knowledge of all modifications without batch variations. Site-specific conjugation can offer a solution to the problem. However, this often requires the modification of the mAb prior to conjugation of mAbs. Although this engineering approach might sound costly and time-consuming, it may be worth pursuing to accelerate the translation of this strategy to the clinic.

One of the main concerns regarding the translation of pretargeting into human applications is often the dilution factor. Human blood volume with body mass typically exceeding 50 kg and blood volume around 5 L far exceeds that of mice models (body mass < 30 g; blood volume ~ 1.5 mL) used in pre-clinical studies. This may lead to a decrease in the concentration of the bioorthogonal reaction components which may impair the reaction rate and efficiency. Recent work by Matiz *et al.* demonstrated the feasibility of pretargeted imaging in a large animal model (canine osteosarcoma) using a bisphosphonate-modified TCO and a radiolabeled tetrazine. This study implied that the increase in mass and volume from mice to large dogs (~ 50kg) caused no decrement in pretargeting. However, it is important to note that the study employed a TCO-modified bisphosphonate rather than a monoclonal antibody, which makes the direct extrapolation of these findings toward humans less precise. Furthermore, the pretargeting interval in this study was only 1 h which is significantly shorter than 24-120 h, typically used in pretargeting with mAbs. Nevertheless, bioorthogonal pretargeting is a rapidly advancing field, and a phase I clinical trial using hu5B-TCO in combination with [^{64}Cu]Cu-Tz-SarAr for imaging of pancreatic cancer has been recently approved.[86]

Recently immuno-PET approaches with smaller antibody fragments such as nanobodies have also been reported to reduce radiation exposure in patients. In contrast to large monoclonal antibodies

(150 kDa), antibody fragments are small (12-15 kDa) and are characterized by their fast clearance from circulation. This enables imaging shortly after radiotracer injection, yielding high-tumor-to-background ratios. Importantly, the short half-life of nanobodies also allows the use of short-lived radioisotopes. While the smaller size of antibody allows for a deeper penetration into solid tumor tissues, it also leads to rapid clearance leading to lower accumulation at the target site.[331] Moreover, these smaller fragments are more susceptible to impaired immunoreactivity when randomly conjugated. Although not always required, a site-specific conjugation approach is often pursued for the modification of these nanobodies. While site-specific conjugates decrease the regulatory hurdles for future clinical translation, they also present numerous challenges during production. Moreover, the high renal uptake of radiolabeled antibody fragments also poses a major limitation for clinical translation with kidneys and bladder identified as dose-limiting organs due to renal reabsorption and retention of nanobodies.[332] Additionally, the development of nanobodies is a recent approach and there are only a few clinically approved nanobodies.[333]

In contrast, many antibodies are readily available and are used in clinical routine as therapy, rendering the transition to clinical use more feasible. Furthermore, the application of pretargeting with mAbs extends beyond diagnostic imaging tools. The modularity of the system allows it to be used as a companion diagnostic or theragnostic tool. Pretargeted radioimmunotherapy using the conventional TCO-modified mAb and radiolabeled tetrazine with therapeutic radioisotopes is a promising strategy for delivering a therapeutic radiation dosage to solid tumors while sparing normal tissues. An initial study by Rossin *et al.* in 2013 used pretargeting to deliver [^{177}Lu]Lu-DOTA-PEG_{11}-Tz in LS174T-tumor-bearing mice pretreated with CC49-TCO. Dosimetry calculations suggested that the pretargeting system could allow for an 8-fold higher tumor dose in mice when compared to directly labeled antibodies.[79] Subsequently, multiple research groups have applied the strategy to achieve therapeutic radiation delivery while minimizing toxicity.[257-259, 261] More recently, Timperanza *et al.* reported the synthesis and characterization of ^{211}At and ^{125}I-labeled tetrazines conjugated to polylysines as a theragnostic pair for disseminated cancer imaging and alpha therapy.[262] This development opens up new prospects for pretargeted therapy involving radioisotopes with shorter half-lives (^{211}At; $t_{1/2}$ =7.2 hours vs ^{225}Ac; $t_{1/2}$ = 9.92 days). The versatility and modularity of bioorthogonal pretargeting through IEDDA makes it an important and relevant tool to consider adding to the clinical toolbox.

To conclude, in this thesis, we explored the synthetic development and evaluation of TCO and d-TCO based probes as radiotracers for pretargeted imaging *in vivo*. The ideal radiotracer for pretargeted imaging requires good balance of reactivity and stability. Moreover, the small molecule radiotracer should also possess favorable pharmacokinetics such as fast distribution and renal clearance to improve image contrast at early time points. Further fine tuning of the pharmacokinetics of these compounds are necessary to push the transition of these compounds from pre-clinical to clinical setting.

Summary of findings:

- TCO and d-TCO-based fluorinated radiotracers were developed and evaluated *in vivo* for pretargeted imaging based on IEDDA;
- Linker replacement from fluoroethyl group on [^{18}F]FTCO to Al[^{18}F]NOTA improved the stability of TCO radiotracer MICA-205;
- All d-TCO derivatives showed high reactivity towards tetrazines;
- The developed pretargeted blocking assay allowed sucessfully for a pre-selection of compounds for *in vivo* ligation;
- Fluorinated d-TCO derivatives UAMC-4129 and UAMC-3711 with the lowest log D values from the series showed the highest blocking efficiency of 95% and 93% respectively in the blocking assay;
- [^{18}F]MICA-214 and [^{18}F]MICA-215 were radiolabeled in good RCY and RCP and both tracers showed excellent PBS stability;
- In plasma, [^{18}F]MICA-215 (94 ± 2.4%) showed excellent stability in comaprison to [^{18}F]MICA-214 (42± 2.9%). However *in vivo* [^{18}F]MICA-215 (7.9 ± 2.3% at 5 min) underwent extensive metabolisation compared to [^{18}F]MICA-214 (24.6 ± 2.4% at 5 min);
- Biodistribution of both tracers showed abdominal uptake, however [^{18}F]MICA-214 showed in general lower non-specific uptake in other organs compared to [^{18}F]MICA-215;
- [^{18}F]MICA-205 and [^{18}F]MICA-214 showed clear delineation of the tumor in mice pre-treated with CC49-tz confirming *in vivo* ligation;
- Despite successful *in vivo* ligation was observed, further radiotracer optimisation is required to improve tumor uptake as well as tumor-to-background ratios;
- Cell-fluorescence assay demonstrated a higher turn-on effect implying a better cell permeability and subsequent intracelluar ligation with Tz for the most lipophilic d-TCO derivative from the series;

6.2 Future Perspectives

One of the main limitations observed in the pretargeted studies in this thesis was the high abdominal background related to tracers clearance pathway and metabolization. Thus, modification to compounds with functional groups to increase renal clearance is required in future studies. Pegylation with longer units up to 11 units has been shown to increase renal clearance without impacting the plasma half-life of tetrazine-based radiotracers.[322] Furthermore, introducing amino acids, diacetic acid to introduce a overall net charge on the moleules or the incorporation of carbohydrate moieties can increase renal clearance of the d-TCO based radiotracers.[80, 93, 95, 327, 328] A systematic study with a larger library of TCOs incorporating such moieties should be the next step.

Recently, geminal-substituted axial 5-hydroxy-trans-cyclooctene (a-TCO) analogs has been reported by Pigga *et al.* An a-TCO derivative was shown to be more reactive than 5-hydroxy-trans-cyclooctene as well as oxo-TCO and exhibited a remarkable rate constant of 150,000 ± 8,000 $M^{-1}s^{-1}$, approaching the kinetics observed for d-TCOs. Through a diastereoselective synthesis, a-TCO can be synthesized in 3-steps, providing only the axial diastereomer and simplifying the TCO-synthesis procedure. Additionally, a-TCO showed similar stability to 5-hydroxy-trans-cyclooctene while demonstrating increased hydrophilicity. Given the easier synthetic preparation and increased hydrophilicity of the compound with potential impact on pharmacokinetics, a-TCO holds the potential to be studied as PET probes.

Nonetheless, improving the renal clearance of the radioligands is not the only factor, a right balance between stability and reactivity, is required for a successful pretargeting approach. Implementation of structural design based on the identification of the metabolization pathway and strategies to circumvent it could also guide the development of TCOs as PET probes in the future.

Additionally, studying internalizing targets is also one of the challenging topics where further research is required. With additional optimization, the cell permeability assay could serve as a pre-screening method for selecting cell-permeable TCOs to study internalizing targets. In the future, we envision translating the assay with internalizing antibodies to investigate the internalization of mAbs and to visualize the intracellular click reaction with the tetrazine tag bound to mAb. This could be further translated *in vivo* in mice models with internalizing targets. Additionally, studying the

mAb internalization can also provide insight in drug development to asses the internalization kinetics of antibody-drug conjugates required for an effective therapeutic effect.

In addition to its application in imaging, pretargeting based on IEDDA holds substantial potential in enhancing radioimmunotherapy. While conventional radioimmunotherapy has shown effectiveness towards non-solid tumors, solid tumors require significantly higher radiation doses to achieve a therapeutic response. This elevated radiation requirement can potentially result in higher off-target toxicity in bone marrow. As the radioactivity is separated from the antibody, pretargeting enables the administration of larger radiation doses while lowering the hematologic toxicities. Previous studies have shown that although the overall effective radiation dose may not be significantly reduced, the dosimetry received by the bone marrow can be halved in comparison to conventional approach.[258] Furthermore, PRIT studies using a theranostic pair of ^{64}Cu/^{67}Cu-labeled Tz showed a notable correlation between the tumoral uptake of ^{64}Cu-labeled-Tz in tumors and therapeutic efficacy in treating colorectal carcinoma with ^{67}Cu. Additionally, when^{67}Cu-labeled-Tz was administered in higher doses in a fractionated manner, a reduced hematological toxicity was observed while maintaining its therapeutic effectiveness.[83] Moreover, with the increasing interest in the use of short-lived therapeutic radioisotope sush as Astatine-211 ($t_{1/2}$ = 7.2 h) the PRIT approach can also offer the dosimetric advantages in therapy as observed with pretargeted imaging.

Pretargeting based on the trans-cyclooctene (TCO) and tetrazine (Tz) ligation is a versatile and promising approach with diverse potential applications *in vivo*. As research advances, in the domains of imaging, radioimmunotherapy, and click-to-release drug delivery based on pretargeting, this technique is still in its infancy and holds significant promise for future development.

Summary

Summary

Immuno-Positron emission tomography (PET) imaging using radiolabeled monoclonal antibodies (mAb) represents a powerful tool in *in vivo* research, with increasing applications in theranostic settings in clinic. The molecular precision of antigen-mAb interaction turns radiolabeled mAbs into highly specific radiotracers with a remarkable affinity. However, the high molecular weight and the long circulation times of mAbs are associated with unsatisfactory target to background ratios, necessitating the use of long-lived radionuclides, which in turn, yields high radiation burden to the patient.

To address this challenge, a pretargeting strategy based on biorthogonal chemistry was proposed. The bioorthogonal inverse electron demands Diels-Alder (IEDDA) reaction between 1,2,4,5-tetrazines and trans-cyclooctene (TCO) exhibits ultra-fast reaction kinetics (>10^6 M^{-1} s^{-1}) enabling *in-vivo* target radiolabeling. In a pretargeting approach based on IEDDA, the mAb with a biorthogonal tag is injected first, to allow its clearance from the non-target tissues. Subsequently, a radiolabeled reaction partner is injected which will covalently bind with the tag conjugated to mAb *in vivo*. This allows the use of short-lived radio isotopes such as Fluorine-18, consequently reducing patient radiation exposure while allowing *in vivo* imaging of the target with superior image contrast. Fluorine-18 is an ideal radioisotope for pretargeted PET-imaging due to its high positron branching ratio, low positron energy and short β-trajectory resulting in high spatial resolution. Moreover Fluorine-18 is readily accessible and can be distributed to other facilities, increasing the feasibility for clinical translation.

Significant research has already explored the pretargeting approach with a TCO-mAb construct and a radiolabeled tetrazine. However, TCO is prone to isomerization to its less reactive *cis* form under physiological conditions. Additionally, the lipophilicity of TCO leads to hydrophobic burying of the TCO tag within the protein core leaving only a few reactive tags available for the reaction with tetrazine. To circumvent this, we aimed to reverse the roles of the bioorthogonal reaction pair, using a stable tetrazine as a biorthogonal tag and a radiolabeled TCO probe. This avoids the extended circulation time of TCO *in vivo* and reduced stability due to isomerisation. Additionally, this approach also allows us to explore new faster reacting cis-dioxolane fused TCOs.

In this doctoral dissertation we described the development of TCO and d-TCO derivatives to assess their potential as radiolabeled reaction partners for bioorthogonal *in vivo* pretargeted imaging, ultimately striving to improve the *in vivo* ligation efficiency.

Previously, our group investigated the potential of ^{18}F-labeled TCO through a fluoroethyl group-^{18}[F]FTCO, as a radiotracer for pretargeting. However, ^{18}[F]FTCO showed poor *in vivo* stability with extensive metabolization. To increase the *in vivo* stability of the previously known ^{18}[F]FTCO probe, in **Chapter 3** we modified the linker, incorporating a 1,4,7-triazacyclononane-1,4,7-triacetic acid (NOTA)-chelator, which also served as a radiolabeling moiety. The chelation of ^{18}F-aluminium fluoride (Al^{18}F) by NOTA facilitated a straightforward radiolabeling of the TCO. When compared to ^{18}[F]FTCO, Al[^{18}F]NOTA-TCO showed improved *in vivo* stability with 50% of intact tracer remaining at a 1h time point. The biodistribution in healthy mice demonstrated hepatobiliary and renal clearance, with a rapid blood clearance and relatively low background in other tissues. The low bone uptake indicated no defluorination of the tracer. Furthermore, *in vivo,* pretargeted immuno-PET imaging of mice bearing LS174T colorectal tumor xenografts pretreated with a tetrazine-modified anti-TAG-72 monoclonal antibody (CC49) showed a significantly higher tumor uptake (0.67 ± 0.16 %ID/g) compared to the control group (0.16 ± 0.08 %ID/g).

Encouraged by this finding, we further explored the potential of faster-reacting d-TCO as PET probe for pretargeted imaging in **Chapter 4**. A small library of fluorinated (^{19}F) d-TCOs with diverse linkers was synthesized to investigate their impact on the reactivity, pharmacokinetics and the feasibility for radiolabeling. These d-TCOs were was assessed for their *in vivo* ligation efficiency in an *in vivo* pretargeted blocking assay in mice bearing human colorectal cancer (LS174T) xenografts. The developed blocking assay facilitated the pre-selection of d-TCO derivatives with highest *in vivo* performance, eliminating the need to radiolabel each compound individually. Two d-TCO derivatives UAMC-3711 and UAMC-4129 showed excellent blocking efficiencies of 93% and 95% respectively, against TCO-Cy5 in a pretargeted blocking study, confirming good *in vivo* ligation with the Tz-conjugated antibody (CC49-Tz). These two d-TCO compounds were selected for radiolabelling with ^{18}F and assessed *in vitro* and *in vivo* for stability and pharmacokinetics. The *ex vivo* biodistribution of [^{18}F]MICA-214 and [^{18}F]MICA-215 showed mixed hepatobiliary and renal clearance of the radiotracer. The fraction of the radiotracer clearing through the liver led to radioactivity accumulation in the small intestines at later time points. Importantly, both tracers

showed an absence of *in vivo* defluorination, with no significant increase in bone uptake. Overall, [^{18}F]MICA-214 exhibited lower radioactivity accumulation in non-target organs at 1h time point when compared to [^{18}F]MICA-215.

In vivo, both radiotracers showed extensive and rapid metabolization, with only 24% (n=3) of tracer remaining intact at 5 min for [^{18}F]MICA-214 and 8% for [^{18}F]MICA-215. Given its superior stability and favorable pharmacokinetics, [^{18}F]MICA-214 was selected for further *in vivo* pretargeted PET imaging. The µPET images demonstrated a clear delineation of the tumor with significantly higher tumor uptake of (2.16 ± 0.08% ID/g) in group pretreated with CC49-Tz. In contrast, in the control group, the activity remained lower (1.34 ± 0.07 %ID/g; $p < 0.0001$). Although higher tumor uptake values were achieved, the tumor-to-background ratio needs further improvement for better image contrast.

One of the challenge in pretargeting is the internalization of antibodies upon binding to cell surface targets. This leads to a reduced number of reactive tags available for the injected radiotracer resulting in lower radiotracer uptake at target site. Importantly, many known cancer biomarkers exist within the intracellular compartment. Therefore, to address this issue, we explored the intrinsic hydrophobicity of the d-TCO derivatives to investigate their capability to cross the cell membrane and react with tetrazines. To test the hypothesis that the d-TCOs derivatives were able to cross the cell membrane, a cell assay based on the turn-on-fluorescence property of turn-on coumarin tetrazine probe was developed (**Chapter 5**). For this a quenched fluorogenic coumarin probe with an excellent turn-on effect was developed which was further conjugated with Ibrutinib, a Bruton's tyrosine kinase (BTK) inhibitor. Ibrutinib binds to intracellular BTK and thus allows for targeted intracellular imaging with the developed probe. This conjugate was employed in a cell fluorescence assay to test the ability of d-TCO compounds to pass the cell membrane and react with the tetrazine bound to BTK. Among the compounds tested, UAMC-3933 showed the best cell permeability with pronounced turn-on fluorescence observed. However, no fluorescence turn-on was observed for compound UAMC-4129 despite its fast reaction kinetics. Although further optimization of the assay and probes is necessary for the development of a robust method, this proof-of-concept assay highlighted the need for careful balance in lipophilicity when designing probes for intracellular imaging.

To conclude, this dissertation involved the synthesis, characterization, and evaluation of TCO and d-TCO derivatives as radiotracers for pretargeted imaging. Additionally, we also evaluated the potential of d-TCO radiotracers to cross the cell membrane and react with an intracellularly located tetrazine with an overarching aim to study the internalizing targets in the future.

Samenvatting

Immuno-Positron Emissie Tomografie (Immuno-PET) beeldvorming van geradiolabelde monoklonale antilichamen (mAb) is een krachtig *in vivo* onderzoekstechniek, met toepassingen in diagnostische, prognostische en therapeutische onderzoek domeinen. De moleculaire precisie van de antigen-antilichaam interactie verandert geradiolabelde mAbs in zeer specifieke radiotracers met opmerkelijke affiniteit. Ondanks deze aantrekkelijke eigenschappen gaat hun hoge moleculaire massa gepaard met lange circulatietijden, trage klaring en lage doelwit tot achtergrond ratio. Om een goede balans tussen de half-levens van biovector en radio isotoop te verzekeren is het gebruik van langlevende radionucliden noodzakelijk -met gevolg een hoge stralingsbelasting voor de patiënt.

Pretargeting met behulp van bioorthogonale chemie kwam als oplossing naar voor om deze probleemstelling aan te pakken. De bioorthogonale inverse-electron demand Diels-Alder (IEDDA)-reactie tussen 1,2,4,5-tetrazines en trans-cyclooctenen (TCO's) vertoont ultrasnelle reactiekinetiek ($>10^6$ M^{-1} s^{-1}) wat mogelijkheden biedt tot het *in vivo* merken van radioactiviteit aan de gewenste doelwitten. In een pretargeting strategie gebaseerd op IEDDA wordt in een eerste fase een bioorthogonaal gelabeld mAb toegediend waarna een wachttijd plaatsvindt om niet-target gebonden antilichaam uit de bloedbaan te klaren. Vervolgens wordt een radioactief snel klarende reactiepartner geïnjecteerd die covalent zal binden met het bioorthogonaal label dat *in vivo* aan het mAb is geconjugeerd. Deze twee-staps strategie maakt het gebruik van kortlevende radio-isotopen mogelijk, resulterend in een vermindering van de stralingsblootstelling en verhoogd *in vivo* beeldcontrast. Het radio-isotoop Fluor-18 is een voorloper in PET-beeldvorming door middel van zijn kort half-leven met voornamelijk β^+-verval met lage positron energie, eigenschappen die belangrijk zijn voor het bekomen van optimale resolutie van de beelden. Bovendien kan Fluor-18 ook gemakkelijk geproduceerd worden door middel van laag energetische cyclotrons die wereldwijd beschikbaar zijn, een factor die belangrijk is voor de haalbaarheid van een translatie van deze tools naar de kliniek.

Pretargeting en het potentieel met TCO-antilichaam bio-conjugaties en radioactief gemerkte tetrazines is reeds uitvoerig bestudeerd. TCO is echter gevoelig voor isomerisatie naar zijn minder

reactieve cis-isomeer onder fysiologische omstandigheden, waardoor lange circulatie tijden in het lichaam suboptimaal zijn. Bovendien leidt de hoge vetoplosbaarheid van TCOs tot hydrofobe maskering van het TCO-label binnenin het antilichaam, waarbij slechts enkele reactieve TCO labels beschikbaar blijven voor de click reactie met tetrazine. Om deze probleemstellingen aan te kaarten, hebben we gebruik gemaakt van een stabiel tetrazine gekoppeld aan het antilichaam als bioorthogonaal label en een radioactief gemerkt TCO. Bovendien stelt deze benadering ons ook in staat om nieuwe snel reagerende cis-dioxolaan-gefuseerde TCOs te onderzoeken.

In dit doctoraatsproefschrift hebben we de ontwikkeling van TCO- en d-TCO-derivaten beschreven om hun potentieel als radiogelabelde reactiepartners voor bioorthogonale *in vivo* pretargeted beeldvorming te beoordelen, met als uiteindelijk doel de efficiëntie van de *in vivo* click reactie te verbeteren.

Eerder heeft onze groep het potentieel van ^{18}F-gelabelde TCOs onderzocht welke gelabeld werden via een fluorethylgroep, ^{18}[F]FTCO, als een radiotracer voor pretargeting. ^{18}[F]FTCO vertoonde een slechte stabiliteit *in vivo* met uitgebreide metabolisatie. In **Hoofdstuk 3** hebben we de fluoroethyl groep vervangen met een (NOTA)-chelator om de *in vivo* stabiliteit te verbeteren van dit ^{18}[F]FTCO. In vergelijking met ^{18}[F]FTCO vertoonde Al[^{18}F]NOTA-TCO een verbeterde *in vivo* stabiliteit, met >50% van de radiotracer intact na 1 uur. De biodistributie in gezonde muizen toonde een gemengde hepatobiliaire en renale klaring, met een snelle bloedklaring en een laag achtergrond signaal in andere weefsels. De lage bot opname van de radiotracer wijst op de afwezigheid van defluorinatie van de radiotracer, een extra indicatie voor de verhoogde stabiliteit. Validatie van pretargeted immuno-PET gebruikmakend van deze radiotracer toonde een specifieke opname van 0,67 ± 0,16 %ID/g in vergelijking met de controlegroep (0,16 ± 0,08 %ID/g).

Aangemoedigd door deze bevindingen, hebben we in **Hoofdstuk 4**, het potentieel van sneller reagerende d-TCO's onderzocht als PET-radiotracer voor pretargeted beeldvorming. Een kleine bibliotheek(^{19}F)d-TCO's met diverse koppelingen werd gesynthetiseerd om hun impact op de reactiviteit, farmacokinetiek en de haalbaarheid voor radioactieve merking van deze moleculen te onderzoeken. Deze d-TCO's werden beoordeeld op hun *in vivo* reactie efficiëntie via een *in vivo* pretargeted blocking experiment bij muizen met tumor (LS174T). De ontwikkelde blocking-assay vergemakkelijkte de voorselectie van d-TCO-derivaten met de beste *in vivo* prestaties voor de

ontwikkeling van radioactieve tracers. Twee d-TCO-derivaten, UAMC-3711 en UAMC-4129, vertoonden een uitstekende blocking-efficiëntie van respectievelijk 93% en 95% ten opzichte van de positieve controle TCO-Cy5. Deze twee d-TCO-verbindingen werden geselecteerd voor radioactieve merking met ^{18}F en werden beoordeeld op hun *in vitro* en *in vivo* stabiliteit en farmacokinetiek. De *ex vivo* biodistributie studie met [^{18}F]MICA-214 en [^{18}F]MICA-215 toonde een gemengde hepatobiliaire en renale klaring van beide radiotracers. De hepatobiliaire klaring, leidde ook tot verhoogde radiotracer opname in de dunne darm op latere tijdstippen door middel van de enterohepatische cyclus. Beide tracers toonden ook afwezigheid van *in vivo* defluorinatie, zonder significante verhoging in botopname. Het aspecifiek achtergrond signaal was minder uitgesproken voor [^{18}F]MICA-214 in vergelijking met [^{18}F]MICA-215.Hiernaast, vertoonden beide radiotracers een uitgebreide en snelle metabolisatie *in vivo*, waarbij slechts 24% van de radiotracer intact bleef na 5 minuten voor [^{18}F]MICA-214 en 8% voor [^{18}F]MICA-215. Gezien de hogere stabiliteit en gunstigere farmacokinetiek werd [^{18}F]MICA-214 geselecteerd voor verdere *in vivo* pretargeted PET-beeldvorming. In µPET-beelden werd de tumor duidelijk gevisualiseerd met een significante hogere opname van de radiotracer in de tumor (2,16 ± 0,08% ID/g) ten opzichte van de controlegroep (1,34 ± 0,07 %ID/g; $p < 0,0001$). Verdere uitdagingen in dit project kunnen de optimalisatie van tumor-achtergrond signaal betreffen.

De grootste uitdaging in de pretargeting strategie is de internalisatie van antilichamen na hun binding aan specifieke doelwitten op het celmembraan. Dit kan aanleiding geven tot een verminderd aantal beschikbare bioorthogonale labels voor de radiotracer om covalent aan te binden en vervolgens een lagere tumoropname. De ontwikkeling van een tool in kanker diagnose die mogelijkheden biedt om de verschillende biomarkers die ook intracellulair aanwezig zijn in beeld te brengen is van uiterst belang in de strijd tegen de ziekte. De d-TCO derivaten bibliotheek ontwikkeld in ons labo maakt gebruik van het instrinsiek hydrofoob karakter van d-TCOs dat het vermogen biedt om het celmembraan te doorkruisen. In deze setting kunnen we de mogelijkheid bieden om ook geïnternaliseerde antilichamen in beeld te brengen zonder verlies aan signaal. Om de hypothese te testen of de d-TCO-derivaten in staat zijn om het celmembraan over te steken, werd een cel assay ontwikkeld op basis van de turn-on-fluorescentie-eigenschap van de turn-on coumarinetetrazine derivaten (**Hoofdstuk 5**). Hiervoor werd een fluorescentie gedempte coumarine-tetrazine probe met een uitstekend turn-on-effect ontwikkeld en verder geconjugeerd met Ibrutinib, een intracellulaire Bruton-tyrosinekinase (BTK) inhibitor. Deze conjugaten werden

dan gebruikt in een cel-fluorescentie-experiment om het vermogen van d-TCO-verbindingen met tetrazines in intracellulaire omgeving te evalueren. UAMC-3933 toonde de beste cel permeabiliteit met hoge turn-on-fluorescentie onder de geteste verbindingen. Voor molecule UAMC-4129 werd er geen turn-on-fluorescentie waargenomen, ondanks zijn snelle reactiekinetiek. Hoewel verdere optimalisatie van het experiment en de probes nodig zijn voor de ontwikkeling van een robustere methode, benadrukte dit proof-of-concept experiment de noodzaak van een zorgvuldige balans in lipofiliciteit bij het ontwerpen van probes voor intracellulaire beeldvorming.

In conclusie, dit proefschrift omvat de synthese, karakterisering en evaluatie van TCO- en d-TCO-derivaten als radiotracers voor pretargeted beeldvorming. Vervolgens hebben we ook het potentieel van d-TCO-radiotracers onderzocht om het celmembraan te penetreren en covalent te binden met intracellulaire tetrazines, met als ultiem doel internaliserende doelwitten te bestuderen.

REFERENCES

References

1. Mankoff, D. A. A definition of molecular imaging. *J Nucl Med* **2007**, *48* (6), 18N, 21N.

2. Pysz, M. A.; Gambhir, S. S.; Willmann, J. K. Molecular imaging: current status and emerging strategies. *Clin Radiol* **2010**, *65* (7), 500-516.

3. Berger, A. How does it work? Positron emission tomography. *BMJ* **2003**, *326* (7404), 1449.

4. Shukla, A. K.; Kumar, U. Positron emission tomography: An overview. *J Med Phys* **2006**, *31* (1), 13-21.

5. *PET-schema*. https://commons.wikimedia.org/wiki/File:PET-schema.png?uselang=en#Licensing (accessed 1/06/2023).

6. Rohren, E. M.; Turkington, T. G.; Coleman, R. E. Clinical applications of PET in oncology. *Radiology* **2004**, *231* (2), 305-332.

7. Otsuka, H.; Graham, M.; Kubo, A.; Nishitani, H. Clinical utility of FDG PET. *J Med Invest* **2004**, *51* (1-2), 14-19.

8. Chen, K.; Chen, X. Positron emission tomography imaging of cancer biology: current status and future prospects. *Semin Oncol* **2011**, *38* (1), 70-86.

9. Scott, A. M.; Wolchok, J. D.; Old, L. J. Antibody therapy of cancer. *Nature Reviews Cancer* **2012**, *12* (4), 278-287.

10. Wei, W.; Rosenkrans, Z. T.; Liu, J.; Huang, G.; Luo, Q. Y.; Cai, W. ImmunoPET: Concept, Design, and Applications. *Chem Rev* **2020**, *120* (8), 3787-3851.

11. Dewulf, J.; Adhikari, K.; Vangestel, C.; Wyngaert, T. V. D.; Elvas, F. Development of Antibody Immuno-PET/SPECT Radiopharmaceuticals for Imaging of Oncological Disorders-An Update. *Cancers (Basel)* **2020**, *12* (7).

12. Carmon, K. S.; Azhdarinia, A. Application of Immuno-PET in Antibody-Drug Conjugate Development. *Mol Imaging* **2018**, *17*, 1536012118801223.

13. Gebhart, G.; Lamberts, L. E.; Wimana, Z.; Garcia, C.; Emonts, P.; Ameye, L.; Stroobants, S.; Huizing, M.; Aftimos, P.; Tol, J.; et al. Molecular imaging as a tool to investigate heterogeneity of advanced HER2-positive breast cancer and to predict patient outcome under trastuzumab emtansine (T-DM1): the ZEPHIR trial. *Ann Oncol* **2016**, *27* (4), 619-624.

14. Bensch, F.; Brouwers, A. H.; Lub-de Hooge, M. N.; de Jong, J. R.; van der Vegt, B.; Sleijfer, S.; de Vries, E. G. E.; Schröder, C. P. ^{89}Zr-trastuzumab PET supports clinical decision making in breast cancer patients, when HER2 status cannot be determined by standard work up. *Eur J Nucl Med Mol Imaging* **2018**, *45* (13), 2300-2306.

15. Bensch, F.; van der Veen, E. L.; Lub-de Hooge, M. N.; Jorritsma-Smit, A.; Boellaard, R.; Kok, I. C.; Oosting, S. F.; Schroder, C. P.; Hiltermann, T. J. N.; van der Wekken, A. J.; et al. (89)Zr-atezolizumab

imaging as a non-invasive approach to assess clinical response to PD-L1 blockade in cancer. *Nat Med* **2018**, *24* (12), 1852-1858.

16. Ulaner, G. A.; Carrasquillo, J. A.; Riedl, C. C.; Yeh, R.; Hatzoglou, V.; Ross, D. S.; Jhaveri, K.; Chandarlapaty, S.; Hyman, D. M.; Zeglis, B. M.; et al. Identification of HER2-Positive Metastases in Patients with HER2-Negative Primary Breast Cancer by Using HER2-targeted (89)Zr-Pertuzumab PET/CT. *Radiology* **2020**, *296* (2), 370-378.

17. Rizzieri, D. Zevalin(®) (ibritumomab tiuxetan): After more than a decade of treatment experience, what have we learned? *Crit Rev Oncol Hematol* **2016**, *105*, 5-17.

18. Parakh, S.; Lee, S. T.; Gan, H. K.; Scott, A. M. Radiolabeled Antibodies for Cancer Imaging and Therapy. *Cancers (Basel)* **2022**, *14* (6).

19. Rondon, A.; Rouanet, J.; Degoul, F. Radioimmunotherapy in Oncology: Overview of the Last Decade Clinical Trials. *Cancers (Basel)* **2021**, *13* (21).

20. Suzuki, T.; Ishii-Watabe, A.; Tada, M.; Kobayashi, T.; Kanayasu-Toyoda, T.; Kawanishi, T.; Yamaguchi, T. Importance of neonatal FcR in regulating the serum half-life of therapeutic proteins containing the Fc domain of human IgG1: a comparative study of the affinity of monoclonal antibodies and Fc-fusion proteins to human neonatal FcR. *J Immunol* **2010**, *184* (4), 1968-1976.

21. Seijsing, J.; Yu, S.; Frejd, F. Y.; Höiden-Guthenberg, I.; Gräslund, T. In vivo depletion of serum IgG by an affibody molecule binding the neonatal Fc receptor. *Sci Rep* **2018**, *8* (1), 5141.

22. Conti, M.; Eriksson, L. Physics of pure and non-pure positron emitters for PET: a review and a discussion. *EJNMMI Phys* **2016**, *3* (1), 8.

23. Protection, I. C. o. R. *The 2007 Recommendations of the International Commission on Radiological Protection. User's Edition*; Elsevier, 2007.

24. Quinn, B.; Dauer, Z.; Pandit-Taskar, N.; Schoder, H.; Dauer, L. T. Radiation dosimetry of 18F-FDG PET/CT: incorporating exam-specific parameters in dose estimates. *BMC Med Imaging* **2016**, *16* (1), 41.

25. Goodwin, D. A. Tumor pretargeting: almost the bottom line. *J Nucl Med* **1995**, *36* (5), 876-879.

26. Goodwin, D.; Meares, C.; Diamanti, C.; McCall, M.; Lai, C.; Torti, F.; McTigue, M.; Martin, B. Use of specific antibody for rapid clearance of circulating blood background from radiolabeled tumor imaging proteins. *Eur J Nucl Med* **1984**, *9* (5), 209-215.

27. Altai, M.; Membreno, R.; Cook, B.; Tolmachev, V.; Zeglis, B. M. Pretargeted Imaging and Therapy. *J Nucl Med* **2017**, *58* (10), 1553-1559.

28. Hnatowich, D. J.; Virzi, F.; Rusckowski, M. Investigations of avidin and biotin for imaging applications. *J Nucl Med* **1987**, *28* (8), 1294-1302.

29. Paganelli, G.; Grana, C.; Chinol, M.; Cremonesi, M.; De Cicco, C.; De Braud, F.; Robertson, C.; Zurrida, S.; Casadio, C.; Zoboli, S. Antibody-guided three-step therapy for high grade glioma with yttrium-90 biotin. *Eur J Nucl Med* **1999**, *26*, 348-357.

30. Weiden, P. L.; Breitz, H. B. Pretargeted radioimmunotherapy (PRIT) for treatment of non-Hodgkin's lymphoma (NHL). *Crit Rev Oncol Hematol* **2001**, *40* (1), 37-51.

31. Breitz, H. B.; Weiden, P. L.; Beaumier, P. L.; Axworthy, D. B.; Seiler, C.; Su, F.-M.; Graves, S.; Bryan, K.; Reno, J. M. Clinical optimization of pretargeted radioimmunotherapy with antibody-streptavidin conjugate and 90Y-DOTA-biotin. *J Nucl Med* **2000**, *41* (1), 131-140.

32. Shen, S.; Forero, A.; LoBuglio, A. F.; Breitz, H.; Khazaeli, M. B.; Fisher, D. R.; Wang, W.; Meredith, R. F. Patient-specific dosimetry of pretargeted radioimmunotherapy using CC49 fusion protein in patients with gastrointestinal malignancies. *J Nucl Med* **2005**, *46* (4), 642-651.

33. Barbet, J.; Peltier, P.; Bardet, S.; Vuillez, J. P.; Bachelot, I.; Denet, S.; Olivier, P.; Leccia, F.; Corcuff, B.; Huglo, D.; et al. Radioimmunodetection of medullary thyroid carcinoma using indium-111 bivalent hapten and anti-CEA x anti-DTPA-indium bispecific antibody. *J Nucl Med* **1998**, *39* (7), 1172-1178.

34. Rousseau, C.; Goldenberg, D. M.; Colombié, M.; Sébille, J. C.; Meingan, P.; Ferrer, L.; Baumgartner, P.; Cerato, E.; Masson, D.; Campone, M.; et al. Initial Clinical Results of a Novel Immuno-PET Theranostic Probe in Human Epidermal Growth Factor Receptor 2-Negative Breast Cancer. *J Nucl Med* **2020**, *61* (8), 1205-1211.

35. Kraeber-Bodere, F.; Rousseau, C.; Bodet-Milin, C.; Frampas, E.; Faivre-Chauvet, A.; Rauscher, A.; Sharkey, R. M.; Goldenberg, D. M.; Chatal, J. F.; Barbet, J. A pretargeting system for tumor PET imaging and radioimmunotherapy. *Front Pharmacol* **2015**, *6*, 54.

36. Santich, B. H.; Cheal, S. M.; Ahmed, M.; McDevitt, M. R.; Ouerfelli, O.; Yang, G.; Veach, D. R.; Fung, E. K.; Patel, M.; Burnes Vargas, D.; et al. A Self-Assembling and Disassembling (SADA) Bispecific Antibody (BsAb) Platform for Curative Two-step Pretargeted Radioimmunotherapy. *Clin Cancer Res* **2021**, *27* (2), 532-541.

37. Liu, G.; Dou, S.; Cheng, D.; Leif, J.; Rusckowski, M.; Streeter, P. R.; Shultz, L. D.; Hnatowich, D. J.; Greiner, D. L. Human islet cell MORF/cMORF pretargeting in a xenogeneic murine transplant model. *Mol Pharm* **2011**, *8* (3), 767-773.

38. He, J.; Wang, Y.; Dou, S.; Liu, X.; Zhang, S.; Liu, G.; Hnatowich, D. Affinity enhancement pretargeting: synthesis and testing of a ^{99}mTc-labeled bivalent MORF. *Mol. pharmaceutics* **2010**, *7* (4), 1118-1124.

39. Patra, M.; Zarschler, K.; Pietzsch, H. J.; Stephan, H.; Gasser, G. New insights into the pretargeting approach to image and treat tumours. *Chem Soc Rev* **2016**, *45* (23), 6415-6431.

40. Knight, J. C.; Cornelissen, B. Bioorthogonal chemistry: implications for pretargeted nuclear (PET/SPECT) imaging and therapy. *Am J Nucl Med Mol Imaging* **2014**, *4* (2), 96-113.

41. Rondon, A.; Degoul, F. Antibody Pretargeting Based on Bioorthogonal Click Chemistry for Cancer Imaging and Targeted Radionuclide Therapy. *Bioconjug Chem* **2020**, *31* (2), 159-173.

42. Oliveira, B. L.; Guo, Z.; Bernardes, G. J. L. Inverse electron demand Diels-Alder reactions in chemical biology. *Chem Soc Rev* **2017**, *46* (16), 4895-4950.

43. Dong, P.; Wang, X.; Zheng, J.; Zhang, X.; Li, Y.; Wu, H.; Li, L. Recent Advances in Targeting Nuclear Molecular Imaging Driven by Tetrazine Bioorthogonal Chemistry. *Curr Med Chem* **2020**, *27* (23), 3924-3943.

44. Sletten, E. M.; Bertozzi, C. R. From mechanism to mouse: a tale of two bioorthogonal reactions. *Acc. Chem. Res.* **2011**, *44* (9), 666-676.

45. Agard, N. J.; Prescher, J. A.; Bertozzi, C. R. A strain-promoted [3 + 2] azide-alkyne cycloaddition for covalent modification of biomolecules in living systems. *J. Am. Chem. Soc.* **2004**, *126* (46), 15046-15047.

46. Saxon, E.; Bertozzi, C. R. Cell surface engineering by a modified Staudinger reaction. *Science* **2000**, *287* (5460), 2007-2010.

47. Sletten, E. M.; Bertozzi, C. R. Bioorthogonal chemistry: fishing for selectivity in a sea of functionality. *Angew. Chem. Int. Ed. Engl.* **2009**, *48* (38), 6974-6998.

48. Tornoe, C. W.; Christensen, C.; Meldal, M. Peptidotriazoles on solid phase: [1,2,3]-triazoles by regiospecific copper(i)-catalyzed 1,3-dipolar cycloadditions of terminal alkynes to azides. *J Org Chem* **2002**, *67* (9), 3057-3064.

49. Rostovtsev, V. V.; Green, L. G.; Fokin, V. V.; Sharpless, K. B. A stepwise huisgen cycloaddition process: copper(I)-catalyzed regioselective "ligation" of azides and terminal alkynes. *Angew Chem Int Ed Engl* **2002**, *41* (14), 2596-2599.

50. Li, L.; Zhang, Z. Development and Applications of the Copper-Catalyzed Azide-Alkyne Cycloaddition (CuAAC) as a Bioorthogonal Reaction. *Molecules* **2016**, *21* (10).

51. Wang, Q.; Chan, T. R.; Hilgraf, R.; Fokin, V. V.; Sharpless, K. B.; Finn, M. G. Bioconjugation by Copper(I)-Catalyzed Azide-Alkyne [3 + 2] Cycloaddition. *J Am Chem Soc* **2003**, *125* (11), 3192-3193.

52. Sen Gupta, S.; Kuzelka, J.; Singh, P.; Lewis, W. G.; Manchester, M.; Finn, M. G. Accelerated bioorthogonal conjugation: a practical method for the ligation of diverse functional molecules to a polyvalent virus scaffold. *Bioconjug Chem* **2005**, *16* (6), 1572-1579.

53. Prescher, J. A.; Bertozzi, C. R. Chemistry in living systems. *Nat Chem Biol* **2005**, *1* (1), 13-21.

54. Prescher, J. A.; Dube, D. H.; Bertozzi, C. R. Chemical remodelling of cell surfaces in living animals. *Nature* **2004**, *430* (7002), 873-877.

55. Bevilacqua, V.; King, M.; Chaumontet, M.; Nothisen, M.; Gabillet, S.; Buisson, D.; Puente, C.; Wagner, A.; Taran, F. Copper-chelating azides for efficient click conjugation reactions in complex media. *Angew Chem Int Ed Engl* **2014**, *53* (23), 5872-5876.

56. Johansson, J. R.; Beke-Somfai, T.; Said Stålsmeden, A.; Kann, N. Ruthenium-Catalyzed Azide Alkyne Cycloaddition Reaction: Scope, Mechanism, and Applications. *Chemical Reviews* **2016**, *116* (23), 14726-14768.

57. Carroll, L.; Evans, H. L.; Aboagye, E. O.; Spivey, A. C. Bioorthogonal chemistry for pre-targeted molecular imaging – progress and prospects. *Org Biomol Chem* **2013**, *11* (35), 5772-5781.

58. van Berkel, S. S.; van Eldijk, M. B.; van Hest, J. C. Staudinger ligation as a method for bioconjugation. *Angew Chem Int Ed Engl* **2011**, *50* (38), 8806-8827.

59. Saxon, E.; Armstrong, J. I.; Bertozzi, C. R. A "traceless" Staudinger ligation for the chemoselective synthesis of amide bonds. *Org Lett* **2000**, *2* (14), 2141-2143.

60. Vugts, D. J.; Vervoort, A.; Stigter-van Walsum, M.; Visser, G. W.; Robillard, M. S.; Versteegen, R. M.; Vulders, R. C.; Herscheid, J. K.; van Dongen, G. A. Synthesis of phosphine and antibody-azide probes

for in vivo Staudinger ligation in a pretargeted imaging and therapy approach. *Bioconjug Chem* **2011**, *22* (10), 2072-2081.

61. Debets, M. F.; van Berkel, S. S.; Dommerholt, J.; Dirks, A. T.; Rutjes, F. P.; van Delft, F. L. Bioconjugation with strained alkenes and alkynes. *Acc Chem Res* **2011**, *44* (9), 805-815.

62. Sletten, E. M.; Bertozzi, C. R. A hydrophilic azacyclooctyne for Cu-free click chemistry. *Org Lett* **2008**, *10* (14), 3097-3099.

63. Jewett, J. C.; Bertozzi, C. R. Cu-free click cycloaddition reactions in chemical biology. *Chem Soc Rev* **2010**, *39* (4), 1272-1279.

64. Baskin, J. M.; Prescher, J. A.; Laughlin, S. T.; Agard, N. J.; Chang, P. V.; Miller, I. A.; Lo, A.; Codelli, J. A.; Bertozzi, C. R. Copper-free click chemistry for dynamic in vivo imaging. *Proc Natl Acad Sci U S A* **2007**, *104* (43), 16793-16797.

65. Karver, M. R.; Weissleder, R.; Hilderbrand, S. A. Bioorthogonal reaction pairs enable simultaneous, selective, multi-target imaging. *Angew Chem Int Ed Engl* **2012**, *51* (4), 920-922.

66. Laughlin, S. T.; Baskin, J. M.; Amacher, S. L.; Bertozzi, C. R. In vivo imaging of membrane-associated glycans in developing zebrafish. *Science* **2008**, *320* (5876), 664-667.

67. Chang, P. V.; Prescher, J. A.; Sletten, E. M.; Baskin, J. M.; Miller, I. A.; Agard, N. J.; Lo, A.; Bertozzi, C. R. Copper-free click chemistry in living animals. *Proc Natl Acad Sci U S A* **2010**, *107* (5), 1821-1826.

68. van den Bosch, S. M.; Rossin, R.; Renart Verkerk, P.; ten Hoeve, W.; Janssen, H. M.; Lub, J.; Robillard, M. S. Evaluation of strained alkynes for Cu-free click reaction in live mice. *Nuclear Medicine and Biology* **2013**, *40* (3), 415-423.

69. Lee, S. B.; Kim, H. L.; Jeong, H.-J.; Lim, S. T.; Sohn, M.-H.; Kim, D. W. Mesoporous Silica Nanoparticle Pretargeting for PET Imaging Based on a Rapid Bioorthogonal Reaction in a Living Body. *Angew Chem Int Ed* **2013**, *52* (40), 10549-10552.

70. Rossin, R.; Robillard, M. S. Pretargeted imaging using bioorthogonal chemistry in mice. *Curr Opin Chem Biol* **2014**, *21*, 161-169.

71. Blackman, M. L.; Royzen, M.; Fox, J. M. Tetrazine ligation: fast bioconjugation based on inverse-electron-demand Diels-Alder reactivity. *J Am Chem Soc* **2008**, *130* (41), 13518-13519.

72. Devaraj, N. K.; Weissleder, R.; Hilderbrand, S. A. Tetrazine-based cycloadditions: application to pretargeted live cell imaging. *Bioconjug Chem* **2008**, *19* (12), 2297-2299.

73. Darko, A.; Wallace, S.; Dmitrenko, O.; Machovina, M. M.; Mehl, R. A.; Chin, J. W.; Fox, J. M. Conformationally Strained trans-Cyclooctene with Improved Stability and Excellent Reactivity in Tetrazine Ligation. *Chem Sci* **2014**, *5* (10), 3770-3776.

74. Royzen, M.; Yap, G. P.; Fox, J. M. A photochemical synthesis of functionalized trans-cyclooctenes driven by metal complexation. *J Am Chem Soc* **2008**, *130* (12), 3760-3761.

75. Pretze, M.; Pietzsch, D.; Mamat, C. Recent trends in bioorthogonal click-radiolabeling reactions using fluorine-18. *Molecules* **2013**, *18* (7), 8618-8665.

76. Bird, R. E.; Lemmel, S. A.; Yu, X.; Zhou, Q. A. Bioorthogonal Chemistry and Its Applications. *Bioconjug Chem* **2021**, *32* (12), 2457-2479.

77. Cheal, S. M.; Chung, S. K.; Vaughn, B. A.; Cheung, N. V.; Larson, S. M. Pretargeting: A Path Forward for Radioimmunotherapy. *J Nucl Med* **2022**, *63* (9), 1302-1315.

78. Rossin, R.; van den Bosch, S. M.; Ten Hoeve, W.; Carvelli, M.; Versteegen, R. M.; Lub, J.; Robillard, M. S. Highly reactive trans-cyclooctene tags with improved stability for Diels-Alder chemistry in living systems. *Bioconjug Chem* **2013**, *24* (7), 1210-1217.

79. Rossin, R.; Lappchen, T.; van den Bosch, S. M.; Laforest, R.; Robillard, M. S. Diels-Alder reaction for tumor pretargeting: in vivo chemistry can boost tumor radiation dose compared with directly labeled antibody. *J Nucl Med* **2013**, *54* (11), 1989-1995.

80. Steen, E. J. L.; Jorgensen, J. T.; Denk, C.; Battisti, U. M.; Norregaard, K.; Edem, P. E.; Bratteby, K.; Shalgunov, V.; Wilkovitsch, M.; Svatunek, D.; et al. Lipophilicity and Click Reactivity Determine the Performance of Bioorthogonal Tetrazine Tools in Pretargeted In Vivo Chemistry. *ACS Pharmacol Transl Sci* **2021**, *4* (2), 824-833.

81. Rossin, R.; van Duijnhoven, S. M.; Lappchen, T.; van den Bosch, S. M.; Robillard, M. S. Trans-cyclooctene tag with improved properties for tumor pretargeting with the diels-alder reaction. *Mol Pharm* **2014**, *11* (9), 3090-3096.

82. Houghton, J. L.; Zeglis, B. M.; Abdel-Atti, D.; Sawada, R.; Scholz, W. W.; Lewis, J. S. Pretargeted Immuno-PET of Pancreatic Cancer: Overcoming Circulating Antigen and Internalized Antibody to Reduce Radiation Doses. *J Nucl Med* **2016**, *57* (3), 453-459.

83. Keinanen, O.; Fung, K.; Brennan, J. M.; Zia, N.; Harris, M.; van Dam, E.; Biggin, C.; Hedt, A.; Stoner, J.; Donnelly, P. S.; et al. Harnessing (64)Cu/(67)Cu for a theranostic approach to pretargeted radioimmunotherapy. *Proc Natl Acad Sci U S A* **2020**, *117* (45), 28316-28327.

84. Keinanen, O.; Fung, K.; Pourat, J.; Jallinoja, V.; Vivier, D.; Pillarsetty, N. K.; Airaksinen, A. J.; Lewis, J. S.; Zeglis, B. M.; Sarparanta, M. Pretargeting of internalizing trastuzumab and cetuximab with a (18)F-tetrazine tracer in xenograft models. *EJNMMI Res* **2017**, *7* (1), 95.

85. Zeglis, B. M.; Sevak, K. K.; Reiner, T.; Mohindra, P.; Carlin, S. D.; Zanzonico, P.; Weissleder, R.; Lewis, J. S. A pretargeted PET imaging strategy based on bioorthogonal Diels-Alder click chemistry. *J Nucl Med* **2013**, *54* (8), 1389-1396.

86. *PET Imaging Using ^{64}Cu-Tz-SarAr and hu5B1-TCO in People With Pancreatic Cancer. NCT05737615*. U.S National Library of Medicine, **2023**. https://classic.clinicaltrials.gov/ct2/show/NCT05737615 (accessed 2023 24/07).

87. Billaud, E. M. F.; Belderbos, S.; Cleeren, F.; Maes, W.; Van de Wouwer, M.; Koole, M.; Verbruggen, A.; Himmelreich, U.; Geukens, N.; Bormans, G. Pretargeted PET Imaging Using a Bioorthogonal (18)F-Labeled trans-Cyclooctene in an Ovarian Carcinoma Model. *Bioconjug Chem* **2017**, *28* (12), 2915-2920.

88. Ruivo, E.; Elvas, F.; Adhikari, K.; Vangestel, C.; Van Haesendonck, G.; Lemiere, F.; Staelens, S.; Stroobants, S.; Van der Veken, P.; Wyffels, L.; Augustyns, K. Preclinical Evaluation of a Novel (18)F-Labeled dTCO-Amide Derivative for Bioorthogonal Pretargeted Positron Emission Tomography Imaging. *ACS Omega* **2020**, *5* (9), 4449-4456.

89. Rossin, R.; Verkerk, P. R.; van den Bosch, S. M.; Vulders, R. C.; Verel, I.; Lub, J.; Robillard, M. S. In vivo chemistry for pretargeted tumor imaging in live mice. *Angew Chem Int Ed Engl* **2010**, *49* (19), 3375-3378.

90. van Duijnhoven, S. M.; Rossin, R.; van den Bosch, S. M.; Wheatcroft, M. P.; Hudson, P. J.; Robillard, M. S. Diabody Pretargeting with Click Chemistry In Vivo. *J Nucl Med* **2015**, *56* (9), 1422-1428.

91. Altai, M.; Perols, A.; Tsourma, M.; Mitran, B.; Honarvar, H.; Robillard, M.; Rossin, R.; ten Hoeve, W.; Lubberink, M.; Orlova, A.; et al. Feasibility of Affibody-Based Bioorthogonal Chemistry-Mediated Radionuclide Pretargeting. *J Nucl Med* **2016**, *57* (3), 431-436.

92. Meyer, J. P.; Houghton, J. L.; Kozlowski, P.; Abdel-Atti, D.; Reiner, T.; Pillarsetty, N. V.; Scholz, W. W.; Zeglis, B. M.; Lewis, J. S. ^{18}F-Based Pretargeted PET Imaging Based on Bioorthogonal Diels-Alder Click Chemistry. *Bioconjug Chem* **2016**, *27* (2), 298-301.

93. Garcia-Vazquez, R.; Battisti, U. M.; Jorgensen, J. T.; Shalgunov, V.; Hvass, L.; Stares, D. L.; Petersen, I. N.; Crestey, F.; Loffler, A.; Svatunek, D.; et al. Direct Cu-mediated aromatic (18)F-labeling of highly reactive tetrazines for pretargeted bioorthogonal PET imaging. *Chem Sci* **2021**, *12* (35), 11668-11675.

94. Battisti, U. M.; Bratteby, K.; Jorgensen, J. T.; Hvass, L.; Shalgunov, V.; Mikula, H.; Kjaer, A.; Herth, M. M. Development of the First Aliphatic (18)F-Labeled Tetrazine Suitable for Pretargeted PET Imaging-Expanding the Bioorthogonal Tool Box. *J Med Chem* **2021**, *64* (20), 15297-15312.

95. Garcia-Vazquez, R.; Jorgensen, J. T.; Bratteby, K. E.; Shalgunov, V.; Hvass, L.; Herth, M. M.; Kjaer, A.; Battisti, U. M. Development of (18)F-Labeled Bispyridyl Tetrazines for In Vivo Pretargeted PET Imaging. *Pharmaceuticals (Basel)* **2022**, *15* (2).

96. Shah, P.; Westwell, A. D. The role of fluorine in medicinal chemistry. *J Enzyme Inhib Med Chem* **2007**, *22* (5), 527-540.

97. Cai, L.; Lu, S.; Pike, V. W. Chemistry with [^{18}F]Fluoride Ion. *Eur J Org Chem* **2008**, *2008* (17), 2853-2873.

98. Luurtsema, G.; Pichler, V.; Bongarzone, S.; Seimbille, Y.; Elsinga, P.; Gee, A.; Vercouillie, J. EANM guideline for harmonisation on molar activity or specific activity of radiopharmaceuticals: impact on safety and imaging quality. *EJNMMI Radiopharm Chem* **2021**, *6* (1), 34.

99. Edem, P. E.; Steen, E. J. L.; Kjær, A.; Herth, M. M. Fluorine-18 Radiolabeling Strategies—Advantages and Disadvantages of Currently Applied Labeling Methods. In *Late-Stage Fluorination of Bioactive Molecules and Biologically-Relevant Substrates*, Postigo, A. Ed.; Elsevier, 2019; pp 29-103.

100. Coenen, H. H. Fluorine-18 labeling methods: Features and possibilities of basic reactions. *Ernst Schering Res Found Workshop* **2007**, (62), 15-50.

101. Miller, P. W.; Long, N. J.; Vilar, R.; Gee, A. D. Synthesis of 11C, 18F, 15O, and 13N radiolabels for positron emission tomography. *Angew Chem Int Ed Engl* **2008**, *47* (47), 8998-9033.

102. van der Born, D.; Pees, A.; Poot, A. J.; Orru, R. V. A.; Windhorst, A. D.; Vugts, D. J. Fluorine-18 labelled building blocks for PET tracer synthesis. *Chem Soc Rev* **2017**, *46* (15), 4709-4773.

103. Smith, G. E.; Sladen, H. L.; Biagini, S. C.; Blower, P. J. Inorganic approaches for radiolabelling biomolecules with fluorine-18 for imaging with positron emission tomography. *Dalton Trans* **2011**, *40* (23), 6196-6205.

104. Farkas, E.; Fodor, T.; Kálmán, F. K.; Tircsó, G.; Tóth, I. Equilibrium and dissociation kinetics of the [Al(NOTA)] complex (NOTA = 1,4,7-triazacyclononane-1,4,7-triacetate). *Reaction Kinetics, Mechanisms and Catalysis* **2015**, *116* (1), 19-33.

105. McBride, W. J.; Sharkey, R. M.; Karacay, H.; D'Souza, C. A.; Rossi, E. A.; Laverman, P.; Chang, C. H.; Boerman, O. C.; Goldenberg, D. M. A novel method of ^{18}F radiolabeling for PET. *J Nucl Med* **2009**, *50* (6), 991-998.

106. Archibald, S. J.; Allott, L. The aluminium-[(18)F]fluoride revolution: simple radiochemistry with a big impact for radiolabelled biomolecules. *EJNMMI Radiopharm Chem* **2021**, *6* (1), 30.

107. McBride, W. J.; D'Souza, C. A.; Sharkey, R. M.; Karacay, H.; Rossi, E. A.; Chang, C. H.; Goldenberg, D. M. Improved 18F labeling of peptides with a fluoride-aluminum-chelate complex. *Bioconjug Chem* **2010**, *21* (7), 1331-1340.

108. Wan, W.; Guo, N.; Pan, D.; Yu, C.; Weng, Y.; Luo, S.; Ding, H.; Xu, Y.; Wang, L.; Lang, L.; et al. First experience of 18F-alfatide in lung cancer patients using a new lyophilized kit for rapid radiofluorination. *J Nucl Med* **2013**, *54* (5), 691-698.

109. Pauwels, E.; Cleeren, F.; Tshibangu, T.; Koole, M.; Serdons, K.; Boeckxstaens, L.; Dekervel, J.; Vandamme, T.; Lybaert, W.; den Broeck, B. V.; et al. (18)F-AlF-NOTA-Octreotide Outperforms (68)Ga-DOTATATE/NOC PET in Neuroendocrine Tumor Patients: Results from a Prospective, Multicenter Study. *J Nucl Med* **2023**, *64* (4), 632-638.

110. Boeckxstaens, L.; Pauwels, E.; Vandecaveye, V.; Deckers, W.; Cleeren, F.; Dekervel, J.; Vandamme, T.; Serdons, K.; Koole, M.; Bormans, G.; et al. Prospective comparison of [(18)F]AlF-NOTA-octreotide PET/MRI to [(68)Ga]Ga-DOTATATE PET/CT in neuroendocrine tumor patients. *EJNMMI Res* **2023**, *13* (1), 53.

111. Cleeren, F.; Lecina, J.; Ahamed, M.; Raes, G.; Devoogdt, N.; Caveliers, V.; McQuade, P.; Rubins, D. J.; Li, W.; Verbruggen, A.; et al. Al(18)F-Labeling Of Heat-Sensitive Biomolecules for Positron Emission Tomography Imaging. *Theranostics* **2017**, *7* (11), 2924-2939.

112. Hao, G.; Mastren, T.; Silvers, W.; Hassan, G.; Öz, O. K.; Sun, X. Copper-67 radioimmunotheranostics for simultaneous immunotherapy and immuno-SPECT. *Scientific Reports* **2021**, *11* (1), 3622.

113. Ahenkorah, S.; Murce, E.; Cawthorne, C.; Ketchemen, J. P.; Deroose, C. M.; Cardinaels, T.; Seimbille, Y.; Fonge, H.; Gsell, W.; Bormans, G.; et al. 3p-C-NETA: A versatile and effective chelator for development of Al(18)F-labeled and therapeutic radiopharmaceuticals. *Theranostics* **2022**, *12* (13), 5971-5985.

114. Ziegler, K.; Wilms, H. Uber vielgliedrige Ringsysteme XIII: Ungesättigte Kohlenwasserstoff-8-Ringe. *Justus Liebigs Annalen der Chemie* **1950**, *567* (1), 1-43.

115. Cope, A. C.; Pike, R. A.; Spencer, C. F. Cyclic Polyolefins. XXVII. cis- and trans-Cycloöctene from N,N-Dimethylcycloöctylamine1. *J. Am. Chem. Soc.* **2002**, *75* (13), 3212-3215.

116. Cope, A. C.; Ganellin, C. R.; Johnson, H. W.; Van Auken, T. V.; Winkler, H. J. S. Molecular Asymmetry of Olefins. I. Resolution of trans-Cyclooctene1-3. *J. Am. Chem. Soc.* **2002**, *85* (20), 3276-3279.

117. Cope, A. C.; Pawson, B. A. Molecular Asymmetry of Olefins. IV. Kinetics of Racemization of (+ or -)-trans-Cyclooctene1. *J. Am. Chem. Soc.* **2002**, *87* (16), 3649-3651.

118. Bach, R. D.; Mazur, U.; Hamama, I.; Lauderback, S. K. The stereochemistry of trans-cyclooctene derivatives. *Tetrahedron* **1972**, *28* (7), 1955-1963.

119. Allinger, N. L.; Sprague, J. T. Conformational analysis. LXXXIV. Study of the structures and energies of some alkenes and cycloalkenes by the force field method. *J. Am. Chem. Soc.* **2002**, *94* (16), 5734-5747.

120. Barrows, S. E.; Eberlein, T. H. Cis and trans isomers of cycloalkenes. *J Chem Educ* **2005**, *82* (9), 1334-1339.

121. Ermer, O. Conformation of Trans-Cyclooctene. *Angew Chem Int Edit* **1974**, *13* (9), 604-606.

122. Weyler, W., Jr.; Byrd, L. R.; Caserio, M. C.; Moore, H. W. Cycloaddition of tert-butylcyanoketene to 1,2-cyclononadiene and cis- and trans-cyclooctene. *J. Am. Chem. Soc.* **1972**, *94* (3), 1027-1029.

123. Palacios, F.; Deheredia, I. P.; Rubiales, G. Preparation and Reactivity of Electron-Poor 2-Azadienes - Diels-Alder Reaction with Trans-Cyclooctene. *Tetrahedron Lett.* **1993**, *34* (27), 4377-4380.

124. Palacios, F.; Deheredia, I. P.; Rubiales, G. Synthesis and Reactivity of Electron-Poor 2-Azadienes - [4+2] Cycloaddition Reactions with Alkenes and Enamines. *J. Org. Chem.* **1995**, *60* (8), 2384-2390.

125. Shea, K. J.; Kim, J. S. Influence of Strain on Chemical-Reactivity - Relative Reactivity of Torsionally Strained Double-Bonds in 1,3-Dipolar Cycloadditions. *J. Am. Chem. Soc.* **1992**, *114* (12), 4846-4855.

126. Ganis, P.; Lepore, U.; Martusce.E. Crystal and Molecular Structure of Di-Mu-Chlorotris(Trans-Cyclooctene)Dicopper(I). *J. Phys. Chem.* **1970**, *74* (12), 2439-&.

127. Kinoshita, I.; Terai, Y.; Kashiwabara, K.; Kido, H.; Saito, K. Preparation and Circular-Dichroism of Rhodium(I) Complexes Containing Optically-Active Trans-Cyclooctene. *J. Organomet. Chem.* **1977**, *127* (2), 237-243.

128. Komiya, S.; Kochi, J. K. Studies of Cationic Gold(I) Complexes - Preparation of Tris(Trans-Cyclooctene)Gold Trifluoromethanesulfonate. *J. Organomet. Chem.* **1977**, *135* (1), 65-72.

129. Nicolaides, A.; Smith, J. M.; Kumar, A.; Barnhart, D. M.; Borden, W. T. Synthesis and Study of the (Ph3P)2Pt Complexes of Three Members of a Series of Highly Pyramidalized Alkenes. *Organometallics* **2002**, *14* (7), 3475-3485.

130. Hecht, J. K. Polymerization of Trans-Cyclooctene. *J Polym Sci Pol Lett* **1968**, *6* (5), 333-334.

131. Lee, S. J.; McGinnis, J.; Katz, T. J. Directional specificity and stereoselectivity in the metathesis of a trisubstituted olefin. *J. Am. Chem. Soc.* **2002**, *98* (24), 7818-7819.

132. Einaru, S.; Shitamichi, K.; Nagano, T.; Matsumoto, A.; Asano, K.; Matsubara, S. trans-Cyclooctenes as Halolactonization Catalysts. *Angew Chem Int Ed Engl* **2018**, *57* (42), 13863-13867.

133. Handula, M.; Chen, K. T.; Seimbille, Y. IEDDA: An Attractive Bioorthogonal Reaction for Biomedical Applications. *Molecules* **2021**, *26* (15).

134. Pagel, M. Inverse electron demand Diels-Alder (IEDDA) reactions in peptide chemistry. *J. Pept. Sci.* **2019**, *25* (1), e3141.

135. Haiber, L. M.; Kufleitner, M.; Wittmann, V. Application of the Inverse-Electron-Demand Diels-Alder Reaction for Metabolic Glycoengineering. *Front. Chem.* **2021**, *9*, 654932.

136. Ravasco, J.; Coelho, J. A. S. Predictive Multivariate Models for Bioorthogonal Inverse-Electron Demand Diels-Alder Reactions. *J Am Chem Soc* **2020**, *142* (9), 4235-4241.

137. Pipkorn, R.; Waldeck, W.; Didinger, B.; Koch, M.; Mueller, G.; Wiessler, M.; Braun, K. Inverse-electron-demand Diels-Alder reaction as a highly efficient chemoselective ligation procedure: synthesis and function of a BioShuttle for temozolomide transport into prostate cancer cells. *J. Pept. Sci.* **2009**, *15* (3), 235-241.

138. Carboni, R. A.; Lindsey, R. V. Reactions of Tetrazines with Unsaturated Compounds - a New Synthesis of Pyridazines. *J Am Chem Soc* **1959**, *81* (16), 4342-4346.

139. Boger, D. L.; Schaum, R. P.; Garbaccio, R. M. Regioselective Inverse Electron Demand Diels-Alder Reactions of N-Acyl 6-Amino-3-(methylthio)-1,2,4,5-tetrazines. *J Org Chem* **1998**, *63* (18), 6329-6337.

140. Karver, M. R.; Weissleder, R.; Hilderbrand, S. A. Synthesis and evaluation of a series of 1,2,4,5-tetrazines for bioorthogonal conjugation. *Bioconjug Chem* **2011**, *22* (11), 2263-2270.

141. Kele, P.; Wagenknecht, H.-A.; Cserép, G.; Demeter, O.; Bätzner, E.; Kállay, M. Synthesis and Evaluation of Nicotinic Acid Derived Tetrazines for Bioorthogonal Labeling. *Synthesis* **2015**, *47* (18), 2738-2744.

142. Yang, J.; Liang, Y.; Seckute, J.; Houk, K. N.; Devaraj, N. K. Synthesis and reactivity comparisons of 1-methyl-3-substituted cyclopropene mini-tags for tetrazine bioorthogonal reactions. *Chemistry* **2014**, *20* (12), 3365-3375.

143. Svatunek, D.; Wilkovitsch, M.; Hartmann, L.; Houk, K. N.; Mikula, H. Uncovering the Key Role of Distortion in Bioorthogonal Tetrazine Tools That Defy the Reactivity/Stability Trade-Off. *J Am Chem Soc* **2022**, *144* (18), 8171-8177.

144. Battisti, U. M.; Garcia-Vazquez, R.; Svatunek, D.; Herrmann, B.; Loffler, A.; Mikula, H.; Herth, M. M. Synergistic Experimental and Computational Investigation of the Bioorthogonal Reactivity of Substituted Aryltetrazines. *Bioconjug Chem* **2022**, *33* (4), 608-624.

145. Wijnen, J. W.; Zavarise, S.; Engberts, J. B. F. N.; Charton, M. Substituent effects on an inverse electron demand hetero Diels-Alder reaction in aqueous solution and organic solvents: Cycloaddition of substituted styrenes to di(2-pyridyl)-1,2,4,5-tetrazine. *J Org Chem* **1996**, *61* (6), 2001-2005.

146. Meijer, A.; Otto, S.; Engberts, J. B. F. N. Effects of the hydrophobicity of the reactants on Diels-Alder reactions in water. *J Org Chem* **1998**, *63* (24), 8989-8994.

147. Thalhammer, F.; Wallfahrer, U.; Sauer, J. Reaktivität einfacher offenkettiger und cyclischer dienophile bei Diels-Alder-reaktionen mit inversem elektronenbedarf. *Tetrahedron Lett.* **1990**, *31* (47), 6851-6854.

148. Liu, F.; Paton, R. S.; Kim, S.; Liang, Y.; Houk, K. N. Diels-Alder reactivities of strained and unstrained cycloalkenes with normal and inverse-electron-demand dienes: activation barriers and distortion/interaction analysis. *J Am Chem Soc* **2013**, *135* (41), 15642-15649.

149. Bach, R. D. Ring strain energy in the cyclooctyl system. The effect of strain energy on [3 + 2] cycloaddition reactions with azides. *J Am Chem Soc* **2009**, *131* (14), 5233-5243.

150. Leong, M. K.; Mastryukov, V. S.; Boggs, J. E. Structure and conformation of cyclopentene, cycloheptene and trans-cyclooctene. *J. Mol. Struct.* **1998**, *445* (1-3), 149-160.

151. Liu, F.; Liang, Y.; Houk, K. N. Theoretical elucidation of the origins of substituent and strain effects on the rates of Diels-Alder reactions of 1,2,4,5-tetrazines. *J Am Chem Soc* **2014**, *136* (32), 11483-11493.

152. Taylor, M. T.; Blackman, M. L.; Dmitrenko, O.; Fox, J. M. Design and synthesis of highly reactive dienophiles for the tetrazine-trans-cyclooctene ligation. *J Am Chem Soc* **2011**, *133* (25), 9646-9649.

153. Wagner, J. A.; Mercadante, D.; Nikic, I.; Lemke, E. A.; Grater, F. Origin of Orthogonality of Strain-Promoted Click Reactions. *Chemistry* **2015**, *21* (35), 12431-12435.

154. Hoffmann, J. E.; Plass, T.; Nikic, I.; Aramburu, I. V.; Koehler, C.; Gillandt, H.; Lemke, E. A.; Schultz, C. Highly Stable trans-Cyclooctene Amino Acids for Live-Cell Labeling. *Chemistry* **2015**, *21* (35), 12266-12270.

155. Reese, C. B.; Shaw, A. Silver Perchlorate Promoted Ring Expansion of Halocarbene Adducts of Cyclic Olefins - a Facile Synthesis of Trans-Cyclooctene and Trans-Cyclononene Derivatives. *J Am Chem Soc* **1970**, *92* (8), 2566-2568.

156. Braddock, D. C.; Cansell, G.; Hermitage, S. A.; White, A. J. P. An asymmetric synthesis of enantiopure chair and twist trans-cyclooctene isomers. *Tetrahedron Asymmetry* **2004**, *15* (19), 3123-3129.

157. Whitham, G. H.; Wright, M. trans-Cycloalkenes. Part II. Application of the dioxolan olefin synthesis to the stereospecific formation of trans-cyclo-octene derivatives. (1SR,2RS)-trans-Cyclo-oct-2-en-1-ol. *J. Chem. Soc. C* **1971**, 886-891.

158. Whitham, G. H.; Wright, M. trans-Cycloalkenes. Part III. Stereochemistry and mechanism of some reactions of diastereoisomeric 3-substituted trans-cyclo-octenes. *J. Chem. Soc. C.* **1971**, (0), 891-896.

159. Hines, J. N.; Peagram, M. J.; Thomas, E. J.; Whitham, G. H. Some reactions of benzaldehyde acetals with alkyl-lithium reagents; a stereospecific olefin synthesis from 1,2-diols. *J. Chem. Soc., Perkin trans. 1* **1973**, 2332-2337.

160. Corey, E. J.; Shulman, J. I. The direct synthesis of optically active -cyclooctene. Optically active -bicyclo[6.1.0]nonane. *Tetrahedron Letters* **1968**, *9* (33), 3655-3658.

161. Vedejs, E.; Snoble, K. A. J.; Fuchs, P. L. Phosphorus Betaines Derived from Cycloheptene and Cyclooctene Oxides - Inversion of Cyclooctenes. *J Org Chem* **1973**, *38* (6), 1178-1183.

162. Vedejs, E.; Fuchs, P. L. Inversion of acyclic olefins by the phosphorus betaine method. Scope and limitations. *J Am Chem Soc* **2002**, *95* (3), 822-825.

163. Bridges, A. J.; Whitham, G. H. *J. Chem. Soc., Perkin Trans.* **1974**, *1*, 142.

164. Wang, X. N.; Krenske, E. H.; Johnston, R. C.; Houk, K. N.; Hsung, R. P. Torquoselective ring opening of fused cyclobutenamides: evidence for a cis,trans-cyclooctadienone intermediate. *J Am Chem Soc* **2014**, *136* (28), 9802-9805.

165. Wang, X. N.; Krenske, E. H.; Johnston, R. C.; Houk, K. N.; Hsung, R. P. $AlCl_3$-Catalyzed Ring Expansion Cascades of Bicyclic Cyclobutenamides Involving Highly Strained Cis,Trans-Cycloheptadienone Intermediates. *J Am Chem Soc* **2015**, *137* (16), 5596-5601.

166. Ito, T.; Tsutsumi, M.; Yamada, K. I.; Takikawa, H.; Yamaoka, Y.; Takasu, K. Synthesis of Functionalized Medium-Sized trans-Cycloalkenes by 4pi Electrocyclic Ring Opening/Alkylation Sequence. *Angew Chem Int Ed Engl* **2019**, *58* (34), 11836-11840.

167. Lambert, W. D.; Scinto, S. L.; Dmitrenko, O.; Boyd, S. J.; Magboo, R.; Mehl, R. A.; Chin, J. W.; Fox, J. M.; Wallace, S. Computationally guided discovery of a reactive, hydrophilic trans-5-oxocene dienophile for bioorthogonal labeling. *Org Biomol Chem* **2017**, *15* (31), 6640-6644.

168. Prevost, M.; Ziller, J. W.; Woerpel, K. A. Strained organosilacyclic compounds: synthesis of anti-Bredt olefins and trans-dioxasilacyclooctenes. *Dalton Trans* **2010**, *39* (39), 9275-9281.

169. Tomooka, K.; Miyasaka, S.; Motomura, S.; Igawa, K. Planar chiral dialkoxysilane: introduction of inherent chirality and high reactivity in conventional achiral alkene. *Chemistry* **2014**, *20* (25), 7598-7602.

170. Machida, K.; Yoshida, Y.; Igawa, K.; Tomooka, K. Efficient Approach to Medium-sized Cyclic Molecules Containing (E)-Alkene via Z to E Photochemical Isomerization in the Presence of AgNO3-impregnated Silica Gel. *Chem Lett* **2018**, *47* (2), 186-188.

171. Pigga, J. E.; Rosenberger, J. E.; Jemas, A.; Boyd, S. J.; Dmitrenko, O.; Xie, Y.; Fox, J. M. General, Divergent Platform for Diastereoselective Synthesis of trans-Cyclooctenes with High Reactivity and Favorable Physiochemical Properties*. *Angew Chem Int Ed Engl* **2021**, *60* (27), 14975-14980.

172. Wilkovitsch, M.; Haider, M.; Sohr, B.; Herrmann, B.; Klubnick, J.; Weissleder, R.; Carlson, J. C. T.; Mikula, H. A Cleavable $C_{(2)}$-Symmetric trans-Cyclooctene Enables Fast and Complete Bioorthogonal Disassembly of Molecular Probes. *J Am Chem Soc* **2020**, *142* (45), 19132-19141.

173. Kuba, W.; Sohr, B.; Keppel, P.; Svatunek, D.; Humhal, V.; Stoger, B.; Goldeck, M.; Carlson, J. C. T.; Mikula, H. Oxidative Desymmetrization Enables the Concise Synthesis of a trans-Cyclooctene Linker for Bioorthogonal Bond Cleavage. *Chemistry* **2023**, *29* (3), e202203069.

174. Liu, B.; Ten Hoeve, W.; Versteegen, R. M.; Rossin, R.; Kleijn, L. H. J.; Robillard, M. S. A Concise Synthetic Approach to Highly Reactive Click-to-Release Trans-Cyclooctene Linkers. *Chemistry* **2023**, *29* (45), e202300755.

175. Sondag, D.; Maartense, L.; de Jong, H.; de Kleijne, F. F. J.; Bonger, K. M.; Lowik, D.; Boltje, T. J.; Dommerholt, J.; White, P. B.; Blanco-Ania, D.; Rutjes, F. Readily Accessible Strained Difunctionalized trans-Cyclooctenes with Fast Click and Release Capabilities. *Chemistry* **2023**, *29* (6), e202203375.

176. Maeda, R.; Wada, T.; Mori, T.; Kono, S.; Kanomata, N.; Inoue, Y. Planar-to-planar chirality transfer in the excited state. Enantiodifferentiating photoisomerization of cyclooctenes sensitized by planar-chiral paracyclophane. *J Am Chem Soc* **2011**, *133* (27), 10379-10381.

177. Kaneda, M.; Asaoka, S.; Ikeda, H.; Mori, T.; Wada, T.; Inoue, Y. Discontinuous pressure effect upon enantiodifferentiating photosensitized isomerization of cyclooctene. *Chem Commun (Camb)* **2002**, (12), 1272-1273.

178. Inoue, T.; Matsuyama, K.; Inoue, Y. Diastereodifferentiating Z-E photoisomerization of 3-benzoyloxycyclooctene: Diastereoselectivity switching controlled by substrate concentration

through competitive intra- vs intermolecular photosensitization processes. *J Am Chem Soc* **1999**, *121* (42), 9877-9878.

179. Shi, M.; Inoue, Y. Geometrical photoisomerization of (Z)-cyclooctene sensitized by aromatic phosphate, phosphonate, phosphinate, phosphine oxide and chiral phosphoryl esters. *J Chem Soc Perk T 2* **1998**, (11), 2421-2427.

180. Inoue, Y.; Matsushima, E.; Wada, T. Pressure and temperature control of product chirality in asymmetric photochemistry. Enantiodifferentiating photoisomerization of cyclooctene sensitized by chiral benzenepolycarboxylates. *J Am Chem Soc* **1998**, *120* (41), 10687-10696.

181. Tsuneishi, H.; Inoue, Y.; Hakushi, T.; Tai, A. Direct and Sensitized Geometrical Photoisomerization of 1-Methylcyclooctene. *J Chem Soc Perk T 2* **1993**, (3), 457-462.

182. Inoue, Y.; Yamasaki, N.; Yokoyama, T.; Tai, A. Highly enantiodifferentiating photoisomerization of cyclooctene by congested and/or triplex-forming chiral sensitizers. *J Org Chem* **2002**, *58* (5), 1011-1018.

183. Inoue, Y.; Kunitomi, Y.; Takamuku, S.; Sakurai, H. Asymmetric Cis-Trans Photoisomerization of Cyclo-Octene Sensitized by Chiral Aromatic Esters. *J Chem Soc Chem Comm* **1978**, (23), 1024-1025.

184. Inoue, Y.; Ueoka, T.; Kuroda, T.; Hakushi, T. Singlet photosensitization of simple alkenes. Part 4. cis-trans Photoisomerization of cycloheptene sensitized by aromatic esters. Some aspects of the chemistry of trans-cycloheptene. *J Chem Soc Perk T 2* **1983**, (7), 983-988.

185. Pigga, J. E.; Fox, J. M. Flow Photochemical Syntheses of trans-Cyclooctenes and trans-Cycloheptenes Driven by Metal Complexation. *Israel Journal of Chemistry* **2020**, *60* (3-4), 207-218.

186. Blanco-Ania, D.; Maartense, L.; Rutjes, F. P. J. T. Rapid Production of trans-Cyclooctenes in Continuous Flow. *Chemphotochem* **2018**, *2* (10), 898-905.

187. Cedeño, D. L.; Sniatynsky, R. Metal−Olefin Interactions in M(CO)5(cycloolefin) (M = Cr, Mo, W; Cycloolefin = Cyclopropene to Cyclooctene): Strain Relief and Metal−Olefin Bond Strength. *Organometallics* **2005**, *24* (16), 3882-3890.

188. Mander, L. N.; Williams, C. M. Chromatography with silver nitrate: part 2. *Tetrahedron* **2016**, *72* (9), 1133-1150.

189. Sanzone, J. R.; Woerpel, K. A. High Reactivity of Strained Seven-Membered-Ring trans-Alkenes. *Angew Chem Int Ed Engl* **2016**, *55* (2), 790-793.

190. Siegl, S. J.; Galeta, J.; Dzijak, R.; Vazquez, A.; Del Rio-Villanueva, M.; Dracinsky, M.; Vrabel, M. An Extended Approach for the Development of Fluorogenic trans-Cyclooctene-Tetrazine Cycloadditions. *Chembiochem* **2019**, *20* (7), 886-890.

191. Kara, S. S.; Ates, M. Y.; Deveci, G.; Cetinkaya, A.; Kahveci, M. U. Direct synthesis of tetrazine functionalities on polymer backbones. *J Polym Sci Pol Chem* **2019**, *57* (6), 673-680.

192. Dadhwal, S.; Fairhall, J. M.; Goswami, S. K.; Hook, S.; Gamble, A. B. Alkene-Azide 1,3-Dipolar Cycloaddition as a Trigger for Ultrashort Peptide Hydrogel Dissolution. *Chem Asian J* **2019**, *14* (8), 1143-1150.

193. Versteegen, R. M.; Ten Hoeve, W.; Rossin, R.; de Geus, M. A. R.; Janssen, H. M.; Robillard, M. S. Click-to-Release from trans-Cyclooctenes: Mechanistic Insights and Expansion of Scope from Established Carbamate to Remarkable Ether Cleavage. *Angew Chem Int Ed Engl* **2018**, *57* (33), 10494-10499.

194. van der Gracht, A. M. F.; de Geus, M. A. R.; Camps, M. G. M.; Ruckwardt, T. J.; Sarris, A. J. C.; Bremmers, J.; Maurits, E.; Pawlak, J. B.; Posthoorn, M. M.; Bonger, K. M.; et al. Chemical Control over T-Cell Activation in Vivo Using Deprotection of trans-Cyclooctene-Modified Epitopes. *ACS Chem Biol* **2018**, *13* (6), 1569-1576.

195. Siegl, S. J.; Vazquez, A.; Dzijak, R.; Dracinsky, M.; Galeta, J.; Rampmaier, R.; Klepetarova, B.; Vrabel, M. Design and Synthesis of Aza-Bicyclononene Dienophiles for Rapid Fluorogenic Ligations. *Chemistry* **2018**, *24* (10), 2426-2432.

196. DeMeester, K. E.; Liang, H.; Jensen, M. R.; Jones, Z. S.; D'Ambrosio, E. A.; Scinto, S. L.; Zhou, J.; Grimes, C. L. Synthesis of Functionalized N-Acetyl Muramic Acids To Probe Bacterial Cell Wall Recycling and Biosynthesis. *J Am Chem Soc* **2018**, *140* (30), 9458-9465.

197. Bruins, J. J.; Blanco-Ania, D.; van der Doef, V.; van Delft, F. L.; Albada, B. Orthogonal, dual protein labelling by tandem cycloaddition of strained alkenes and alkynes to ortho-quinones and azides. *Chem Commun (Camb)* **2018**, *54* (53), 7338-7341.

198. Bernard, S.; Kumar, R. A.; Porte, K.; Thuery, P.; Taran, F.; Audisio, D. A Practical Synthesis of Valuable Strained Eight-Membered-Ring Derivatives for Click Chemistry. *Eur J Org Chem* **2018**, *2018* (17), 2000-2008.

199. Vazquez, A.; Dzijak, R.; Dracinsky, M.; Rampmaier, R.; Siegl, S. J.; Vrabel, M. Mechanism-Based Fluorogenic trans-Cyclooctene-Tetrazine Cycloaddition. *Angew Chem Int Ed Engl* **2017**, *56* (5), 1334-1337.

200. Marjanovic, J.; Baranczak, A.; Marin, V.; Stockmann, H.; Richardson, P. L.; Vasudevan, A. Development of inverse electron demand Diels-Alder ligation and TR-FRET assays for the determination of ligand-protein target occupancy in live cells. *Medchemcomm* **2017**, *8* (4), 789-795.

201. Maggi, A.; Ruivo, E.; Fissers, J.; Vangestel, C.; Chatterjee, S.; Joossens, J.; Sobott, F.; Staelens, S.; Stroobants, S.; Van Der Veken, P.; et al. Development of a novel antibody-tetrazine conjugate for bioorthogonal pretargeting. *Org Biomol Chem* **2016**, *14* (31), 7544-7551.

202. Lorenzo, M. M.; Decker, C. G.; Kahveci, M. U.; Paluck, S. J.; Maynard, H. D. Homodimeric Protein-Polymer Conjugates via the Tetrazine-trans-Cyclooctene Ligation. *Macromolecules* **2016**, *49* (1), 30-37.

203. Kozma, E.; Nikic, I.; Varga, B. R.; Aramburu, I. V.; Kang, J. H.; Fackler, O. T.; Lemke, E. A.; Kele, P. Hydrophilic trans-Cyclooctenylated Noncanonical Amino Acids for Fast Intracellular Protein Labeling. *Chembiochem* **2016**, *17* (16), 1518-1524.

204. Denk, C.; Svatunek, D.; Mairinger, S.; Stanek, J.; Filip, T.; Matscheko, D.; Kuntner, C.; Wanek, T.; Mikula, H. Design, Synthesis, and Evaluation of a Low-Molecular-Weight (11)C-Labeled Tetrazine for Pretargeted PET Imaging Applying Bioorthogonal in Vivo Click Chemistry. *Bioconjug Chem* **2016**, *27* (7), 1707-1712.

205. Mohamed, A.; Anna, P.; Maria, T.; Bogdan, M.; Hadis, H.; Marc, R.; Raffaella, R.; Wolter ten, H.; Mark, L.; Anna, O.; et al. Feasibility of Affibody-Based Bioorthogonal Chemistry–Mediated Radionuclide Pretargeting. *J Nucl Med* **2016**, *57* (3), 431.

206. Wang, K.; Wang, D.; Ji, K.; Chen, W.; Zheng, Y.; Dai, C.; Wang, B. Post-synthesis DNA modifications using a trans-cyclooctene click handle. *Org Biomol Chem* **2015**, *13* (3), 909-915.

207. Blizzard, R. J.; Backus, D. R.; Brown, W.; Bazewicz, C. G.; Li, Y.; Mehl, R. A. Ideal Bioorthogonal Reactions Using A Site-Specifically Encoded Tetrazine Amino Acid. *J Am Chem Soc* **2015**, *137* (32), 10044-10047.

208. Wollack, J. W.; Monson, B. J.; Dozier, J. K.; Dalluge, J. J.; Poss, K.; Hilderbrand, S. A.; Distefano, M. D. Site-specific labeling of proteins and peptides with trans-cyclooctene containing handles capable of tetrazine ligation. *Chem Biol Drug Des* **2014**, *84* (2), 140-147.

209. Mejia Oneto, J. M.; Gupta, M.; Leach, J. K.; Lee, M.; Sutcliffe, J. L. Implantable biomaterial based on click chemistry for targeting small molecules. *Acta Biomater* **2014**, *10* (12), 5099-5105.

210. Schoch, J.; Staudt, M.; Samanta, A.; Wiessler, M.; Jaschke, A. Site-specific one-pot dual labeling of DNA by orthogonal cycloaddition chemistry. *Bioconjug Chem* **2012**, *23* (7), 1382-1386.

211. Devaraj, N. K.; Upadhyay, R.; Haun, J. B.; Hilderbrand, S. A.; Weissleder, R. Fast and sensitive pretargeted labeling of cancer cells through a tetrazine/trans-cyclooctene cycloaddition. *Angew Chem Int Ed Engl* **2009**, *48* (38), 7013-7016.

212. Svatunek, D.; Denk, C.; Rosecker, V.; Sohr, B.; Hametner, C.; Allmaier, G.; Frohlich, J.; Mikula, H. Efficient low-cost preparation of trans-cyclooctenes using a simplified flow setup for photoisomerization. *Monatsh Chem* **2016**, *147* (3), 579-585.

213. Billaud, E. M. F.; Shahbazali, E.; Ahamed, M.; Cleeren, F.; Noel, T.; Koole, M.; Verbruggen, A.; Hessel, V.; Bormans, G. Micro-flow photosynthesis of new dienophiles for inverse-electron-demand Diels-Alder reactions. Potential applications for pretargeted in vivo PET imaging. *Chem Sci* **2017**, *8* (2), 1251-1258.

214. Darko, A.; Boyd, S. J.; Fox, J. M. Large-Scale Flow Photochemical Synthesis of Functionalized trans-Cyclooctenes Using Sulfonated Silica Gel. *Synthesis (Stuttg)* **2018**, *50* (24), 4875-4882.

215. Pickel, T. C.; Genung, N. E.; Guckian, K. M.; Shi, X. L. A Simple, Readily Accessible, and Effective Apparatus for the -Photoisomerization of cis-Cyclooctenes to trans-Cyclooctenes. *Synlett* **2021**, *32* (17), 1711-1713.

216. Plass, T.; Milles, S.; Koehler, C.; Szymanski, J.; Mueller, R.; Wiessler, M.; Schultz, C.; Lemke, E. A. Amino acids for Diels-Alder reactions in living cells. *Angew Chem Int Ed Engl* **2012**, *51* (17), 4166-4170.

217. Nikic, I.; Plass, T.; Schraidt, O.; Szymanski, J.; Briggs, J. A.; Schultz, C.; Lemke, E. A. Minimal tags for rapid dual-color live-cell labeling and super-resolution microscopy. *Angew Chem Int Ed Engl* **2014**, *53* (8), 2245-2249.

218. Versteegen, R. M.; Rossin, R.; ten Hoeve, W.; Janssen, H. M.; Robillard, M. S. Click to release: instantaneous doxorubicin elimination upon tetrazine ligation. *Angew Chem Int Ed Engl* **2013**, *52* (52), 14112-14116.

219. Dommerholt, J.; Schmidt, S.; Temming, R.; Hendriks, L. J.; Rutjes, F. P.; van Hest, J. C.; Lefeber, D. J.; Friedl, P.; van Delft, F. L. Readily accessible bicyclononynes for bioorthogonal labeling and three-dimensional imaging of living cells. *Angew Chem Int Ed Engl* **2010**, *49* (49), 9422-9425.

220. Seitchik, J. L.; Peeler, J. C.; Taylor, M. T.; Blackman, M. L.; Rhoads, T. W.; Cooley, R. B.; Refakis, C.; Fox, J. M.; Mehl, R. A. Genetically encoded tetrazine amino acid directs rapid site-specific in vivo bioorthogonal ligation with trans-cyclooctenes. *J Am Chem Soc* **2012**, *134* (6), 2898-2901.

221. Lang, K.; Davis, L.; Wallace, S.; Mahesh, M.; Cox, D. J.; Blackman, M. L.; Fox, J. M.; Chin, J. W. Genetic Encoding of bicyclononynes and trans-cyclooctenes for site-specific protein labeling in vitro and in live mammalian cells via rapid fluorogenic Diels-Alder reactions. *J Am Chem Soc* **2012**, *134* (25), 10317-10320.

222. Fang, Y.; Judkins, J. C.; Boyd, S. J.; Am Ende, C. W.; Rohlfing, K.; Huang, Z.; Xie, Y.; Johnson, D. S.; Fox, J. M. Studies on the Stability and Stabilization of trans-Cyclooctenes through Radical Inhibition and Silver (I) Metal Complexation. *Tetrahedron* **2019**, *75* (32), 4307-4317.

223. Ravasco, J. M. J. M.; Coelho, J. A. S.; Trindade, A. F.; Afonso, C. A. M. Synthesis and reactivity/stability study of double-functionalizable strained trans-cyclooctenes for tetrazine bioorthogonal reactions. *Pure and Applied Chemistry* **2020**, *92* (1), 15-23.

224. Uttamapinant, C.; Howe, J. D.; Lang, K.; Beranek, V.; Davis, L.; Mahesh, M.; Barry, N. P.; Chin, J. W. Genetic code expansion enables live-cell and super-resolution imaging of site-specifically labeled cellular proteins. *J Am Chem Soc* **2015**, *137* (14), 4602-4605.

225. Jendralla, H. The Influence of Endocyclic Oxygen-Atoms on the Cycloaddition Reactivity of Trans-Cyclo-Octene. *Tetrahedron* **1983**, *39* (8), 1359-1363.

226. S. Hilderbrand, B. R. V., R Weissleder. Cyclooctenes for Bioorthogonal Reactions. US 044655, 2015.

227. Knorr, G.; Kozma, E.; Herner, A.; Lemke, E. A.; Kele, P. New Red-Emitting Tetrazine-Phenoxazine Fluorogenic Labels for Live-Cell Intracellular Bioorthogonal Labeling Schemes. *Chemistry* **2016**, *22* (26), 8972-8979.

228. Gold, B.; Dudley, G. B.; Alabugin, I. V. Moderating strain without sacrificing reactivity: design of fast and tunable noncatalyzed alkyne-azide cycloadditions via stereoelectronically controlled transition state stabilization. *J Am Chem Soc* **2013**, *135* (4), 1558-1569.

229. Jendralla, H. (5RS, 7RS)-7 Methoxy-1,3dioxacyclooct-5(E)-en Synthese eines stabilen Bisheterotrans-cyclooctens; ein neues heterocyclisches System. *Chemische Berichte* **2006**, *115* (1), 201-209.

230. Prevost, M.; Woerpel, K. A. Insertions of silylenes into vinyl epoxides: diastereoselective synthesis of functionalized, optically active trans-dioxasilacyclooctenes. *J Am Chem Soc* **2009**, *131* (40), 14182-14183.

231. Cerè, V.; Peri, F.; Pollicino, S.; Antonio, A. Acid-catalyzed transannular cyclization of medium ring unsaturated sulfides. The effect of ring size and double bond geometry on rate. *Journal of the Chemical Society, Perkin Transactions 2* **1998**, (4), 977-980.

232. Royzen, M.; Taylor, M. T.; Deangelis, A.; Fox, J. M. Total Synthesis of Hyacinthacine A2: Stereocontrolled 5-aza-cyclooctene Photoisomerization and Transannular Hydroamination with Planar-to-Point Chirality Transfer. *Chem Sci* **2011**, *2* (11), 2162-2165.

233. Li, Z.; Cai, H.; Hassink, M.; Blackman, M. L.; Brown, R. C.; Conti, P. S.; Fox, J. M. Tetrazine-trans-cyclooctene ligation for the rapid construction of ^{18}F labeled probes. *Chem Commun (Camb)* **2010**, *46* (42), 8043-8045.

234. Selvaraj, R.; Liu, S.; Hassink, M.; Huang, C. W.; Yap, L. P.; Park, R.; Fox, J. M.; Li, Z.; Conti, P. S. Tetrazine-trans-cyclooctene ligation for the rapid construction of integrin alphavbeta(3) targeted PET tracer based on a cyclic RGD peptide. *Bioorg Med Chem Lett* **2011**, *21* (17), 5011-5014.

235. Liu, S.; Hassink, M.; Selvaraj, R.; Yap, L. P.; Park, R.; Wang, H.; Chen, X.; Fox, J. M.; Li, Z.; Conti, P. S. Efficient 18F labeling of cysteine-containing peptides and proteins using tetrazine-trans-cyclooctene ligation. *Mol Imaging* **2013**, *12* (2), 121-128.

236. Wu, Z.; Liu, S.; Hassink, M.; Nair, I.; Park, R.; Li, L.; Todorov, I.; Fox, J. M.; Li, Z.; Shively, J. E.; et al. Development and evaluation of 18F-TTCO-Cys40-Exendin-4: a PET probe for imaging transplanted islets. *J Nucl Med* **2013**, *54* (2), 244-251.

237. Wang, Y.; Lim, K.; Normandin, M.; Zhao, X.; Cline, G. W.; Ding, Y. S. Synthesis and evaluation of [18F]exendin (9-39) as a potential biomarker to measure pancreatic beta-cell mass. *Nucl Med Biol* **2012**, *39* (2), 167-176.

238. Keliher, E. J.; Reiner, T.; Turetsky, A.; Hilderbrand, S. A.; Weissleder, R. High-yielding, two-step 18F labeling strategy for 18F-PARP1 inhibitors. *ChemMedChem* **2011**, *6* (3), 424-427.

239. Reiner, T.; Keliher, E. J.; Earley, S.; Marinelli, B.; Weissleder, R. Synthesis and in vivo imaging of a 18F-labeled PARP1 inhibitor using a chemically orthogonal scavenger-assisted high-performance method. *Angew Chem Int Ed Engl* **2011**, *50* (8), 1922-1925.

240. Wang, M.; Wang, H.; Niu, C. Q.; Zhang, T.; Wu, Z.; Li, Z. Tetrazine-TCO Ligation: A Potential Simple Approach to Improve Tumor Uptake through Enhanced Blood Circulation. *Bioconjug Chem* **2020**, *31* (7), 1795-1803.

241. Feng, H.; Zhang, H.; Wang, M.; Vannam, R.; Wang, H.; Yan, X.; Ouyang, W.; Jia, X.; Fox, J. M.; Li, Z. Improving Tumor-to-Background Contrast through Hydrophilic Tetrazines: The Construction of (18) F-Labeled PET Agents Targeting Nonsmall Cell Lung Carcinoma. *Chemistry* **2020**, *26* (21), 4690-4694.

242. Wang, M.; Vannam, R.; Lambert, W. D.; Xie, Y.; Wang, H.; Giglio, B.; Ma, X.; Wu, Z.; Fox, J.; Li, Z. Hydrophilic (18)F-labeled trans-5-oxocene (oxoTCO) for efficient construction of PET agents with improved tumor-to-background ratios in neurotensin receptor (NTR) imaging. *Chem Commun (Camb)* **2019**, *55* (17), 2485-2488.

243. Evans, H. L.; Nguyen, Q. D.; Carroll, L. S.; Kaliszczak, M.; Twyman, F. J.; Spivey, A. C.; Aboagye, E. O. A bioorthogonal (68)Ga-labelling strategy for rapid in vivo imaging. *Chem Commun (Camb)* **2014**, *50* (67), 9557-9560.

244. Cook, B. E.; Adumeau, P.; Membreno, R.; Carnazza, K. E.; Brand, C.; Reiner, T.; Agnew, B. J.; Lewis, J. S.; Zeglis, B. M. Pretargeted PET Imaging Using a Site-Specifically Labeled Immunoconjugate. *Bioconjug Chem* **2016**, *27* (8), 1789-1795.

245. Garcia, M. F.; Zhang, X.; Shah, M.; Newton-Northup, J.; Cabral, P.; Cerecetto, H.; Quinn, T. (99m)Tc-bioorthogonal click chemistry reagent for in vivo pretargeted imaging. *Bioorg Med Chem* **2016**, *24* (6), 1209-1215.

246. Lumen, D.; Vugts, D.; Chomet, M.; Imlimthan, S.; Sarparanta, M.; Vos, R.; Schreurs, M.; Verlaan, M.; Lang, P. A.; Hippelainen, E.; et al. Pretargeted PET Imaging with a TCO-Conjugated Anti-CD44v6 Chimeric mAb U36 and [(89)Zr]Zr-DFO-PEG(5)-Tz. *Bioconjug Chem* **2022**, *33* (5), 956-968.

247. Keinanen, O.; Li, X. G.; Chenna, N. K.; Lumen, D.; Ott, J.; Molthoff, C. F.; Sarparanta, M.; Helariutta, K.; Vuorinen, T.; Windhorst, A. D.; Airaksinen, A. J. A New Highly Reactive and Low Lipophilicity Fluorine-18 Labeled Tetrazine Derivative for Pretargeted PET Imaging. *ACS Med Chem Lett* **2016**, *7* (1), 62-66.

248. Hersom, M.; Helms, H. C.; Pretzer, N.; Goldeman, C.; Jensen, A. I.; Severin, G.; Nielsen, M. S.; Holm, R.; Brodin, B. Transferrin receptor expression and role in transendothelial transport of transferrin in cultured brain endothelial monolayers. *Mol Cell Neurosci* **2016**, *76*, 59-67.

249. Syvanen, S.; Fang, X. T.; Faresjo, R.; Rokka, J.; Lannfelt, L.; Olberg, D. E.; Eriksson, J.; Sehlin, D. Fluorine-18-Labeled Antibody Ligands for PET Imaging of Amyloid-beta in Brain. *ACS Chem Neurosci* **2020**, *11* (24), 4460-4468.

250. Bredack, C.; Edelmann, M. R.; Borroni, E.; Gobbi, L. C.; Honer, M. Antibody-Based In Vivo Imaging of Central Nervous System Targets-Evaluation of a Pretargeting Approach Utilizing a TCO-Conjugated Brain Shuttle Antibody and Radiolabeled Tetrazines. In *Pharmaceuticals*, 2022; Vol. 15.

251. Shalgunov, V.; Lopes van den Broek, S.; Vang Andersen, I.; Garcia Vazquez, R.; Raval, N. R.; Palner, M.; Mori, Y.; Schafer, G.; Herrmann, B.; Mikula, H.; et al. Pretargeted imaging beyond the blood-brain barrier. *RSC Med Chem* **2023**, *14* (3), 444-453.

252. Yazdani, A.; Bilton, H.; Vito, A.; Genady, A. R.; Rathmann, S. M.; Ahmad, Z.; Janzen, N.; Czorny, S.; Zeglis, B. M.; Francesconi, L. C.; Valliant, J. F. A Bone-Seeking trans-Cyclooctene for Pretargeting and Bioorthogonal Chemistry: A Proof of Concept Study Using (99m)Tc- and (177)Lu-Labeled Tetrazines. *J Med Chem* **2016**, *59* (20), 9381-9389.

253. Maitz, C. A.; Delaney, S.; Cook, B. E.; Genady, A. R.; Hoerres, R.; Kuchuk, M.; Makris, G.; Valliant, J. F.; Sadeghi, S.; Lewis, J. S.; et al. Pretargeted PET of Osteodestructive Lesions in Dogs. *Mol Pharm* **2022**, *19* (9), 3153-3162.

254. Hou, S.; Choi, J. S.; Garcia, M. A.; Xing, Y.; Chen, K. J.; Chen, Y. M.; Jiang, Z. K.; Ro, T.; Wu, L.; Stout, D. B.; et al. Pretargeted Positron Emission Tomography Imaging That Employs Supramolecular Nanoparticles with in Vivo Bioorthogonal Chemistry. *ACS Nano* **2016**, *10* (1), 1417-1424.

255. Poty, S.; Carter, L. M.; Mandleywala, K.; Membreno, R.; Abdel-Atti, D.; Ragupathi, A.; Scholz, W. W.; Zeglis, B. M.; Lewis, J. S. Leveraging Bioorthogonal Click Chemistry to Improve (225)Ac-Radioimmunotherapy of Pancreatic Ductal Adenocarcinoma. *Clin Cancer Res* **2019**, *25* (2), 868-880.

256. Li, L.; Turatti, F.; Crow, D.; Bading, J. R.; Anderson, A. L.; Poku, E.; Yazaki, P. J.; Williams, L. E.; Tamvakis, D.; Sanders, P.; et al. Monodispersed DOTA-PEG-conjugated anti-TAG-72 diabody has low kidney uptake and high tumor-to-blood ratios resulting in improved 64Cu PET. *J Nucl Med* **2010**, *51* (7), 1139-1146.

257. Houghton, J. L.; Membreno, R.; Abdel-Atti, D.; Cunanan, K. M.; Carlin, S.; Scholz, W. W.; Zanzonico, P. B.; Lewis, J. S.; Zeglis, B. M. Establishment of the In Vivo Efficacy of Pretargeted Radioimmunotherapy Utilizing Inverse Electron Demand Diels-Alder Click Chemistry. *Mol Cancer Ther* **2017**, *16* (1), 124-133.

258. Membreno, R.; Cook, B. E.; Fung, K.; Lewis, J. S.; Zeglis, B. M. Click-Mediated Pretargeted Radioimmunotherapy of Colorectal Carcinoma. *Mol Pharm* **2018**, *15* (4), 1729-1734.

259. Shah, M. A.; Zhang, X.; Rossin, R.; Robillard, M. S.; Fisher, D. R.; Bueltmann, T.; Hoeben, F. J. M.; Quinn, T. P. Metal-Free Cycloaddition Chemistry Driven Pretargeted Radioimmunotherapy Using alpha-Particle Radiation. *Bioconjug Chem* **2017**, *28* (12), 3007-3015.

260. Lappchen, T.; Rossin, R.; van Mourik, T. R.; Gruntz, G.; Hoeben, F. J. M.; Versteegen, R. M.; Janssen, H. M.; Lub, J.; Robillard, M. S. DOTA-tetrazine probes with modified linkers for tumor pretargeting. *Nucl Med Biol* **2017**, *55*, 19-26.

261. Rondon, A.; Schmitt, S.; Briat, A.; Ty, N.; Maigne, L.; Quintana, M.; Membreno, R.; Zeglis, B. M.; Navarro-Teulon, I.; Pouget, J. P.; et al. Pretargeted radioimmunotherapy and SPECT imaging of peritoneal carcinomatosis using bioorthogonal click chemistry: probe selection and first proof-of-concept. *Theranostics* **2019**, *9* (22), 6706-6718.

262. Timperanza, C.; Jensen, H.; Back, T.; Lindegren, S.; Aneheim, E. Pretargeted Alpha Therapy of Disseminated Cancer Combining Click Chemistry and Astatine-211. *Pharmaceuticals (Basel)* **2023**, *16* (4).

263. Wyffels, L.; Thomae, D.; Waldron, A. M.; Fissers, J.; Dedeurwaerdere, S.; Van der Veken, P.; Joossens, J.; Stroobants, S.; Augustyns, K.; Staelens, S. In vivo evaluation of ^{18}F-labeled TCO for pre-targeted PET imaging in the brain. *Nucl Med Biol* **2014**, *41* (6), 513-523.

264. Ruivo, E.; Adhikari, K.; Elvas, F.; Fissers, J.; Vangestel, C.; Staelens, S.; Stroobants, S.; Van der Veken, P.; Wyffels, L.; Augustyns, K. Improved stability of a novel fluorine-18 labeled TCO analogue for pretargeted PET imaging. *Nucl Med Biol* **2019**, *76-77*, 36-42.

265. Fan, X.; Ge, Y.; Lin, F.; Yang, Y.; Zhang, G.; Ngai, W. S.; Lin, Z.; Zheng, S.; Wang, J.; Zhao, J.; et al. Optimized Tetrazine Derivatives for Rapid Bioorthogonal Decaging in Living Cells. *Angew Chem Int Ed Engl* **2016**, *55* (45), 14046-14050.

266. Carlson, J. C. T.; Mikula, H.; Weissleder, R. Unraveling Tetrazine-Triggered Bioorthogonal Elimination Enables Chemical Tools for Ultrafast Release and Universal Cleavage. *J Am Chem Soc* **2018**, *140* (10), 3603-3612.

267. Sarris, A. J. C.; Hansen, T.; de Geus, M. A. R.; Maurits, E.; Doelman, W.; Overkleeft, H. S.; Codee, J. D. C.; Filippov, D. V.; van Kasteren, S. I. Fast and pH-Independent Elimination of trans-Cyclooctene by Using Aminoethyl-Functionalized Tetrazines. *Chemistry* **2018**, *24* (68), 18075-18081.

268. Davies, S.; Qiao, L.; Oliveira, B. L.; Navo, C. D.; Jimenez-Oses, G.; Bernardes, G. J. L. Tetrazine-Triggered Release of Carboxylic-Acid-Containing Molecules for Activation of an Anti-inflammatory Drug. *Chembiochem* **2019**, *20* (12), 1541-1546.

269. Davies, S.; Oliveira, B. L.; Bernardes, G. J. L. Development of a self-immolative linker for tetrazine-triggered release of alcohols in cells. *Org Biomol Chem* **2019**, *17* (23), 5725-5730.

270. van Onzen, A.; Versteegen, R. M.; Hoeben, F. J. M.; Filot, I. A. W.; Rossin, R.; Zhu, T.; Wu, J.; Hudson, P. J.; Janssen, H. M.; Ten Hoeve, W.; Robillard, M. S. Bioorthogonal Tetrazine Carbamate Cleavage by Highly Reactive trans-Cyclooctene. *J Am Chem Soc* **2020**, *142* (25), 10955-10963.

271. Mejia Oneto, J. M.; Khan, I.; Seebald, L.; Royzen, M. In Vivo Bioorthogonal Chemistry Enables Local Hydrogel and Systemic Pro-Drug To Treat Soft Tissue Sarcoma. *ACS Cent Sci* **2016**, *2* (7), 476-482.

272. Zhang, G.; Li, J.; Xie, R.; Fan, X.; Liu, Y.; Zheng, S.; Ge, Y.; Chen, P. R. Bioorthogonal Chemical Activation of Kinases in Living Systems. *ACS Cent Sci* **2016**, *2* (5), 325-331.

273. Li, J.; Jia, S.; Chen, P. R. Diels-Alder reaction-triggered bioorthogonal protein decaging in living cells. *Nat Chem Biol* **2014**, *10* (12), 1003-1005.

274. Rossin, R.; van Duijnhoven, S. M.; Ten Hoeve, W.; Janssen, H. M.; Kleijn, L. H.; Hoeben, F. J.; Versteegen, R. M.; Robillard, M. S. Triggered Drug Release from an Antibody-Drug Conjugate Using Fast "Click-to-Release" Chemistry in Mice. *Bioconjug Chem* **2016**, *27* (7), 1697-1706.

275. Wu, K.; Yee, N. A.; Srinivasan, S.; Mahmoodi, A.; Zakharian, M.; Mejia Oneto, J. M.; Royzen, M. Click activated protodrugs against cancer increase the therapeutic potential of chemotherapy through local capture and activation. *Chem Sci* **2021**, *12* (4), 1259-1271.

276. Rossin, R.; Versteegen, R. M.; Wu, J.; Khasanov, A.; Wessels, H. J.; Steenbergen, E. J.; Ten Hoeve, W.; Janssen, H. M.; van Onzen, A.; Hudson, P. J.; Robillard, M. S. Chemically triggered drug release from an antibody-drug conjugate leads to potent antitumour activity in mice. *Nat Commun* **2018**, *9* (1), 1484.

277. Okamoto, K.; Kondo, T.; Goto, T. Synthetic Studies on Gangliosides .2. Functionalization of 2-Deoxy-2,3-Dehydro-N-Acetylneuraminic Acid Methyl-Ester. *Bulletin of the Chemical Society of Japan* **1987**, *60* (2), 631-636.

278. Czuban, M.; Srinivasan, S.; Yee, N. A.; Agustin, E.; Koliszak, A.; Miller, E.; Khan, I.; Quinones, I.; Noory, H.; Motola, C.; et al. Bio-Orthogonal Chemistry and Reloadable Biomaterial Enable Local Activation of Antibiotic Prodrugs and Enhance Treatments against Staphylococcus aureus Infections. *ACS Cent Sci* **2018**, *4* (12), 1624-1632.

279. *Trials C. Phase 1/2a Study of SQ3370 in Patients with Advanced Solid Tumors. NCT04106492*. U.S. National Library of Medicine, **2023**. https://clinicaltrials.gov/ct2/show/NCT04106492 (accessed 2023 11 May).

280. Yao, Q.; Lin, F.; Fan, X.; Wang, Y.; Liu, Y.; Liu, Z.; Jiang, X.; Chen, P. R.; Gao, Y. Synergistic enzymatic and bioorthogonal reactions for selective prodrug activation in living systems. *Nat Commun* **2018**, *9* (1), 5032.

281. Khan, I.; Agris, P. F.; Yigit, M. V.; Royzen, M. In situ activation of a doxorubicin prodrug using imaging-capable nanoparticles. *Chem Commun (Camb)* **2016**, *52* (36), 6174-6177.

282. Zuo, L.; Ding, J.; Li, C.; Lin, F.; Chen, P. R.; Wang, P.; Lu, G.; Zhang, J.; Huang, L. L.; Xie, H. Y. Coordinating bioorthogonal reactions with two tumor-microenvironment-responsive nanovehicles for spatiotemporally controlled prodrug activation. *Chem Sci* **2020**, *11* (8), 2155-2160.

283. Khan, I.; Seebald, L. M.; Robertson, N. M.; Yigit, M. V.; Royzen, M. Controlled in-cell activation of RNA therapeutics using bond-cleaving bio-orthogonal chemistry. *Chem Sci* **2017**, *8* (8), 5705-5712.

284. Du, S.; Wang, D.; Lee, J. S.; Peng, B.; Ge, J.; Yao, S. Q. Cell type-selective imaging and profiling of newly synthesized proteomes by using puromycin analogues. *Chem Commun (Camb)* **2017**, *53* (60), 8443-8446.

285. Agustin, E.; Asare Okai, P. N.; Khan, I.; Miller, M. R.; Wang, R.; Sheng, J.; Royzen, M. A fast click-slow release strategy towards the HPLC-free synthesis of RNA. *Chem Commun (Camb)* **2016**, *52* (7), 1405-1408.

286. Steiger, A. K.; Yang, Y.; Royzen, M.; Pluth, M. D. Bio-orthogonal "click-and-release" donation of caged carbonyl sulfide (COS) and hydrogen sulfide (H(2)S). *Chem Commun (Camb)* **2017**, *53* (8), 1378-1380.

287. Li, Z.; Conti, P. S. Radiopharmaceutical chemistry for positron emission tomography. *Adv Drug Deliv Rev* **2010**, *62* (11), 1031-1051.

288. Wang, M.; Svatunek, D.; Rohlfing, K.; Liu, Y.; Wang, H.; Giglio, B.; Yuan, H.; Wu, Z.; Li, Z.; Fox, J. Conformationally Strained trans-Cyclooctene (sTCO) Enables the Rapid Construction of (18)F-PET Probes via Tetrazine Ligation. *Theranostics* **2016**, *6* (6), 887-895.

289. Meyer, J.-P.; Houghton, J. L.; Kozlowski, P.; Abdel-Atti, D.; Reiner, T.; Pillarsetty, N. V. K.; Scholz, W. W.; Zeglis, B. M.; Lewis, J. S. (18)F-Based Pretargeted PET Imaging Based on Bioorthogonal Diels-Alder Click Chemistry. *Bioconjug Chem* **2016**, *27* (2), 298-301.

290. Rahim, M. K.; Kota, R.; Haun, J. B. Enhancing reactivity for bioorthogonal pretargeting by unmasking antibody-conjugated trans-cyclooctenes. *Bioconjug Chem* **2015**, *26* (2), 352-360.

291. Wyffels, L.; Thomae, D.; Waldron, A. M.; Fissers, J.; Dedeurwaerdere, S.; Van der Veken, P.; Joossens, J.; Stroobants, S.; Augustyns, K.; Staelens, S. In vivo evaluation of (18)F-labeled TCO for pre-targeted PET imaging in the brain. *Nucl Med Biol* **2014**, *41* (6), 513-523.

292. Nicolet, C. M.; Siegel, D. H.; Surfus, J. E.; Sondel, P. M. TAG-72-reactive antibody CC49 recognizes molecules expressed by hematopoietic cell lines. *Tumour Biol* **1997**, *18* (6), 356-366.

293. Thor, A.; Ohuchi, N.; Szpak, C. A.; Johnston, W. W.; Schlom, J. Distribution of oncofetal antigen tumor-associated glycoprotein-72 defined by monoclonal antibody B72.3. *Cancer Res* **1986**, *46* (6), 3118-3124.

294. Wyffels, L.; Muccioli, G. G.; Kapanda, C. N.; Labar, G.; De Bruyne, S.; De Vos, F.; Lambert, D. M. PET imaging of fatty acid amide hydrolase in the brain: synthesis and biological evaluation of an 11C-labelled URB597 analogue. *Nucl Med Biol* **2010**, *37* (5), 665-675.

295. Heskamp, S.; Laverman, P.; Rosik, D.; Boschetti, F.; van der Graaf, W. T.; Oyen, W. J.; van Laarhoven, H. W.; Tolmachev, V.; Boerman, O. C. Imaging of human epidermal growth factor receptor type 2 expression with 18F-labeled affibody molecule ZHER2:2395 in a mouse model for ovarian cancer. *J Nucl Med* **2012**, *53* (1), 146-153.

296. Dijkgraaf, I.; Franssen, G. M.; McBride, W. J.; D'Souza, C. A.; Laverman, P.; Smith, C. J.; Goldenberg, D. M.; Oyen, W. J.; Boerman, O. C. PET of tumors expressing gastrin-releasing peptide receptor with an 18F-labeled bombesin analog. *J Nucl Med* **2012**, *53* (6), 947-952.

297. Laverman, P.; McBride, W. J.; Sharkey, R. M.; Eek, A.; Joosten, L.; Oyen, W. J.; Goldenberg, D. M.; Boerman, O. C. A novel facile method of labeling octreotide with (18)F-fluorine. *J Nucl Med* **2010**, *51* (3), 454-461.

298. Steen, E. J. L.; Edem, P. E.; Norregaard, K.; Jorgensen, J. T.; Shalgunov, V.; Kjaer, A.; Herth, M. M. Pretargeting in nuclear imaging and radionuclide therapy: Improving efficacy of theranostics and nanomedicines. *Biomaterials* **2018**, *179*, 209-245.

299. Hapuarachchige, S.; Artemov, D. Theranostic Pretargeting Drug Delivery and Imaging Platforms in Cancer Precision Medicine. *Front Oncol* **2020**, *10*, 1131.

300. Devaraj, N. K.; Thurber, G. M.; Keliher, E. J.; Marinelli, B.; Weissleder, R. Reactive polymer enables efficient in vivo bioorthogonal chemistry. *Proc Natl Acad Sci U S A* **2012**, *109* (13), 4762-4767.

301. Poulie, C. B. M.; Jorgensen, J. T.; Shalgunov, V.; Kougioumtzoglou, G.; Jeppesen, T. E.; Kjaer, A.; Herth, M. M. Evaluation of [(64)Cu]Cu-NOTA-PEG(7)-H-Tz for Pretargeted Imaging in LS174T Xenografts-Comparison to [(111)In]In-DOTA-PEG(11)-BisPy-Tz. *Molecules* **2021**, *26* (3).

302. Edem, P. E.; Sinnes, J. P.; Pektor, S.; Bausbacher, N.; Rossin, R.; Yazdani, A.; Miederer, M.; Kjaer, A.; Valliant, J. F.; Robillard, M. S.; et al. Evaluation of the inverse electron demand Diels-Alder reaction in rats using a scandium-44-labelled tetrazine for pretargeted PET imaging. *EJNMMI Res* **2019**, *9* (1), 49.

303. van der Kolk, M. R.; Janssen, M.; Rutjes, F.; Blanco-Ania, D. Cyclobutanes in Small-Molecule Drug Candidates. *ChemMedChem* **2022**, *17* (9), e202200020.

304. Molineux, G. Pegylation: engineering improved pharmaceuticals for enhanced therapy. *Cancer Treat Rev* **2002**, *28 Suppl A*, 13-16.

305. Marchetti, L. A.; Kumawat, L. K.; Mao, N.; Stephens, J. C.; Elmes, R. B. P. The Versatility of Squaramides: From Supramolecular Chemistry to Chemical Biology. *Chem* **2019**, *5* (6), 1398-1485.

306. Kuchar, M.; Mamat, C. Methods to Increase the Metabolic Stability of (18)F-Radiotracers. *Molecules* **2015**, *20* (9), 16186-16220.

307. Miranda, A.; Bertoglio, D.; Glorie, D.; Stroobants, S.; Staelens, S.; Verhaeghe, J. Validation of a spatially variant resolution model for small animal brain PET studies. *Biomed Phys Eng Express* **2020**, *6* (4), 045001.

308. Andrews, U. H.; Baldwin, J. E.; Grayston, M. W. On the Thermal-Isomerization of Trans-Cyclooctene to Cis-Cyclooctene. *Journal of Organic Chemistry* **1982**, *47* (2), 287-292.

309. Liu, B.; Thayumanavan, S. Substituent Effects on the pH Sensitivity of Acetals and Ketals and Their Correlation with Encapsulation Stability in Polymeric Nanogels. *J Am Chem Soc* **2017**, *139* (6), 2306-2317.

310. Darko, A.; Wallace, S.; Dmitrenko, O.; Machovina, M. M.; Mehl, R. A.; Chin, J. W.; Fox, J. M. Conformationally strained trans-cyclooctene with improved stability and excellent reactivity in tetrazine ligation. *Chemical Science* **2014**, *5* (10), 3770-3776.

311. Nielsen, U. B.; Marks, J. D. Internalizing antibodies and targeted cancer therapy: direct selection from phage display libraries. *Pharmaceutical Science & Technology Today* **2000**, *3* (8), 282-291.

312. Devaraj, N. K.; Hilderbrand, S.; Upadhyay, R.; Mazitschek, R.; Weissleder, R. Bioorthogonal turn-on probes for imaging small molecules inside living cells. *Angew Chem Int Ed Engl* **2010**, *49* (16), 2869-2872.

313. Kozma, E.; Demeter, O.; Kele, P. Bio-orthogonal Fluorescent Labelling of Biopolymers through Inverse-Electron-Demand Diels-Alder Reactions. *Chembiochem* **2017**, *18* (6), 486-501.

314. Meimetis, L. G.; Carlson, J. C.; Giedt, R. J.; Kohler, R. H.; Weissleder, R. Ultrafluorogenic coumarin-tetrazine probes for real-time biological imaging. *Angew Chem Int Ed Engl* **2014**, *53* (29), 7531-7534.

315. Galeta, J.; Dzijak, R.; Oboril, J.; Dracinsky, M.; Vrabel, M. A Systematic Study of Coumarin-Tetrazine Light-Up Probes for Bioorthogonal Fluorescence Imaging. *Chemistry* **2020**, *26* (44), 9945-9953.

316. Turetsky, A.; Kim, E.; Kohler, R. H.; Miller, M. A.; Weissleder, R. Single cell imaging of Bruton's tyrosine kinase using an irreversible inhibitor. *Sci Rep* **2014**, *4*, 4782.

317. Vogenberg, F. R.; Isaacson Barash, C.; Pursel, M. Personalized medicine: part 1: evolution and development into theranostics. *P t* **2010**, *35* (10), 560-576.

318. Connal, S.; Cameron, J. M.; Sala, A.; Brennan, P. M.; Palmer, D. S.; Palmer, J. D.; Perlow, H.; Baker, M. J. Liquid biopsies: the future of cancer early detection. *J Transl Med* **2023**, *21* (1), 118.

319. Meredith, R. F.; Buchsbaum, D. J. Pretargeted radioimmunotherapy. *Int. J. Radiat. Oncol. Biol. Phys.* **2006**, *66* (2, Supplement), S57-S59.

320. Bruce Martin, R. Ternary complexes of Al3+ and F− with a third ligand. *Coordination Chemistry Reviews* **1996**, *149*, 23-32.

321. McBride, W. J.; D'Souza, C. A.; Karacay, H.; Sharkey, R. M.; Goldenberg, D. M. New Lyophilized Kit for Rapid Radiofluorination of Peptides. *Bioconjug Chem* **2012**, *23* (3), 538-547.

322. Zeglis, B. M.; Brand, C.; Abdel-Atti, D.; Carnazza, K. E.; Cook, B. E.; Carlin, S.; Reiner, T.; Lewis, J. S. Optimization of a Pretargeted Strategy for the PET Imaging of Colorectal Carcinoma via the Modulation of Radioligand Pharmacokinetics. *Mol Pharm* **2015**, *12* (10), 3575-3587.

323. Meyer, J. P.; Kozlowski, P.; Jackson, J.; Cunanan, K. M.; Adumeau, P.; Dilling, T. R.; Zeglis, B. M.; Lewis, J. S. Exploring Structural Parameters for Pretargeting Radioligand Optimization. *J Med Chem* **2017**, *60* (19), 8201-8217.

324. Veronese, F. M.; Pasut, G. PEGylation, successful approach to drug delivery. *Drug Discov Today* **2005**, *10* (21), 1451-1458.

325. Alavijeh, M. S.; Chishty, M.; Qaiser, M. Z.; Palmer, A. M. Drug metabolism and pharmacokinetics, the blood-brain barrier, and central nervous system drug discovery. *NeuroRx* **2005**, *2* (4), 554-571.

326. Wu, Y.-J.; Meanwell, N. A. Geminal Diheteroatomic Motifs: Some Applications of Acetals, Ketals, and Their Sulfur and Nitrogen Homologues in Medicinal Chemistry and Drug Design. *J. Med. Chem.* **2021**, *64* (14), 9786-9874.

327. Potemkin, R.; Strauch, B.; Kuwert, T.; Prante, O.; Maschauer, S. Development of 18F-Fluoroglycosylated PSMA-Ligands with Improved Renal Clearance Behavior. *Mol Pharm* **2020**, *17* (3), 933-943.

328. Lindner, T.; Altmann, A.; Krämer, S.; Kleist, C.; Loktev, A.; Kratochwil, C.; Giesel, F.; Mier, W.; Marme, F.; Debus, J.; Haberkorn, U. Design and Development of (99m)Tc-Labeled FAPI Tracers for SPECT Imaging and (188)Re Therapy. *J Nucl Med* **2020**, *61* (10), 1507-1513.

329. Schlom, J.; Eggensperger, D.; Colcher, D.; Molinolo, A.; Houchens, D.; Miller, L. S.; Hinkle, G.; Siler, K. Therapeutic advantage of high-affinity anticarcinoma radioimmunoconjugates. *Cancer Res* **1992**, *52* (5), 1067-1072.

330. Liu, G. A Revisit to the Pretargeting Concept-A Target Conversion. *Front Pharmacol* **2018**, *9*, 1476.

331. Kolkman, J. A.; Law, D. A. Nanobodies – from llamas to therapeutic proteins. *Drug Discovery Today: Technologies* **2010**, *7* (2), e139-e146.

332. Keyaerts, M.; Xavier, C.; Heemskerk, J.; Devoogdt, N.; Everaert, H.; Ackaert, C.; Vanhoeij, M.; Duhoux, F. P.; Gevaert, T.; Simon, P.; et al. Phase I Study of ⁶⁸Ga-HER2-Nanobody for PET/CT Assessment of HER2 Expression in Breast Carcinoma. *Journal of Nuclear Medicine* **2016**, *57* (1), 27-33.

333. Jin, B.-k.; Odongo, S.; Radwanska, M.; Magez, S. Nanobodies: A Review of Generation, Diagnostics and Therapeutics. *International Journal of Molecular Sciences* **2023**, *24* (6), 5994.

334. Owonikoko, T. K.; Moser, J. C.; Yoon, J.; Slotkin, E. K.; Dowlati, A.; Ma, V. T.; Düring, M.; Sveistrup, J. Phase 1 trial of GD2-SADA:177Lu-DOTA drug complex in patients with recurrent or refractory metastatic solid tumors known to express GD2 including small cell lung cancer (SCLC), sarcoma, and malignant melanoma. *Journal of Clinical Oncology* **2023**, *41* (16_suppl), TPS3162-TPS3162.

335. *GD2-SADA:177Lu-DOTA Complex in Patients With Solid Tumors Known to Express GD2. NCT05130255*. U.S National Library of Medicine, 2023. https://www.clinicaltrials.gov/study/NCT05130255 (accessed 2024 8/01).

SCIENTIFIC CURRICULUM VITAE

Scientific Curriculum Vitae

Personal Information

First Name	Karuna
Surname	Adhikari
Date of birth	25/04/1992
Place of birth	Kathmandu, Nepal
Email	Adhikarikaruna.ka@gmail.com

Education and Training

09/2018 - 01/2024	**PhD in Pharmaceutical Sciences** Faculty of Pharmaceutical, Biomedical and Veterenary Sciences University of Antwerp, Antwerp, Belgium Laboratory of Medicinal chemistry
10/2021 - 12/2021	**Research Internship** Institute of Applied Synthetic Chemistry Vienna University of Technology, Vienna, Austria Laboratory of Molecular chemistry and chemical biology
09/2018 - 02/2019	**FELASA Accredited Course- Scientist -Cat C** Faculty of Pharmaceutical Biomedical and Veterenary Sciences University of Antwerp, Antwerp, Belgium
09/2016 – 07/2018	**Master in Drug Development: Pharmacist** Faculty of Pharmaceutical Biomedical and Veterenary Sciences University of Antwerp, Antwerp, Belgium
02/2018 – 05/2018	**Research Internship – Erasmus Exchange** Faculty of Pharmacy University of Helsinki, Helsinki, Finland Division of pharmaceutical chemistry and Technology
09/2013 – 09/2016	**Bachelor in Pharmaceutical Sciences** Faculty of Pharmaceutical Biomedical and Veterenary Sciences

	University of Antwerp, Antwerp, Belgium
10/2014 – 09/2016	**Honours College**
	Faculty of Pharmaceutical Biomedical and Veterinary Sciences, University of Antwerp, Antwerp, Belgium
	Research internship at Laboratory of Peripheral Neuropathy
	VIB-Department of Molecular Genetics

Funding and Academic Awards

11/2019 - 10/2023	PhD Fellowship Fundamental Research (renewable once)
	Research Foundation Flanders (FWO)
10/2021 – 12/2021	Travel grant FWO (Long stay abroad)
10/2018 - 10/2019	University Research Fund (BOF -Umbrella grant)
	University of Antwerp
2016	Faculty Prize Pharmaceutical, Biomedical and Veterinary Sciences, University of Antwerp

Scientific Publications

Adhikari, K.; Dewulf, J.; Vangestel, C.; Van der Veken, P.; Stroobants, S.; Elvas, F.; Augustyns, K. Characterization of Structurally Diverse ^{18}F-Labeled d-TCO Derivatives as a PET Probe for Bioorthogonal Pretargeted Imaging. *ACS Omega* **2023**, 8 (41), 38252-38262.

Leino, T. O.; Turku, A.; Urvas, L.; **Adhikari, K**.; Oksanen, J.; Steynen, Y.; Yli-Kauhaluoma, J.; Xhaard, H.; Kukkonen, J. P.; Wallén, E. A. A. Azulene as a biphenyl mimetic in orexin/hypocretin receptor agonists. *Bioorg Med Chem* **2023**, 88-89, 117325.

Dewulf, J.; Adhikari, K.; Vangestel, C.; Wyngaert, T. V. D.; Elvas, F. Development of Antibody Immuno-PET/SPECT Radiopharmaceuticals for Imaging of Oncological Disorders-An Update. *Cancers (Basel)* **2020**, 12 (7).

Ruivo, E.; Elvas, F.; **Adhikari, K**.; Vangestel, C.; Van Haesendonck, G.; Lemiere, F.; Staelens, S.; Stroobants, S.; Van der Veken, P.; Wyffels, L.; Augustyns, K. Preclinical Evaluation of a Novel (18)F-Labeled dTCO-Amide Derivative for Bioorthogonal Pretargeted Positron Emission Tomography Imaging. *ACS Omega* **2020**, 5 (9), 4449-4456.

Ruivo, E.; **Adhikari, K**.; Elvas, F.; Fissers, J.; Vangestel, C.; Staelens, S.; Stroobants, S.; Van der Veken, P.; Wyffels, L.; Augustyns, K. Improved stability of a novel fluorine-18 labeled TCO analogue for pretargeted PET imaging. *Nucl Med Biol* **2019**, 76-77, 36-42.

Oral Presentations

Evaluation of a ^{18}F-labeled d-TCO (*Trans*cyclooctene) derivative as a PET probe for pretargeted imaging of tumors *in vivo*. Departmental Research Day-Pharmaceutical Sciences,University of Antwerp, 2023 Antwerp, Belgium.

Development and pre-clinical evaluation of an ^{18}F-labeled d-TCO (*Trans*cyclooctene) derivative for bioorthogonal pretargeted PET imaging of cancer. Cancer Research Day-University of Antwerp, 2022 Antwerp, Belgium

Development and evaluation of a *trans*-cyclooctene (TCO) probe for a pretargeted PET imaging (UAMC-3711). BELNUC, 2022, Antwerp, Belgium

Poster Presentations

Adhikari, K., Elvas, F., Stroobants, S., Van der Veken, P., Augustyns, K. Development and evaluation of a *trans*-cyclooctene (TCO) probe for pretargeted PET imaging. EFMC-ISMC 2022, Nice, France

Adhikari, K., Elvas, F., Stroobants, S., Van der Veken, P., Augustyns, K. Evaluation of a *trans*-cyclooctene (TCO) probe for pretargeted PET imaging. ISRS 2022, Nantes, France

Adhikari, K., Ruivo, E., Elvas, F., Staelens, S., Stroobants, S., Van der Veken, P., Augustyns, K. Development of novel trans-cyclooctene (TCO) derived-probes for pretargeted molecular imaging based on the Inverse Electron Demand Diels-Alder addition (IEDDA). ABPP 2019, Leuven, Belgium.

ACKNOWLEDGMENTS

Acknowledgments

"Great is the art of beginning, but greater is the art of ending" - this sentiment rings especially true for me now, as I am nearing the end of my PhD research journey. This journey has been a life-changing experience both personally and professionally. Many people have contributed in this journey to reach this milestone and I would like to express my deepest gratitude to those.

First of all, I would like to express my heartfelt gratitude to **Prof. Koen Augustyns** for giving me the opportunity to start this PhD programme at UAMC. I am truly indebted to you for your trust and support in accomplishing this dream. Thank you for your valuable guidance and supervision throughout the years, as well as the freedom you gave us to grow as a scientist and learn to work independently. Your unwavering optimism, even when I was dissatisfied with my results, lifted my spirit and encouraged me to move forward. Working with you has been a very pleasant experience. Thank your for being an inspiration, and I wish you all the best for your future endeavors.

To **Prof. Filipe Elvas**, the support and guidance you have provided has been instrumental in elevating the scientific content of this thesis to its current level. Thank you for your insights, scientific ideas, and inputs that have helped improve this project. Your critical comments and scientific discussions have been invaluable for achieving each milestone in this project. Thank you for always seeing the bigger picture, even when the experiments failed, and for brainstorming to make the next one work. I have learned a great deal from you, from radiolabeling chemistry to *in vivo* work. Thank you for your patience in teaching me even when I was stubborn. Thank you for your encouragement to participate in conferences and your efforts to organize social gatherings. I have enjoyed our dinners, beers, and conversations. Thank you for everything.

I would also like to thank **Prof. Sigrid Stroobants** for the constructive input and scientific discussions that you have provided over the years and for welcoming me at the radiopharmacy department with open arms.

To the Internal Doctoral Committee members, **Prof. Alexander Van Nuijs** and **Prof. Nina Hermans** thank you for revising the thesis and your kind and constructive feedback.

I would like to express my gratitude to the external jury members **Prof. Frederik Cleeren** and **Prof. François Guérard** for accepting the task of evaluating this PhD dissertation and for the feedback.

I would also like to thank **Prof. Hannes Mikula** for his warm welcome and guidance during my research internship at the MolBioChem lab. Thank you for making it possible a midst of a COVID pandemic. Especially, thanks to **Patrick** for showing me around the lab and sharing his knowlegde on tetrazine chemistry. Also a huge thanks to **Barbara S**, **Nicole**, **Nadine**, **Andreas**, **Nikolaus**, **Barbara H**, **Dorian**, **Birgit**, **Birgitte** and **Martin** for their support and good times at TU Wien. Despite the lockdown, I had an enjoyable experience.

To **Eduardo**, I appreciate your kind welcome and supervision in the lab during the first year. Thank you for sharing the knowledge with me. I couldn't have asked for a smoother start.

Over the past five years, UAMC has felt more like a second home to me, and it has been an incredible experience to work alongside such wonderful colleagues, and I am thankful to all of you. **Pieter** thank you for your help with chemistry questions, honest opinions, and encouraging words. **Hans**, it is a joy to see you around every day with a smile. Working with both of you for organic chemistry and practical classes has been a fun experience.The group has grown insanely and many have left in the meanwhile. To all the present and past members, **Sophie L**, **Alba**, **Camilla**, **Greta**, **Caroline**, **Henri-Philippe**, **Philipp**, **Vanessa**, **Pawel**, **Adrian**, **Gustavo**, **Roy**, **Roberta**, **Aaron**, **Margarida**, **Michaela**, **Martijn**, **Lorenzo**, **Murat**, **Maarten**, **Nikita**, **Magda**, **Louis**, **Nicolò**, **Sergei**, **Mélissa**, **Joep**, **Alan**, **Olivier**, **Stijn**, **Paz**, **Pooja**, **Quanyi**, **Sarah P**, **Sarah V**, **Vani**, **Yanna**, **Eduardo**, **Muhammet**, **Thomas**, **Alejandro**, **Nicco**, **Nik**, **Theresa**, **Pedro**, **Siham**, **Kenneth**, **Rafaela**, **Johannes**, **Valerie**, **Sophie V**, **Zunigha** and **Birgit** thank you for the exceptional work environment you have created. I have truly enjoyed the lunch breaks, group meetings, conferences, thirstdays, and vrijmibos we have shared together.

Special shout out goes to **Sophie Lyssens** for her tireless efforts to keep the lab running over the years. You make our lives so much easier! Thank you for being the Sint and Paashaas and coming up with all the nice ideas. Also thank you for being a friend and listening to me during difficult times.

To **Mélissa**, you were the first proper lab partner and the best one i ever had (the one before you doesn't count :p). I enjoyed working next to you, our conversations, and our shared love for the

plants. **Alba**, **Camilla**, we all started the same year, and it has been a great support to share this journey with you. Thank you for your companionship, engaging conversations, and for allowing me to vent my frustrations and all the good times we had toegether. And offcourse, thank you for all the administrative tips. **Alba**, thank you for being the event planner of the UAMC and giving us unforgettable experiences. **Greta** and **Caroline** thank you for literally taking care of everyone in the lab. Your support in the past years meant a lot to me whether it was scientific dilemma or life advice.

I would also like to thank the Radiopharmacy and MICA team for warmly receiving me and providing invaluable assistance with all my experiments. I would like to express my gratitude to **Prof. Tim Van den Wyngaert** for his kind and encouraging words, always showing us the bright side, and supporting us in difficult times. I would like to extend a special thanks to **Dominique** for rescuing countless radiolabeling experiments and always being available to help. Many thanks to **Stef, Caroline, Romy, Wouter, Andreas, Tommy, Astrid,** and **Annelies** for their help and for ensuring that everything is running well in the lab. Additionally, thank you all for the delicious lunchtime cakes and drinks to celebrate each of our accomplishments. I would like to thank **Phillipe** for all the assitance with *in vivo* experiments, organizing the best quiz every year and team building events. **Caroline**, **Eleni** and **Annemie** for their contributions to countless bioDs and IHC experiments. Thanks to **Christel** for the cells and animal models and helping me in planning and executing animal studies and **Alan** for the image reconstructions and **Tina** for administration. .I would also like to thank **Lucas** for having my back at UZA and **Sofie** for the lunchtime talks, and I wish good luck to **Louis** and **Noémie** for their Phd journey and **Maarten** and **Quanyi** on their TCO-adventure.

To my friends, **Nanet**, **Jeroen**, **Michiel**, **Pauline**, **Marit and Carst** thank you all for keeping me mentally sane for the past five years, for bringing me out of the cave (lab) every now and then, for supporting me without hesitation through dark times and celebrating with me in good times. Thank you for being the constants in an ever changing world. We have all come so far and i am lucky to have you all in my life. Also thanks to **Mathias**, **Clara,** and **Tatiana,** for keeping my friends happy, the group has gotten merrier with your presence.

Jonatan, the list of things that you have helped me with during this PhD is too long that i can't seem to sum up. You have been there for me from the very beginning, whether it was for getting stuffs from the high shelves at UZA or performing *in vivo* experiments to co-authoring papers. You were

there to save the day when important experiments failed and to celebrate the little milestones with me (even though we both know how skeptic we both are about that). Thank you for your patience, understanding and above all for being my biggest support system. The PhD journey was undoubtedly a roller coaster ride and having you by my side has made all the difference. Thank you for being my colleague, confidant, friend and my partner. I look forward to share more adventures with you.

To my family, thank you **mom** and **dad** for everything you've done for us. I know it hasn't been easy for you and you've had to go through some tough times to get where we are today. I am very grateful to you both for bringing us to the right places where we could create and grab the opportunities. Thank you for your support in the past years. Special thanks to my sister, **Kalyani** for always being there, listening to my PhD frustrations even though you don't understand it. Thank you for being a reality check mirror when i am being delusional but most of all thank you for looking after Faya when i could not. We have walked a long road together and I am proud of what we both have achieved. Thanks to **Ishwor** our newest addition to the fam, for the good vibes and kind words. Also a big thanks to **familie Dewulf** for the support, I am blessed to have you all in my life. Finally, i would like to thank my dog **Faya** (a never ending side project) for bringing me so much joy, for pushing me to do better for both of us. Your yard is almost ready 😊